NITRIDING OF ALUMINIUM-CONTAINING STEELS

by

ABBAS ABDUL-HUSSEIN

A Dissertation submitted in fulfilment of the requirements for the degree of Doctor of Philosophy at the University of Leeds

Department of Metallurgy
Houldsworth School of Applied Science
The University of Leeds

April, 1984

Lacking p. vi.

Dedicated

to

Haj Abdul-Hussein's family

ACKNOWLEDGEMENTS

The author expresses his sincere gratitude to Dr. D.H. Jack under whose supervision this research was carried out. His personal advise and stimulating discussion have been invaluable and made this thesis possible.

Thanks are due to Professor J. Nutting, Head of the Department of Metallurgy for providing the necessary facilities for this research. The author greatly values the help, encouragement and good will of his friends and laboratory staff in the department.

The author acknowledges the financial support of the Ministry of Higher Education, Government of Iraq.

The experimental results and deductions contained in this thesis are original except where reference is made to the work of others.

Department of Metallurgy

The University of Leeds

A. A- Hussein

April, 1984

ABSTRACT

This thesis describes a study of the nitriding behaviour of some aluminium-containing low alloy steels with and without chromium. The main aim of the study has been to establish the relationship between prior heat treatment and nitriding process variables on the nitriding response of the aluminium containing steels. Emphasis was placed on establishing the metallography of the steels nitrided under controlled conditions, using transmission electron microscopy of thin foils and carbon replicas, optical microscopy and microhardness measurements. A potentiostatic etching method was used for the extraction of carbides and nitrides, and those phases which were present were determined by X-ray diffraction and X-ray microanalysis.

In addition to the known nitride phases, i.e. f.c.c CrN and hexagonal AlN, another phase with α-Fe type d-spacing was observed, and subsequently identified as f.c.c. AlN of NaCl structure with a ∿ 4.05 A. This phase transforms to hexagonal AlN if the nitrided specimen is annealed at 700°C. The latter phase was found to be rich in silicon. Unlike CrN, the precipitation of AlN is greatly influenced by the nitriding temperature and the NH_3 content of the gas mixture.

The formation of the carburized layer depends on the internal compressive stress of nitrided layer. The size of the carbides is an impórtant factor in the formation of this layer. Larger carbides are more stable and less likely to dissolve during nitriding. In bulk specimens, nitrided

in high NH_3 content so as to form a white layer on the surface, carbide concentration takes place under the white layer.

The effect of process variables on the fatigue resistance of nitrided steel has been investigated. Specimens of "Nitralloy" En41A have been gas nitrided under controlled conditions to produce steep and shallow case-hardness profiles with and without white layer. The resultant fatigue properties have been related to the microstructure, hardness profile, residual stress and case depth. The fatigue resistance of the nitrided En41A steel depend on the residual stress level in the case, and to a certain extent on the microstructure of the nitrided layer. Nitriding at 570^{o}C produces low residual stress and also causes embrittlement of the nitrided layer.

CONTENTS

PAGE

MISSING

IN

ORIGINAL

Figs. 4.1 to 4.21 and Tables 4.1 to 4.18 are between pages 68 and 69

Figs. 5.1 to 5.27 are between pages 92 and 93

Figs. 6.1 to 6.29 are between pages 115 and 116

CHAPTER 1

INTRODUCTION

1.1 Nitriding process

Iron and steel alloys can have their surface layers hardened by the introduction of atomic nitrogen into the ferrite phase in the temperature range 500-700^{o}C. The basis of the nitriding reaction is the interaction of atomic nitrogen with nitride forming alloying elements in the iron or steel so as to form a dispersion of fine alloy nitrides in the ferrite matrix. The known nitride forming elements are Al, Cr, V, Ti, Mo, W, Mn and Si; but not all of these elements have the capability of inducing high surface hardness. Among the above alloying elements Al, Cr, Si, Mn and Mo occur in commercial nitriding steels, and can achieve surface hardnesses that exceed 1000 VHN.

Although the main purpose of nitriding is to produce a wear resistance surface for steels it is found that corrosion resistance and fatigue properties are also improved.

The main advantage of nitriding over carburising as a surface hardening treatment is that a far greater surface hardness is achieved which has a greater resistance to softening at elevated temperatures; also the core retains its strength since the nitriding process is commonly carried out at temperatures (about 500^{o}C) lower than the temperature (about 600^{o}C) at which the steels are usually tempered prior to nitriding. The distortion and dimensional changes are

reduced to a minimum since the process does not involve a phase change in the matrix.

1.2 Historical

The reaction between iron and nitrogen (as ammonia) was first established in 1905 by Braune (1), and the increase in the surface hardness of nitrided iron was observed by Hodkinson in 1906 (2).

In 1913, Adolph W. Machlet (3) was granted a U.S. patent covering the treating of iron and steel articles in ammonia at temperatures above 900^{o}F.

According to his patent, the articles have the following characteristics:

"The articles when examined after cooling, are found to be provided with an integral alloyed skin, casing, shell or coating which when polished has a dull silvery colour, and is very compact and close-grained and hard, and is capable of taking a very high polish closely resembling polished silver. It is so hard that it is difficult to polish, and difficult or impossible to cut with an ordinary machinist's file. This coating is extremely reluctant to tarnish, corrode, rust or oxidize, and under ordinary conditions may be regarded as practically proof against oxidation or rust, as for instance in indoor use, or where it is not unduly exposed to the elements".

In 1921 Aldolph Fry (4) of the Krupp works in Germany applied for a patent on a method of hardening alloy steels containing aluminium, chromium, manganese or silicon by

nitriding at temperatures below the euctectoidal transformation.

Fry's work in developing special alloy steels, specifically for nitriding, led to the so called "Nitralloy" steels.

Many attempts at improvements in gas nitriding technique have since taken place, e.g. pressure nitriding (5), agitation of the work piece by high frequency oscillation (6), nitriding at two different temperatures (7), and additions to the nitriding atmosphere of organic or inorganic compounds such as aniline and ammonium chloride (8),(9).

The main objective in these attempts was to shorten the nitriding time or to obtain an increased depth of hardening.

In commercial nitriding, there are three different nitriding methods. These are, gas nitriding, salt bath nitriding and ion-nitriding. Gaseous nitriding was the first method to be developed and is still the main commercial process. It involves the use of partially dissociated (about 30%) anhydrous ammonia at temperatures of 500-570^{o}C. When in contact with hot iron, ammonia catalycally dissociates into hydrogen and atomic nitrogen, the latter diffuses into the steel surface and reacts with those alloying elements which have a strong affinity towards nitrogen to form fine nitrides. The formation of soft and brittle iron nitrides on the surface of the nitrided articles is still a major problem in nitriding. However, attempts have been made to reduce the thickness of this so-called "white-layer". In 1937 Fisher and Shaw (10) showed that "white-layer" thickness can be reduced by increasing the degree of dissociation after

the first few hours of nitriding. This work was complemented by Floe (11) who developed a two stage nitriding process (12). The process involves nitriding at 500^{o}C for a short period (5-10h) in 30% dissociated ammonia, the rest of the nitriding period then would be carried out with 85% dissociation. This limits the white layer thickness to a maximum of 12 µm with no sacrifice in case depth. The process also offers great savings by recirculating the exhaust gases to produce the high percentage of dissociation required for the second stage.

Liquid nitriding was introduced by Komarnitsky (13) in 1930's. The liquid bath is composed of a mixture of sodium and potassium salts, which comprise 60-70% (by weight) of the total mixture, and consist of 96.5% NaCN, 2.5% Na_2CO_3 and 0.5% NaCNO. The potassium salts, 30-40% of the mixture, consist of 96% KCN, 0.6% K_2CO_3, 0.75% KCNO and 0.5 KCl. By ageing the bath at 575^{o}C for 12 h, the cyanate can be raised to the desired level, about 45%. After the ageing process the steel parts are then immersed in the bath, at a normal working temperature of 550-570^{o}C for a maximum period of 2 h. Up to the middle of the 1950's, salt bath nitriding was used only on a very restricted scale, and mainly for short periods (10-30 min) to avoid pitting which occurs on the steel surfaces. In addition the results of the nitriding can be irregular. This occurs due to the variations in the cyanate content at different levels of the bath. This defect is eliminated by injecting air through the bath. The introduction of air provides agitation and stimulates chemical activity.

Increasing interest in the process for commercial purposes led to further improvements, leading to the "Tuffride"

(14) and Sulfinuz (15) processes.

The essential ingredients of the baths for both processes are normally the same i.e. sodium and potassium cyanide and cyanate, but with the "Sulfinuz" treatment, sodium sulphide is added which accelerates the reaction to produce cyanate.

In 1928 Bason (16) reported that metal surfaces can be hardened if bombarded with nitrogen ions. The process called glow-discharge or ion-nitriding was first used industrially by Berghaus (17) who patented it at the beginning of the 1930's.

The principle of ion-nitriding is similar to that of galvanic plating where a current-carrying medium between an anode and a cathode supplies the coating material to the cathode. With ion-nitriding, the current carrying medium is a low-pressure nitrogen gas contained in a vacuum furnace (1-10 Torr). Under the influence of the high voltage (over 500 volts) the gas is ionized and thus become electrically conductive. The positive nitrogen ions so produced are attracted by the cathodic work piece; they impinge upon the surface, are thus occluded, and heat up the piece to the necessary diffusion temperature (~ 500^{o}C), so no external heating is required (18,19,20,21).

It has been shown that ion-nitriding has several advantages over conventional gas nitriding. One major advantage is the ease with which the nature and thickness of the "white layer" can be controlled simply by changing the treatment gas composition. Also parts grow only slightly

when ion-nitrided (22). This is attributed to sputtering occurring at the metal surface being bombarded, i.e. material which sputters away compensates for the growth which is a normal characteristic of the conventional nitriding process. Little distortion takes place in ion-nitrided parts, and the resulting cases are quite uniform. In commercial practice the process offers other advantages (18) like faster nitriding rate; parts can be masked with re-usable sheets of thin low-carbon steel to prevent selected area from nitriding, and it provides a more pleasant work environment than gas or salt-bath nitriding shops.

1.3 Nitriding Steels

The development of special alloy steels for nitriding was based on the fundamental work carried out by Fry (23); who discovered that the addition of aluminium, chromium, manganese and silicon increases the hardness of the nitrided steel. Steels containing these elements gave a commercially satisfactory result. Although molybdenum was not mentioned by Fry, it developed later that Mo was of greater importance and essential for commercially satisfactory nitriding steel.

The molybdenum decreases softening on tempering so that high strengths can be retained even after tempering at well over the nitriding temperature, and it minimizes susceptibility to temper embrittlement during nitriding. The early analysis of nitriding steel was: 1.30 to 1.80% Cr, 1.30 to 1.80% Al and 0.20 to 0.30% Mo (24); this was further improved and the steel composition became: 0.80-1.30% Cr,

0.60 to 1.20% Al and 0.15 to 0.25% Mo. The later analysis gave excellent surface hardness and penetration with better adaptability to forging and machining.

The present aluminium containing steels are the En 41 type with chemical composition: 1.40-1.80% Cr, 0.90-1.30% Al and 0.10-0.25% Mo, plus Si, Mn and Ni.

A new type of aluminium-free nitriding steel was developed in the 1950's based on the En 40 type with 2.5-3.5% Cr plus Mo and V (25). These steels have better hot strength and hardenability in heavy section than the aluminium-containing grades. They can sometimes be hardened by air cooling instead of oil quenching in certain size ranges, which is an advantage for complicated shapes. Also they have adequate cleanness and high toughness in the air melted condition. The case hardness is lower than that of the aluminium-containing steels, and therefore, the nitrided cases of the Cr-Mo-V steels are less brittle and less susceptible to spalling and flaking. These nitriding steels are selected where a combination of properties is required, such as high core strength to support the nitrided case and give the requisite load carrying capacity, or where heavy sections are involved and optimum hot strength and hot hardness are needed for elevated temperature service.

Regarding the mechanism of nitrogen hardening, Fry (26) originally suggested that the nitrogen hardening was not due to the presence of alloy nitrides but to the influence of nitrogen on the lattice spacing of iron. Other workers were of the opinion that only iron nitride formed and the alloying

elementary merely determined the "case quality". However, Jones and Morgan (22) and Jones (27,28) established that aluminium produced the greatest hardening in steels due to the formation of fine insoluble particles of aluminium nitride, with chromium and vanadium having lesser effects.

1.4 Ammonia-hydrogen gas mixture nitriding

At the nitriding temperature (500-570^{o}C) ammonia is metastable and decomposes on contact with iron. The products of the dissociation are molecular hydrogen plus either molecular nitrogen or nitrogen dissolved interstitially in iron. The nitrogen solubility at the surface of the iron is determined by the equilibrium:

$$NH_3 \rightleftharpoons 3/2\ H_2 + [N]\ \text{(dissolved in Fe)} \qquad 1.1$$

hence

$$[\%N] = k\ P_{NH_3}/(P_{H_2})^{3/2} \qquad 1.2$$

where k is the equilibrium constant at a given temperature and P_{NH_3} and P_{H_2} are the partial pressures of the ammonia and hydrogen, respectively, in the gas. The equilibrium constant k has been determined experimentally by Lehrer (29) and Emmett et al. (30) and can be used to determine the concentration of nitrogen in ferrite in equilibrium with any ammonia-hydrogen mixture.

There are other possible reactions that can occur when ammonia reacts with iron at elevated temperature. One possible reaction involves solid solution of hydrogen:

$$NH_3 = \tfrac{1}{2} N_2 + 3[H] \qquad 1.3$$

but this is found to occur only to limited extent (31). The other possible reaction involves the decomposition of ammonia to both molecular nitrogen and hydrogen.

$$2\,NH_3 = N_2 + 3\,H_2 \qquad 1.4$$

However, a high flowrate and smooth metal surfaces suppress this reaction at least up to a temperature of 600°C (32). On an experimental scale, nitriding gas atmospheres are usually mixtures of ammonia and hydrogen, and the nitriding potential of the gas, defined as $P_{NH_3}/P_{H_2}^{3/2}$, can be calculated from equation (1.1). More typically, pure ammonia is introduced into the furnace and decomposes to some extent at the surfaces of the furnace and the charge. If a fraction (X) has dissociated according to the reaction in equation 1.4 then

$$\frac{pNH_3}{(pH_2)^{3/2}} = \left\{\frac{1-X}{1+X}\right\} \quad \left\{\frac{1+X}{3X/2}\right\}^{3/2} \qquad 1.5$$

If, as often happens, the composition of the furnace atmosphere is expressed as a fraction (1-Y) of ammonia plus a fraction (Y) of fully dissociated ammonia as determined by the exit gas composition, then equation (1.5) becomes:

$$\frac{pNH_3}{(pH_2)^{3/2}} = (1-Y)/(3Y/4)^{3/2} \qquad 1.6$$

Fig. 1.1 illustrates the relationship between the amount of fully dissociated ammonia (Y), the ammonia content of a binary ammonia-hydrogen mixture and nitrogen potential.

1.5 The iron-nitrogen system

For any ammonia-hydrogen gas mixture there is an equivalent chemical potential or activity of nitrogen dissolved in iron, and as the ammonia content of an ammonia-hydrogen gas mixture increases, the nitrogen content of the iron increases until at some point the nitrogen potential equals that in equilibrium with γ'-Fe_4N, Fig. 1.2. By equilibrating iron with ammonia-hydrogen mixtures at different temperatures the phase diagram shown in Fig. 1.3, has been constructed. The appropriate conditions for γ'-Fe4N and ε -Fe_3N formation in pure iron are shown in Fig. 1.4, the Lehrer diagram (29), which relates the proportion of ammonia in the nitriding gas atmosphere to the phase present at equilibrium on the surface of the iron.

A detailed structural analysis of the phases occuring in the iron nitrogen system was performed by Jack (33,34). Structural data for α''-$Fe_{16}N_2$, γ'-Fe4N, ε -Fe_3N and ξ -Fe_2N are given in Table 1.1. α''-$Fe_{16}N_2$ has a fully ordered nitrogen atom arrangement in a slightly distorted b.c.c. iron atom array, see Fig. 1.5.

This phase is formed by tempering nitrogen martensite or by ageing supersaturated nitrogen ferrite.

The precipitation of γ'-Fe_4N in supersaturated nitrogen ferrite was found to occur in two stages, the intermediate stage being the precipitation of α'' -$Fe_{16}N_2$.

In γ'-Fe_4N, the metal-atom arrangement is f.c.c. The nitrogen atoms occupy one-quarter of the number of octahedral holes in a fully ordered manner so as to minimise the strain energy and the mutual repulsion between nitrogen atoms;

see Fig. 1.6. The phase is stable only below 680°C, see Fig. 1.3. The metal atom arrangement in ε - Fe_3N is close packed hexagonal. Octahedral interstices in such a structure are arranged in layers perpendicular to the c-axis with spacing c/2 and with two dimensional close packing within each layer of "holes". At the composition Fe_3N one third of the interstices in each layer are occupied such that each nitrogen atom is surrounded by six unoccupied holes in its own plane and two others respectively above and below it.

The homogeneity range of ε-iron nitride extends almost to the composition Fe_2N and the additional nitrogen atoms enter the unoccupied interstices only in alternate layers to give a sequence in which successive layers are one third and two thirds filled. Just before the ideal ε-Fe_2N composition is reached there is a phase change to ξ-Fe_2N.

1.6 Nitride formation in iron and steel alloys

It has been established that the extreme hardness of the binary iron alloys e.g. Fe-Mo, Fe-Ti, Fe-V, Fe-Cr is caused by very fine scale precipitation of alloy nitrides on the cube planes of the matrix (35,36,37).

However under similar nitriding conditions the alloying elements in iron show different levels of interaction with nitrogen.

The nitride phases of the more commonly occuring alloying elements in steel are listed in Table 1.2.

The strength of interaction between nitrogen and the alloying element is related to the heat of fomration and the

crystal structure of the nitride phase. Face centred cubic nitride phases which have 'a' approximately 415 pm can form with a Bain orientation (38) as coherent or semi-coherent plates on the cubic planes of ferrite. Such precipitates can nucleate homogeneously, whereas it is known that AlN with a more complicated hexagonal crystal structure only nucleates on dislocation (39). The stresses generated by growing particles of AlN are sufficient to produce further dislocations on which more precipitates can form.

The nucleation difficulty of the hexagonal AlN was attributed to the fact that unlike TiN, VN or CrN it is a covalent compound and not an interstitial phase (40). In interstitial nitrides the nitrogen atoms occupy the same octahedral sites as they do in the matrix. However, AlN has the hexagonal wurtzite structure with the nitrogen atoms occupying tetrahedral sites. The aluminium atom arrangement cannot be derived simply from the ferrite structure but can only occur by a large rearrangement in the metal atom positions.

In the iron-molybdenum-nitrogen system nucleation of the nitride presents few problems as it occurs by a continuous clustering process. The slow rate of reaction is attributed to the weak interaction of molybdenum and nitrogen.

1.7 Hardness of nitrided iron and steel alloys

Nitriding of iron alloys and steels in an NH_3/H_2 atmosphere at temperatures between 450-650^{o}C produces structures with varying hardness profiles, i.e. variation of

hardness with distance from the surface. The nature and type of hardness profile developed depends on the following factors:

a) the nitriding temperature

b) the activity of the nitrogen in the ammonia-hydrogen mixtures, which is proportional to the ammonia content of the gas

c) the ease of nucleation of the nitride precipitate

d) the concentration substitutional alloying element

e) the strength of the solute-nitride interaction.

The response to nitriding in gaseous ammonia-hydrogen mixtures of iron alloys can be classified into two extreme types of behaviour as follows.

1.7.1 Strong interaction with easy nucleation

When there is a strong interaction between nitrogen and the substitutional solute, and nucleation of the nitride is easy, the nitriding reaction proceeds by the formation of a uniform hard subscale, which advances progressively into the core forming a steep hardness profile.

A generalised mathematical model for this reaction has been developed from models for internal oxidation by Wagner (41) and assumes that:

a) diffusion of the substitutional alloying element can be neglected

b) all the alloying element at the interface between nitrided and non-nitrided regions is completely reacted before the nitriding front moves on

c) the solubility product K_s, of the nitrogen concentration times the alloying el-ment concentration is negligibly small for homogeneous precipitation.

d) nitrogen is taken up rapidly from the nitriding atmosphere to maintain an equilibrium surface nitrogen concentration Fig. 1.7 shows the respective nitrogen alloying element and nitride concentrations for such a model.

If we consider a unit area of reaction front, then the diffusive flux or rate of transfer of atoms through this unit area

$$\text{flux} = \frac{dn}{dt} \quad \text{in atoms/cm}^2\text{/s}$$

where n = number of atoms

By Fick's first law

$$\frac{dn}{dt} = D_N^{\alpha} [N'_s - N'_c]/\xi$$

Assuming the concentration of nitrogen in equilibrium with alloy nitride at the nitriding front, N'_c is zero, then:

$$\frac{dn}{dt} = D_N^{\alpha} [N'_s]/\xi \qquad 1.7$$

Again the number of atoms transferred across unit area

$$dn = r[x'].d\xi \qquad 1.8$$

from which $r[x'].d\xi/dt = D_N^{\alpha} [N'_s]/\xi$

or $\xi d\xi = D_N^{\alpha} [N'_s] dt/r[x']$

Integraing $\xi^2 = 2 D_N^{\alpha} [N'_s]t/r[x']$

or $\xi^2 = \frac{2[N_s]}{r[x]} D_N^{\alpha} t$ 1.9

where ξ = depth of nitrogen penetration

$[N'_s]$ = surface nitrogen concentration in atom/cm^3

$[N_s]$ = surface nitrogen concentration in atomic %

$[x']$ = original alloying element concentration in atom/cm^3

$[x]$ = original alloying element concentration in atomic %

r = the ratio of nitrogen to substitutional solute in the phase formed by nitriding (r = y/x, when phase formed is MxNy)

D_N^{α} = the diffusivity of nitrogen in α-iron

Such a relation is accurately obeyed by a number of binary iron alloys, e.g. iron-titanium alloys nitrided over a wide range of temperature and nitriding potentials (42). The implications of the model are that faster nitriding rates can be achieved by increasing the ammonia content of the gas mixture, and thus the surface nitrogen concentration (so long as the critical level for iron nitride formation is not exceeded) or by decreasing the amount of alloying element, which would have the disadvantage of reducing the nitrided hardness. Similar behaviour is observed in iron containing 5 wt.% Cr (37) and with certain iron vanadium

alloys (36). In such alloys the sub-scale depth can be detected both metallographically and by the sharp cut-off in the hardness profile.

1.7.2 Weak interaction or difficult nucleation

This type of behaviour occurs either when there is a relatively weak interaction between solute and nitrogen or there is a barrier to nucleation of the nitride precipitates. Under these conditions the nitriding reaction is controlled by the rate of reaction to form the nitride phase. Such behaviour has been observed in annealed iron-aluminium alloy (39), in Fe-5 wt% Mo nitrided at 575^{o}C (42) and in Fe-1.2 wt % Cr nitrided at 575^{o}C (36). An alternative explanation has been proposed by Hayes and Grieveson (43) in which nitrogen adsorption through the surface, rather than diffusion through the matrix is considered to be rate controlling. At low alloy contents the nitriding front can potentially move rapidly, but if transport through the surface is limiting, the solubility of nitrogen at the surface never reaches its equilibrium value.

Fig. (1.8) illustrates the two main types of the behaviour occurring during nitriding.

1.7.3 Intermediate behaviour

The behaviour of iron-chromium alloys can be considered as following an intermediate type of interaction (44). With high (5%) or low (1%) chromium concentrations, iron-chromium alloys show nitriding responses characteristic

of "strong" or of "weak" interactions. With intermediate concentration (2%) the case/core transition is less abrupt than for a strong interaction but maximum surface hardness is achieved at the onset of nitriding.

The sharpness of the nitrided boundary depends on the rate of nucleation of the nitride precipitates. If the nucleation rate is high as in the case of iron-titanium alloys, then the case/core interface is sharp as nitrogen cannot advance until all the solute at the interface has been converted into the alloy nitride.

Meijering (45) has shown that the diffuseness of the interface $\Delta X/\xi$ is proportional to

$$\frac{K_S}{[N][Cr]} \quad \text{(see Fig. 1.9)}$$

where ΔX = the extent of the interface

ξ = the total nitriding depth

K_s = the critical solubility product for the nucleation of homogeneous precipitation

[N] = the surface nitrogen concentration

[Cr] = the original chromium concentration.

Thus, as the temperature of nitriding is increased, K_s will increase and with it the diffuseness of the interface. With increasing ammonia in the gas mixture and increasing alloy content the boundary will become sharper. When a sharp cut off is not observed as in the case of chromium steels nitrided under specific conditions, the mathematical model shown in the previous section based on strong interaction and

easy nucleation, i.e. Equation 1.9, cannot be applied. However, the nitriding kinetics can be investigated by following the increase of nitrogen concentration during nitriding.

1.8 Scope of the present investigation

The present investigation aims to:

(1) establish the relationships between prior heat treatment and nitriding process variables on the nitriding response of aluminium-containing low alloy steels and as such complements previous work in this laboratory on the nitriding of chromium-containing irons and steels (46,47,48).

(2) Study the microstructure of the nitrided aluminium-containing steels, and to identify the nitride phases that precipitate during nitriding, under various conditions, in order to understand the hardening responses of these steels.

Table 1.1

Unit cell dimensions and composition limits of iron-nitrogen phases

phase symbol	crystal structure	composition limits	unit cell dimensions, Å	wt% N	Reference No.
$\gamma'(Fe_4N)$	f.c.c. metal atom arrangement	5.29-5.7 wt% N	a = 3.791	5.29	(33)
		$FeN_{0.23}$-$FeN_{0.24}$	a = 3.801	5.71	
		5.75-6.1 wt% N	a = 2.787	5.75	(31)
		$FeN_{0.24}$-$FeN_{0.26}$	a = 3.795	6.10	
$\varepsilon\{Fe_2N_{(1-x)}\}$	c.p.h. metal atom arrangement	5.70-11.0 wt% N	a = 2.66, c = 4.344	5.70	(31)
		$FeN_{0.24}$-$FeN_{0.49}$	a = 2.764, c = 4.420	11.00	
			a = 2.657, c = 4.380	7.30	(33)
			a = 2.770, c = 4.432	11.00	
$\alpha''(Fe_{16}N_2)$	b.c. tetragonal	3.1 wt% N	a = 5.72	3.1	(32,34)
		$FeN_{0.13}$	c = 6.29		

phase	Bravais lattice	unit cell dimensions pm x 10^2	heats of formation KJ/mole nitride
TiN	f.c.c.	a = 4.244	-335
AlN	hexagonal	a = 3.110 c = 4.975	-301
VN	f.c.c.	a = 4.139	-218
CrN	f.c.c.	a = 4.149	-126
Mo_2N	f.c.c.	a = 4.169	-82
W_2N	f.c.c.	a = 4.126	-71

Table 1.2 Nitride phases of the more commonly occurring alloying elements in nitrided steels.

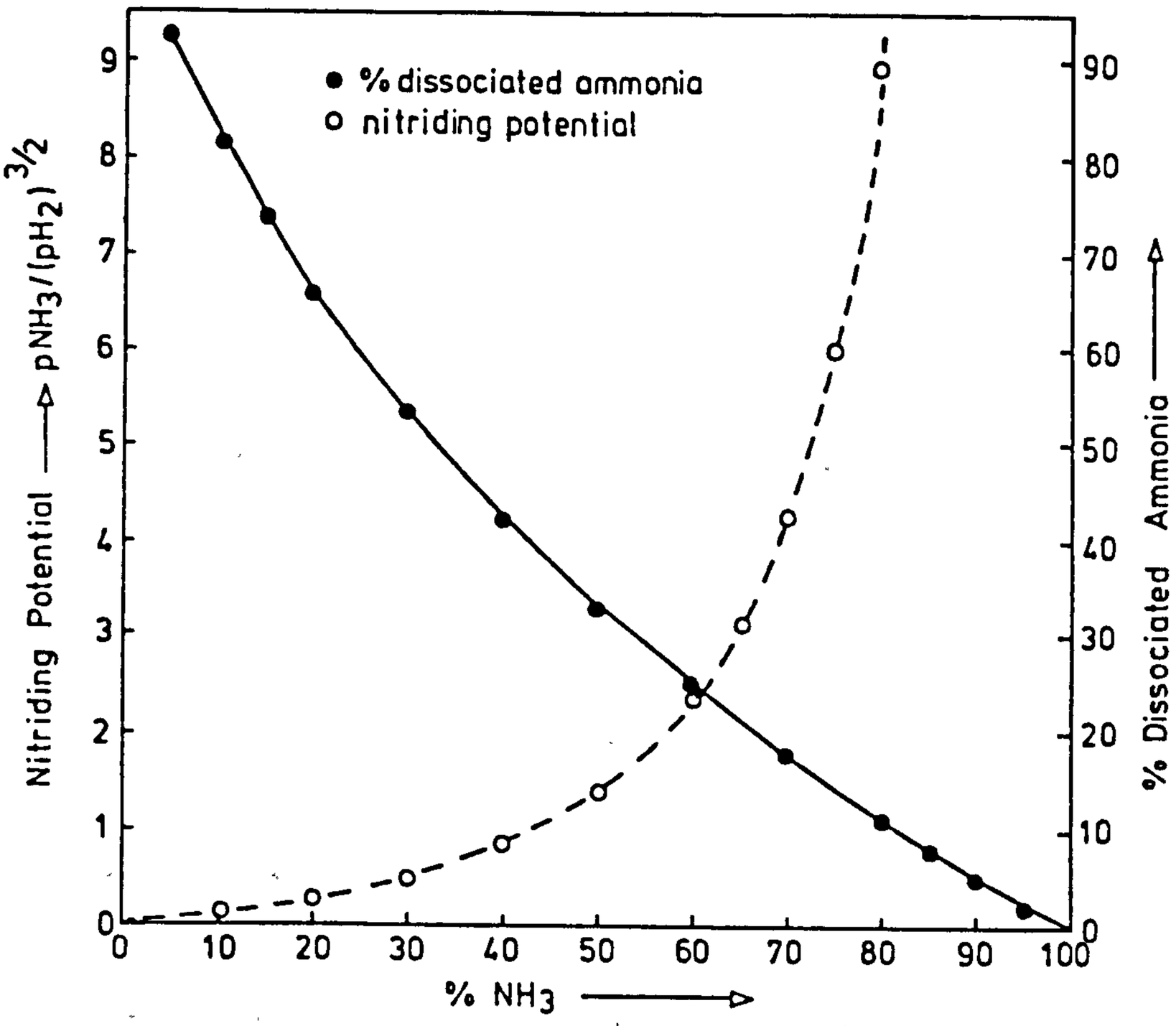

Fig. 1.1 The relationships between ammonia content, nitriding potential, and dissociated ammonia in the nitriding atmosphere

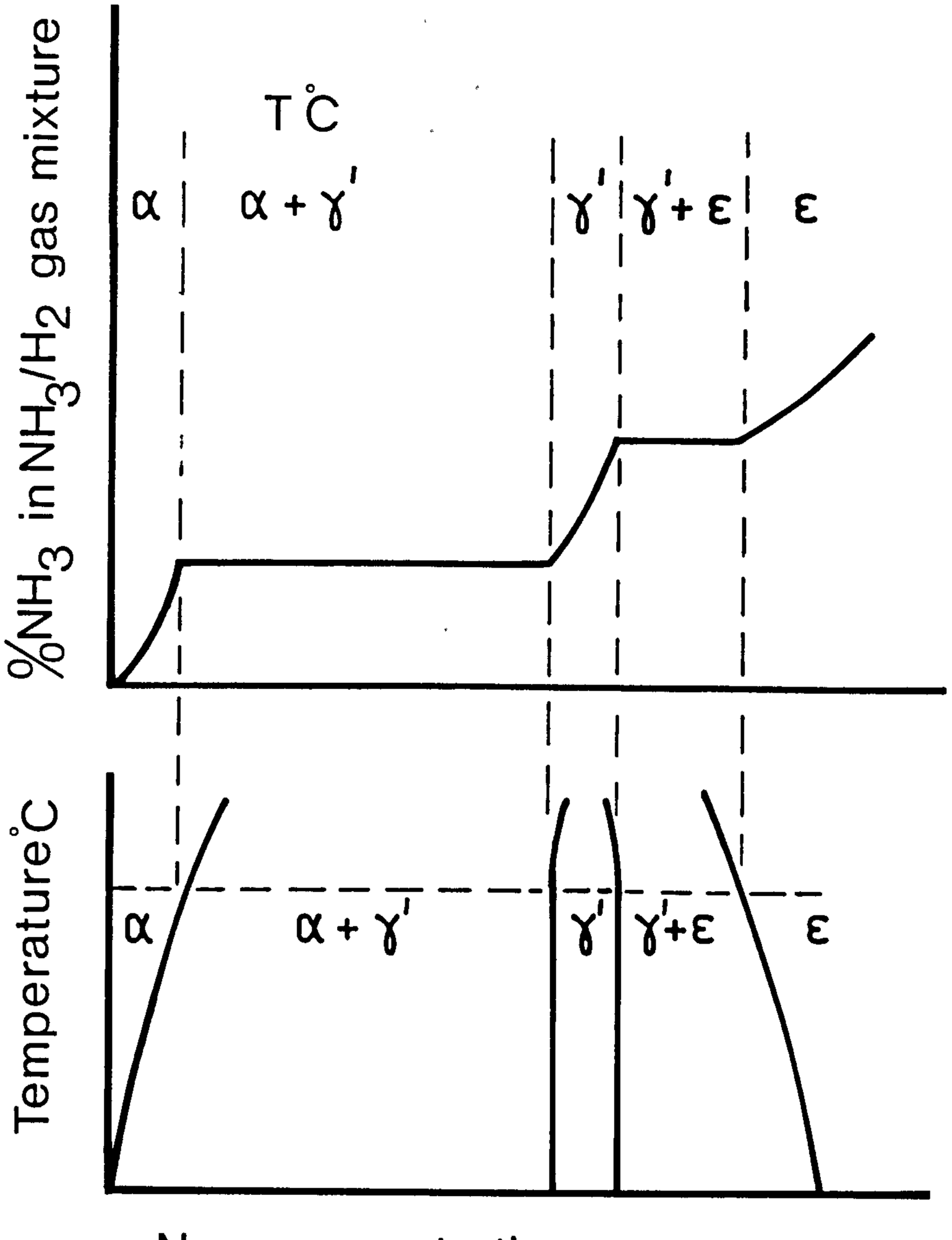

Fig. 1.2 Determination of phase boundaries in the Fe-N system by the action of ammonia-hydrogen gas mixtures on iron.

Fig. 1.3 Part of the iron-nitrogen phase diagram as determined by the action of ammonia on iron.

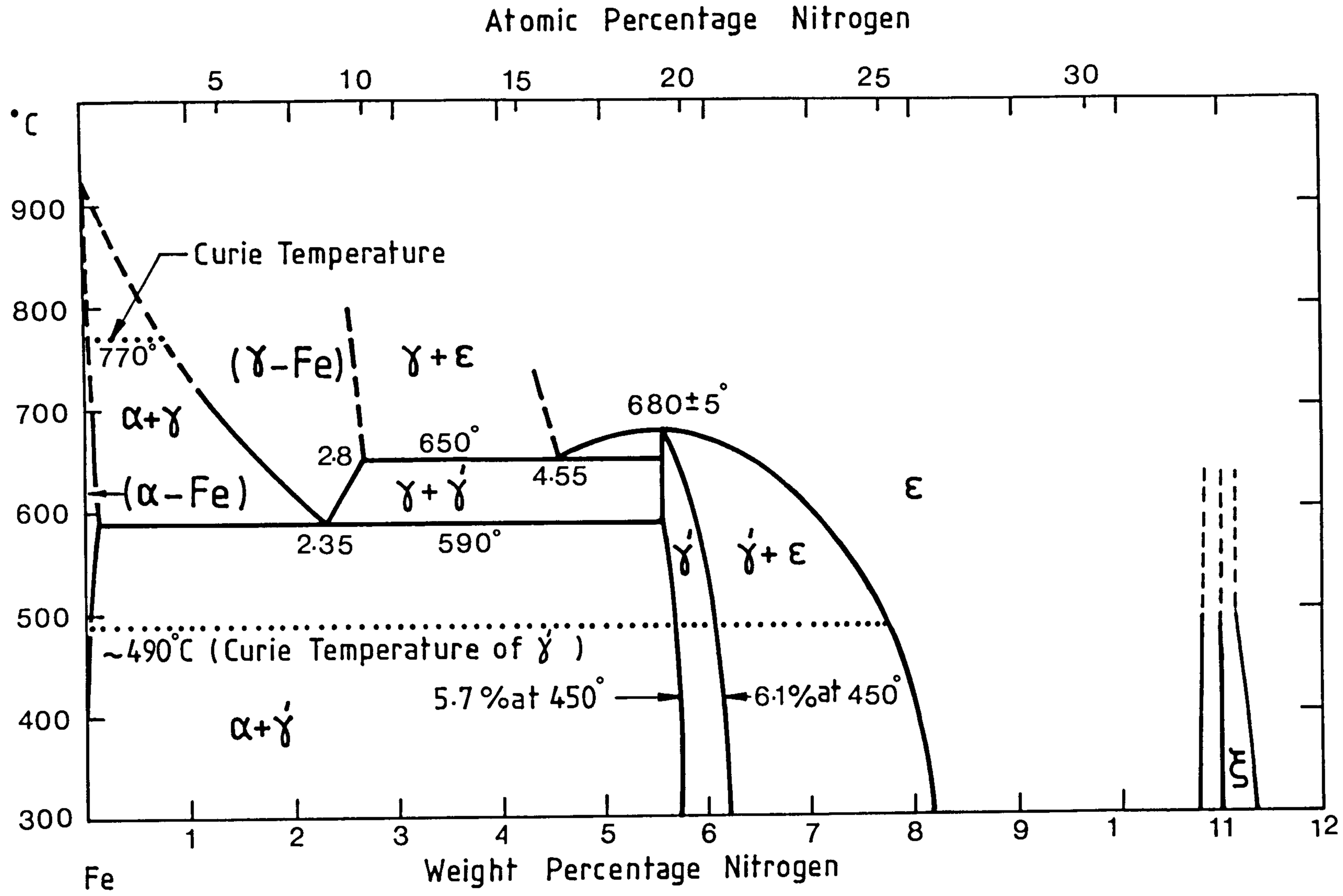

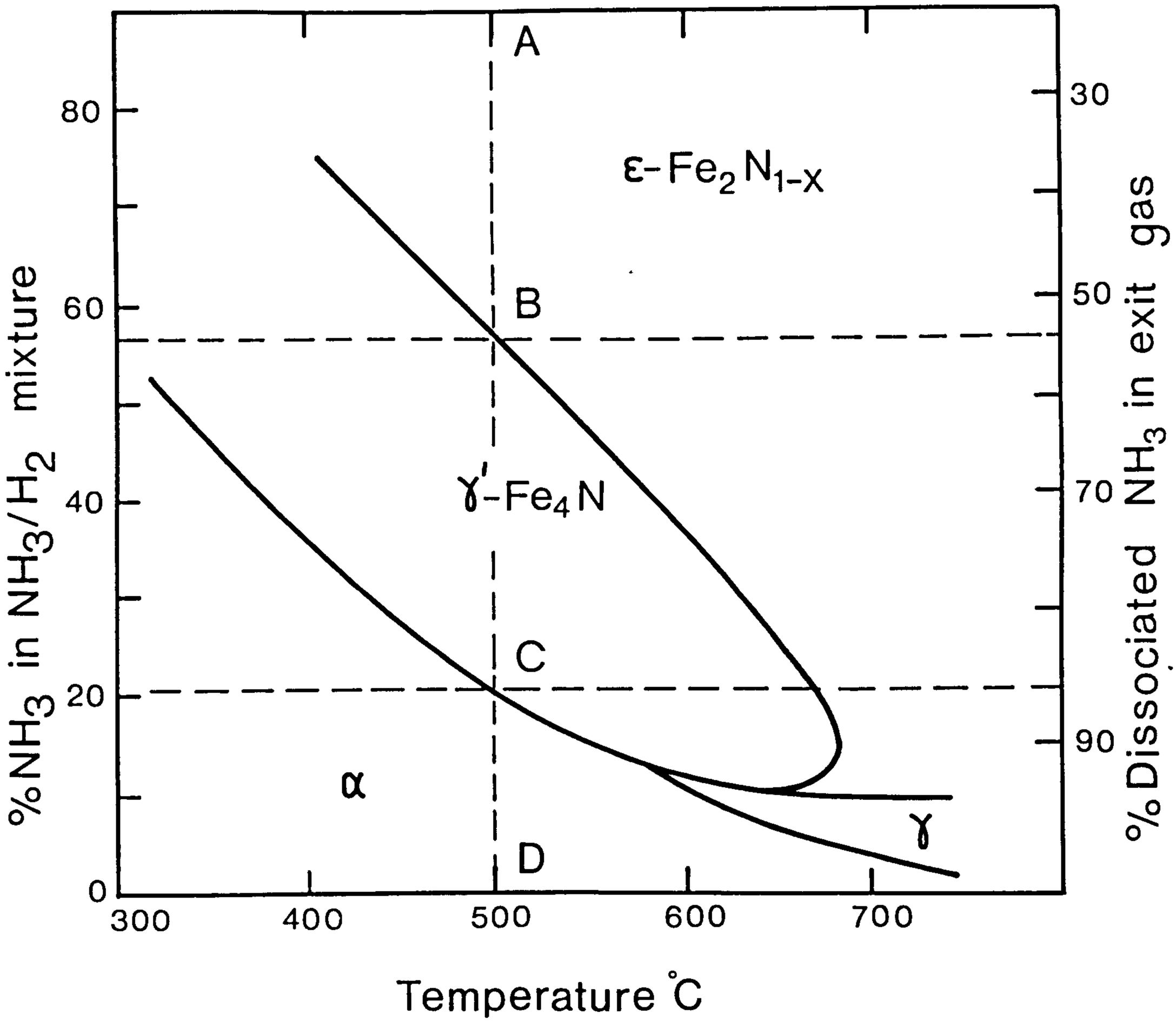

Fig. 1.4 The lehrer diagram from the equilibration of iron with ammonia-hydrogen mixtures showing critical ammonia concentrations for the formation of iron nitride.

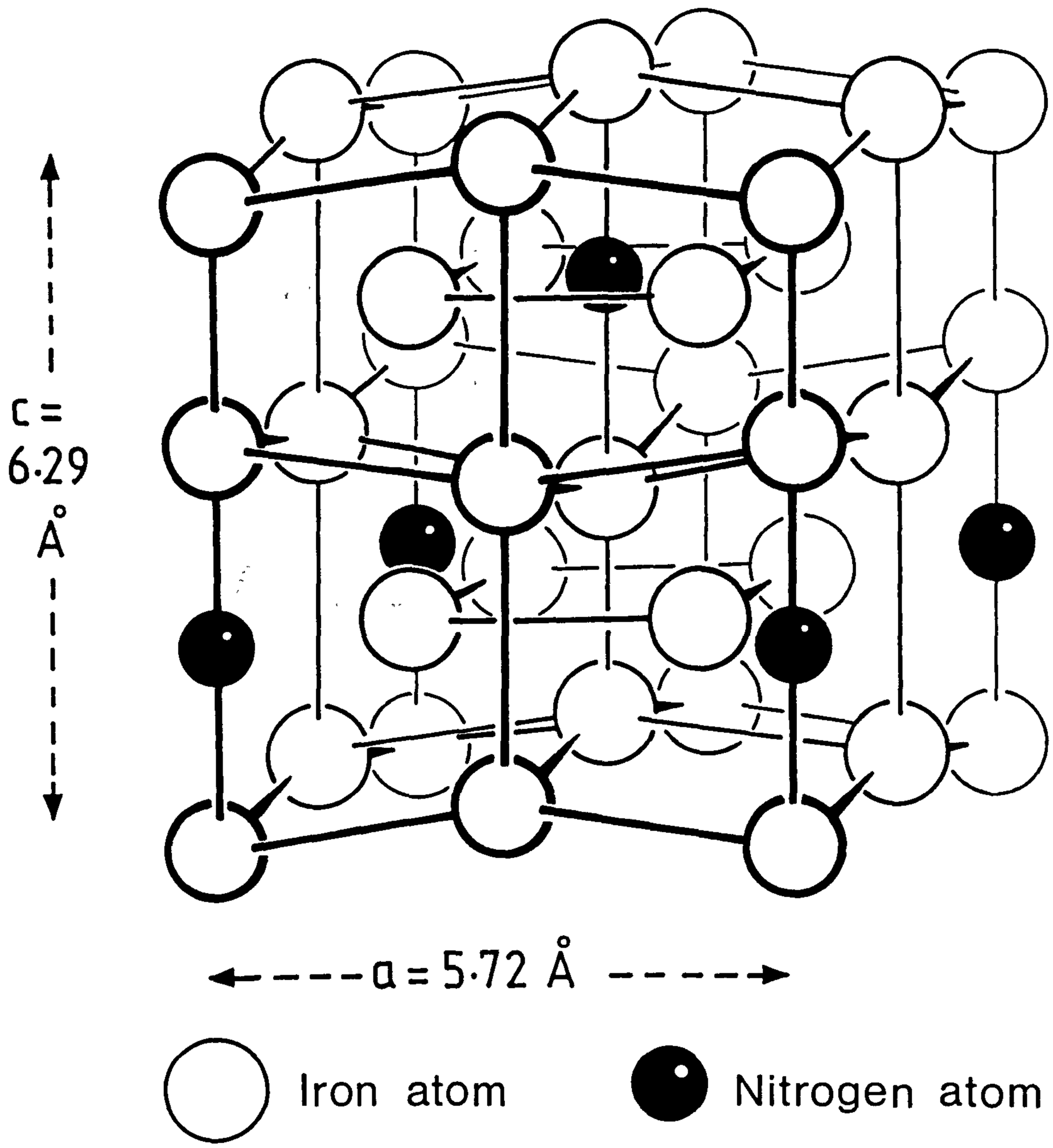

Fig. 1.5 The crystal structure of α''-$Fe_{16}N_2$

● Nitrogen atom

X Unoccupied interstices

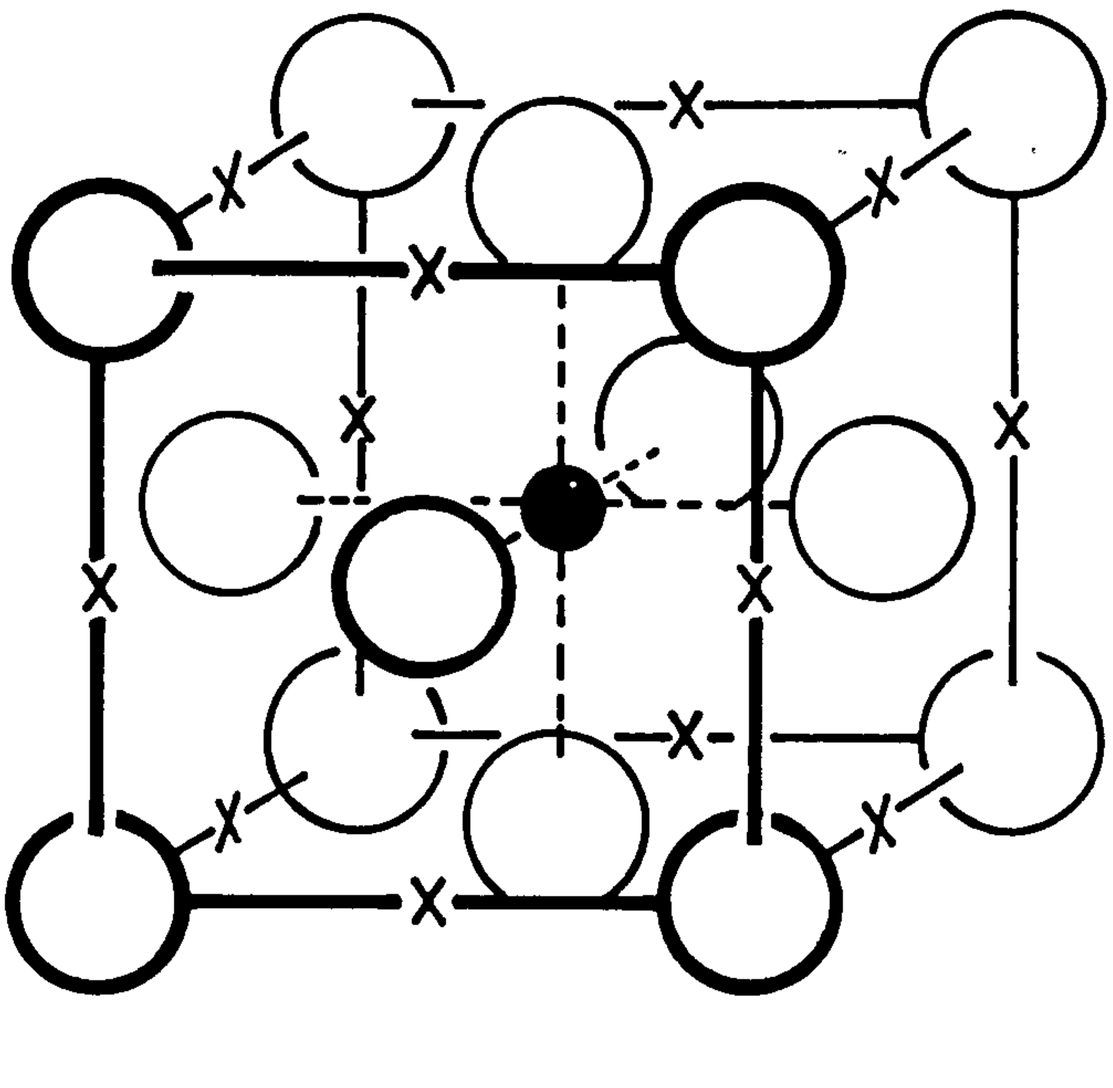

$\gamma'-F_4N$

Fig. 1.6 The crystal structure of γ'-Fe_4N

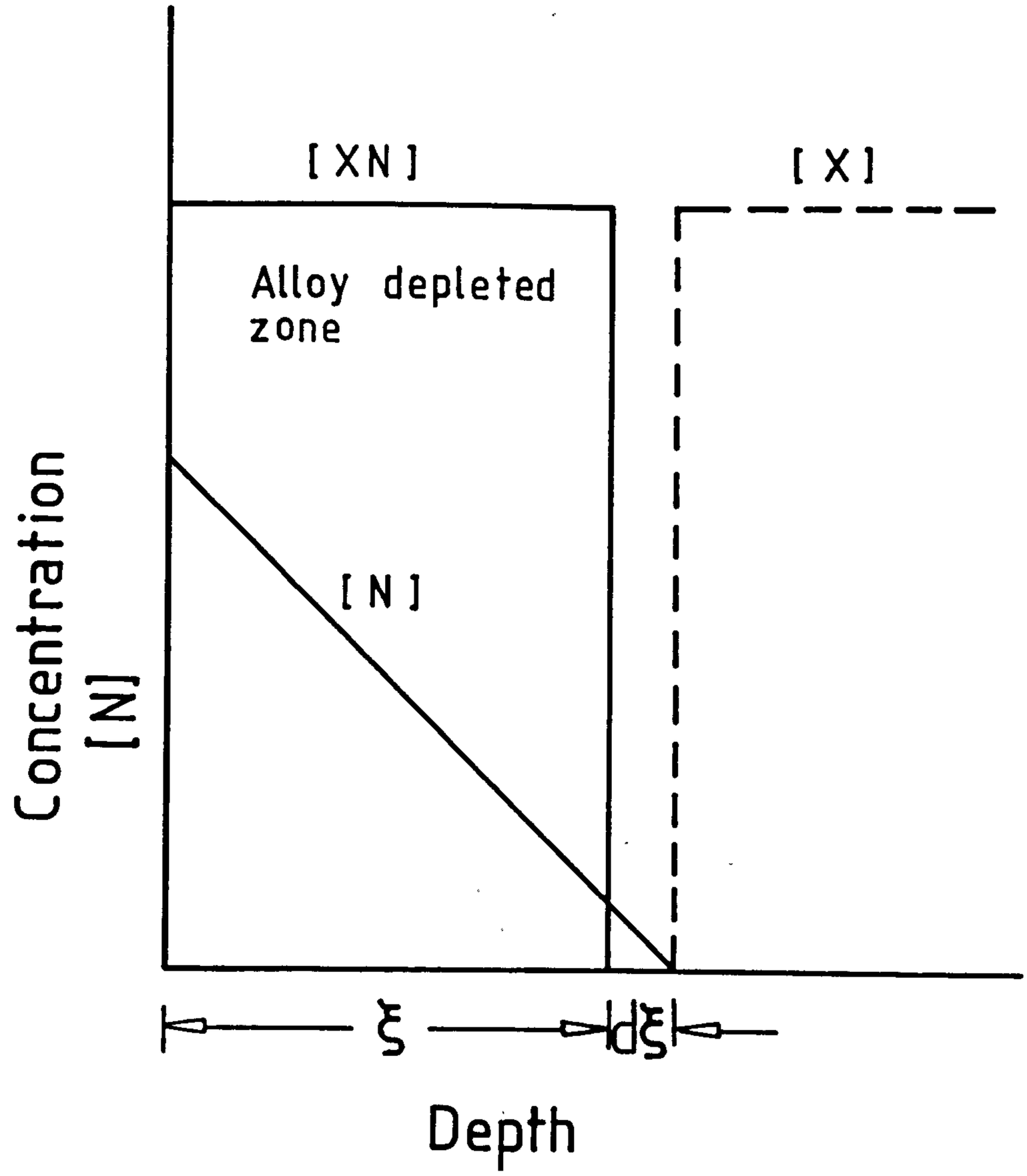

Fig. 1.7 Schematic drawing showing the concentration of nitrogen, alloying element and alloy nitride at a given nitriding time.

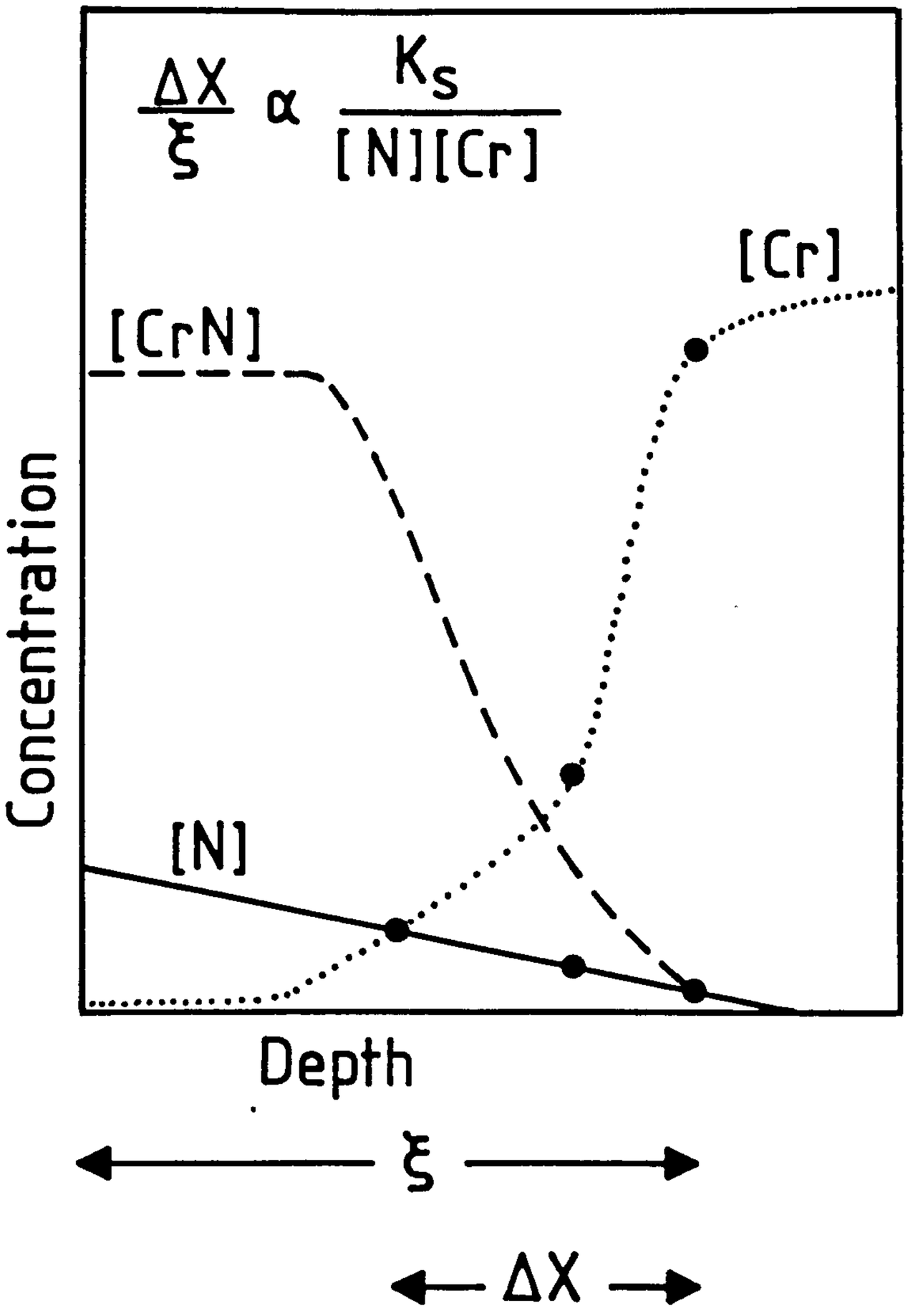

Fig. 1.8 Schematic drawing of the concentrations of CrN, Cr and N. At all points on the curves the product K_s = [wt. % Cr][wt.% N] is constant and non-zero.

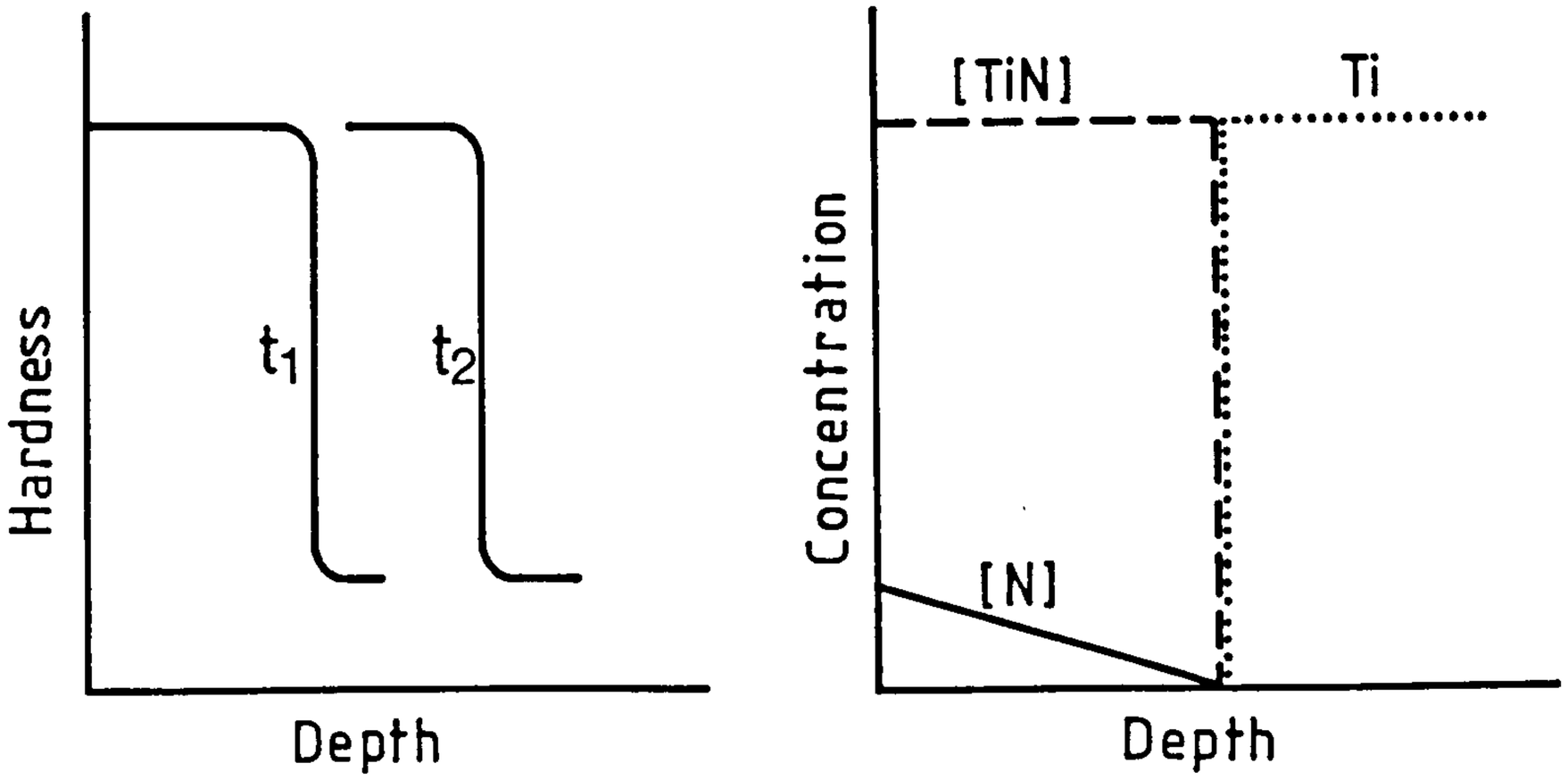

BEHAVIOUR OF A STRONG NITRIDE FORMER

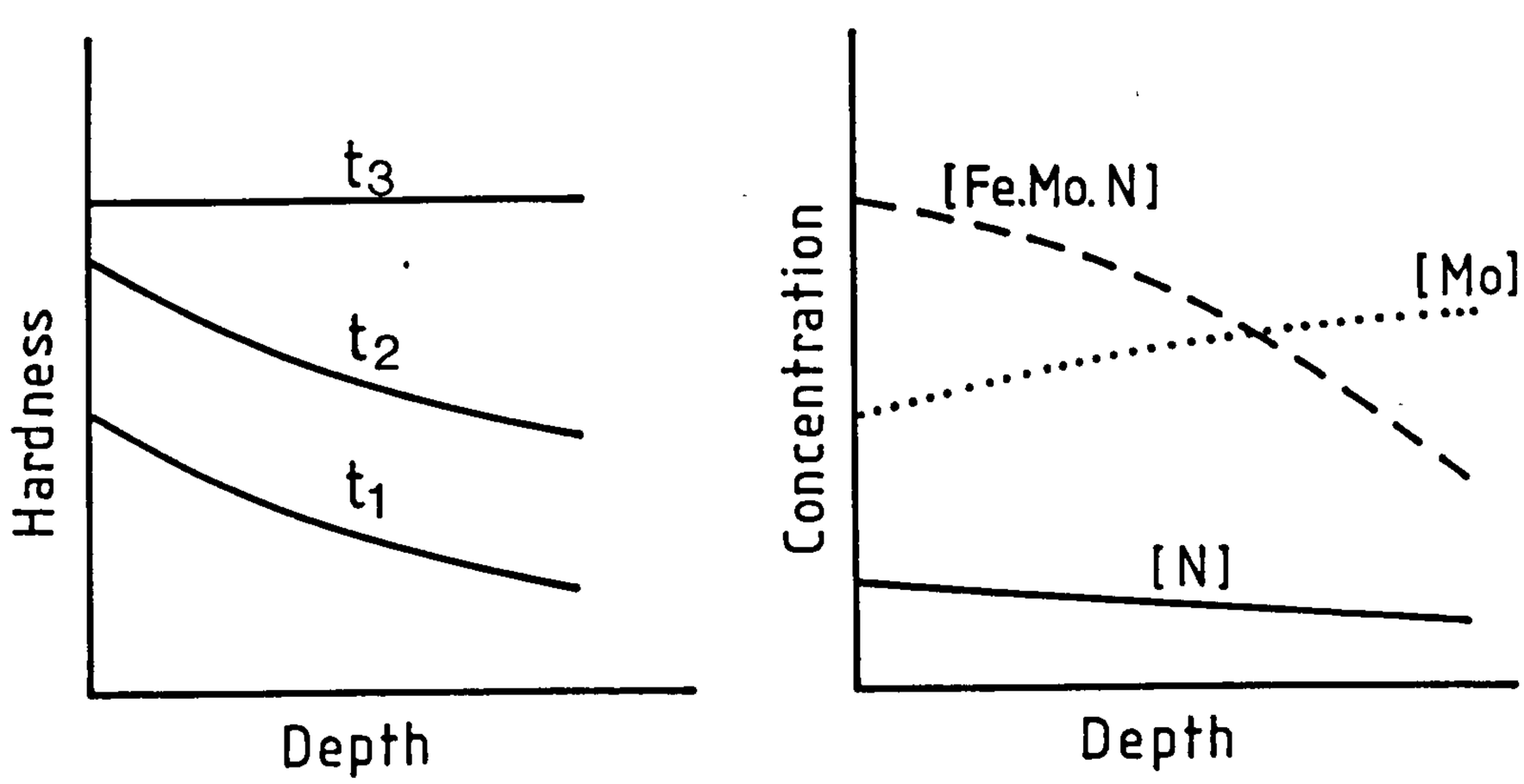

BEHAVIOUR OF A WEAK NITRIDE FORMER

Fig. 1.9 Behaviour of strong and weak interaction

CHAPTER 2

EXPERIMENTAL METHODS

2.1 Material used

A variety of aluminium and chromium - containing steels were used in the present investigations. The materials fell into three different categories, according to their chemical composition; these were:

a) aluminium and chromium-containing steels (En41B and En41A).

b) aluminium-free, chromium-containing steels (En19 and En40B).

c) Chromium-free, aluminium-containing steels (En41(-Cr) and Fe-C-Al). These were supplemented by a binary Iron aluminium alloy containing 0.52% aluminium.

The chemical composition of the above alloys are given in Table 2.1. En41B, En41A, En19 and En40B steels are all of a commercial quality and these were supplied in the form of hot rolled bars. En41(-Cr), Fe-C-Al and Fe-Al are experimental materials used for comparative studies. These were melted by the process of vacuum induction, using high purity iron (Japanese electrolytic iron). They were prepared in the Department of Metallurgy at Leeds University. The reason for making En41(-Cr) and Fe-C-Al steels was in the need to study the role of aluminium in steel without interference from chromium and other alloying elements e.g. silicon, manganese, molybdenum and nickel. Both steels were made to

contain amounts of carbon and aluminium similar to the levels found in commercial En41B.

2.2 Treatment prior to nitriding

To ensure that all the starting material used for nitriding was homogeneous and therefore comparable, a high temperature heat treatment was used prior to tempering. The hot rolled bars, measuring 10-12 mm in diameter, were abrasively cleaned and degreased before encapsulating in fused silica tubes at a vacuum of 10^{-3} torr. Before final sealing, the silica tube was repeatedly flushed with argon and evacuated to reduce the oxygen to the minimum. The encapsulated bars were then heat treated at 1200°C for 24 h. This heat treatment was sufficient to remove all the bands that originated from the segregation during ingot solidification. These bars were then further hot rolled to a thickness of approximately 6 mm. After grinding off the scale and the decarburised layer, rectangular specimens of approximately 8 × 15 mm were cut from these rolled strips. The specimens were then abrasively cleaned and degreased before encapsulating in an evacuated fused silica tube. After austentizing for 0.5 h at 900°C in the silica tube the specimens were hardened by quenching in oil. This was done by breaking the silica tube during quenching. The quenched specimens were tempered at the required temperature and time, then cooled in air.

Before nitriding, all specimens were abraded with silicon carbide paper to 600 mesh then degreased and thoroughly washed in alcohol.

2.3 Nitriding apparatus

The nitriding apparatus consisted of two main parts; one containing the gas flowmeters and gas purification train, and the other the furnace containing the reaction tube. A line diagram of the apparatus is shown in Fig. 2.1.

Anhydrous ammonia, high purity hydrogen and nitrogen were supplied from cylinders. Their respective flow rates were controlled by constant pressure head capillary flowmeters (49). A schematic diagram of the flowmeter used is shown in Fig. 2.2. It consists of a manometer, capillary tube and bleeder. The flow rates of each flow meter were calibrated in terms of the pressure differences across the capillary, as measured by the manometer. Calibration was made by measuring the rate of ascent of a soap bubble in a graduated glass tube of a uniform cross section at different pressures across the capillary tube. From these readings, a calibration curve for each capillary flowmeter was drawn, showing the relationship between the pressure difference across the capillary as measured by the manometer and the flow rates of each individual gas. Control of the flow rate was obtained by altering the head of oil in the bleeder tubes. Thus the actual flow rate of the gas was found from the manometer pressure difference and flowmeter curve. Two different capillary tubes were calibrated for each gas, one for high flow rates and the other for low flow rates, thus providing a wider range of NH_3/H_2 gas mixtures for nitriding experiments. Throughout the investigation a total gas flow rate of approximately 500 cm^3/min was maintained, given a linear flow across the specimens of 100 cm/min. Vacuum pump oil was used in the manometers and

bubblers because of its low vapour pressure and comparative inertness to hydrogen and ammonia.

Before entering the reaction tube, the gases were purified by standard methods (50). Hydrogen was first passed over a heated bed of activated copper catalyst which was pre-reduced in hydrogen for several days at 140°C and maintained at 100°C during use. The purpose of the activated copper was to remove the oxygen from the hydrogen. After this treatment, the hydrogen was dried by passing over silica gel, molecular sieve and phosphorous pentoxide successively. Ammonia was dried by passing it over potassium hydroxide pellets. The purified gases were first mixed in a mixing manifold then passed through a column containing glass beads before entering the reaction tube. The exhaust gases were expelled via a bubbler which again contained vacuum pump oil.

A rotary pump and mercury manometer were connected to the mixing manifold so that air in the reaction tube could be exhausted prior to a nitriding run, and any gas leaks could be detected. Two nitriding furnaces were connected to the mixing column, one with a horizontal reaction-tube arrangement which was used for general purpose specimens, and anothdr, with a vertical reaction-tube arrangement was used for fatigue specimens. Recrystallised alumina work tubes were used in both furnaces.

In the horizontal furnace, the specimen holder was a silica glass boat connected to a silica rod. A cylindrical piece of iron was connected to the other end of the rod so that the specimen holder could be slid in and out of the furnace by means of a magnet, while the system was sealed.

Details of the horizontal furnace are shown in Fig. 2.3.

The specimen loading procedure was as follows: first the specimens were placed in the boat which was then kept in the cold zone of the reaction tube. The system was then sealed, evacuated and filled with nitrogen. After flushing the reaction tube several times with nitrogen, the required mixture of ammonia and hydrogen was then admitted and allowed to flow for half an hour to purge any nitrogen. The boat and the specimens were then moved into the hot reaction zone by means of a magnet. After nitriding for a predetermined period, the boat together with the specimens were withdrawn to the cold zone (which was cooled by a water cooling coil), and were then removed from the apparatus after the nitriding gases had been flushed out with nitrogen.

As mentioned before, the vertical furnace was used for nitriding fatigue specimens. The furnace was basically the same as the horizontal one, but some minor changes were made to cope with a different type of specimen holder. This consisted of a smooth iron rod linked to a second detachable iron rod, smaller in cross section than the first, which had a cross-shaped iron piece attached on to the other end. At each tip of the cross a hole was made so that a total of four specimens could be suspended and nitrided at the same time. Unlike the horizontal furnace, the specimens were lowered by hand into the hot zone while the system was sealed; thus greater control on specimen movement was achieved. Details of the vertical furnace and the specimen holder are shown in Fig. 2.4. The temperature, in both furnaces, was controlled to $\pm$ 3^{o}C by Eurotherm proportional controllers using a Pt-Rt/Rh

thermocouple near the furnace resistance winding. The temperature at the reaction-zone was measured by a chromel-alumel thermocouple situated inside the reaction tube and protected by a silica sheath.

2.4 Metallographic techniques

2.4.1 Optical microscopy and microhardness testing

The nitrided specimens were first ground to a depth of 2-2.5 mm, which is beyond the nitrided case, so that the case and the core were clearly revealed in cross-section. The specimens were then mounted in a bakelite mounting compound at a temperature of 150^{o}C in a Struers mounting press. These were polished by various grades of wet silicon carbide paper to 600 mesh. Final polishing was carried out on a series of rotating wheels (containing diamond paste) up to 0.5 micron. Before microhardness testing, the specimens were lightly etched in 2% Nital. Microhardness measurements were carried out using a standard Reichert microhardness attachment with a 50 g load being used throughout. At the same time the depth of each hardness reading was measured using a micrometer eyepiece fitted to the Reichert microscope.

Optical photomicrography was carried out using a Vickers M41 photoplan microscope. The mounted and polished nitrided specimens were etched in different solutions to reveal the various zones of the nitrided layer. The white layer and the nitrided layer were revealed by etching in 2% nital. The grain boundary phase and the carbide concentration

under the white layer were revealed by etching in ferricyanide solution. The carbon-rich layer at the case/core interface was revealed by etching in oberhoffer's reagent, see Table 2.2.

2.4.2 Scanning electron microscopy

Scanning electron microscopy was used to examine the microstructure of the white layer, and the fracture surfaces of the fatigue specimens. The majority of the work was carried out using a Cambridge S600 S.E.M., but a Hitachi S700 field emission S.E.M. was also used.

The nitrided specimens were prepared as for optical microscopy. These were deeply etched in nital and thoroughly washed in alcohol. The specimens were then coated with a thin layer of carbon using a carbon evaporation unit, thus making the specimens conduct electrically to prevent charging effects in the microscope.

The broken fatigue specimens were sputter coated with gold-palladium to protect the fracture surface from the atmosphere. These were then mounted on standard aluminium stubs using a conducting glue.

2.4.3 Transmission electron microscopy

The larger share of the microstructural investigation was made by T.E.M. The high resolution of these microscopes allowed the very fine scale precipitation to be resolved and identified.

The investigation was carried out using Philips EM300, 100 KV and Jeol 120CX electron microscopes. Thin foils and

carbon replicas of both tempered and nitrided spceimens were examined using these microscopes.

2.4.3.1 Thin foil preparation

The materials were first rolled to strips of 100-150μm thick, then cut in to smaller strips of 15 x 25 mm. These were encapsulated in evacuated fused silica tubes then quenched from 900°C and tempered at 600°C for 1 h (these are the standard heat treatment conditions, used in the present work, before nitriding thin specimens). After nitriding, the specimens were chemically thinned to approximately 15 microns in a solution containing 2% hydrofluoric acid (40%), 49% hydrogen peroxide (100 vols.) and 49% distilled water. Final polishing was carried out in a constantly agitated chromic-acetic acid electrolyte, using an improved window technique (51). This method was found to be the most practical as it works at a relatively moderate temperature (15-25°C), and consistently produced large areas of electron transparent material. A schematic representation of the electropolishing equipment is shown in Fig. 2.5. The details of the thin foil preparation and conditions for electropolishing are given in table 2.3.

2.4.3.2 Extraction carbon replica

Two techniques were used for the preparation of extraction carbon replicas.

2.4.3.2(a) Direct-extraction replicas

Extraction replicas were produced from optical microscopy specimens. These were etched in 2% nital then thoroughly washed in alcohol and dried in hot air. The specimens were then immediately coated with a thin film of carbon, using a carbon evaporation unit. The carbon film was then scratched by a scalpel blade into small squares approximately 1.5 x 1.5 mm. Extraction was achieved by immersing the specimens in a solution of 5% nital.

2.4.3.2(b) Two-stage extraction replicas

This particular technique was used on the nitrided specimens to avoid the decomposition of aluminium nitride in nital. According to previous work (52), aluminium nitride decomposes in water as well as in acidic and alkaline solutions. However, the method used in the present work gave satisfactory results, in which aluminium nitride was successfully extracted.

The nitrided specimens were mounted and metallographically polished. Using the potentiostatic etching method described in section 2.5, the specimens were etched for approximately 15 seconds in a solution containing 10% acetyl acetone, 1% tetramethylammonium chloride in methanol. After etching, the specimens were carefully rinsed in alcohol and left to dry. A thin cellulose acetate film was softened in acetone and then laid on the etched specimen. This was then left to dry and harden. When hard the film was peeled off the specimen, attached to a glass slide and then coated with

carbon. Selected sections were cut from the film. These were positioned on copper grids and placed above a boiling acetone bath for 30 minutes. The acetone vapour dissolves the cellulose acetate film to leave the extracted particles attached to the carbon film.

2.5 Precipitate extraction for x-ray analysis

A potentiostatic electrolytic extraction method was used to isolate the carbides and nitrides from the matrix. This method has been used for the isolation of carbides in steels (53). The circuit diagram of the apparatus used is shown in Fig. 2.6. The specimens used were first polished using an emery paper and thoroughly washed in methanol by means of an ultrasonic washer. These were hung in the electrolytic cell. The electrolyte was 10% acetyl acetone, 1% tetramethylammonium chloride in methanol. The matrix dissolution was carried out under an anodic potential of ∿ 100 mV vs S.C.E. Once the sample was totally dissolved or sufficient precipitates were available, the precipitates were then isolated from the solution using a centrifuge. They were washed in alcohol and centrifuged again. This process was repeated several times to clean the precipitates. Finally, the precipitate suspension was poured into a glass dish and left for the residual methanol to evaporate. The precipitates were then collected and used to prepare specimens for X-ray diffraction and for X-ray microanalysis.

Another solution was also used for the extraction of nitrides. Chromium nitride and aluminium nitrides were both successfully extracted in a 2% H_3PO_4 aqueous solution (52). But this method had several disadvantages. Micro-chemical X-ray analysis results showed that the extracted particles were contaminated with phosphorous even though the precipitates had been twice diluted with water and centrifuged. When diluted with water, the fine particles tended to stay in suspension and the very fine ones tended to float on the water surface. This mainly occurred with aluminium nitride. As a result, part of the extracted precipitates were lost. Furthermore the extracts could not be washed with methanol because the latter reacted with the electrolytic solution and produced a solid white substance which contaminated the precipitates.

2.6 X-ray diffraction

The extracted particles were used to prepare wire-shaped specimens for insertion in a Debye-Scherrer X-ray camera which was used throughout the investigation. FeK_α and CuK_α radiation were both used.

2.7 Micro-chemical X-ray analysis

The extracted particles of each material were chemically analysed by using the microanalysis attachment on the Cambridge S600 scanning electron microscope. Analysis was carried out at 15 kV for 100 seconds, with a working distance of 15 mm throughout.

2.8 Fatigue testing

Fatigue tests were carried out using a Wohler rotating bend machine at a speed of 2800 r.p.m., using Rolls Royce-type unnotched test specimens.

The specimens were machined from bars 10mm in diameter. The bars were first quenched from 900^{o}C and then tempered at 600^{o}C for 1 h. The dimensions of the fatigue specimens and a schematic diagram of the fatigue test machine are shown in Fig. 2.7 and Fig. 2.8 respectively.

Table 2.1

Chemical compositions of the alloys investigated

Alloy	Composition in wt%									
	C	Cr	Al	Mo	Ni	V	Si	Mn	S*	P*
En41B	0.46	1.6	0.85	0.30	0.40	-	0.40	0.6	0.05	0.05
En41A	0.33	1.65	1.04	0.20	0.39	-	0.30	0.59	0.05	0.05
En19	0.37	1.03	-	-	0.23	0.02	0.1 - 0.35*	0.5 - 0.8*	0.05	0.05
En40B	0.26	2.88	-	0.53	0.40	0.06	0.1 - 0.35*	0.4 - 0.65*	0.05	0.05
En41(-Cr)	0.39	-	1.15	0.35	0.40	-	0.46	0.40		
Fe-C-Al	0.46	-	1.0							
Fe-Al			0.52							

* Specifications only, no analysis obtained

Reagent	Etching conditions
<u>Nital</u> 2 ml nitric acid, 98 ml ethyl alcohol	5 - 8 S at room temperature
<u>Ferricyanide solution</u> 1 to 4 gm potassium ferricyanide, 10g potassium hydroxide, 100 ml distilled water	60 S in boiling solution
<u>Oberhoffer's reagent</u> 1 g cupric chloride, 30 g ferric chloride, 0.5 g stanneous chloride, 50 ml HCl, 500 ml distilled water, 500 ml ethyl alcohol	5 - 8 S at room temperature

<u>Table 2.2</u>

List of the etching reagent used and the etching conditions

strips of 100-150 μm thick cut into 25 × 15mm

↓

Chemically thined to ~ 15 μm in a solution containing

2% HF (40% vol.)

49% H_2O_2 (100% vol.)

49% distilled water

↓

electro polished in a chromic-acetic electrolyte containing 60 g chromic acid, 10 ml distilled water and 250 ml acetic acid, at 15-25°C and a potential of 24V.

↓

Thoroughly washed in methanol and then in glycerol. Wash in methanol before use

Table 2.3

Details of thin foil preparation for transmission electron microscopy

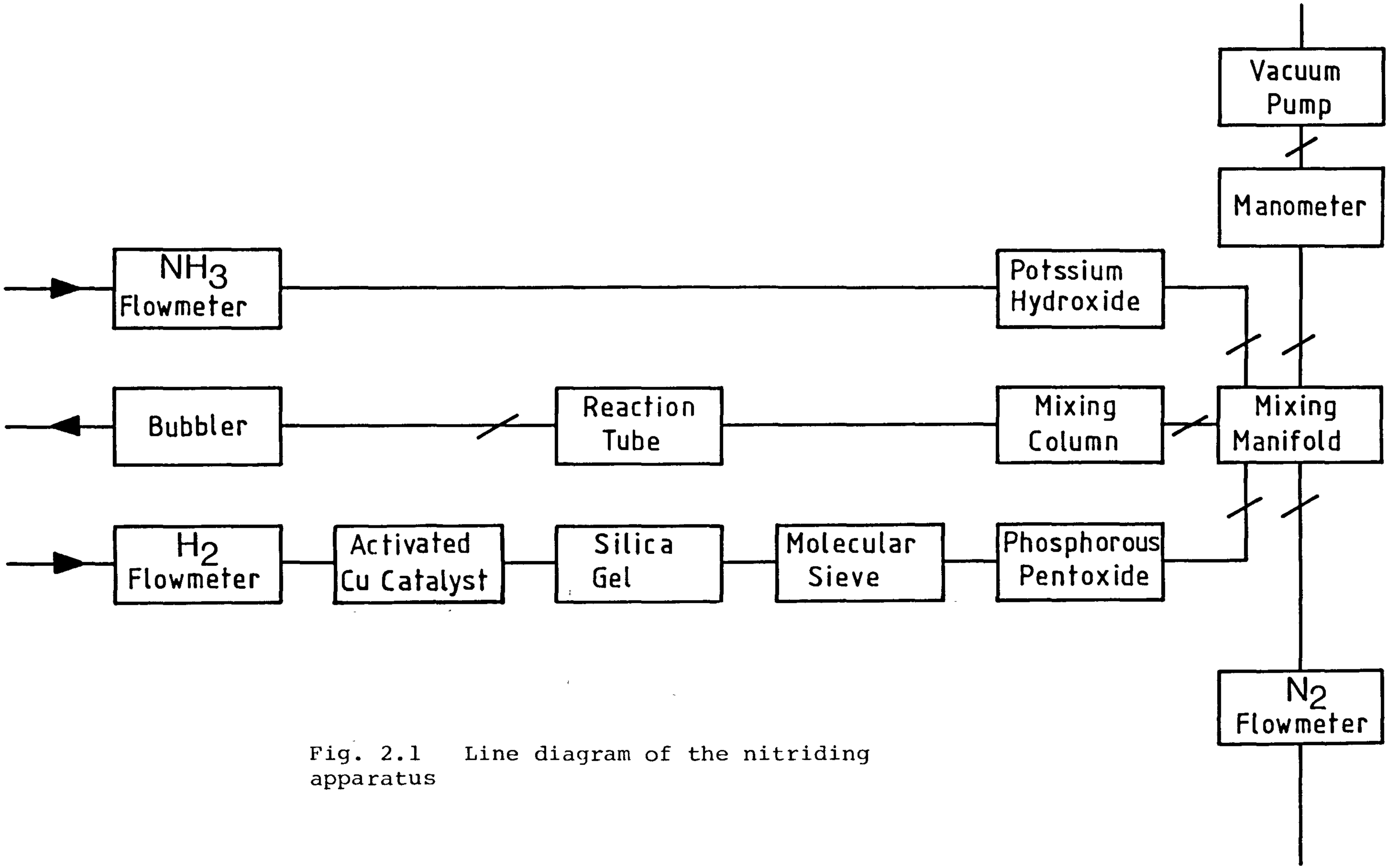

Fig. 2.1 Line diagram of the nitriding apparatus

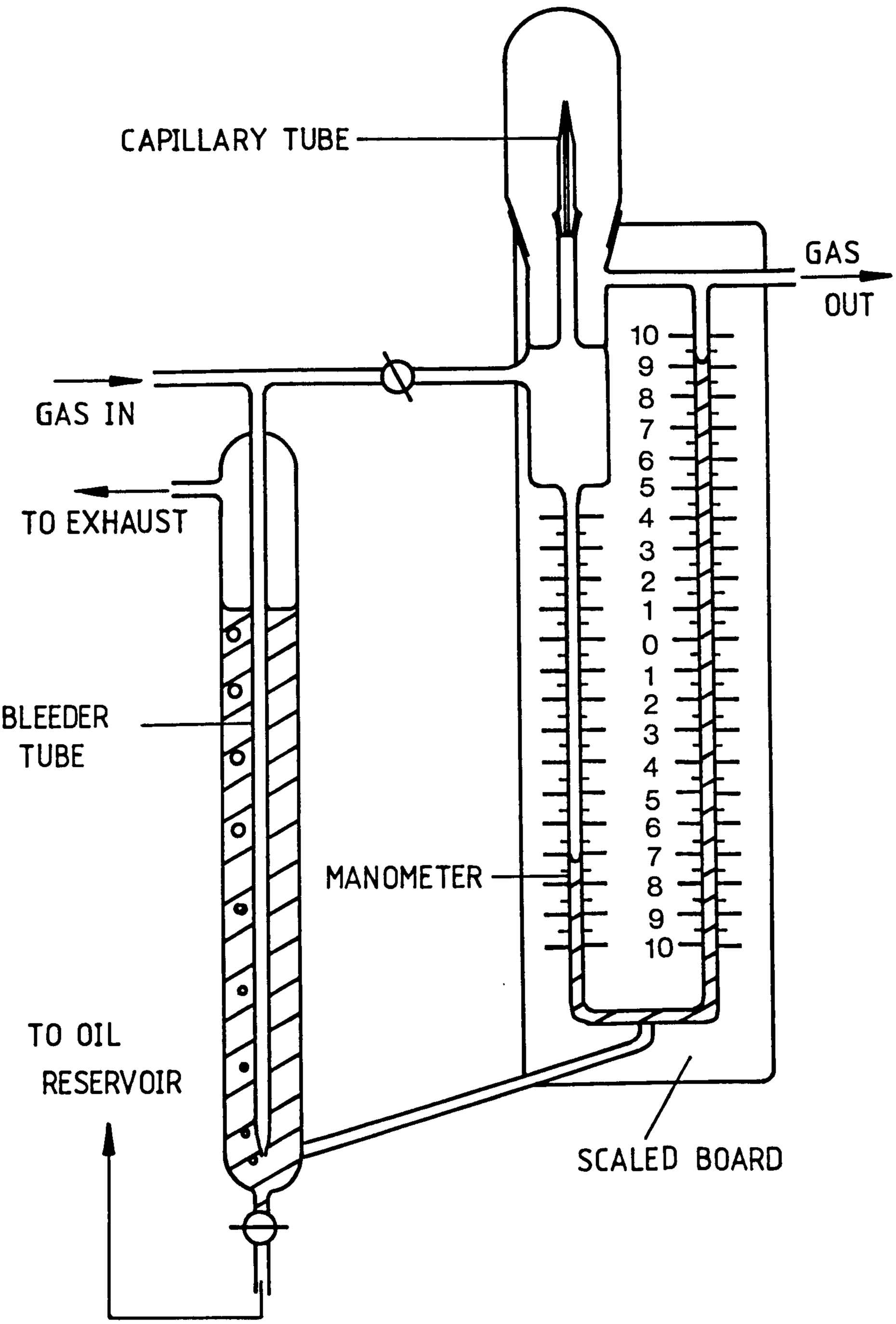

Fig. 2.2 Schematic drawing of the constant pressure head capillary flowmeter

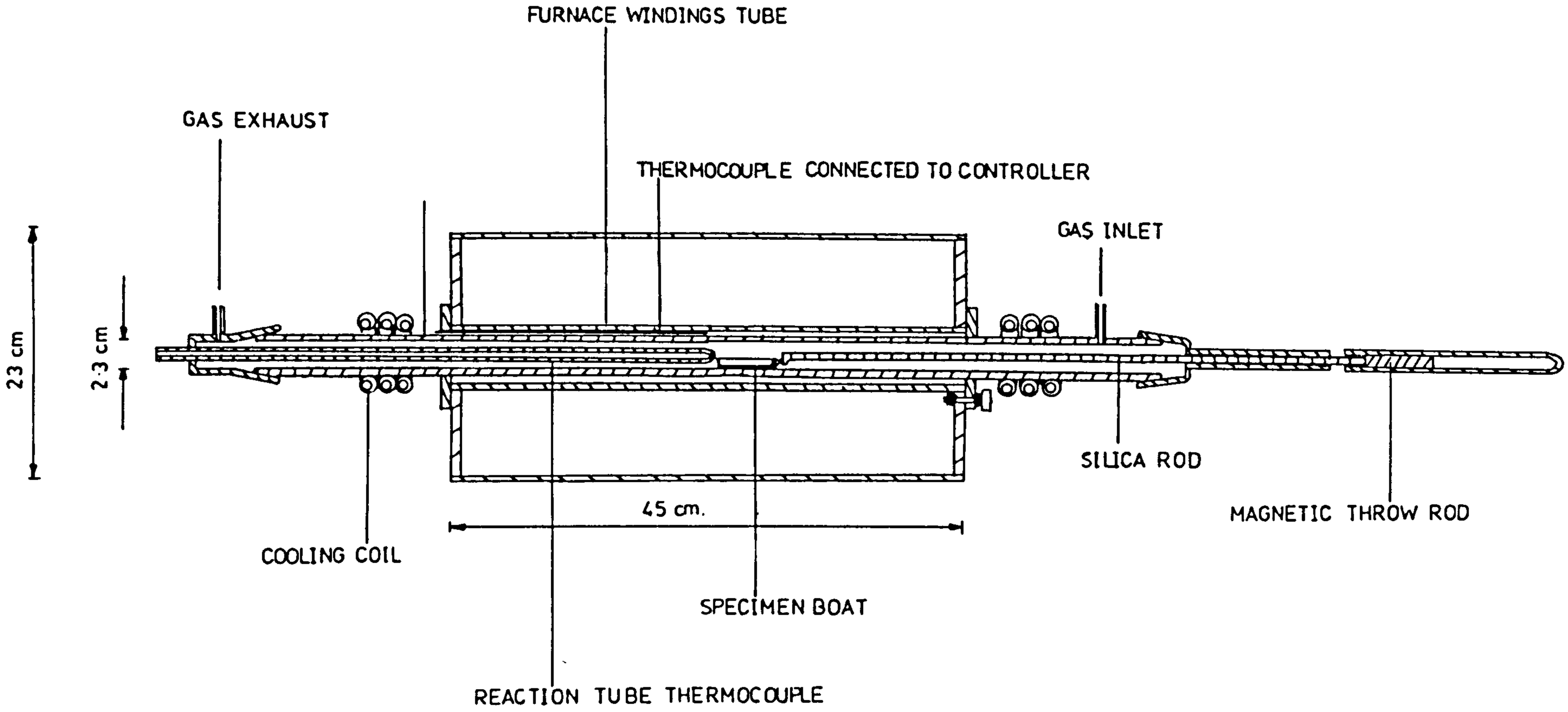

Fig.(2·3) Schematic diagram of the horizontal nitriding furnace

Fig. 2.4

Schematic drawing showing details of the vertical furnace and the cross-shaped specimens holder

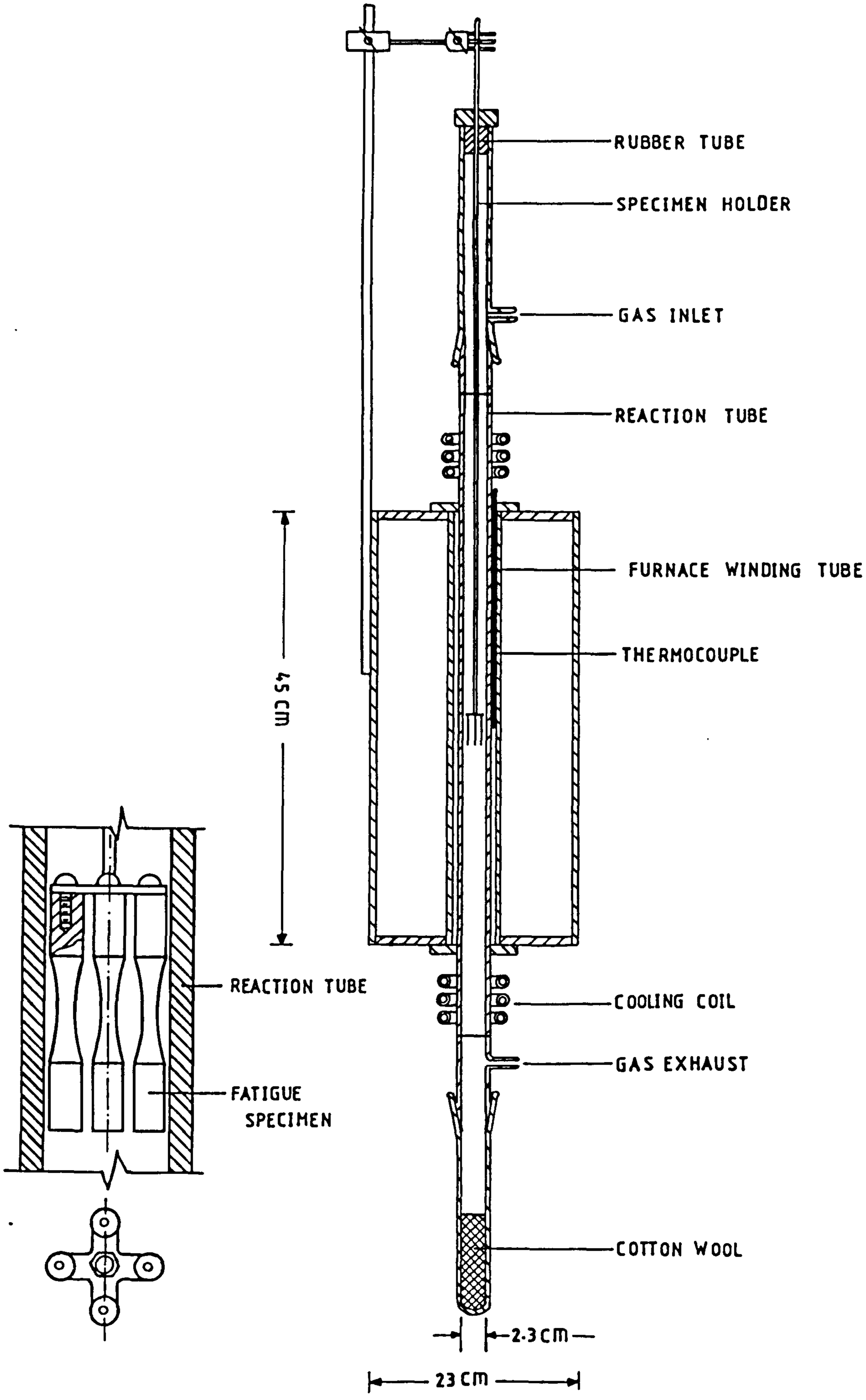
RUBBER TUBE
SPECIMEN HOLDER
GAS INLET
REACTION TUBE
FURNACE WINDING TUBE
THERMOCOUPLE
45 cm
REACTION TUBE
FATIGUE SPECIMEN
COOLING COIL
GAS EXHAUST
COTTON WOOL
2.3 cm
23 cm

Fig. 2.5 Schematic presentation of the electro-polishing apparatus used to prepare thin foils

(a) Side view

1 - Spacer block cum safety support-one (stainless steel).

2 - Cylindrical clamp (three are identical)

3 - Clamping screw for fore electrode/ specimen holder

4 - Cathode holder laquered at shaded area

5 - Properly aligned serrated stainless steel (0.5 mm sheet) cathode.

6 - Thin foil specimen (laquered at edges); holder moved by d/2 up or down every 15 minutes

7 - Electrolyte

8 - Magnetically stirring capsule

(b) Top view

9 - Bakelite or insulating frame (one pair)

10- Electrical connection with insulated wire

11- Washer for electrical connection

12- Clamping bolts for main support frame

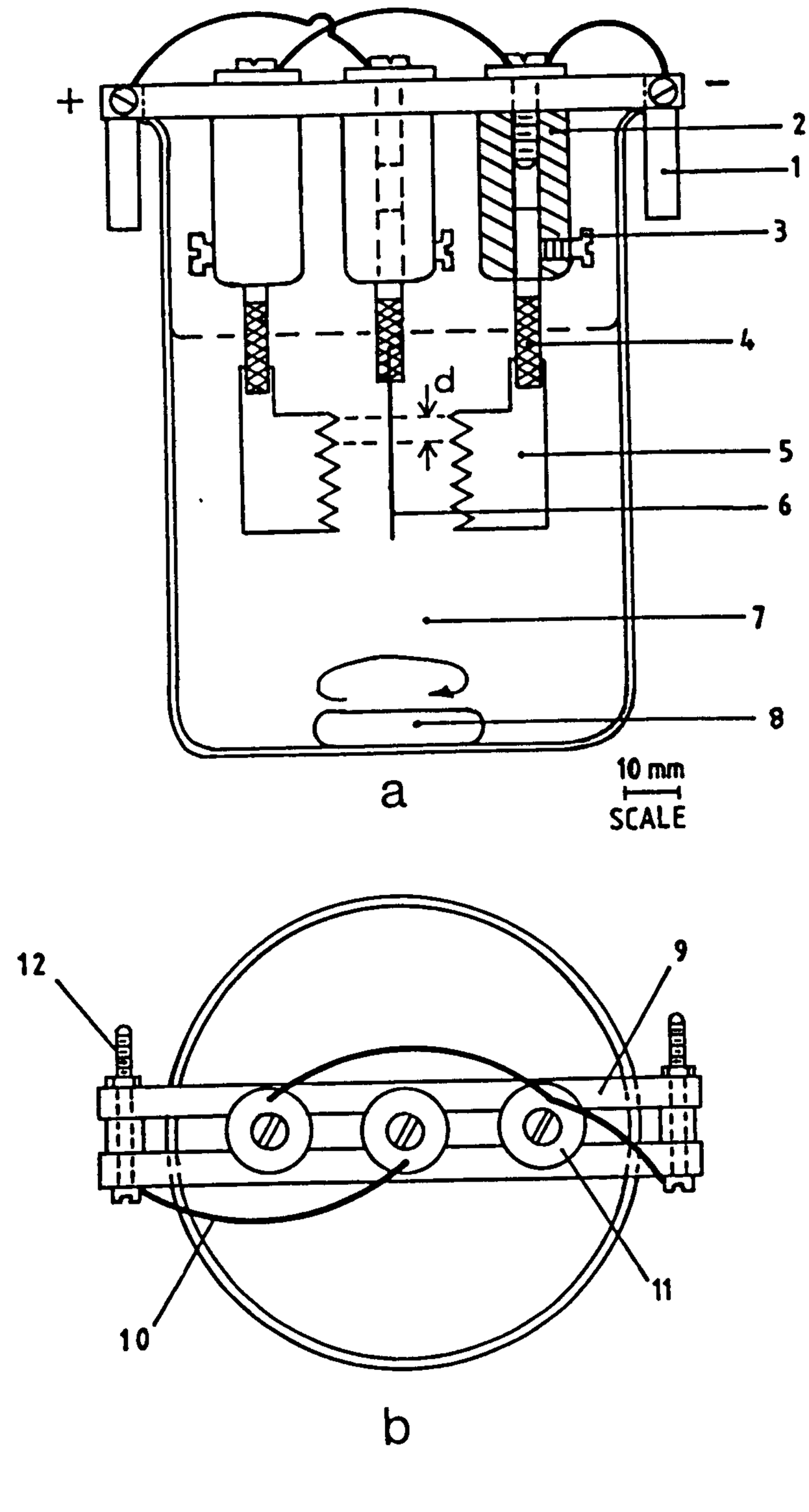

FIG.(2.5)

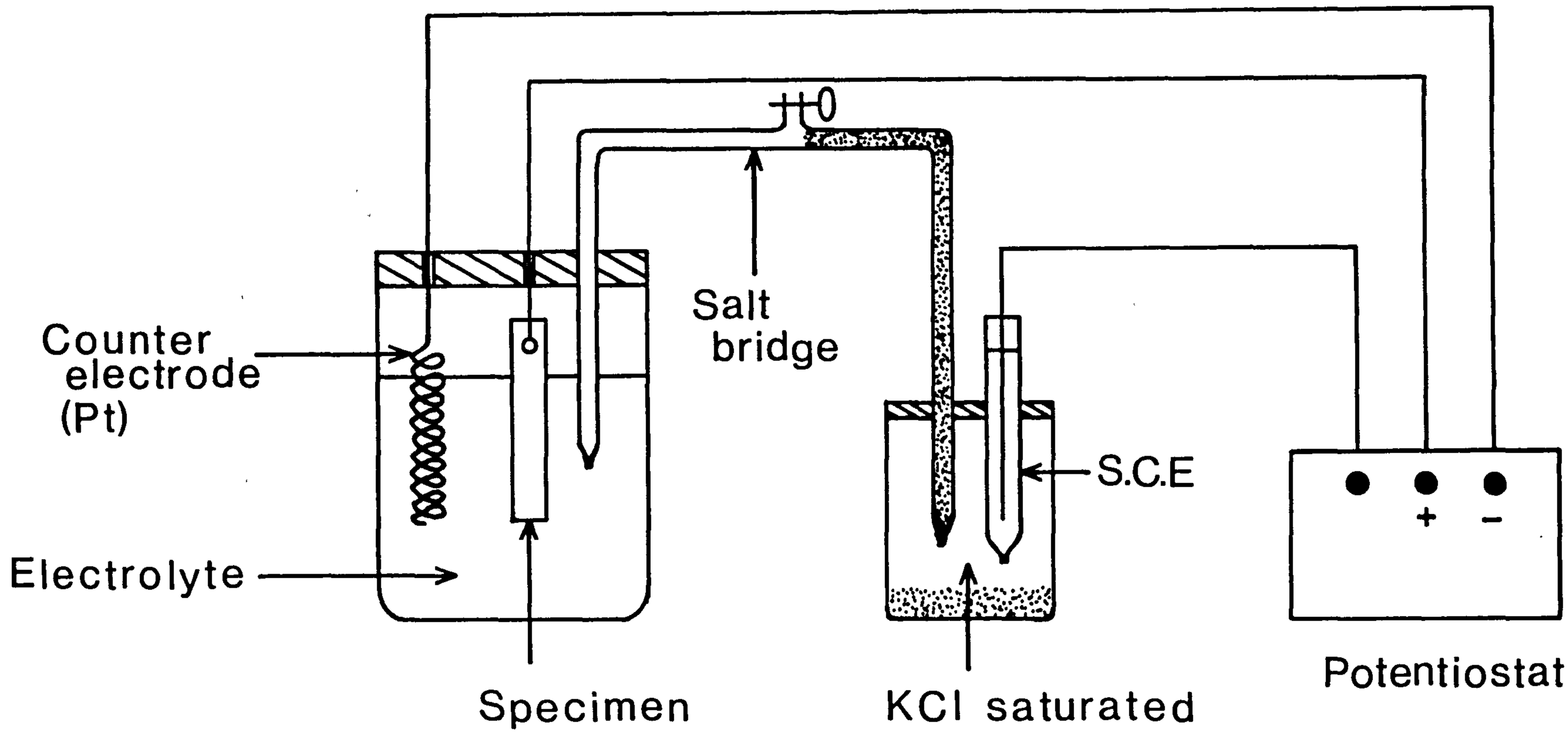

Fig. 2.6 Circuit diagram of the apparatus used to extract nitrides and carbides from steel (51)

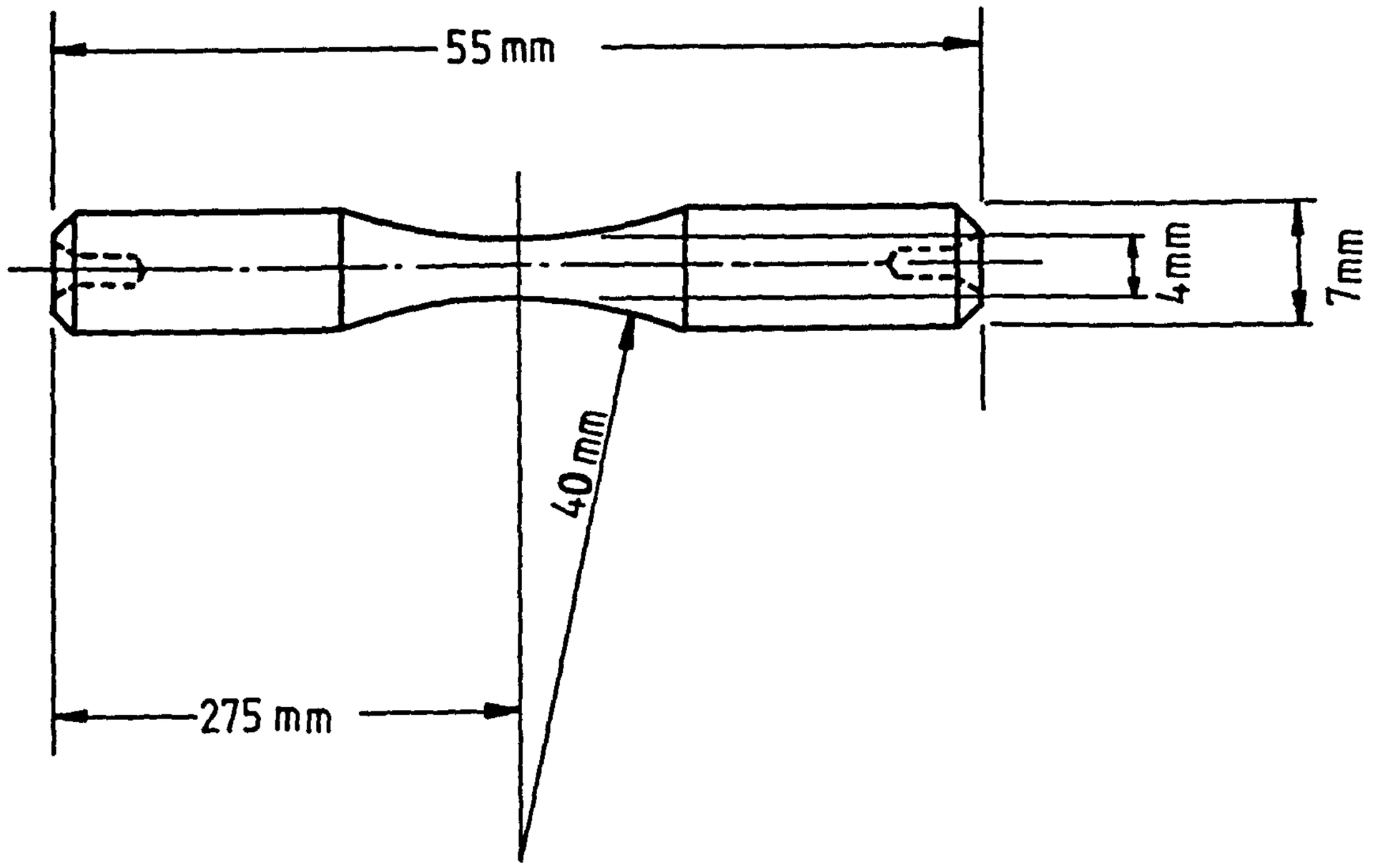

FIG. (2·7) ROLLS ROYCE TYPE FATIGUE SPECIMEN

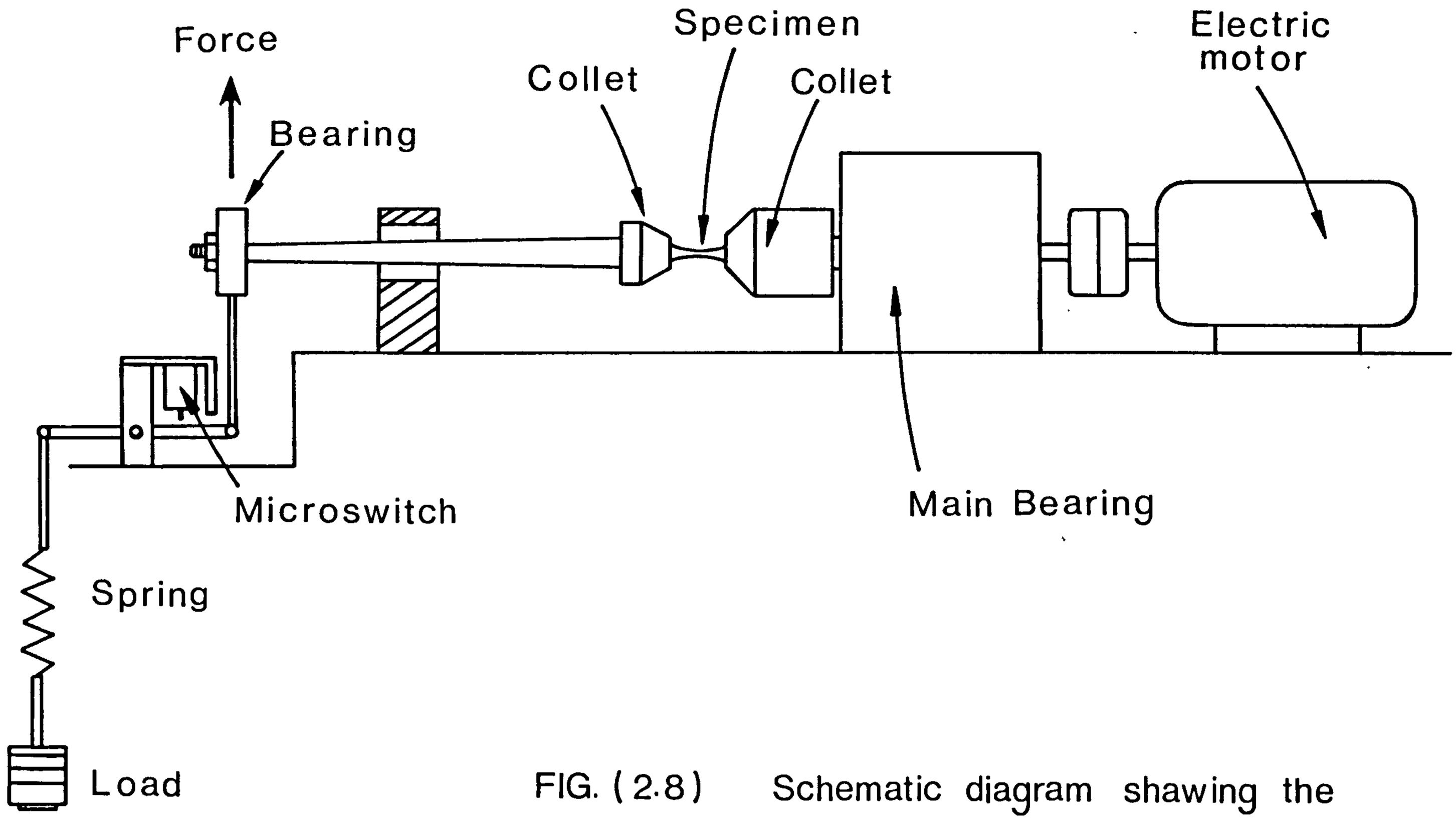

FIG. (2.8) Schematic diagram shawing the fatigue-testing machine

CHAPTER 3

TEMPERING CHARACTERISTICS OF ALUMINIUM CONTAINING STEELS

3.1 Introduction

Previous work carried out on chromium-containing steels has shown that the hardness and depth of the nitrided case is influenced by the steel heat treatment prior to nitriding. Using 1-3% chromium-molybdenum steels, Hodgson and Waring (54) reported that the nitrided surface hardness showed a progressive decrease with increasing tempering within the range 500-700^{o}C. Hodgson and Baron (55) using steels of the En40 type, and subsequently Kunze (56), concluded that the maximum nitriding case hardness and the case depth tend to decrease when the previous tempering time or temperature is increased. Barker and Smith (57) using En19C steel (1% Cr-Mo) came to a similar conclusion and also stated, in agreement with Hodgson and Baron (55), that in general the nitrided surface hardness will be largely dependent on the initial hardness of the tempered steel.

This dependence of the maximum case hardness on pre-nitriding treatment is due to the incorporation of the nitride-forming elements in the carbides formed on tempering. Because elements like chromium are strong carbide formers, the amount of alloying element left as a solid solution in the matrix, and hence available to react with nitrogen, will be reduced as treatment time and temperature increase. However, for aluminium-containing steels this argument cannot apply, since

aluminium is not a carbide forming element, and will not segregate to the carbides. Thus the pre-nitriding tempering treatment should not affect the concentration of aluminium in the ferrite matrix, and hence the nitriding response.

En41B contains both chromium and aluminium plus other alloying elements e.g. silicon, manganese and molybdenum. The combination of carbide and non-carbide forming elements in this steel made it necessary to investigate its tempering behaviour, in particular the degree of segregation of nitride-forming elements to the carbides. No investigation of the detailed tempering behaviour of "Nitralloy" En41 type steel has been found in the literature.

In the present work, commercial En41B and En19 plus certain other aluminium-containing steels, shown in table 2.1, were investigated in the quenched and tempered condition. Different temperatures and times were used, and tempered products were investigated in terms of hardness, microstructure, and composition.

3.2 Influence of tempering temperature and time on hardness

3.2.1 Materials Used

The majority of the work was carried on En41B and En19 steels. The aluminium-free En19 steel was chosen because its content of carbon and other alloying elements closely resembles that of En41B steel. Some work was also carried out on Fe-C-Al, En41(-Cr) and En41A, as they were useful in clarifying the effect of alloying elements and carbon content

on the hardness and microstructure of the tempered steel, as well as the characteristics of the nitrided steel.

3.22 Experimental methods

Disc shaped specimens 6 mm in thickness were cut from a bar 10-12 mm in diameter, which had first been homogenised at 1200°C for 24h. The homogenisation treatment was carried out under argon atmosphere, in a partially evacuated and sealed fused silica tube, to avoid oxidation and decarburisation. The specimens were austenitized for 0.5h at 900°C and subsequently hardened by quenching in oil at room temperature to produce a martensitic structure.

Five tempering temperatures were employed within the range 500-700°C, with increments of 50°C, and six tempering times were used: 0.5, 1, 2, 8, 32 and 128 h.
All tempering treatments were carried out in a resistance wound furnace and the specimens were left to be air-cooled after tempering. The opposite flat sides of the disc-shaped specimens were ground to remove the decarburized layer and to get the two sides exactly parallel, after which they were metallographically polished. Hardness readings were taken using a Vickers hardness tester and a 30 kg load throughout. At least three hardness measurements were made on each specimen in order to obtain an average hardness.

3.2.3 Experimental results

The relationships between hardness, tempering time and temperature are represented graphically. With three

independent variables i.e. time, temperature and alloying elements, the results can be represented in different ways. Figs. 3.1 and 3.2 are the isochronal tempering curves for En41B and En19 respectively, and they illustrate the effect of tempering temperature on hardness at different times. The overall level of hardness is higher in En41B than in En19, but the drop in hardness especially in the temperature range 500-600^{o}C is greater in En41B and the curves are steeper than those of En19.

Figs. 3.3a and 3.3b are the isothermal curves for the same steels, and they illustrate the influence of time on hardness at a given temperature. Prolonged tempering at 500^{o}C has little effect on the decrease in hardness, but the effect increases steadily as temperature rises.

The tempering data can also be represented in another way. Hollomon and Jaffe (58) derived a relationship of hardness as a function of both time and temperature in which all tempering data could be combined as a single curve. The form of this combined time/temperature parameter is T(C+Logt), where T is the tempering temperature in degrees Kelvin and t the time in hours. The value of the constant C varies for different steels, and appears to decrease linearly with increasing carbon content. The value of C = 20 was found to be sufficiently accurate for the low alloy steels. However the value is not critical.

The tempering data of En41B and En19 steels are both represented in Fig. 3.4 as a function of the Hollomon tempering parameter. It clearly shows the hardness level of En19 is

always lower than En41B when tempered under the same conditions. The difference in hardness between the two steels is gradually reduced with increasing tempering temperature and time.

The effect of tempering temperature on the hardness of different types of steels is shown in Fig. 3.5. The overall hardness levels of the alloy steels are greater than that of Fe-C-Al steel, even though the carbon content of this steel is the same as that in En41B and higher than those found in the other investigated alloys. The higher hardness in the alloy steels confirms that in steels of similar carbon content, the presence of chromium and other alloying elements such as molybdenum and manganese have a considerable effect on hardness after tempering by retarding the spherodization of the carbide particles. Baluffi et al. (59) observed that in chromium steels the spherodization of Fe_3C is retarded, the particles of Fe_3C remaining small and plate-like. The hardness is retained even at higher temperatures unlike plain carbon steel.

Transmission electron microscopy examination of En41B and Fe-C-Al steels, tempered at 600^{o}C for 1 h, showed that the size, shapes and sites of the carbide particles are completely different in the two steels (see Figs. 3.15 and 3.19). En41B has smaller carbides which are evenly distributed. There are precipitates on the lath boundaries and within the laths, whereas in Fe-C-Al the carbides are much larger and precipitates on the lath boundaries only.

Table 3.1 lists the averages of the hardness readings for the investigated steels in the quenched condition (from 900°C) and after tempering at 600°C for 1 h. The figures indicate that the hardness of the quenched steel is mainly influenced by the carbon content. Fe-C-Al, containing 0.46%C, has higher hardness than other steels with the exception of En41B. This also contains 0.46%C, but in addition chromium and other alloying elements as well. On tempering the situation is different, the hardness is influenced by the alloying elements which affect the size, shape and distribution of the carbides. The drop in the hardness of the quenched steels after tempering is highest in Fe-C-Al with ΔH = 420 VHN and lowest in En40B with ΔH = 221 VHN, despite the fact that the latter steel contains only 0.26% carbon. This emphasises the role of chromium in retarding tempering.

3.3 X-ray microanalysis of carbides

The carbide particles were extracted from specimens which had been quenched from 900°C and tempered at 600°C for 1h. The potentiostatic-etching method was used to isolate the carbides, in a solution containing 10% acetyl acetone, 1% tetramethylammonium chloride in methanol and voltage of ∿100mV being the most suitable for the isolation of cementite (51).

Analysis was carried out using a Cambridge S600 scanning electron microscope with a Link system X-ray micro-analysis attachment. The conditions under which the analyses were performed were 15 keV, at a working distance of 15 mm and analysis time of 100 secs. The same conditions were used

for all the carbide samples, which were extracted from different steels, in order to keep the peak ratios of CrK_α to FeK_α fixed so that the results could be used for the purpose of comparison.

The analyses of carbides from chromium containing steels are shown in Figs. 3.6, 3.7 and 3.8 which illustrate the X-ray analysis plots of En19, En41B and En40B respectively. It is obvious that the height of CrK_α peaks in proportion to FeK_α peaks increases with the increase in chromium content of the steel. The ratio of $\frac{CrK_\alpha}{FeK_\alpha}$ in the above steels increases according to the following sequence:

$$En19 < En41B < En40B.$$

Since the chromium content of these steels are 1.03%, 1.65% and 2.88% respectively, this means that the proportion of chromium in carbides is positively correlated with the chromium content of the steel.

Elements other than Fe and Cr were also detected. The X-ray plot of En40B (Fig. 3.8) indicates the presence of a significant proportion of molybdenum. Manganese was difficult to detect because the peak coincides with that of chromium, that is the MnK_α position coincides with CrK_β. However the presence of manganese can be deduced by checking the proportion of CrK_α to CrK_β. The X-ray plot of En19 clearly demonstrates the presence of manganese because the Cr K_β/K_α ratio is higher than it should be.

The analyses of the chromium-free steels, Fe-C-Al and En41(-Cr) are illustrated in Figs. 3.9 and 3.10.

Fe-C-Al steel shows peaks from iron only, which indicates that the carbides in this steel are pure Fe_3C. The same peaks were obtained from En41(-Cr) steel together with very small peaks of Mo and Mn, which suggests the presence of both elements in minute quantities.

3.4 X-ray Diffraction

Wire-shaped specimens were prepared from each sample of the extracted carbides. These were then inserted in a Debye-Scherrer X-ray camera, which was found to be the most suitable for producing clear X-ray diffraction patterns.

Figs. 3.11 and 3.12 are X-ray diffraction powder patterns of extracted carbides from En41B and Fe-C-Al. Indexing of these X-ray patterns showed the extracted particles are Fe_3C for the both steels. Tables 3.2 and 3.3 list the observed interplanar spacing values of cementite obtained from the En41B and Fe-C-Al samples. The quality of the lines on the X-ray film for each steel were significantly different. Carbides from Fe-C-Al steel reflected sharper and clearer lines than those reflected from En41B and En4(-Cr). Carbides from En40B did not produce clear X-ray patterns, the lines were very weak and so diffuse that it was not possible to measure them accurately. This means the carbides were extremely small.

3.5 Microstructure of tempered steels

3.5.1 Material and techniques

The investigation was carried out using Fe-C-Al, En41(-Cr), En19 and En41B steels. Thin foils and carbon

extraction replicas were prepared from the alloys which were first quenched from 900°C and tempered at 600°C for 1 h. Transmission electron microscopy was used to examine the microstructure of the tempered steels.

3.5.2 Results

Figs. 3.13 and 3.14 are thin foil micrographs of Fe-C-Al steel. The cementite particles precipitated mainly on the boundaries of the tempered martensite laths. The shape of these carbides are spheroidal with an average size of 220 nm. The micrographs also indicate that the steel has completely recovered and started to recrystallise, causing a considerable decrease in the dislocation density.

In En41(-Cr), recovery and recrystallisation also occurred, but to a much lesser extent. The dislocation density is higher than in Fe-C-Al and the average size of the carbides is approximately 100 nm. These were mainly precipitated on the lath boundaries, see Figs. 3.15 and 3.16. The carbides in this steel have two different shapes, spheroidal and rod-shaped.

Figs. 3.17 and 3.18 are thin foil micrographs of En41B steel. Fig. 3.17 indicates that recovery and recrystallisation have begun to take place, but the main features of the micrographs are the examples of the typical types of cementite particles in this steel, and these are:

a) rod-like particles on the lath boundaries, which can grow to more than 1000 nm long, see Fig. 3.18.

b) spheroidal carbides, also mainly on the lath boundaries, and having an average size of 125 nm, see Fig. 3.17.

c) short needle-shaped particles within the laths, with an average length of approximately 25 nm, see also Fig. 3.18.

These different types of carbides were all found to be cementite and this is clearly demonstrated in Fig. 3.19a, b and c. The diffraction pattern (b) is indexed as cementite see table (3.4). While in the dark field, each type of the precipitate shows up confirming that all carbides are in fact cementite with different morphologies.

Tempering at 600°C for a long period or at 700°C, appears to produce carbides with faulted crystal structures. Fig. 3.20a, is a micrograph of an extraction carbon-replica obtained from a specimen tempered at 700°C for 1 h. The micrograph indicates faults in a large cementite particle. The streaks in the diffraction pattern, as shown in Fig. 3.20b are diffracted from the same particle, and are due to the faulted crystal lattice. These faults occur parallel to the (001) plane of the cementite particle (also see Table 3.5).

The general distribution of the carbides in En41B is shown in Fig. 3.21, in which the micrograph was obtained from a carbon extraction replica.

The shape, size and distribution of the carbides in En19 steel is shown in Fig. 3.22. The spheroidal carbides seem to dominate the structure. The average size of these particles is approximately 180 nm and is larger than those in En41B.

3.6 Discussion

The loss of hardness in En41B over the temperature range investigated, 500-700°C, is not associated with any phase change in the carbide, which is identified as Fe_3C throughout, but to recovery and recrystallisation of the ferrite, which is closely connected with the coarsening of the carbide particles.

Tempering is retarded by alloying elements which reduce the rate of carbide coarsening, the finer carbides being more effective in restricting recovery and recrystallisation in the ferrite.

The effect of chromium on growth of Fe_3C is clearly demonstrated by comparing micrographs from tempered En41B (Figs. 3.17, 3.18) with those from En41(-Cr), (Figs. 3.15, 3.16). In the absence of chromium the fine intralath-carbides have completely redissolved.

The lack of alloying elements such as Mn, Mo and Si in the chromium-free Fe-C-Al steel results in very large Fe_3C particles of average size 220 nm. which leads to a severe fall in the hardness during tempering, even though the hardness in the quenched condition is still higher than all the other steels except En41B.

The cementite produced by tempering chromium-containing steels i.e. En19, En41B and En40 contain different proportions of chromium, which is positively correlated to the chromium content of the steel. It is known however, that chromium in steel is concentrated in cementite in preference to ferrite, and previous work (60) (61) has shown that it can replace up to 18% of the iron atoms in the M_3C type carbide.

3.7 Summary and Conclusions

1. For En41B and En19 steels the combinations of tempering time and temperature to obtain a given hardness obey the Hollomon relationship in which all tempering data can be represented on one curve.

2. The hardness of tempered steel depends to a large extent on the size and distribution of the carbides. This is largely influenced by the presence of alloying elements such as Cr, Mo, Mn and Si.

3. Three different carbide morphologies were observed in tempered En41B; firstly spheroidal carbides which precipitated mainly on the grain boundaries, secondly rod-like carbides which also precipitated and grew along the grain boundaries, and thirdly smaller, needle-shaped carbides which precipitated within the laths.

4. The only carbide observed in En41B was Fe_3C. There was no evidence of Cr_7C_3 even at high temperatures and prolonged tempering times.

5. In tempered chromium-containing steel, the proportion of dissolved chromium in Fe_3C was positively correlated to the increase of chromium in the steel.

6. Tempering at 600^{o}C for 1 h produces a structure which is significantly recovered and more or less recrystallized, depending on the type of steel. The degree of recrystallization is greater with lower alloy contents.

7. In chromium-free steel tempered 1 h at 600°C the fine intralath carbide referred to in (3) above was redissolved.

8. In Fe-C-Al alloys spheroidisation of carbide has taken place after tempering 1 h at 600°C and is associated with considerable recrystallization.

Steel	wt% C	wt% Cr	Hardness HV_{30}	
			Oil quenched from 900°C	Tempered at 600°C for 1h
EN41B	0.46	1.6	750	380
En41A	0.33	1.65	568	330
En19	0.37	1.03	610	360
En40B	0.26	2.88	566	345
Fe-C-Al	0.46	-	650	230
En41(-Cr)	0.39	-	623	330

Table 3.1 Shows the effect of carbon and chromium contents on hardness of the quenched and tempered steels.

Fig. 3.1 The isochronal tempering curves for En41B steel

Fig. 3.2 The isochronal tempering curves for En19 steel

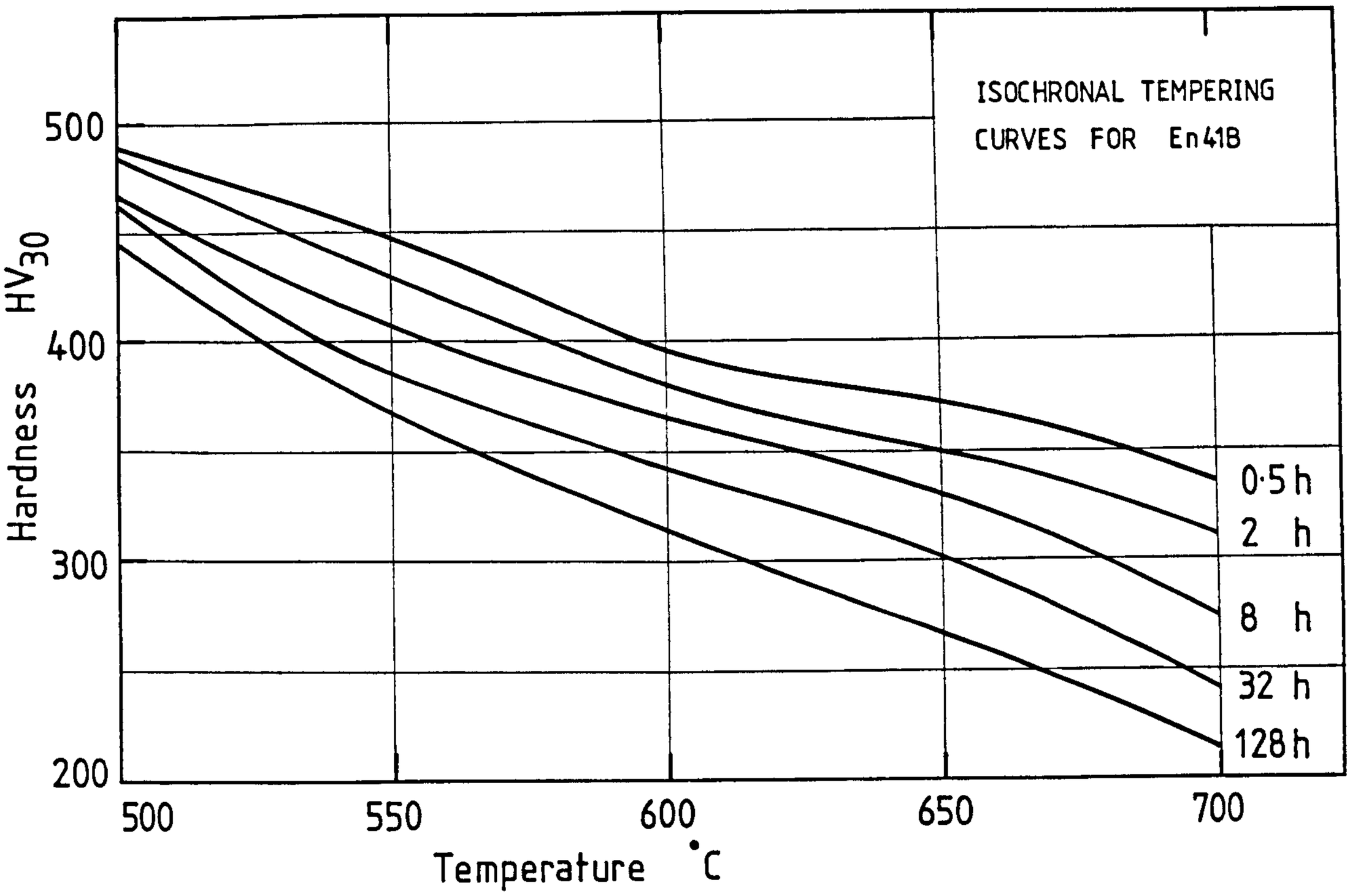
ISOCHRONAL TEMPERING
CURVES FOR En41B
Hardness HV30
500
400
300
200
500
550
600
650
700
Temperature °C
0·5 h
2 h
8 h
32 h
128 h

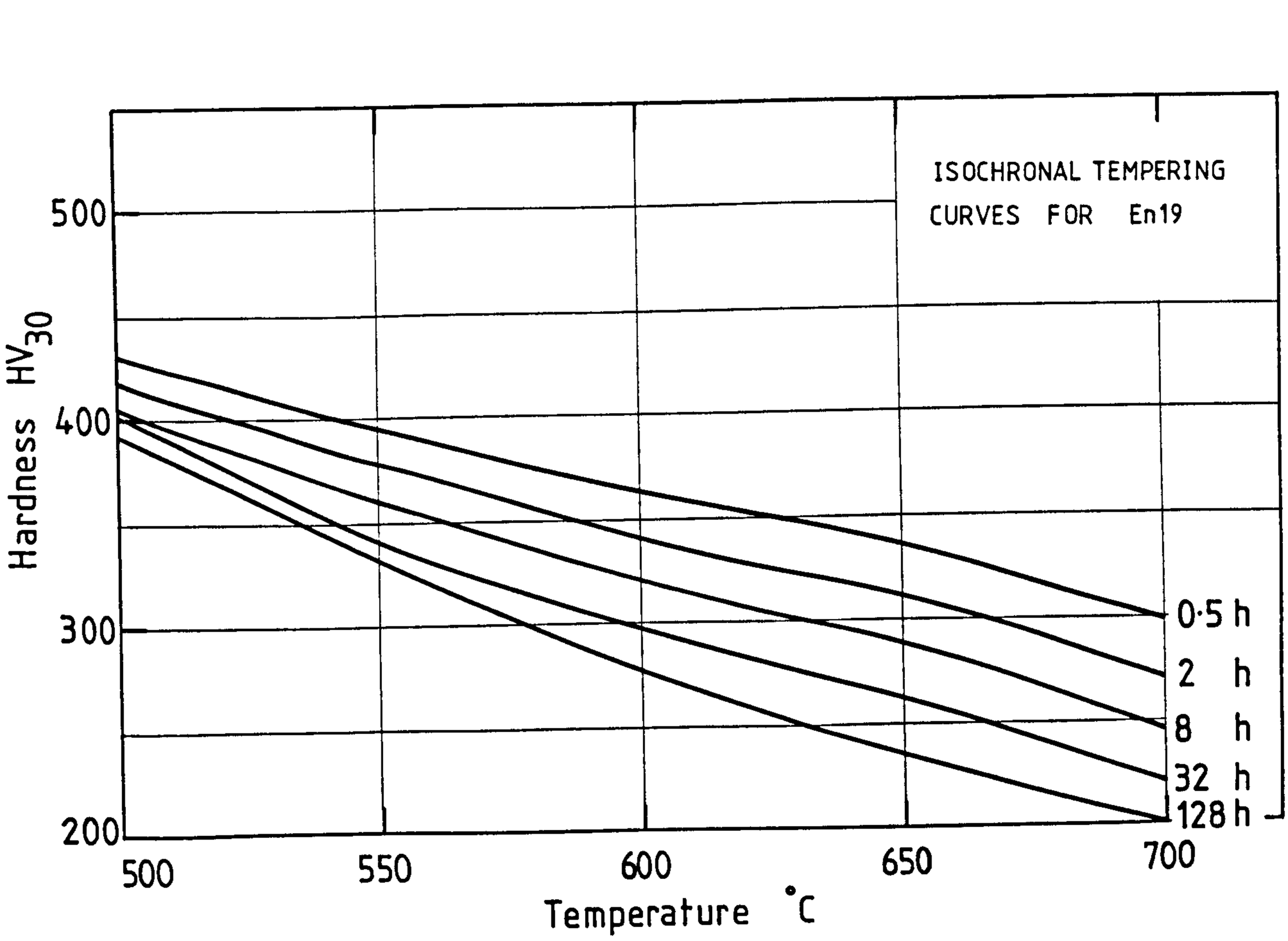
ISOCHRONAL TEMPERING
CURVES FOR En19
Hardness HV30
500
400
300
200
500
550
600
650
700
Temperature °C
0·5 h
2 h
8 h
32 h
128 h

Fig. 3.3 The isothermal tempering curves showing the effect of tempering time on hardness

a - En41B steel

b - En19 Steel

a) En41B

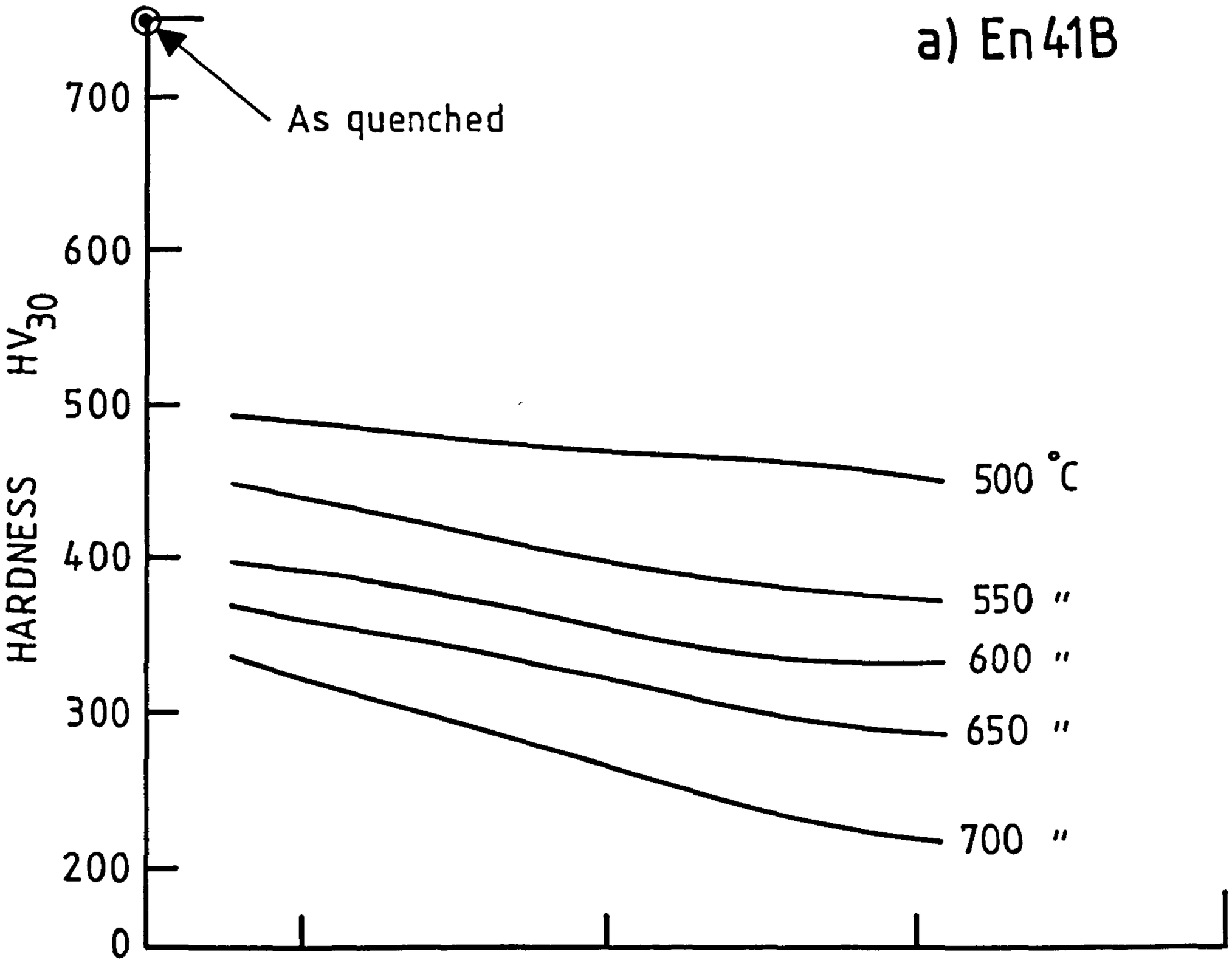

b) En19

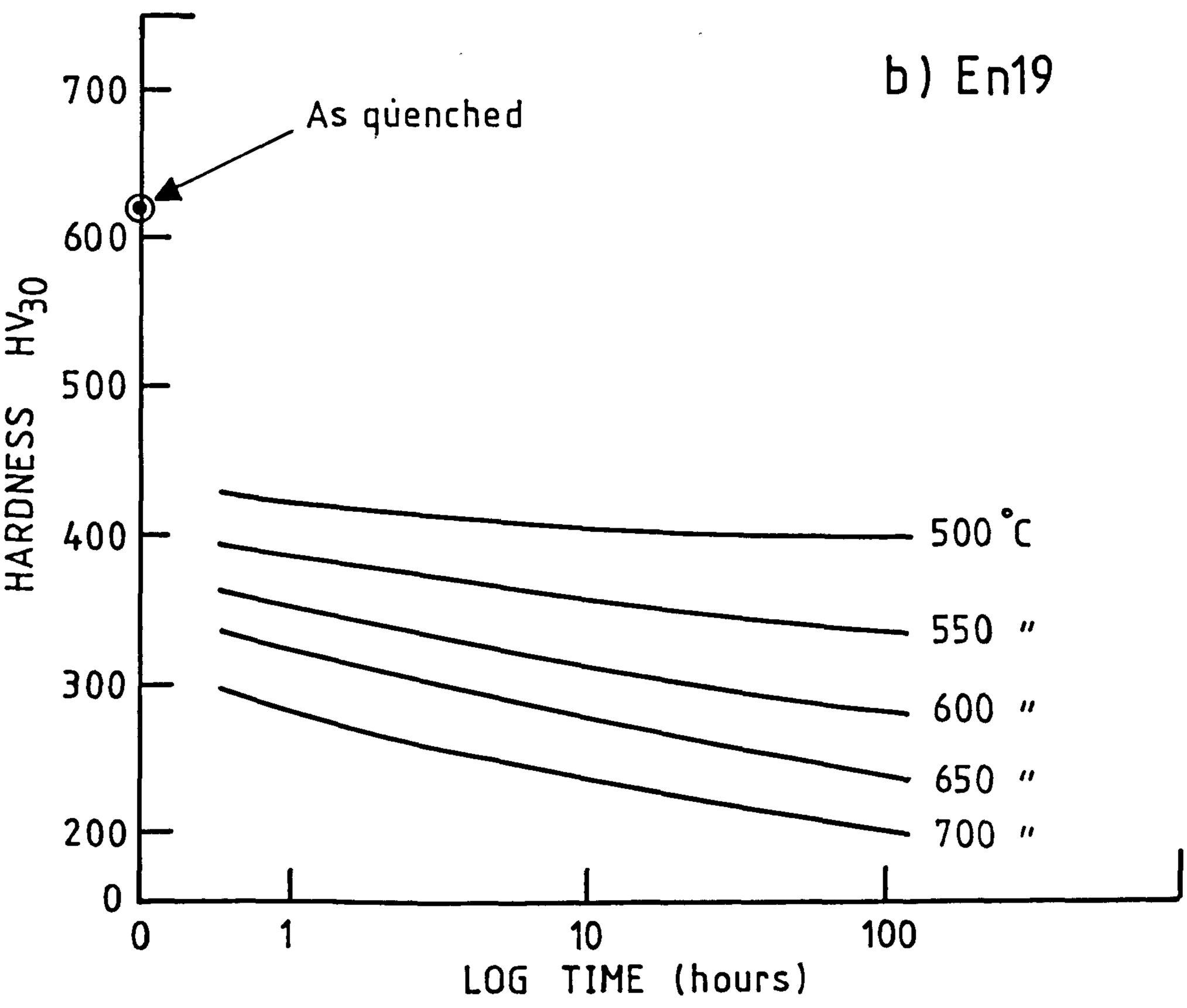

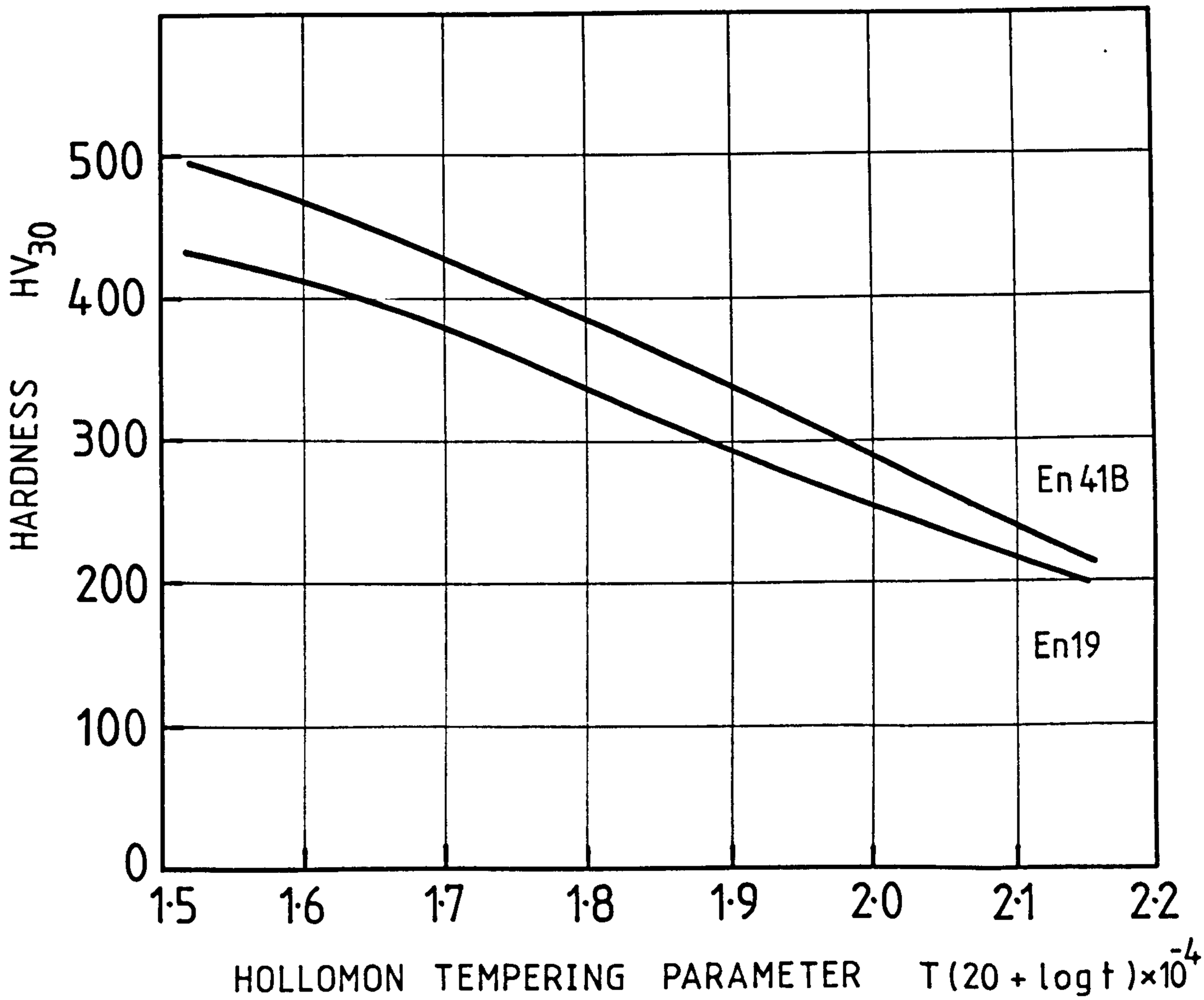

Fig. 3.4 Showing the tempering data as a function of the Hollomon tempering parameter

Fig. 3.5 Effect of tempering temperature on the hardness of different types of steels. Note the low hardness of Fe-C-Al

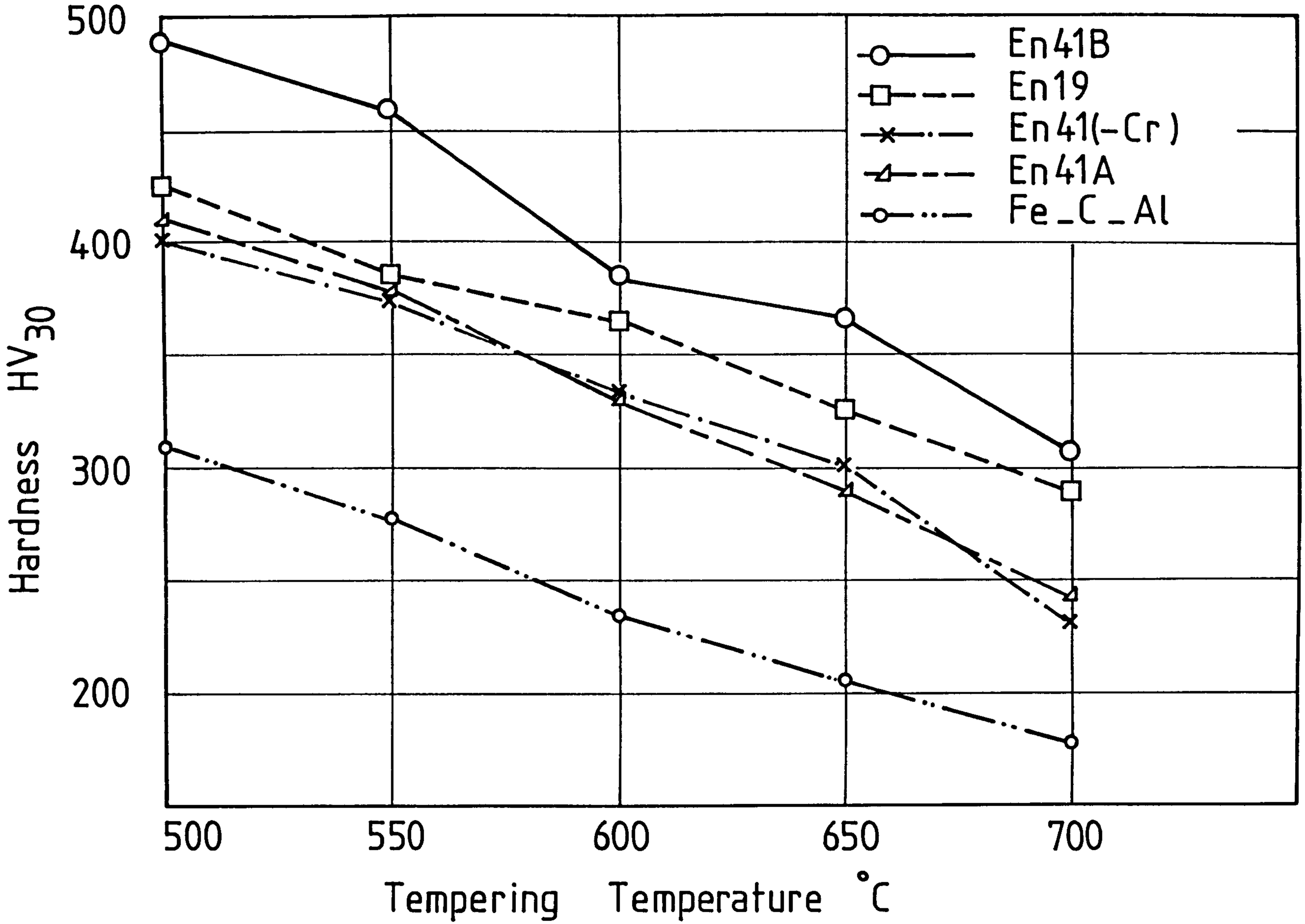
500
400
300
200
Hardness HV30
En41B
En19
En41(-Cr)
En41A
Fe_C_Al
500
550
600
650
700
Tempering Temperature °C

Fig. 3.6 X-ray microanalysis traces of the carbide particles extracted from En19 steel, tempered at 600°C for 1 h

Fig. 3.7 X-ray microanalysis of the carbide particles extracted from En41B, tempered at 600°C for 1h

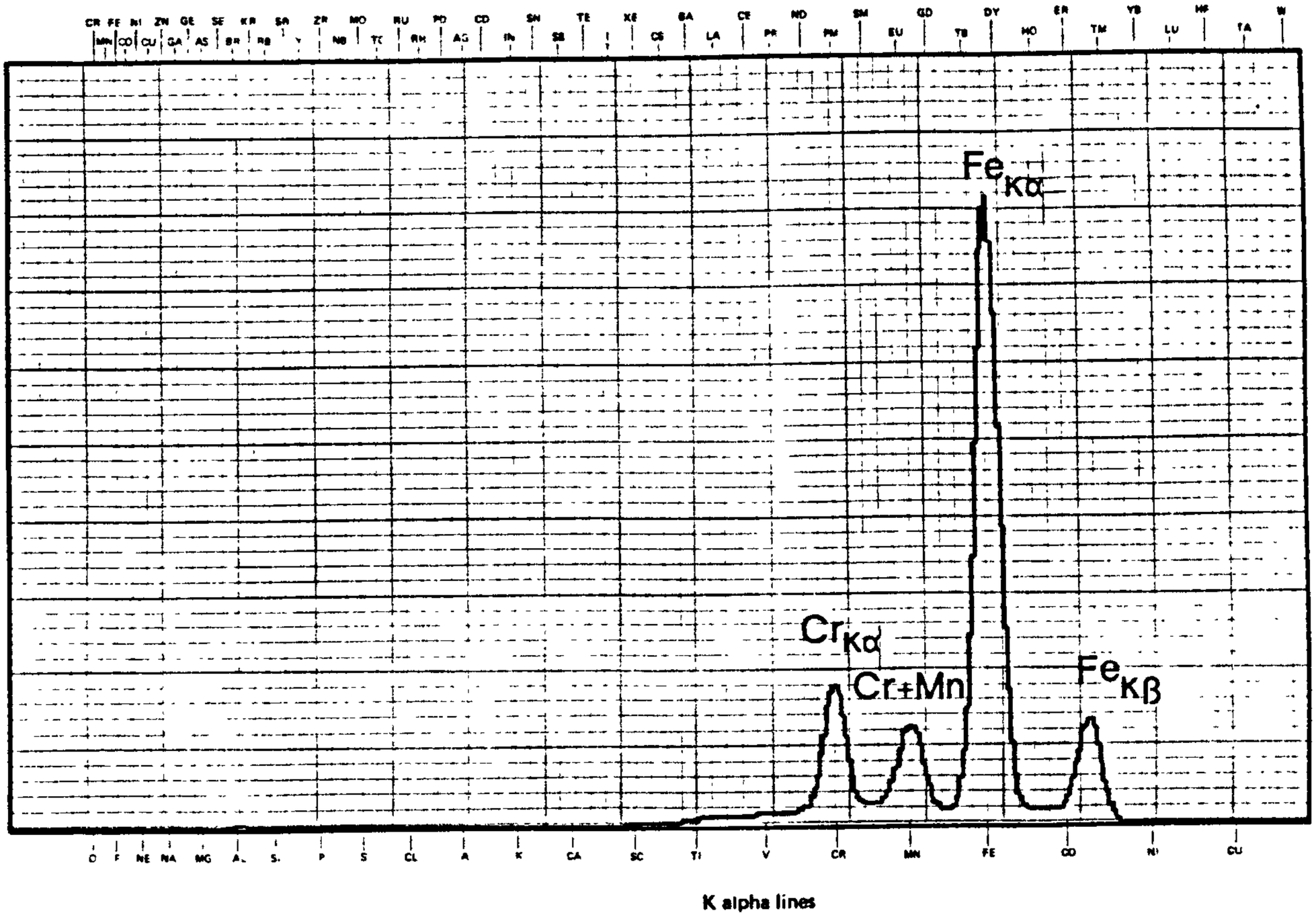
L alpha lines
CR FE NI ZN GE SE KR SR ZR MO RU PD CD SN TE XE BA CE ND SM GD DY ER YB HF W
MN CO CU GA AS BR RB Y NB TC RH AG IN SB I CS LA PR PM EU TB HO TM LU TA
Fe Kα
Cr Kα
Cr+Mn
Fe Kβ
O F NE NA MG AL SI P S CL A K CA SC TI V CR MN FE CO NI CU
K alpha lines

Fig. (3.6)

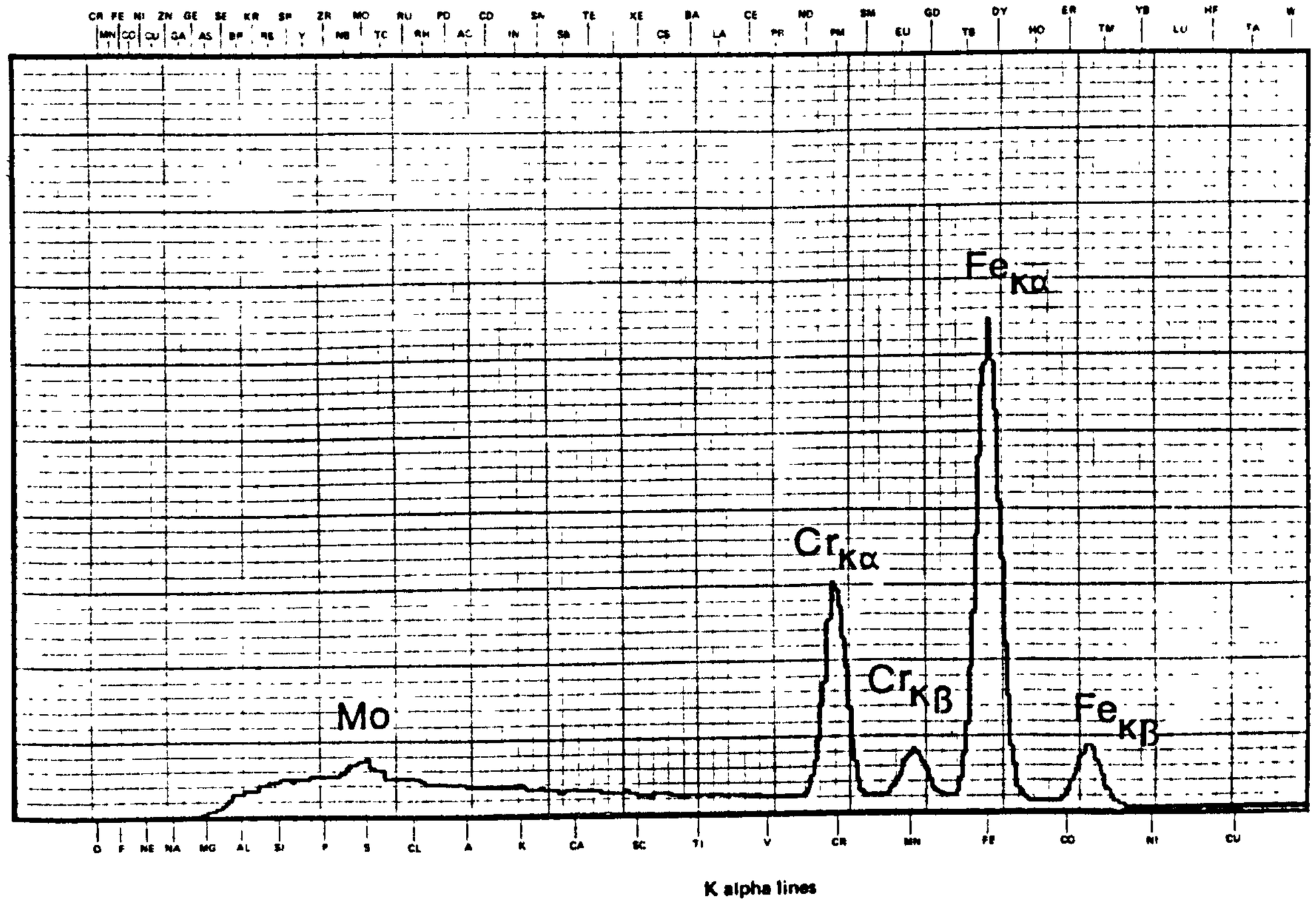
L alpha lines
CR FE NI ZN GE SE KR SR ZR MO RU PD CD SN TE XE BA CE ND SM GD DY ER YB HF W
MN CO CU GA AS BR RB Y NB TC RH AG IN SB CS LA PR PM EU TB HO TM LU TA
Fe Kα
Cr Kα
Cr Kβ
Fe Kβ
Mo
O F NE NA MG AL SI P S CL A K CA SC TI V CR MN FE CO NI CU
K alpha lines

Fig. (3.7)

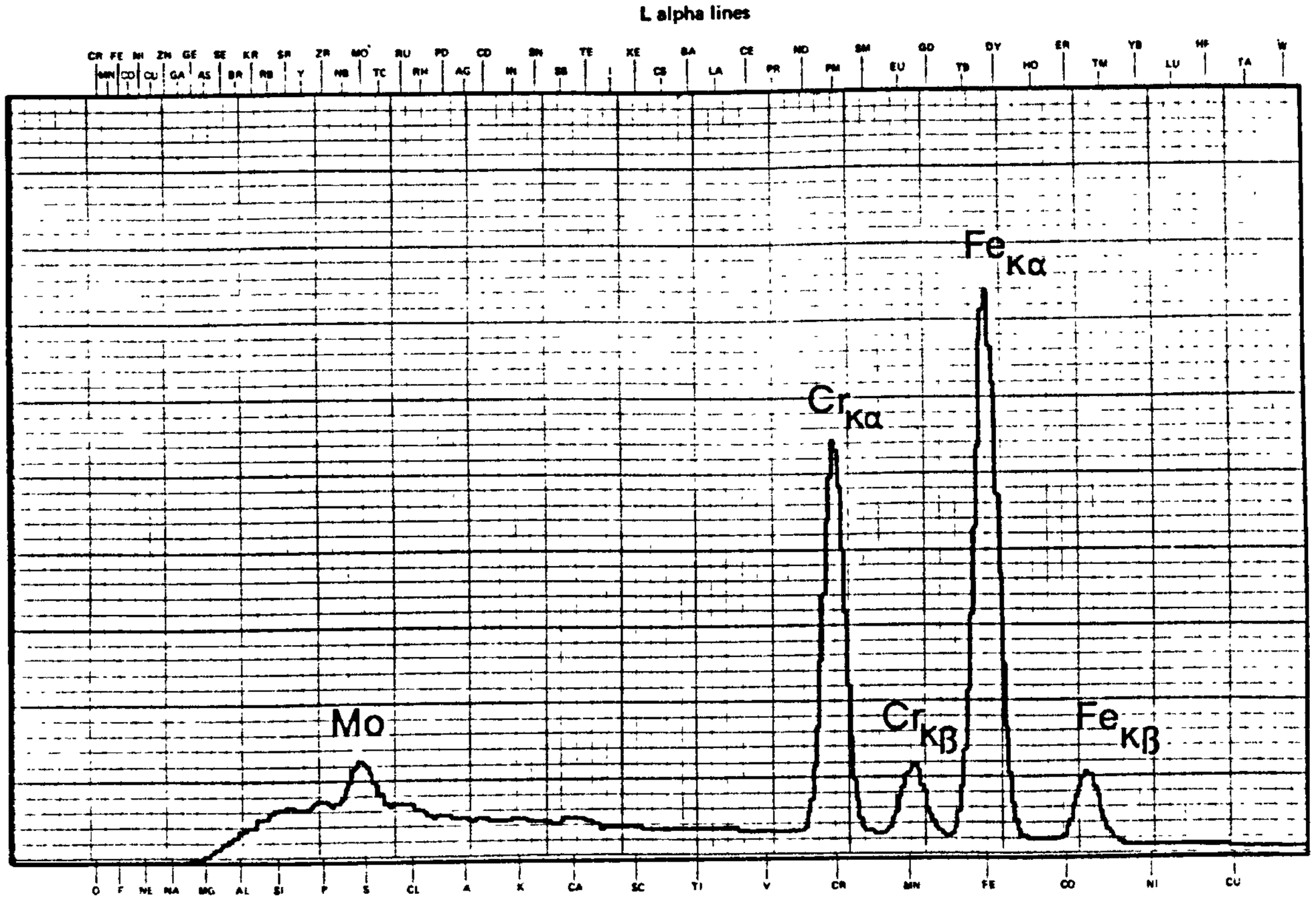

Fig. 3·8 X-ray microanalysis traces of the carbide particles extracted from En40B, tempered at 600°C for 1 h, showing the carbides contain a high proportion of chromium and significant amount of molybdenum

Fig. 3.9 X-ray microanalysis traces of the carbides extracted from Fe-C-Al, tempered at 600°C for 1 h, indicating pure Fe_3C

Fig. 3.10 X-ray microanalysis traces of the carbides extracted from En41(-Cr) tempered at 600°C for 1 h, showing traces of Mo and Mn

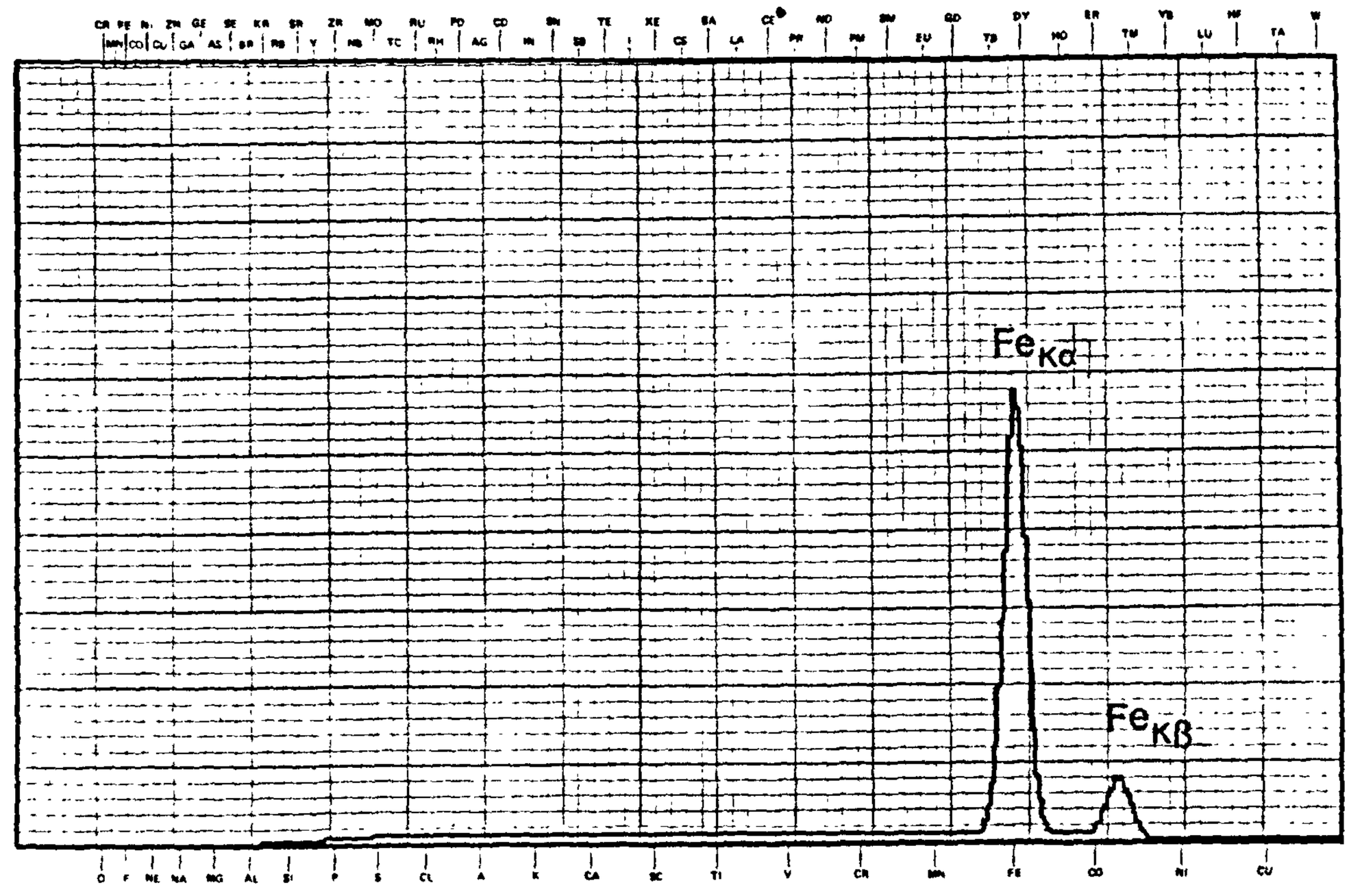

Fig.(3.9)

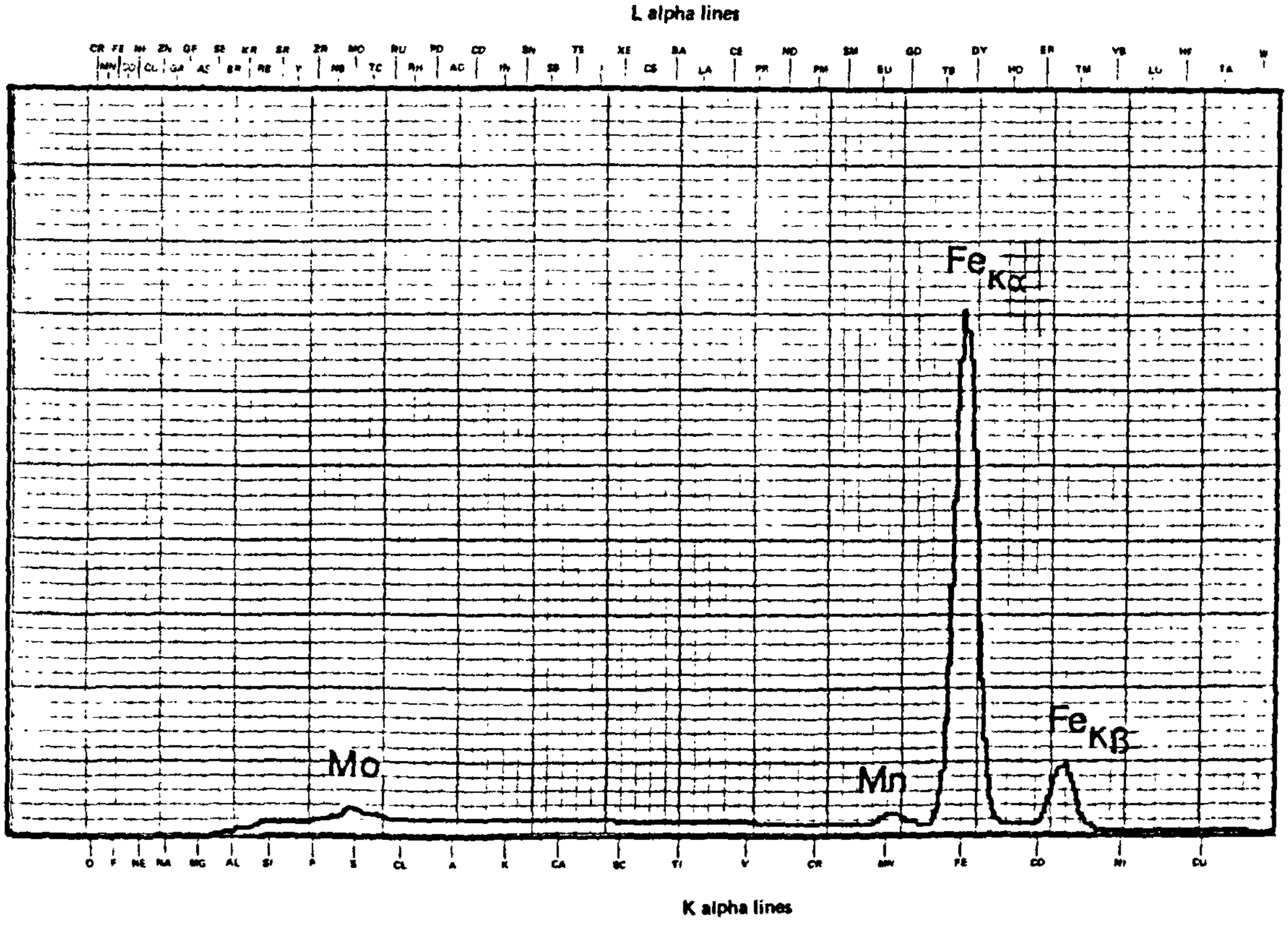

Fig.(3.10)

Fig. 3.11 X-ray diffraction powder pattern (using Cu K_α radiation) of carbides extracted from En41B, tempered at 600°C for 1 h.

Table 3.2 X-ray data for $(Fe, Cr)_3C$.
Calculated values using the parameters
$a_o = 4.524$ Å, $b_o = 5.088$ Å, $c_o = 6.742$ Å

Table 3.2

$d_{obs.}$ Å	$d_{cal.}$ Å	hkl
2.375	2.380	021
2.260	2.262	200
2.21	2.218	120
2.10	2.107	121
2.062	2.067	210
2.005	2.013	103
1.970	1.976	211
1.863	1.872	113
1.843	1.853	122
1.760	1.762	212
1.682	1.684	004
1.638	1.640	221
1.580	1.588	130
1.546	1.546	131
1.514	1.515	032
1.430	1.437	132
1.404	1.405	024
1.327	1.329	312
1.260	1.259	232
1.225	1.225	140
1.215	1.216	313
1.191	1.191	025
1.161	1.162	233
1.152	1.152	125
1.127	1.127	330
1.106	1.107	043
1.096	1.097	314,016
1.089	1.090	411
1.069	1.069	332
1.054	1.054	225
0.9974	1.005	305
0.9896	1.002	126

Fig. 3.11

Fig. 3.12 X-ray diffraction powder pattern (using Cu K_α radiation) of carbides extracted from Fe-C-Al steel, tempered at 600°C for 1 h.

Table 3.3 X-ray data for Fe_3C.

Calculated values using the parameters $a_o = 4.524$ Å, $b_o = 5.088$ Å, and $c_o = 6.742$ Å.

Fig. 3.12

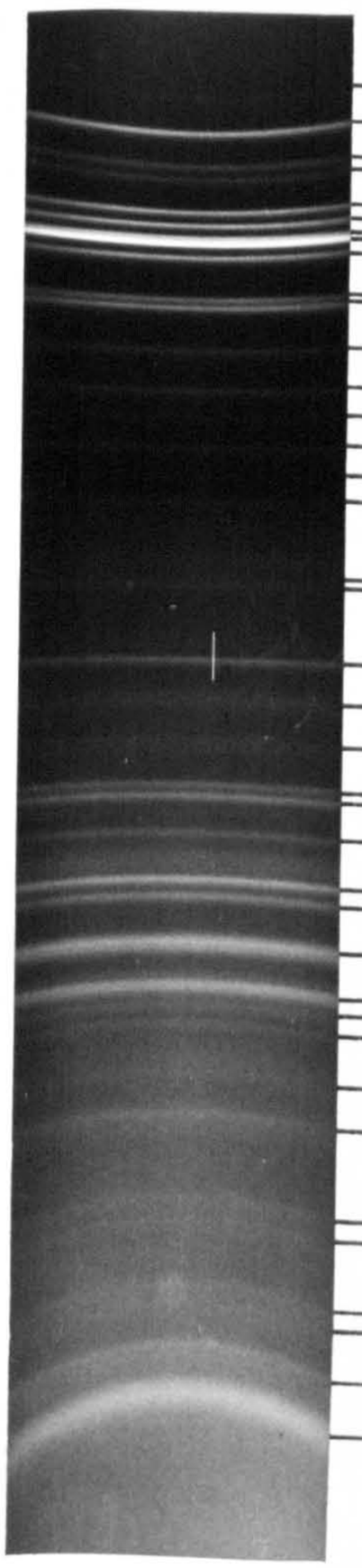

d_{obs} A°	$d_{cal.}$ Å	hkl
2.530	2.544	020
2.381	2.380	021
2.260	2.262	200
2.210	2.218	120
2.100	2.107	121
2.065	2.067	210
2.030	2.031	022
2.007	2.013	103
1.972	1.976	211
1.870	1.872	113
1.848	1.853	122
1.760	1.762	212
1.682	1.685	004
1.638	1.640	221
1.586	1.588	130
1.546	1.546	131
1.514	1.515	032
1.430	1.437	132
1.404	1.405	024
1.327	1.329	312
1.293	1.292	105
1.260	1.259	232
1.225	1.225	140
1.215	1.216	313
1.191	1.191	025
1.161	1.162	233
1.152	1.152	125
1.127	1.127	330
1.106	1.107	043
1.096	1.097	314,016
1.089	1.090	411
1.069	1.069	332
1.054	1.054	225
1.028	1.028	324,135
1.021	1.022	421
1.0065	1.007	333
1.003	1.006	051,206
0.9974	1.005	305
0.9896	1.002	126

Table 3.3

Fig. 3.13 Thin foil micrograph of Fe-C-Al steel, tempered at 600°C for 1 h, showing recrystallized grains

Fig. 3.14 Thin foil micrograph of Fe-C-Al steel, tempered at 600°C for 1 h, showing large spheroidal carbides and recovered grains.

Fig(3·13) 0.5 u

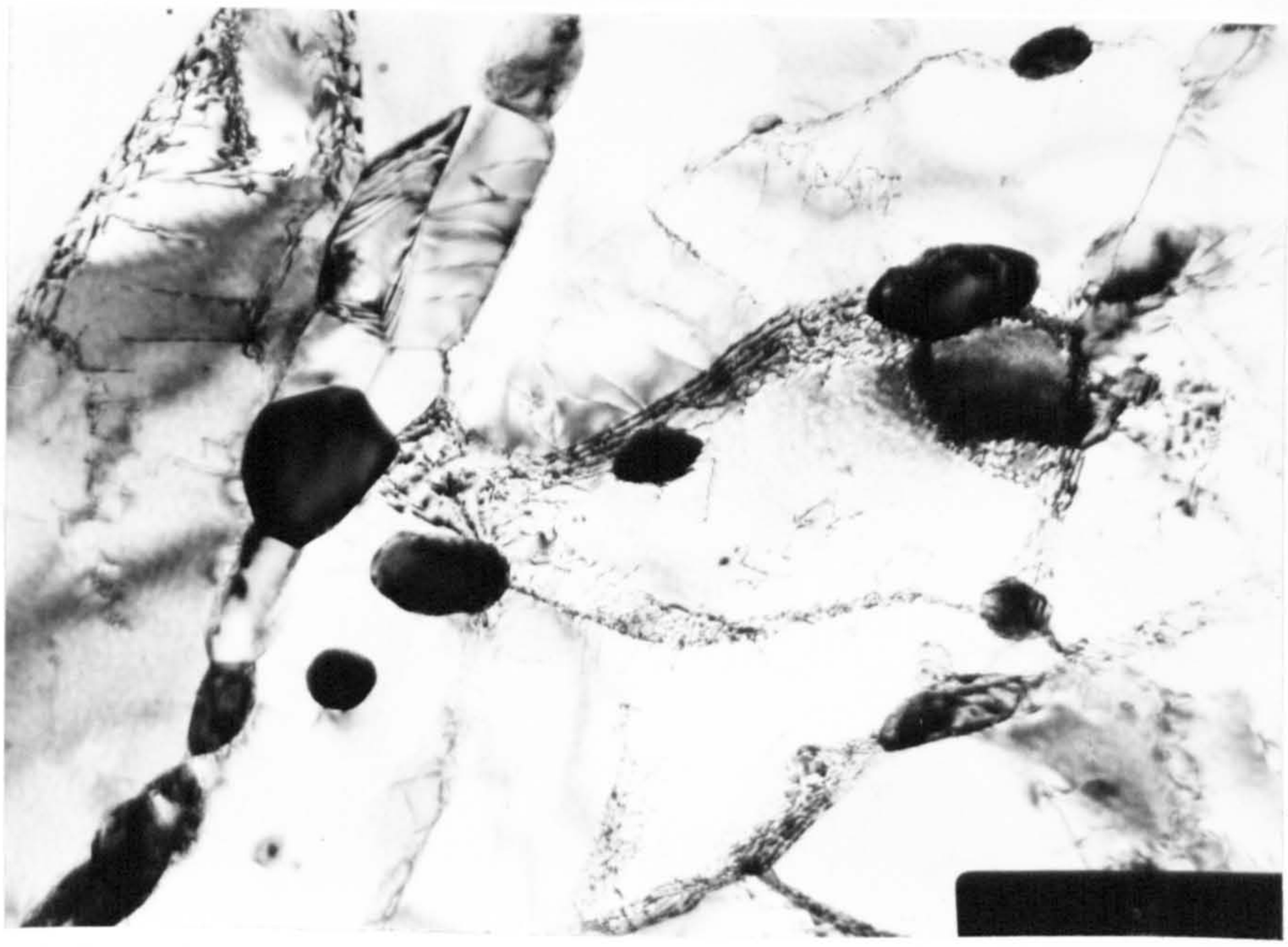

Fig(3.14) 0.5u

Fig. 3.17 Thin foil micrograph of En41B tempered at 600°C for 1 h, showing recrystallized grains and spheroidal carbides at lath boundaries

Fig. 3.18 Thin foil micrograph of En41B tempered at 600°C for 1 h, showing rod shaped carbides along the lath boundaries and short needles within the laths.

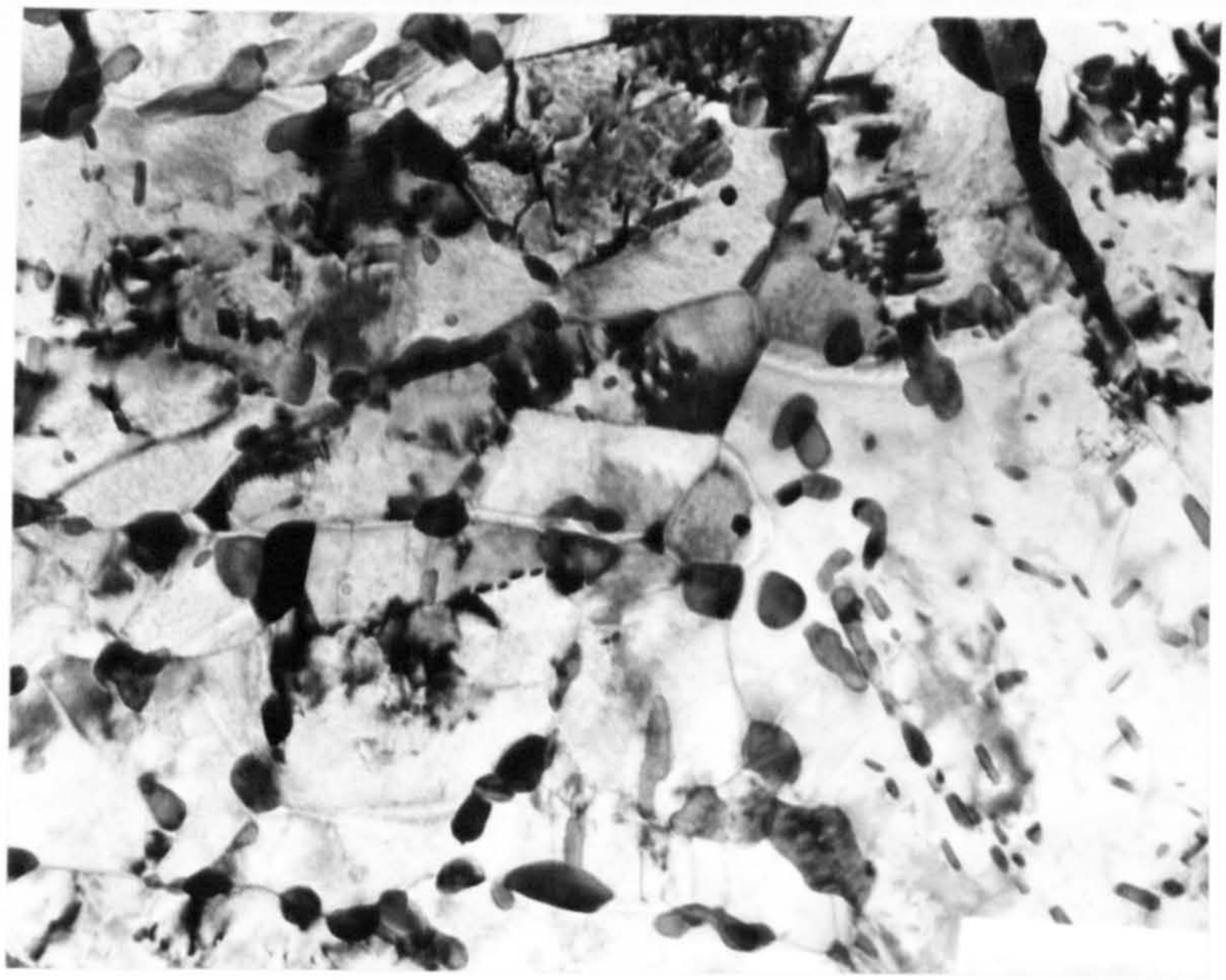

0.5 um

Fig.(3.17)

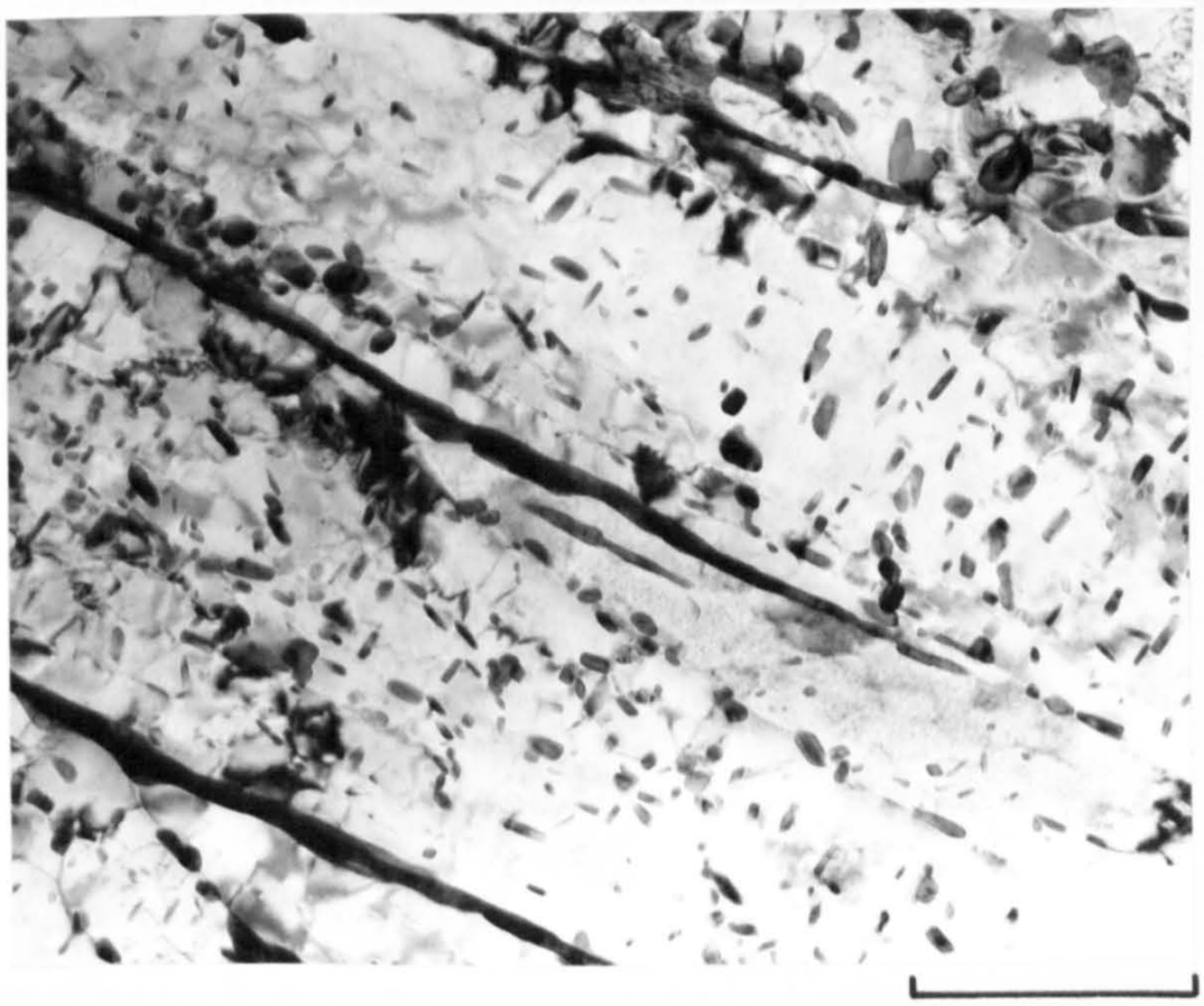

0.25 um

Fig.(3.18)

Fig. 3.19

(a) Bright field micrograph of tempered En41B (600^{o}C, 1h) showing different shapes and size of carbides.

(b) Electron diffraction pattern of $(Fe, Cr)_3C$

(c) Diffraction pattern interpretation

(d) Dark field micrograph of (a) showing all the different types of carbides are $(Fe,Cr)_3C$

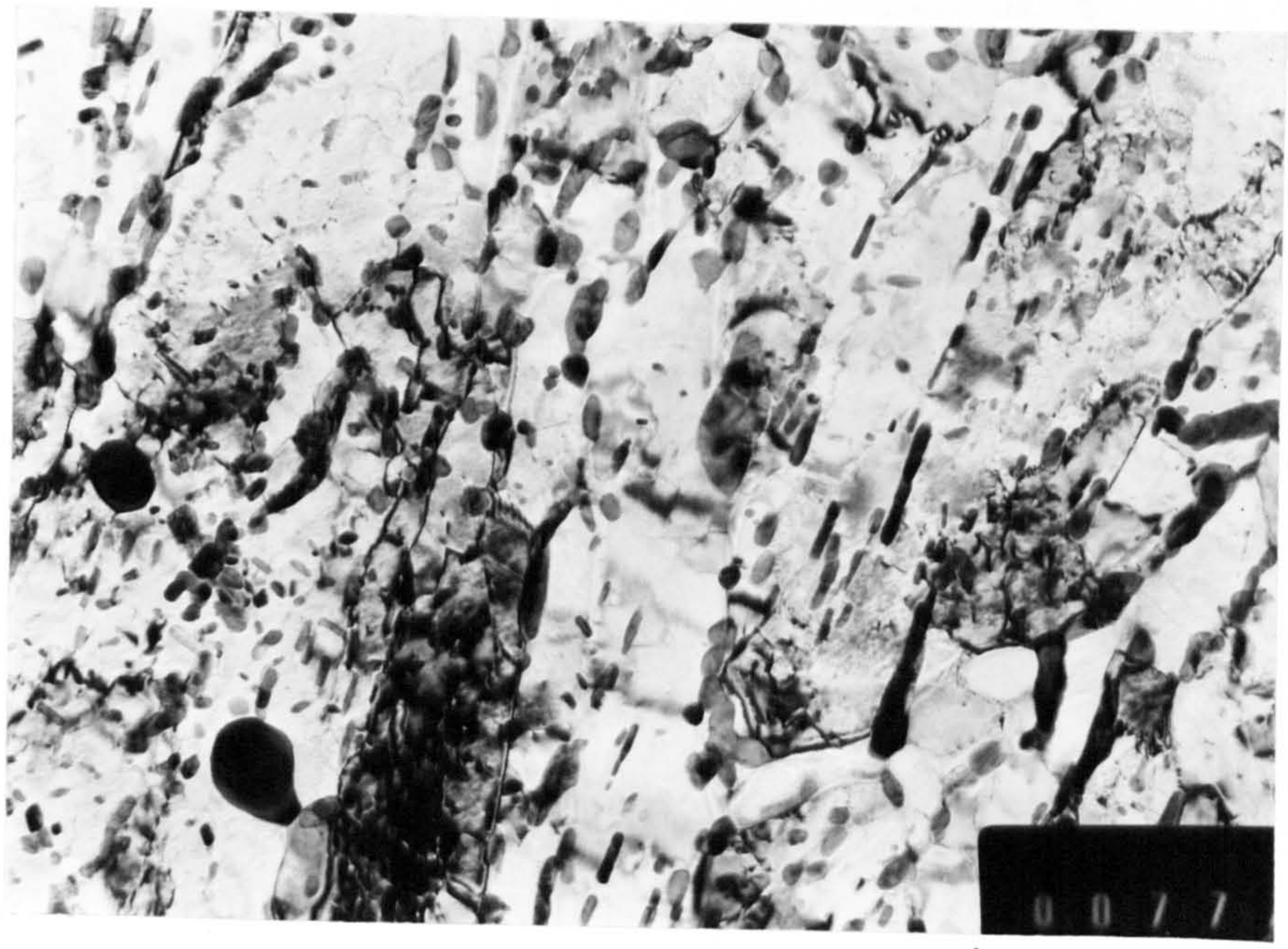

a

0.5 um

b

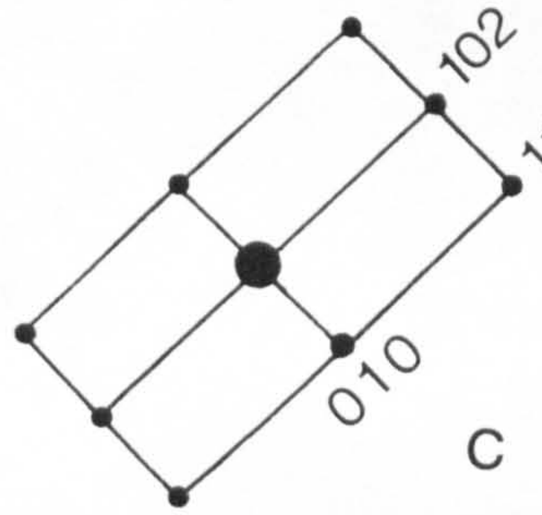

c

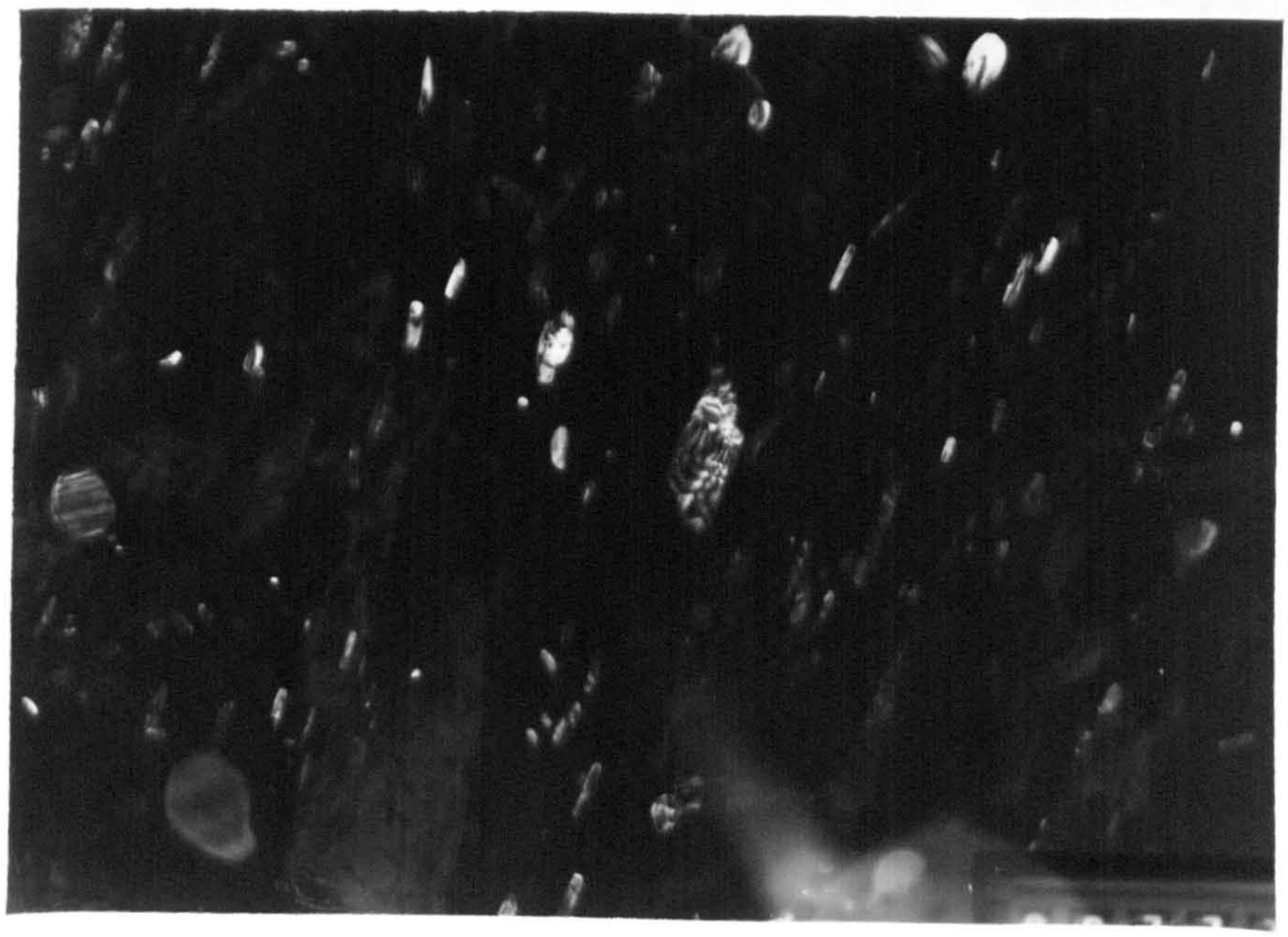

d

Fig.(3 .19)

Table 3.4

Electron diffraction data for $(Fe,Cr)_3C$, zone axis $[20\bar{1}]$, see Fig. 3.19

$d_{obs.}$	$d^*_{cal.}$ Å	hkl
5.066	5.088	010
2.384	2.387	112
2.702	2.703	102

* calculated from : a = 4.524 Å
b = 5.088 Å
c = 6.742 Å

Fig. 3.20

(a) Bright field micrograph from an extraction carbon-replica obtained from En41B steel, tempered at 700°C for 1h, showing the faulted crystal structure of a carbide particles. The faults are parallel to (001)

(b) Electron diffraction pattern of $(Fe,Cr)_3C$. The streaks are due to the faulted structure.

(c) Interpretation of the diffraction pattern.

(d) Dark field image of the same particle as in (a).

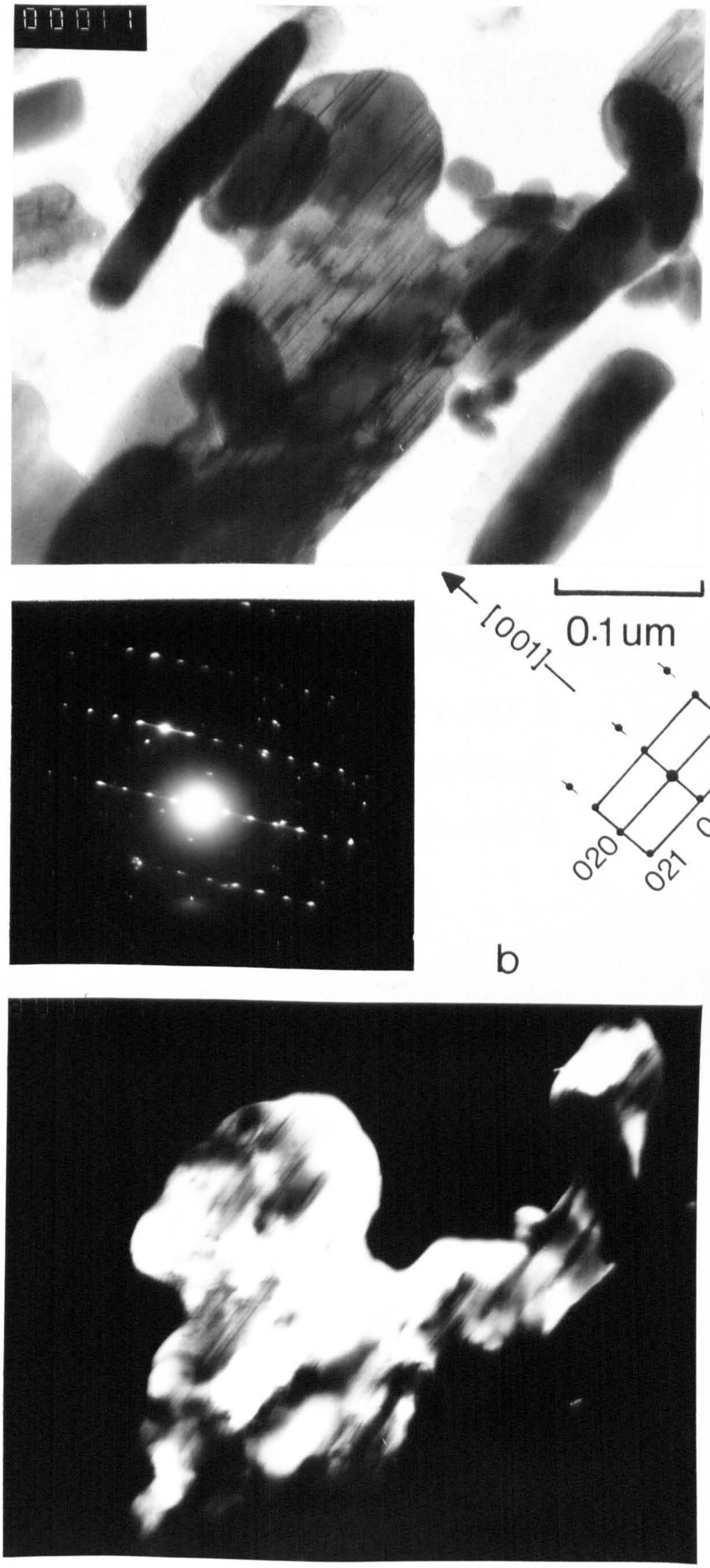

Fig.(3.20)

Table 3.5

Electron diffraction data for $(Fe,Cr)_3C$, zone axis [200]. see Fig. 3.20

d_{obs} Å	d_{cal} Å	hkl
6.742	6.742	001
2.573	2.544	020
2.399	2.380	021

Calculated from : a = 4.524 Å

b = 5.088 Å

c = 6.742 Å

Fig. 3.21 Micrograph from an extraction carbon replica obtained of En41B, tempered at 600°C for 1h, showing general distribution of the carbides

Fig. 3.22 Micrograph from an extraction carbon replica of En19, tempered at 600°C for 1h, showing general distribution of carbides. Note the large spheroidal particles

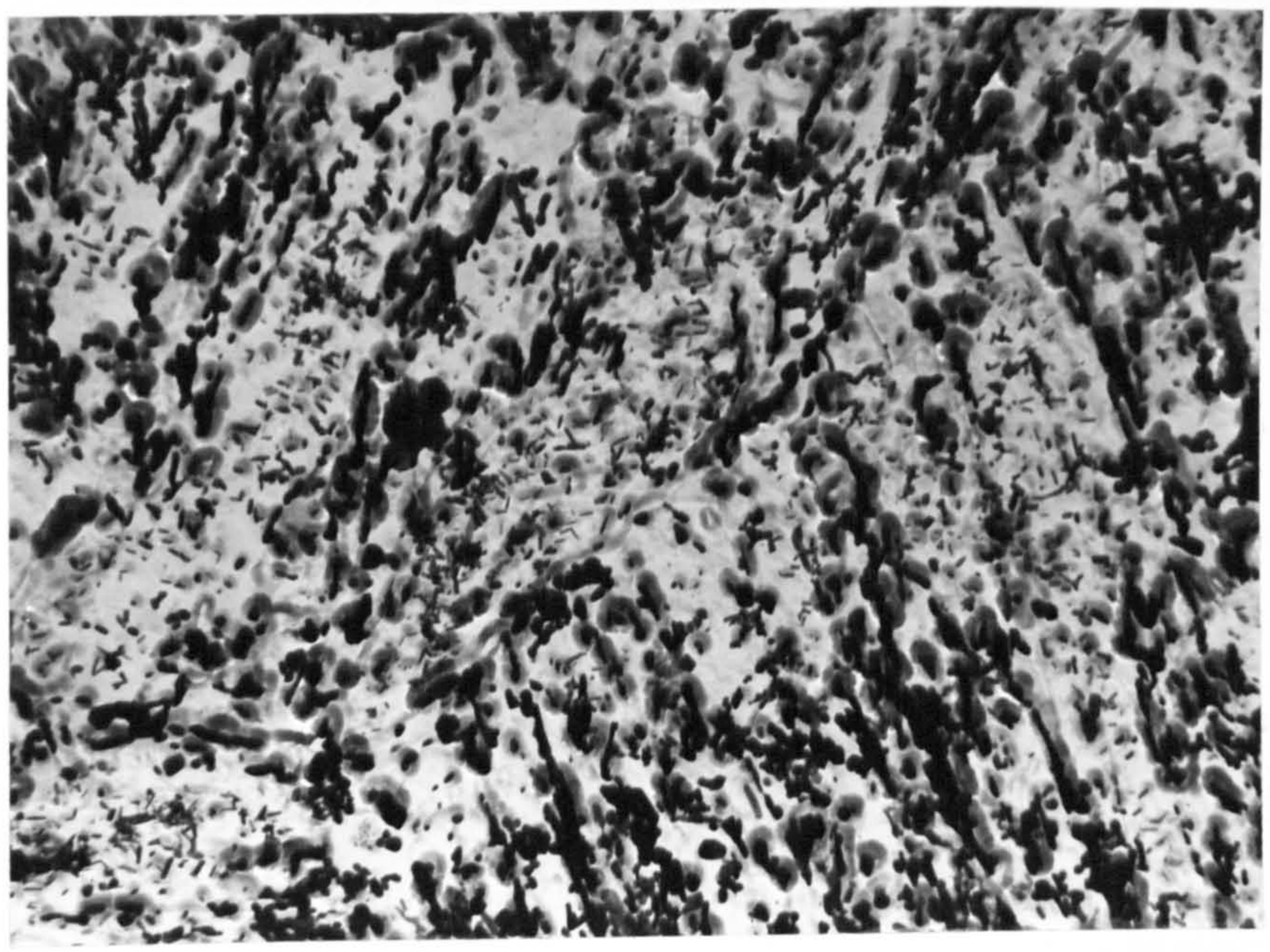

Fig.(3.21)

1um

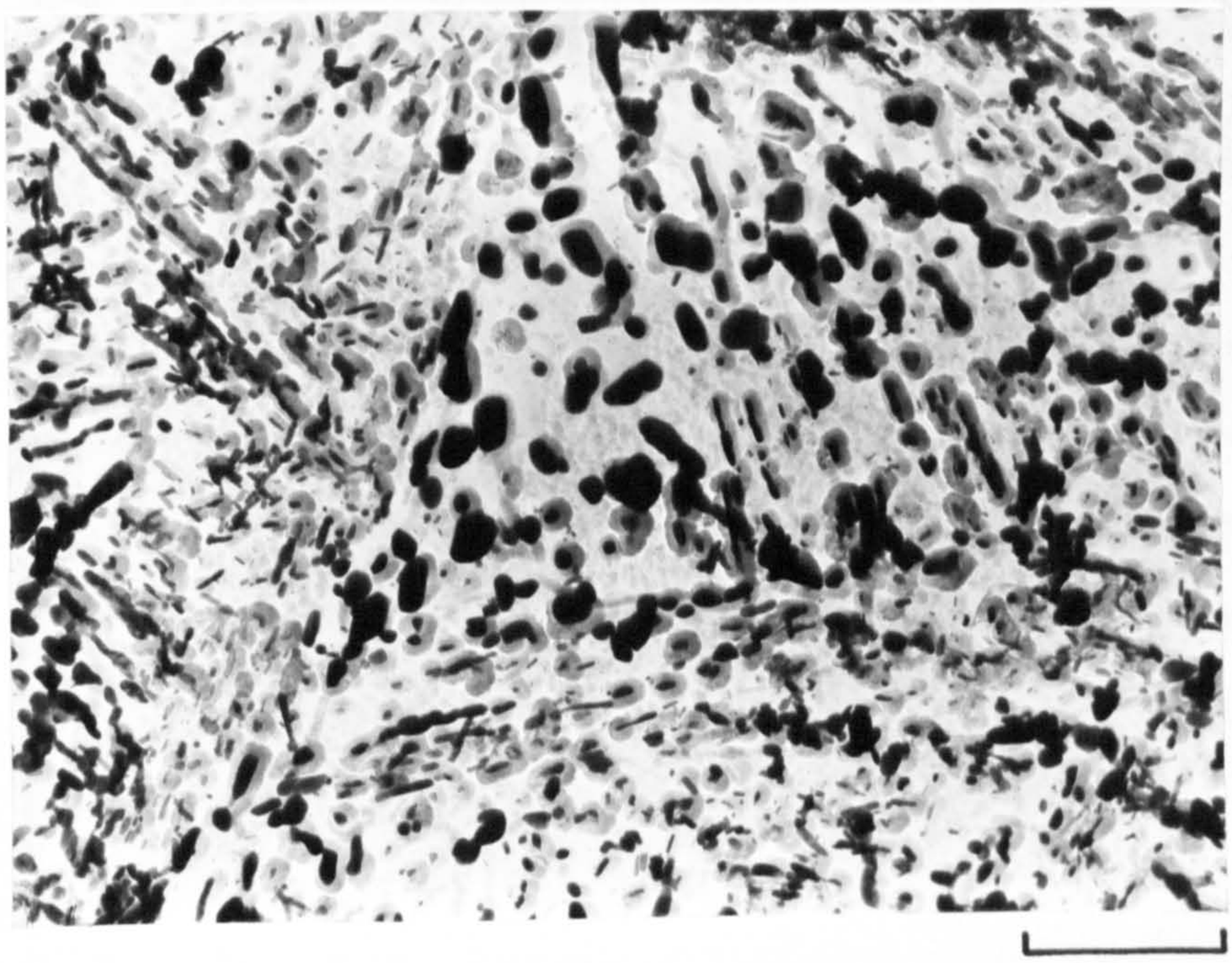

Fig. (3·22)

1um

CHAPTER 4

NITRIDE FORMATION IN ALUMINIUM CONTAINING STEELS

4.1 Introduction

Upon nitriding iron and steels containing metallic elements with a strong affinity for nitrogen, different types of nitride can precipitate. The nitride phases of the more commonly occuring alloying elements in nitrided steels are TiN, AlN, VN, CrN, Mo_2N and W_2N (see Table 1.2). All these phases have the metal atoms arranged on a f.c.c. lattice with the exception of AlN which is hexagonal,

Face centered cubic nitride phases which have a lattice parameter in the region of 4.1 $\mathring{A}$ can form with a Bain orientation relation (38) as coherent or semi coherent plates on the cube planes of ferrite. These can nucleate homogeneously, whereas nucleation of the complicated hexagonal AlN is more difficult and requires dislocations as nucleating sites. Podgurski et al's (39) investigations, using dilute Fe-Al alloys, showed that annealed Fe-Al alloys do not react readily to form AlN when held at 500^{o}C in a NH_3/H_2 gas mixture but do so upon the introduction of dislocations. The nucleation of the nitride phase occurs on dislocation sites initially, but the growth of the aluminium nitride particles causes the ferrite phase to yield plastically, generating more dislocations and hence further nucleation. The nitride phase was identified as a stoichiometric aluminium nitride with the hexagonal crystal lattice. The same alloys readily formed

aluminium nitride at 570°C in the annealed state

The precipitation of hexagonal AlN in nitrided irons and steels has been reported previously by other authors. Philips and Seybolt (62) investigated a binary iron alloy containing 1% Al and also a chromium steel containing 1.2% Al. These were ion nitrided at 550°C and 600°C in N_2/H_2 mixtures. Two separate aluminium nitride populations were observed, one consisting of coarse chain-linked clusters and a very fine essentially unresolved dispersion of smaller particles about 10 Å in size. It was suggested that the fine particles may act as an intermediate precipitate, having a low nucleation barrier. The coarse AlN structures were interpreted in terms of a low nucleation frequency caused by a high energy barrier imposed by surface energy and strain energy requirements.

Regarding the severe nucleation difficulties of AlN, it has been proposed (62), that a high surface energy requirement might be imposed at the AlN/steel interface because of the predominantly ionic nature of AlN when compared to more "metallic" nitrides like TiN, or VN. Jack et al. (40) explained the behaviour of AlN thus: unlike other nitrides it is a covalent compound and not an interstitial phase. In interstitial nitrides the nitrogen atom occupy the same octahedral sites as they do in the matrix. AlN has the hexagonal wurtzite structure with the nitrogen atoms occupying tetrahedral sites, and the aluminium atom arrangement cannot be derived simply from the ferrite structure but can only occur through a large rearrangement in the metal atom positions.

4.2 Detection of the precipitated phases:

4.2.1 Material and techniques

The materials used in this investigation were commercial En41B and experimental En41(-Cr) and Fe-C-Al steels.

Two different types of specimen were prepared from each steel. Thin specimens, with thicknesses in the range 0.1 - 0.15mm, were divided into two batches, each being nitrided at different nitriding conditions, i.e.:

1. 500^{o}C in 16% NH_3 for 24h
2. 570^{o}C in 13% NH_3 for 24h.

These conditions were chosen so as to avoid the formation of "white layer" on the surface.

Bulk specimens were also nitrided under two different conditions:

3. 500^{o}C in 80% NH_3 for 72h
4. 570^{o}C in 80% NH_3 for 48h.

All specimens were subjected to the standard heat treatment before nitriding i.e. quenched from 900^{o}C then tempered at 600^{o}C for 1h. For thin specimens, the above treatments were carried out under an argon atmosphere in silica capsules to avoid decarburization.

The precipitates were extracted from the nitrided thin specimens by a potentiostatic etching technique described in section 2.5, in which the electrolyte used contained 10% Acetyl acetone, and 1% tetramethyl ammonium chloride in methanol, with an anodic potential of 100 mV v.s. S.C.E. Thin wire shaped specimens were prepared from the extracted

particles for X-ray diffraction.

Extraction carbon replicas were prepared from both thin and bulk specimens. The nitrided specimens were first mounted and then metallographically polished. To avoid the dissolution of fine aluminium nitrides, the specimens were etched for a short time using the same technique used for extracting the nitride particles. The specimens were rinsed in methanol and dried in hot air. A two stage technique was used in which the particles were first lifted from the etched specimens and then transfered onto a thin carbon film (see section 2.4.3.2b) to be examined in the transmission electron microscope.

The extracted particles were also chemically analysed using a scanning electron microscope with a Link Systems micro-chemical X-ray analyser attachment.

4.3 X-ray diffraction results

4.3.1 En41B steel

Fig. 4.1 is an X-ray powder diffraction pattern of the extracted particles obtained from specimens nitrided at 570^{o}C in 13% NH_3. The indexing of the pattern is shown in the adjacent Table 4.1. The interplanar spacings correspond to those expected from f.c.c. CrN with a lattice parameter a = 4.10 $\mathring{A}$. An extra line at d = 2.655 $\mathring{A}$ was observed, but it was so very weak that it did not appear on printing.

The precipitates extracted from specimens nitrided at 500^{o}C in 16% NH_3, showed two sets of lines, one set was

indexed as f.c.c. CrN and the other set was indexed as cementite, indicating that the carbide particles were not totally dissolved during nitriding.

4.3.2 En41(-Cr) steel

The extracted particles from specimens nitrided at 570°C in 13% NH_3, showed two sets of diffraction lines which differred in nature, see Fig. 4.2. The set with sharper yet weaker diffraction lines appeared to be ordered in an f.c.c fashion, with a lattice parameter approximately equal to 4.6 Å. In the second set, the diffracted lines are stronger in intensity but more diffuse than in the first set. The values of the interplanar spacings are identical to those of α-Fe, see Table 4.2. However these lines do not correspond to α-Fe but indicate the presence of another f.c.c phase, which is shown later in this chapter to be aluminium nitride.

At this stage no lines corresponding to the hexagonal AlN were observed, which was attributed to either an absence of AlN, or to poor diffraction by what were presumed to be very fine particles. So an attempt was made to coarsen the particles by ageing some specimens at 700°C for 7h in a 4% N_2 - 96% H_2 atmosphere. These specimens were first nitrided at 570°C in 13% NH_3. The precipitates were extracted by potentiostatic etching as before.

The X-ray diffraction results are shown in Fig. 4.3, where again there are two sets of lines. The strong and broad lines were indexed as hexagonal AlN with a = 3.1 Å and b = 4.99 Å, see Table 4.3. The weak and thin lines have

interplanar spacings identical to those listed in Table 4.2 and compared well to an f.c.c phase with a = 4.6 Å. The other set of lines with interplanar spacings equal to those of α-Fe, which were observed in specimens nitrided at 570°C, are not detected after ageing at 700°C.

The particles extracted from specimens nitrided at 500°C in 16% NH_3, showed strong lines of Fe_3C, which again indicates that the carbide particles did not dissolve at 500°C. An attempt was made to check whether there were any other phase precipitated under these conditions. The cementite particles were separated from the powder by means of a magnet. Only a very small residue remained, but it was enough to prepare a thin wire specimen for X-ray diffraction. The results are shown in Fig. 4.4 and the interplanar spacings are listed in the adjacent Table 4.4. There are two sets of lines, the weak ones are indexed as cementite, and come from smaller Fe_3C particles which were not removed during the magnetic separation. The other set of lines appeared to have interplanar spacing values matching those found earlier at 570°C, with an f.c.c arrangement and a lattice parameter of 4.6 Å.

4.3.3 Fe-C-Al steel

The X-ray diffraction pattern from the powder particles extracted from thin specimens nitrided at 570°C in 13% NH_3 again showed two sets of diffracted lines. One set has a very weak intensity and diffuse lines, and was indexed as hexagonal AlN. The other lines were strong but also diffuse,

and the interplanar spacings matched those of α-Fe, see Fig. 4.5 and Table 4.5.

The specimen nitrided at 500°C in 16% NH_3, showed an Fe_3C pattern only.

4.3.4 Fe-0.52 Al alloy

Repeated attempts to extract precipitates from specimens nitrided at 500°C in 16% NH_3, by potentiostatic etching, ended without success. Each time the specimens were totally dissolved away without leaving behind any particles.

The specimens nitrided at 570°C in 13% NH_3 gave a small ammount of precipitates, but it was not possible to get clear X-ray diffraction patterns from the extracted powder. With specimens which had first been cold rolled then nitrided at 570°C in 13% NH_3, however, the amount of the extracted precipitates was much larger than those collected from specimens nitrided in the as-tempered condition. The X-ray diffraction pattern obtained from these particles is shown in Fig. 4.6. There are two sets of lines that can be seen, with d-spacings as listed in the adjacent Table 4.6. The faint lines were indexed as hexagonal AlN and the strong ones have d-spacings matching those of α-Fe.

Some of the specimens which were originally nitrided at 570°C in 13% NH_3 for 24h, were aged at 700°C for 7h and at 900°C for 4h in a 4% N_2 - 96% H_2 atmosphere. This experiment was made to coarsen the particles in order to get stronger diffraction, and also to see the effect of high temperature on the precipitated phases. The diffraction patterns for

each treatment are shown in Fig. 4.7(a) and (b). The pattern obtained from specimens aged at 700°C (Pattern a) shows lines of hexagonal AlN only, the other set of lines which was observed in non-aged specimens has disappeared.

Pattern (b), which was obtained from specimens aged at 900°C shows lines of hexagonal AlN with a stronger intensity, and there are also some extra lines with spacings which do not fit in with any nitride phases that could possibly occur in this alloy, see table 4.7.

4.4 Electron diffraction results

The carbon replica technique described in section 2.4.3.2(b) were found to be most useful in detecting the precipitated phases, especially in the cases where some phases were difficult to detect by X-ray methods or by thin foil techniques. Direct extraction carbon replicas and two stage extraction carbon replicas were used in the present investigation.

4.4.1 En41B steel

Fig. 4.8 is a diffraction pattern obtained from an extraction carbon replica which was taken from a specimen nitrided at 570°C in 80% NH_3 for 48 h. The pattern is indexed as f.c.c CrN. The d-spacings are listed in Table 4.8.

The diffraction lines from hexagonal AlN are much weaker than those diffracted from CrN, and are further weakened as the diffracted beam is transmitted through the carbon film. So in order to avoid this and to get stronger diffraction, the carbon film was cracked and the diffraction

pattern was taken from the precipitates bridging these cracks. The diffraction pattern shown in Fig. 4.9 was taken by this method, and it clearly shows another pattern as well as the f.c.c CrN ring pattern. These extra rings were indexed as hexagonal AlN, see Table 4.9.

4.4.2 En41(-Cr) steel

A two stage extraction carbon replica method was used for this steel to avoid the dissolution of the fine precipitates of AlN. Carbon replicas of both bulk and thin nitrided specimens were examined.

Three different phases were consistently observed in the nitrided specimens of this steel. These phases were:

4.4.2(a) Hexagonal AlN

This phase was found to precipitate under all nitriding conditions, but the size and distribution of the particles in thin specimens nitrided in low NH_3 concentrations appeared to be greatly influenced by the nitriding temperature. Fig. 4.10 is a two stage extraction carbon replica taken from a thin specimen nitrided at $570^{o}C$ in 13% NH_3. It shows a very fine and evenly distributed needle-like precipitate, whereas thin specimens nitrided at $500^{o}C$ in 16% NH_3, showed larger precipitates of hexagonal AlN. These were found to occur in isolated areas in which the individual particles appeared to have been nucleated on dislocations, see Fig. 4.11.

The hexagonal AlN was found to precipitate readily in bulk specimens nitrided at 500^{o} or $570^{o}C$ in 80% NH_3. The

particles were found to be finer and evenly distributed nearer to the surface of the nitrided specimens, and become larger at successive depths in the nitrided layer. The particles appear to be finer in specimens nitrided at 570°C than in specimens nitrided at 500°C.

4.4.2(b) "Cubic-AlN"

Another well defined ring pattern was consistently observed in the extraction replicas of both bulk and thin specimens nitrided at 500° and 570°C. The d-spacings match well with those of α-Fe, as has already been observed by X-ray diffraction. The particles that gave this pattern are very fine and evenly distributed, but it was not possible to distinguish between these precipitates and hexagonal AlN since both are finely dispersed. The particles of both phases appeared to have similar characteristics regarding size and distribution, as can be fairly judged from the diffraction patterns. Table (4.10) lists the d-spacings of this phase as observed in the diffraction pattern shown in Fig. 4.12 which also contains rings of hexagonal AlN.

4.4.2(c) "CaO.MnO"

A third phase which was occasionally observed in the extraction carbon replicas, as a large precipitate, probably single crystal, is shown in Fig. 4.13(a) and (c). The diffraction pattern shown in Fig. 4.13(b), was indexed as a b.c.c phase with a lattice parameter approximately equal to 3.72 Å, see Table 4.11. However, it is believed that the

"phase" is nothing but a large inclusion; and it was found in the ASTM index that the compound CaO.MnO has a b.c.c structure with d-spacings matching the observed ones. This "phase" was only observed in the nitrided specimens of the investigated steels i.e. En41B, En41(-Cr) and Fe-C-Al.

4.4.3 Fe-C-Al steel

In this material, hexagonal AlN was observed in the bulk specimens nitrided at 500^{o} and 570^{o}C in 80% NH_3. The precipitates were found to be much finer at the surface. Also it was noticed that the precipitates are generally larger in the specimens nitrided at 500^{o}C.

The phase with the "α-Fe" type d-spacings also gave a strong diffraction pattern. Typical diffraction patterns that were consistently observed in the nitrided specimens are shown in Fig. 4.14(a) and (b), and the d-spacings measured from these patterns are given in Table 4.12. Pattern (b) which was taken from an area just under the white-layer is clearly less spotty than pattern (a) which was taken from the middle of the nitrided layer. Also the diffraction rings from the (101) and (002) planes of the hexagonal AlN are so diffuse in pattern (b) that together they make just one broad ring, but they are clearly distinguished in pattern (a). This is a further confirmation of the fact that AlN precipitates are much finer near the surface.

The phase with the b.c.c structure and a lattice parameter of 3.72 $\mathring{A}$ which is believed to be CaO.MnO, was also observed in this material occasionally.

4.5 X-ray microanalysis results

The extracted precipitates from nitrided thin specimens were analysed using scanning electron microscopy with a Link Systems X-ray microanalysis attachment.

The specimens for the analysis were prepared by mixing the precipitates with small amounts of gum and distilled water and shaping into small pellets. These were glued on to graphite stubs before analysis. The specimens that had first been used for X-ray diffraction were also used as samples for X-ray microanalysis.

4.5.1 En41B steel

The analysis was made only for precipitates extracted from specimens nitrided at 570^{o}C in 13% NH_3, and under these conditions the specimen will be totally decarburized, which ensures that the carbides do not interfere with the analysis results.

Fig. 4.15 is an analysis trace from the extracted precipitates. It shows that chromium, aluminium and silicon are the dominant elements, and there appears to be a significant amount of molybdenum. Traces of other metallic elements like iron and manganese are also present. The presence of manganese can not be seen directly, but it can be inferred from the high ratio of Cr K_β/Cr K_α. Traces of non-metalic elements like Ca and Cl were also detected.

4.5.2 En41(-Cr) steel

The X-ray traces from the extracted precipitates from a thin specimen nitrided at 570^{o}C in 13% NH_3 is shown in

Fig. 4.16. In this material the dominant elements are aluminium and silicon, but the molybdenum peak is again significantly high, and also there are traces of manganese and iron. The proportions of the Al, Si and Mo in this precipitate appears to be similar to those in En41B.

Thin specimens nitrided at 570°C then further annealed at 700°C, showed a significant decrease in the Si and Mo peaks in proportion to the Al peak, see Fig. 4.17. This could be attributed to the precipitation of further AlN which increases the amount of Al in the extracted powder.

4.5.3 Fe-C-Al steel

The X-ray plot shown in Fig. 4.18 was obtained from precipitates in a thin specimen nitrided at 570°C in 13% NH_3. It is clear that Al is the only dominant element, but also there are traces of Si and Fe. The presence of silicon is attributed to a small contamination of the material which occurs during preparation of the cast, silicon usually coming from the crucible inner walls which were glazed by silica.

4.6 Identification of the precipitated phases

In the previous sections, it has been shown that at least five phases are observed in the nitrided aluminium containing steels, two of which were unequivocally identified. These were f.c.c CrN and hexagonal AlN.

The other phases, whose presence was confirmed either by X-ray diffraction or by electron diffraction or by both methods, were not previously known, taking into consideration

the chemical composition of the investigated material.

In this section, each phase will be dealt with individually, giving details of its identification and occurrence.

Two of the observed phases were clearly identified as nitrides. These are:

4.6(a) f.c.c CrN

This phase was observed only in the commercial steel En41B. It has a lattice parameter equal to approximately 4.1$\mathring{A}$, and was found to precipitate readily at both temperatures i.e. 500^{o} and 570^{o}C, and in low ammonia concentrations. This is a well known phase and it has been reported before by many authors.

4.6(b) Hexagonal AlN

Hexagonal AlN with lattice parameters a = 3.1A and c = 4.96 $\mathring{A}$ was observed in all the investigated materials. It was found to precipitate more readily at 570^{o}C than at 500^{o}C when nitriding was carried out in low ammonia concentrations. The particles produced at 570^{o}C are finer than those produced at 500^{o}C in the same alloy. Also it was noticed that the particle size seems to be finer in En41(-Cr) steel than in Fe-C-Al when both materials are nitrided under the same conditions. This phase has long been recognized, and has been mainly observed in aluminium killed steels.

4.6(c) CaO.MnO

This phase was observed only in the nitrided steels. It has a b.c.c structure with a lattice parameter approximately equal to 3.72 $\mathring{A}$, an occurs as a large precipitate. Although this phase was not observed in the tempered steels, it is assumed that it already existed in the tempered material, but was not detected.

4.6(d) F.c.c phase, a = 4.6 $\mathring{A}$

An f.c.c phase with lattice parameter approximately a = 4.6 $\mathring{A}$ was observed in nitrided En41(-Cr) steel only. The phase can only be detected by X-ray diffraction, which indicates that it has fairly large sized particles and precipitates in small quantities. Fig. 4.19 is an X-ray microanalysis trace of the extracted precipitates from thin specimens nitrided at 500°C in 16% NH_3, showing the presence of silicon, molybdenum, manganese, and traces of aluminium and zirconium. The latter element is not intended to be present in this steel. However, the observed phase characteristics i.e. the d-spacings and the lattice parameter were found to compare well with those of ZrO or ZrN. This is an undesirable contamination of the original material, because a small amount of zirconium in the steel could interfere with the nitriding results and cast some doubt about the true identity of this particular phase. However, when the extracted particles from thin specimens nitrided at 570°C in 13% NH_3 were analysed by the same method, the X-ray plot did not show any trace of zirconium, see Fig. 4.16. Similar tests on

extracted particles from thin specimens first nitrided at 570°C in 13% NH_3 then annealed at 700°C in a 4% N_2/H_2 atmosphere again revealed no traces of zirconium on the X-ray plot. In both cases the f.c.c phase was observed by X-ray diffraction, see Figs. 4.2 and 4.3. This suggest that the zirconium-rich particles are large and randomly dispersed in the steel, so that they give a positive indication when a large volume of extracted particles are examined by X-ray diffraction, but do not appear in the relatively small volumes which are examined on replicas. The source of the zirconium remains unclear.

4.6(e) "α-Iron" phase

The other unknown phase has d-spacings matching those of "α-Fe". The phase was detected by X-ray diffraction and by electron diffraction, and it was observed in En41(-Cr) and Fe-C-Al steels as well as in the Fe-0.52 Al alloy. It was not possible to detect the phase in En41B steel due to the precipitation of CrN, in which the strongly diffracting (200), (220), (222), (400), (420) and (422) planes have matching spacings to those of "α-Fe". The possibility that this phase may in fact be iron was taken into consideration. A quantitative analysis was made on a sample of the extracted precipitates from thin specimens of En41(-Cr) steel nitrided at 570°C in 13% NH_3. The sample was analysed for the elements that showed significant peaks on the X-ray analysis plot, namely Al, Si, Mo, Mn and Fe.

Table 4.13 lists the percentage by weight of the above elements in the sample. The aluminium forms 51 wt.% and

silicon 23.5%. The rest of the elements i.e. Mo, Mn and Fe form 11.8, 7.8 and 5.9 wt.% respectively. These figures show that iron constitutes only a small fraction of the total elements present (in atomic proportions the amount is only 3%). However, it is unlikely that all this amount is in the form of free iron particles, since there is likely to be some iron oxide and even undissolved carbide. Moreover, the samples that were used for X-ray diffraction and for X-ray analysis were treated before hand by a magnet, to ensure the removal of iron carbide from the extracted precipitates, which would also remove iron. The magnetically treated samples gave the same result as the non-treated ones, which implies that the observed "α-Fe" type pattern does not originate from iron itself.

Furthermore, the "α-Fe" type patterns obtained from extraction carbon replicas of nitrided irons and steels containing Al were consistent and very clear. No such pattern was observed in the extraction carbon replica of tempered specimens, when using the same extraction method. And finally the intensities in the diffraction patterns in both electron and X-ray diffraction are different from those of iron. So the possibility that iron might have been responsible for the appearance of the pattern was ruled out.

Careful examination of the electron diffraction patterns and X-ray diffraction patterns, after different nitriding treatments, revealed certain facts:

Firstly, in nitrided bulk specimens the ring patterns obtained from extraction carbon replicas of thick specimens nitrided at 500^{o} and $570^{o}C$ in 80% NH_3, tends to become spottier

at successive distances from the surface of the nitrided layer. This indicates that the particles responsible for the appearance of the pattern are finer nearer to the surface, which is typical of nitride precipitation in bulk specimens.

Secondly the pattern totally disappeared when nitrided thin specimens were annealed at 700°C for 7h in a N_2/H_2 atmosphere, but the pattern was present after nitriding at 570°C in 13% NH_3. This was observed in En41(-Cr) steel and in the Fe-0.52 Al alloy. This sort of behaviour indicates that the precipitates are not stable at higher temperatures, and they either dissolve or transform into another phase. The only other phase that was observed at both nitriding temperatures i.e. 500° and 570°C, and after annealing at 700°C was the hexagonal AlN. So if the particles do transform into another phase then it would be hexagonal aluminium nitride.

In the light of the above observation, the most likely explanation for the appearance of the "α-Fe" type pattern is the precipitation of a f.c.c AlN. This kind of precipitation is not common or widely known, but it has been previously reported on one occasion, in which a f.c.c AlN was observed in aluminium killed low carbon steel. By means of electron microscopy, Hanai et al. (63) found that at an early stage of the precipitation of AlN in the course of annealing cold-rolled and hot-rolled strips of a commercial low-carbon aluminium killed steel, fine cubic precipitates appeared and changed into the well known hexagonal aluminium nitride by extended annealing or by annealing at high temperatures. The authors were able to show that cubic precipitates are closely connected

with recrystallization behaviour.

If the diffraction patterns which were observed in the present work are compared with the ones reported by Hanai et al. it is noticeable that the characteristics of both patterns are very much the same in terms of the interplanar spacing, the relative intensity and the missing planes, see Table 4.14.

It was explained by Hanai et al. that the pattern does not conform to those of carbo-nitrides of aluminium, iron, or manganese charted up to that time. But several of the inter-planar spacings of the cubic precipitates can be seen as conforming to those of iron and other iron-like body centred cubic metals, and to those of aluminium and other aluminium likeface centred cubic metals or to those of Fe_3Al. Iron was ruled out because the intensity at d = 1.1702 Å should have been stronger than at d = 1.4332 Å. Although the interplanar spacings of aluminium fitted those of the cubic precipitates. In f.c.c. metals, diffraction is impossible except when all of theMiller indices h,k,l are odd or even and the intensity of {111} is stronger than that of {200}. In the cubic precipitate, the intensity of {111} is very weak while that of {200} was the strongest. Consequently the cubic precipit-ates cannot be identified as aluminium.

However, the diffraction pattern of the cubic precipitate fits very well with that of the NaCl structure shown in Fig. 4.21. The structure factor for the NaCl

structure is strong when all of the Miller indices h,k,l are even, and weak when all are odd.

By assuming that the cubic precipitates do have the NaCl structure, the lattice parameter is a = 4.05 Å. The authors were able to calculate the intensity ratio for the diffraction peaks according to the following equation (64):

$$I_{hkl} = I_o \cdot |F_{hkl}|^2 \cdot m \cdot \lambda^3 \cdot V/16 \cdot \pi \cdot \nu^2 \cdot \sin^2 \theta \qquad 1$$

where

I_o = The intensity of the incident electron beam

F_{hkl} = The structure factor of {hkl}

m = The multiplicity factor of {hkl}

V = The volume of the crystal

ν = The volume of a unit cell

θ = Bragg angle

λ = The wave length of the electron beam.

The calculated intensity values fitted well with the measured ones, see Table 4.14.

Finally, Hanai et al. pointed out that the structure of cubic AlN is similar to that of hexagonal AlN. The hexagonal AlN has aluminium atoms on close packed hexagonal lattice sites and nitrogen atoms at intermediate sites, where each atom is surrounded symmetrically by four atoms of the other kind, see Fig. 4.20. The cubic AlN, on the other hand, may be considered as two interpenetrating f.c.c lattices of aluminium and nitrogen, where each atom is mutually in the octahedral position, see Fig. 4.21. These two therefore

should be able to transform into each other with little atomic displacement. Also it was presumed that the cubic AlN has a strong metallic bond character, because in it aluminium atoms occupy f.c.c positions and nitrogen atoms of the smaller atomic radius occupy the octahedral position. On the other hand the hexagonal AlN has a covalent character with 4:4 tetrahedral coordination. Consequently, in as much as aluminium metal exists in the f.c.c form, it may be that AlN should exist as NaCl structure with nitrogen atoms on the octahedral positions of the f.c.c lattice of aluminium at low temperatures, lower than about the melting point of aluminium, 660^{o}C, and that AlN at high temperatures should be of a stable compound with covalent bonds with aluminium atoms in close packed hexagonal positions. This behaviour was also noticed in the present work, in which f.c.c AlN was only observed in specimens nitrided at 500^{o} and 570^{o}C, and when specimens nitrided at 570^{o}C were annealed at 700^{o}C, only hexagonal AlN was observed and the f.c.c AlN totally disappeared. This supports Hanai et al's proposals.

4.7 Conditions for the occurrence and detection of the nitride phases

The nitride phases detected in the nitrided aluminium containing steels are shown in Table 4.15. CrN was detected in chromium containing En41B steel only, while hexagonal AlN was detected in En41B, En41(-Cr) and Fe-C-Al steels and Fe-0.52 Al alloy. The cubic AlN was detected in En41(-Cr), Fe-C-Al and Fe-0.52 Al alloy. If this phase does occur in

En41B, it would not be possible to detect because all the interplanar spacings match those from CrN precipitates which are stronger in intensity. The f.c.c zirconium-rich phase was only detected in En41(-Cr).

For En41B steel, CrN was easily detected by both replica and X-ray diffraction techniques at all nitriding conditions. Table 4.16 shows that hexagonal AlN was only detected by extraction carbon replicas of thick specimen nitrided at 570°C in 80% NH_3. Very fine AlN is difficult to detect by X-ray diffraction. In chromium-free En41(-Cr), hexagonal AlN was easily detected by carbon replica techniques at all conditions whereas cubic AlN was detected by both carbon replica and X-ray diffraction techniques, see Table 4.17.

In Fe-C-Al steel, hexagonal AlN and cubic AlN were detected by both carbon replica methods and X-ray diffraction. Neither nitride was detected at 500°C in low NH_3 concentrations, see Table 4.18.

4.8 Discussion

For the aluminium-containing steels, with and without chromium, the isolation of the different nitride phases from the same material at the same time, by potentiostatic etching techniques, needs a correct solution in which none of the particles should dissolve. A solution containing 10% acetyl acetone, 1% tetramethylammonium chloride in methanol was found to be most suitable.

The detected nitride phases, i.e. f.c.c CrN, hexagonal AlN and cubic AlN were all successfully extracted using this

solution. Another advantage of the solution is that it does not contaminate the extracted precipitates.

The X-ray diffraction method is not suitable for detecting very fine precipitates of hexagonal AlN, for which the diffraction lines are usually very weak and diffuse. Electron diffraction is more practical because it produces diffraction patterns that are clearly visible. No explanation is available for why fine hexagonal AlN is so difficult to detect by X-ray diffraction. On the other hand f.c.c CrN and f.c.c AlN were detected by X-ray diffraction, in which both produced clearly visible patterns, but electron diffraction produces even clearer patterns.

In steels, hexagonal AlN, appears to precipitate readily in bulk specimens at both 500^{o} and 570^{o}C in high NH_3 concentration. However, the precipitation behaviour is different in low NH_3 concentrations. At 570^{o}C hexagonal AlN still precipitates in large quantities, while at 500^{o}C the precipitates appear to be scarce and occurred in isolated clusters, perhaps indicating nucleation only in heavily dislocated regions. Consequently, in tempered steel, the presence of dislocations does not seem to help precipitation of hexagonal AlN in the adjacent non-dislocated regions if nitriding is carried out at 500^{o}C in low NH_3 concentrations, but it does so in high NH_3 concentrations. This suggests that the nitrogen activity is an important factor for the nucleation of hexagonal AlN.

In bulk specimens, the precipitated nitrides are much finer nearer to the surface than at successive depths in the

nitrided layer. This behaviour is governed by the rate of nucleation and subsequent growth. At the early stages of nitriding in high NH_3 concentrations, the rate of nucleation is high, but after ∿ 10 h surface iron nitrides start to form at the surface (65), and since the diffusion of nitrogen in iron nitride is considerably less than that in ferrite, this will decrease the nitrogen flux into the bulk of the specimen. Accordingly the nucleation rate decreases, which results in fewer nitride precipitates. These will grow to a larger size over long periods, whereas the precipitates nearer to the surface do not grow larger because most of the solute atoms are consumed in the early stages of nitriding.

Chemical analysis of En41(-Cr) shows that silicon forms 23.5 wt.% of the metal atoms in the extracted powder of a nitrided thin specimen. The possibility that silicon nitrides could be responsible was ruled out because the Mn:Si ratio in the steel is approximately 1:1 which is much lower than the 3:1 ratio needed to form hexagonal manganese-silicon nitride (66), and no pattern was observed which conformed to any silicon nitride. The likely explanation is that silicon is dissolved in the hexagonal AlN, because both aluminium and silicon nitrides are covalent compounds and have the hexagonal wurtzite-type structure (40). So the hexagonal AlN precipitates could in fact contain high proportions of silicon and the nitride should be referred to as (Al,Si)N.

4.9 Summary and conclusions

1. In nitrided Al containing steels with or without chromium, different types of nitride were detected. These

were f.c.c CrN, hexagonal AlN and cubic AlN.

2. In En41B, f.c.c CrN and hexagonal AlN were detected, CrN forms readily under all nitriding conditions, whereas hexagonal AlN was only detected in specimens nitrided at 570^{o}C.

3. In the experimental En41(-Cr) steel, hexagonal AlN and cubic AlN were observed under all nitriding conditions.

4. Hexagonal AlN precipitates readily at 570^{o}C in low and high NH_3 concentration, whereas at 500^{o}C and low NH_3 concentration precipitation is sparse.

5. The X-ray diffraction technique is not suitable to detect very fine hexagonal AlN.

6. In the nitrided steels that contain aluminium and silicon the hexagonal AlN is rich in silicon.

7. Cubic AlN with the NaCl structure also forms under all nitriding conditions. It can be detected by X-ray diffraction and by electron diffraction. This transforms to hexagonal AlN if the nitrided specimen is annealed at 700^{o}C.

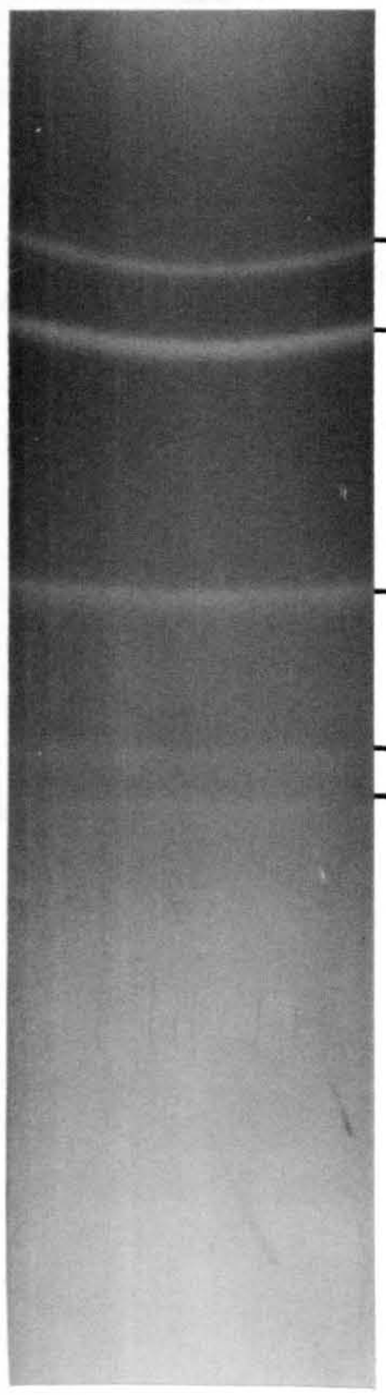

d_{obs} Å	d_{cal} Å	hkl
2.38	2.367	111
2.05	2.05	200
1.45	1.450	220
1.24	1.236	311
1.18	1.184	222

Table 4.1 X-ray data for f.c.c. CrN. Calculated values using a_o = 4.10 Å

Fig. 4.1 X-ray powder pattern of CrN. The particles were extracted from thin specimens of En41B, nitrided at 570°C in 13% NH_3

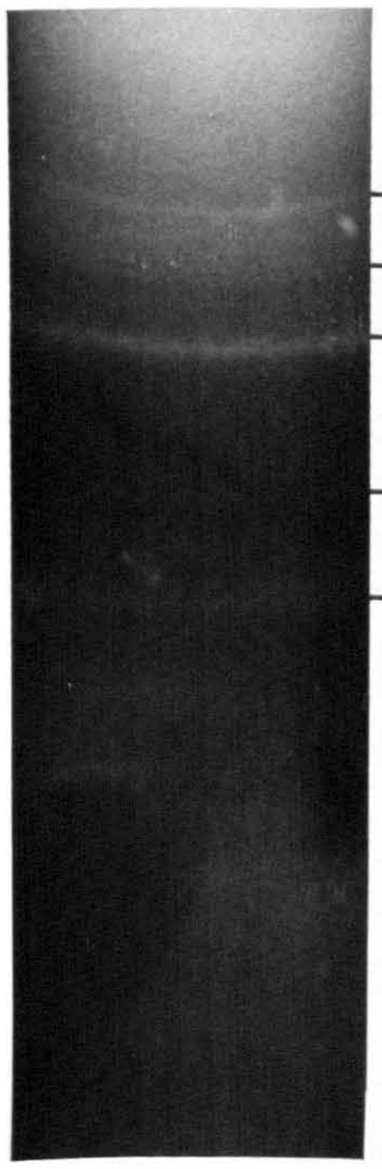

d_{obs} Å	hkl	
	Cubic AlN	f.c.c. phase
2.652		111
2.310		200
2.025	200	
1.622		220
1.435	220	

Table 4.2

X-ray data for "Cubic AlN" and the f.c.c. phase with a = 4.6 Å

Fig. 4.2

X-ray powder pattern of extracted particles from nitrided specimen of En41(-Cr), showing both cubic AlN and f.c.c. phase with a = 4.6Å

$d_{observed}$ Å	h.k.l	
	Hex. AlN	f.c.c phase
2.682	100	111*
2.495	002	
2.367	101	
2.322		200
1.82	102	
1.628		220
1.548	110	
1.388		311
1.319	112	

Table 4.3

X-ray data for hexagonal AlN and f.c.c. phase with a = 4.6Å

Fig. 4.3

X-ray powder pattern showing both hexagonal AlN and f.c.c. phase. Theparticles were extracted from thin specimens of En41(-Cr), nitrided at 570°C in 13% NH_3, then annealed at 700°C

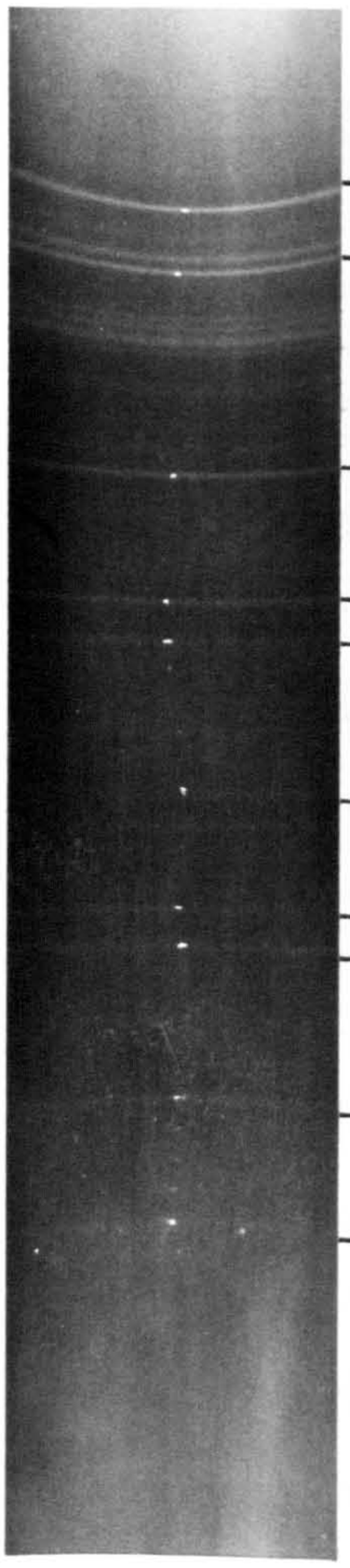

$d_{obs.}$ Å	$d_{cal.}$ Å	hkl
2.665	2.661	111
2.302	2.305	200
1.626	1.629	220
1.390	1.389	311
1.331	1.3307	222
1.159	1.1525	400
1.062	1.0576	331
1.035	1.0308	420
0.945	0.9410	422
0.8907	0.8871	511

Table 4.4

X-ray data for f.c.c. phase with a = 4.6 Å

Fig. 4.4

X-ray powder pattern of f.c.c. phase with a = 4.6 Å, and Fe_3C. The particles extracted from thin specimens of En41(-Cr) nitrided at 500°C in 16% NH_3.

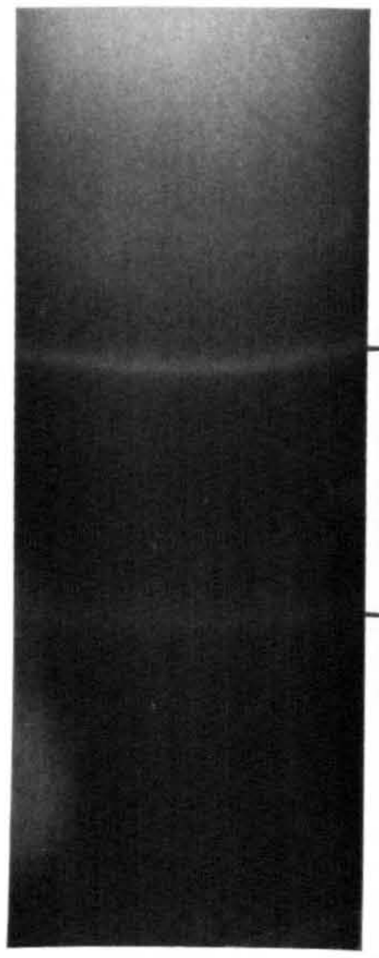

$d_{obs.}$ Å	$d_{cal.}$ Å	hkl
2.035	2.025	200
1.440	1.431	220

Table 4.5

X-ray data for "Cubic AlN" with a = 4.05 Å

Fig. 4.5

X-ray powder pattern showing "Cubic AlN". The particles were extracted from Fe-C-Al specimens, nitrided at 570°C

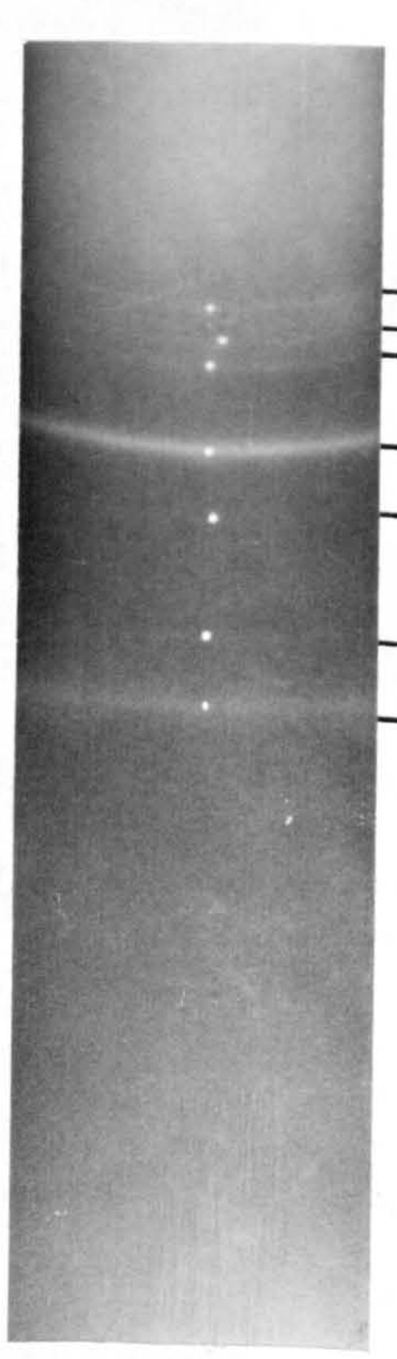

$d_{obs.}$ Å	hkl	
	Hex.AlN	Cub.AlN
2.70	100	
2.49	002	
2.365	101	
2.025		200
1.828	102	
1.552	110	
1.432		220

Table 4.6

X-ray data for hexagonal AlN (a_o = 3.11, b_o = 4.98), and "cubic AlN" (a_o = 4.05 Å) of α-Fe type d spacings.

Fig. 4.6

X-ray powder patterns of hexagonal AlN and "Cubic AlN". The particles were extracted from an Fe-0.52% Al specimen which was first called rolled then nitrided at 570°C in 13% NH_3.

Table 4.7

X-ray data for hexagonal AlN

(a_o = 3.11 Å, b_o = 4.98 Å)

$d_{obs.}$ Å	d_{ASTM} Å	hkl
2.690	2.695	100
2.487	2.490	002
2.355	2.371	101
2.275		
1.988		
1.828	1.829	102
1.612		
1.550	1.5559	110
1.410	1.4133	103
1.372	1.3475	
1.342	1.3475	200
1.318	1.3194	112
1.298	1.3007	201
1.247	1.2450	004
1.182	1.1850	202
1.137	1.1301	104
1.047	1.0461	203
1.019	1.0184	210
0.9985	0.9978	211
0.9720	0.9720	114
0.9335	0.9340	105
0.8940	0.8932	300
0.8680	0.8680	213
0.8485	0.8448	302

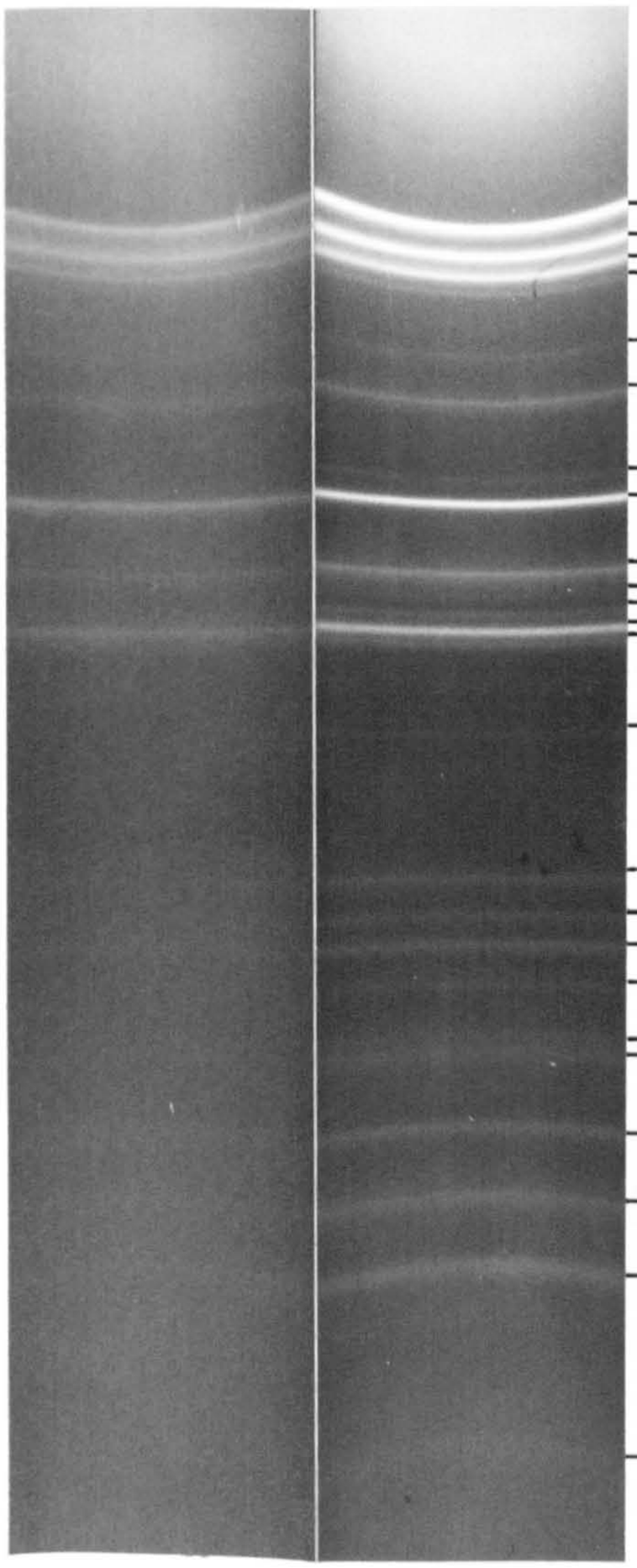

Fig. 4.7

X-ray powder pattern of hexagonal AlN. Thin specimen of Fe-0.52 Al, nitrided at 570°C in 13% NH_3 then annealed at a) 700°C b) 900°C.

Fig. 4.8

(a) Bright field micrograph of an extraction carbon replica from the middle region of a nitrided bulk specimen of En41B, showing large particles of CrN. Specimen was nitrided at $570^{o}C$ in 80% NH_3

(b) Electron diffraction ring pattern of CrN obtained from the same area shown in (a). The spotty pattern indicating large CrN particles.

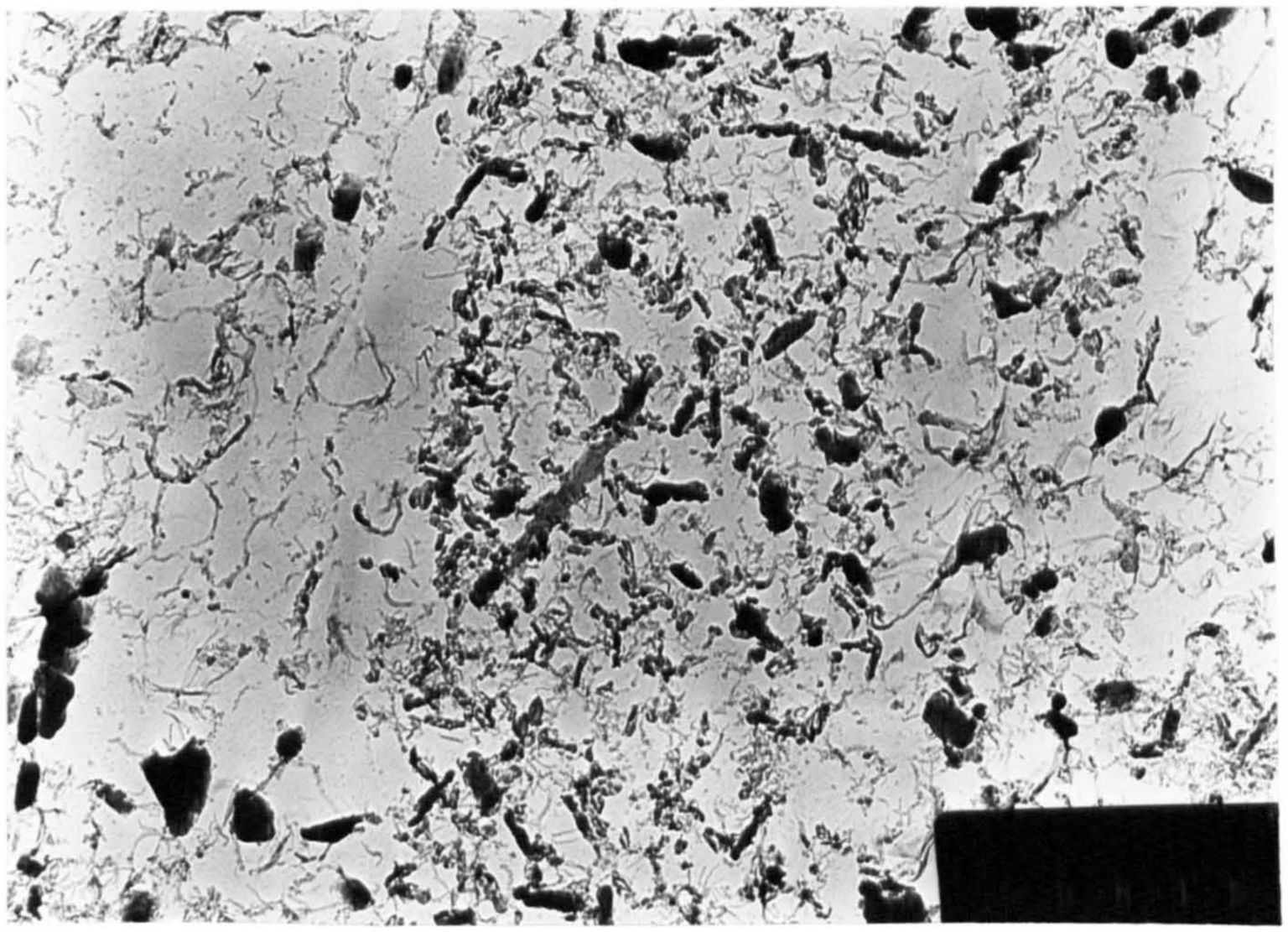

a

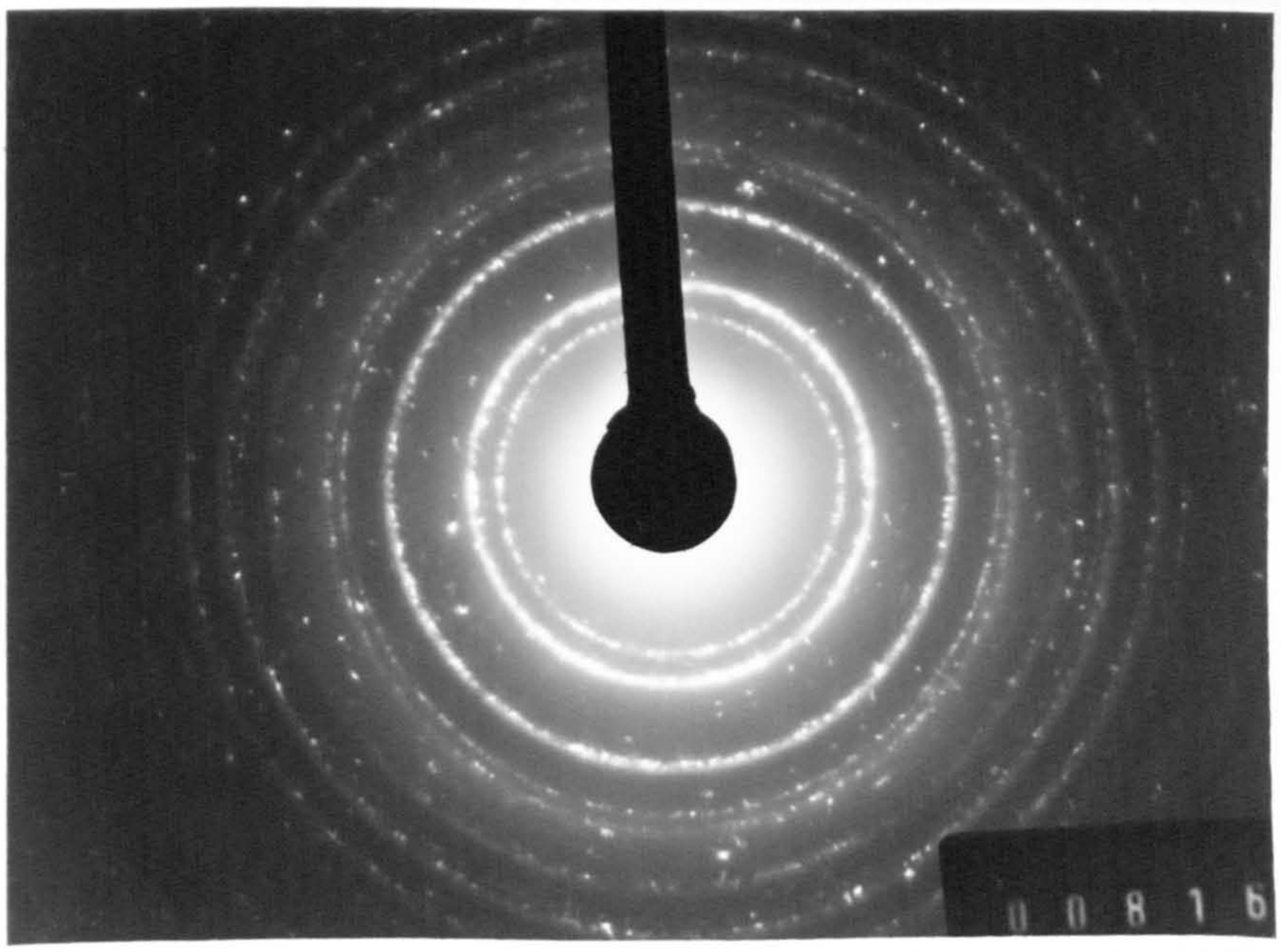

b

Fig.(4.8)

$d_{obs.}$ Å	$d_{cal.}$ Å	hkl
2.394	2.37	111
2.043	2.05	200
1.450	1.45	220
1.25	1.236	311
1.19	1.183	222
1.03	1.025	400
0.92	0.916	420

Table 4.8

Electron diffraction data of CrN as observed in Fig. 4.8(b). Calculated values using a_o = 4.1 Å

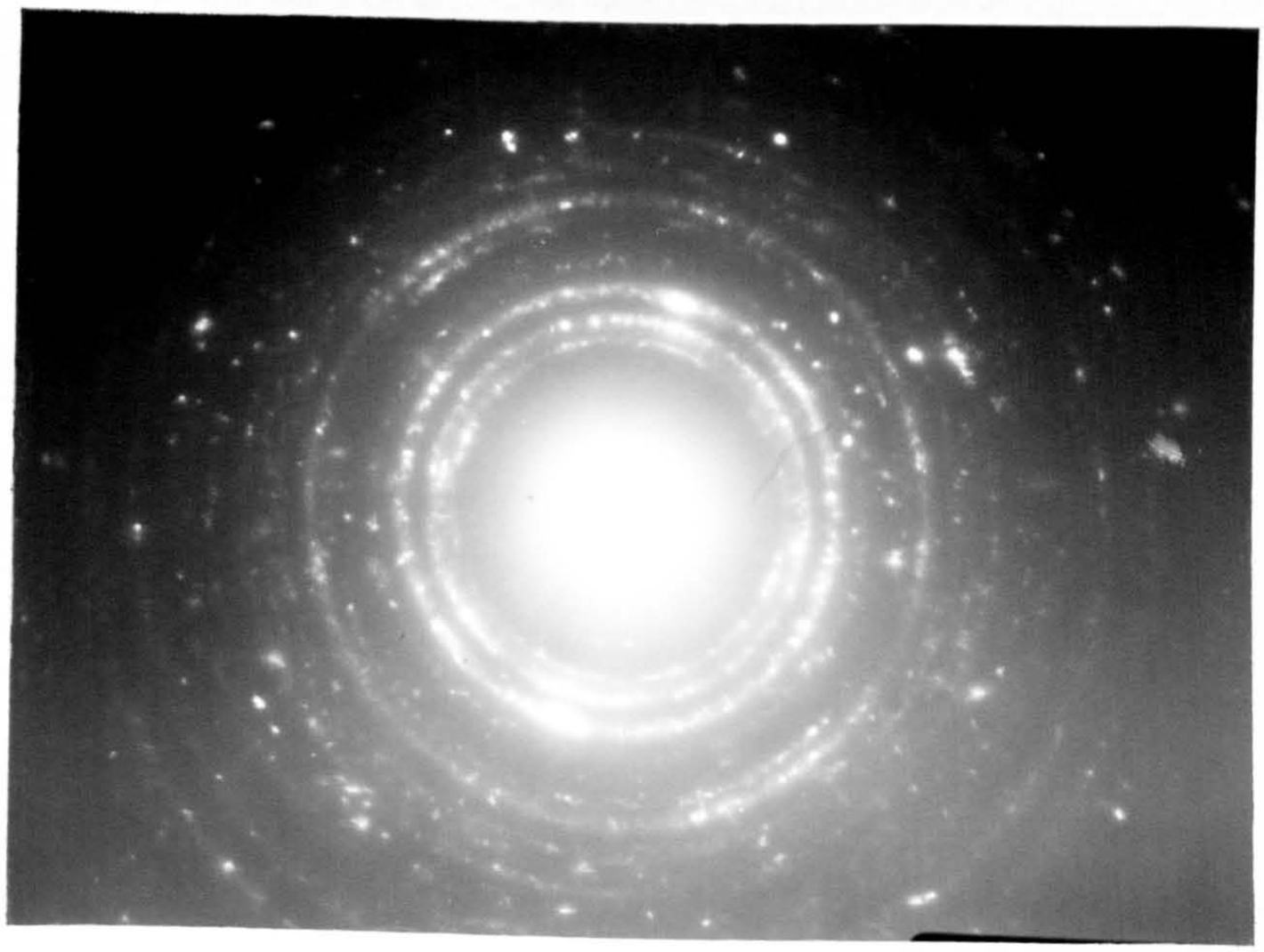

Fig. 4.9

Electron diffraction pattern from a two-stage extraction carbon replica of a bulk specimen of En41B, nitrided at 570°C in 80% NH_3 for 48h

$d_{obs.}$ Å	hkl	
	CrN	Hex. AlN
2.70		100
2.395	111	101
2.066	200	
1.851		102
1.566		110
1.462	220	
1.320		112
1.250	311	

Table 4.9

Electron diffraction data for CrN and hexagonal AlN as measured from the diffraction pattern shown in Fig. 4.9

Fig. 4.10 Transmission electron micrograph of a two-stage extraction carbon replica obtained from a thin specimen of En41(-Cr) nitrided at 570°C in 13% NH_3, showing two types of precipitates; very fine needles and "dotes". The diffraction pattern indicates the presence of hexagonal AlN and "cubic AlN".

Fig. 4.11 As in Fig. 4.10 but nitrided at 500°C in 16% NH_3. Note the larger size of hexagonal AlN, which is confirmed by a spotty ring pattern. No "cubic AlN" was observed.

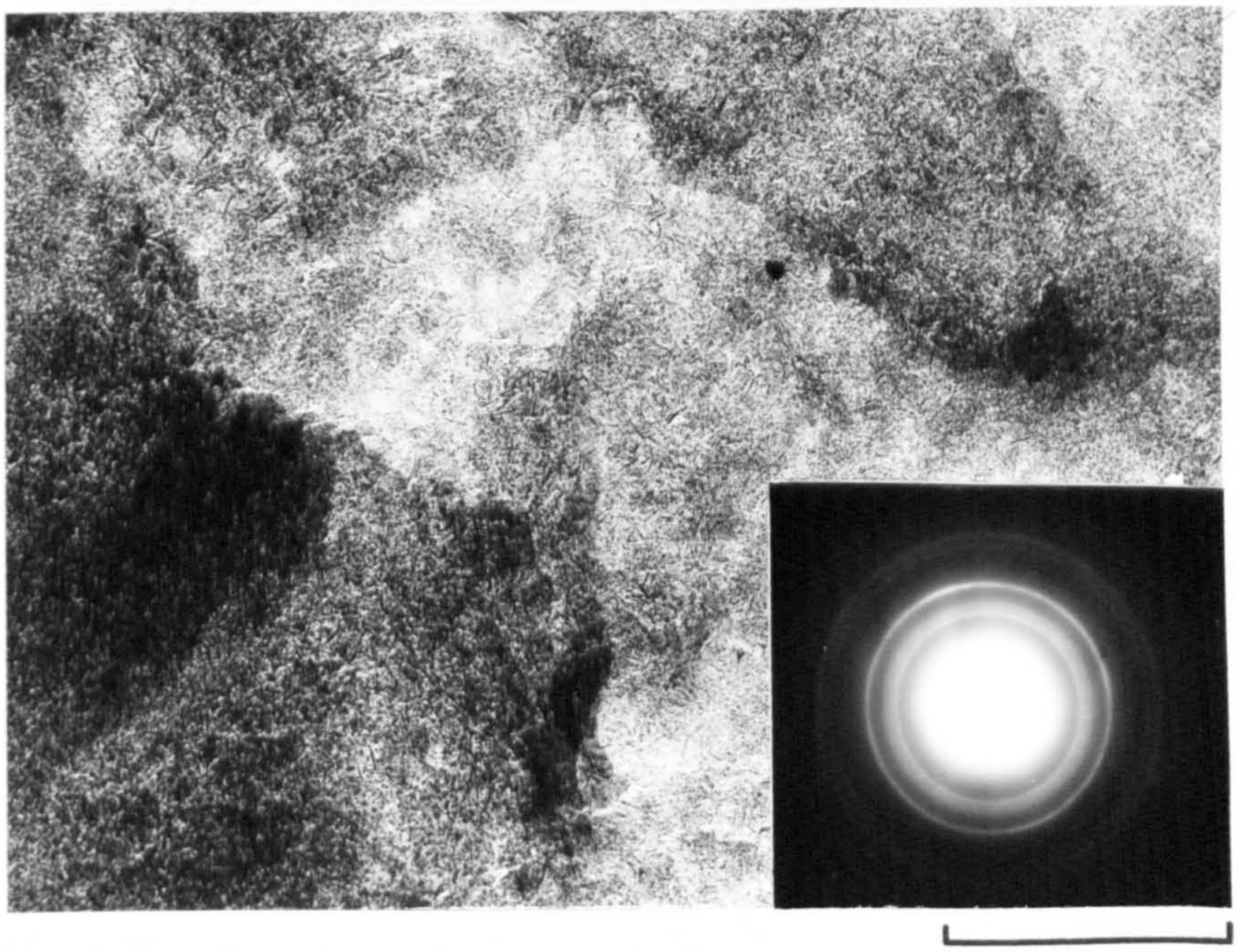

0.5 um

Fig. (4.10)

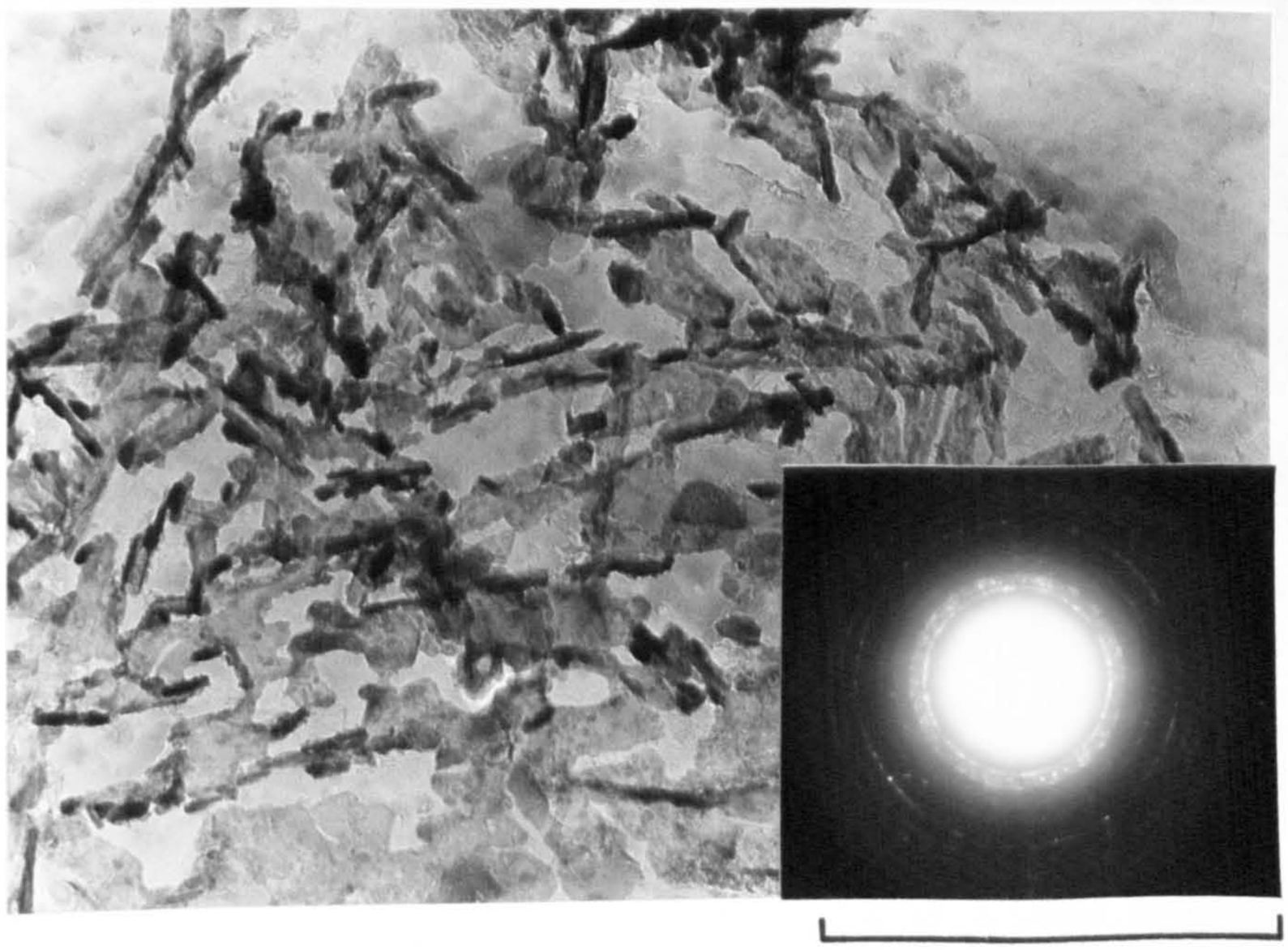

0.5 um

Fig. (4.11)

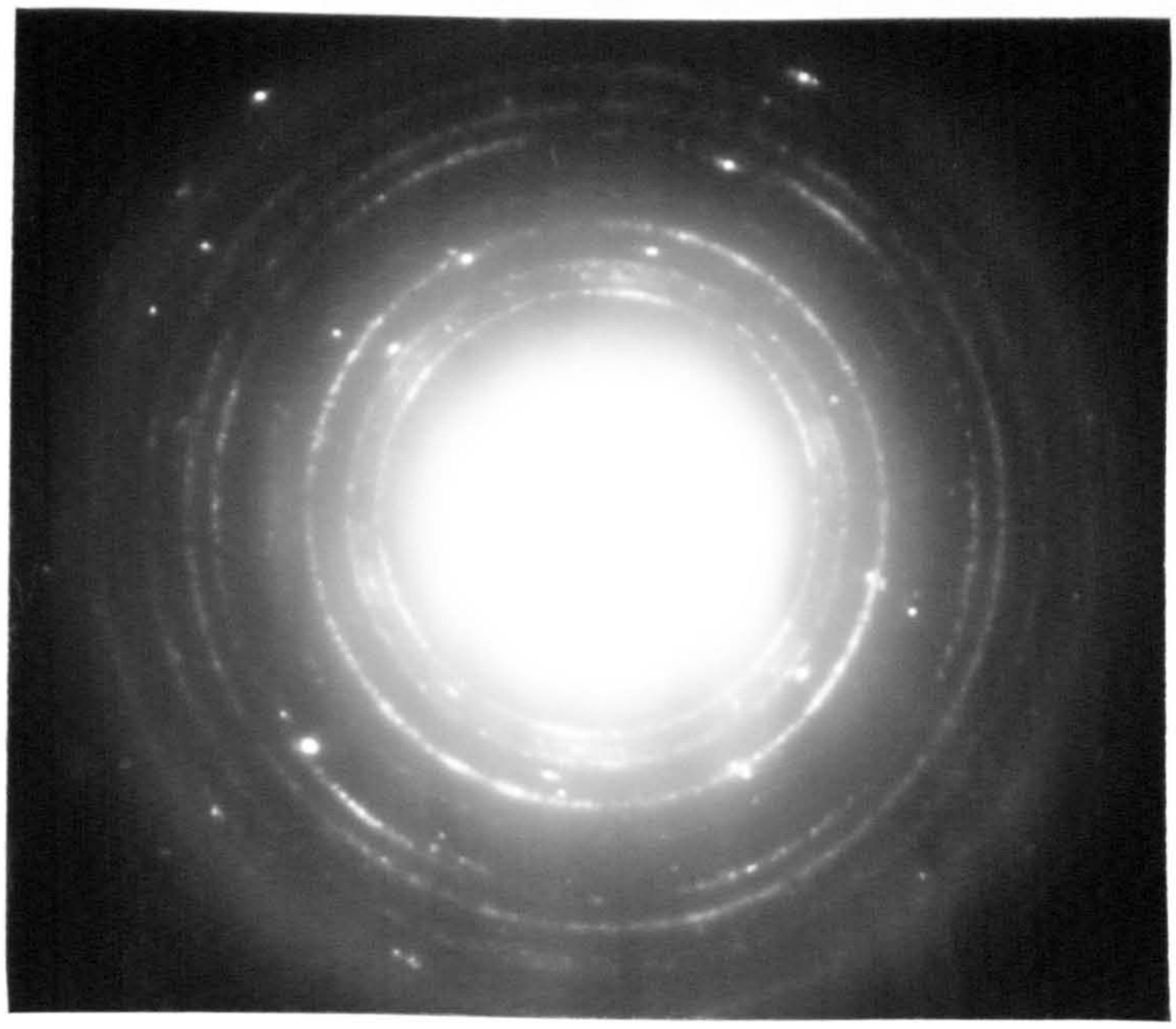

Fig. 4.12 Electron diffraction from an extraction carbon replica of a nitrided En41(-Cr) showing ring patterns of cubic and hexagonal AlN

$d_{obs.}$ Å	$d_{cal.}$ Å	hkl
2.030	2.025	200
1.434	1.432	220
1.164	1.169	222
1.019	1.025	400
0.908	0.906	420
0.826	0.827	422

Table 4.10

Electron diffraction data for cubic AlN as observed in Fig. 4.12.

Calculated values using a_o = 4.05 Å

Fig. 4.13

(a) Bright field micrograph of a two-stage extraction replica, showing large size precipitate of CaO.MnO, in a nitrided thin specimen of En41(-Cr).

(b) Diffraction pattern from the above

(c) Dark field of the same particle in (a)

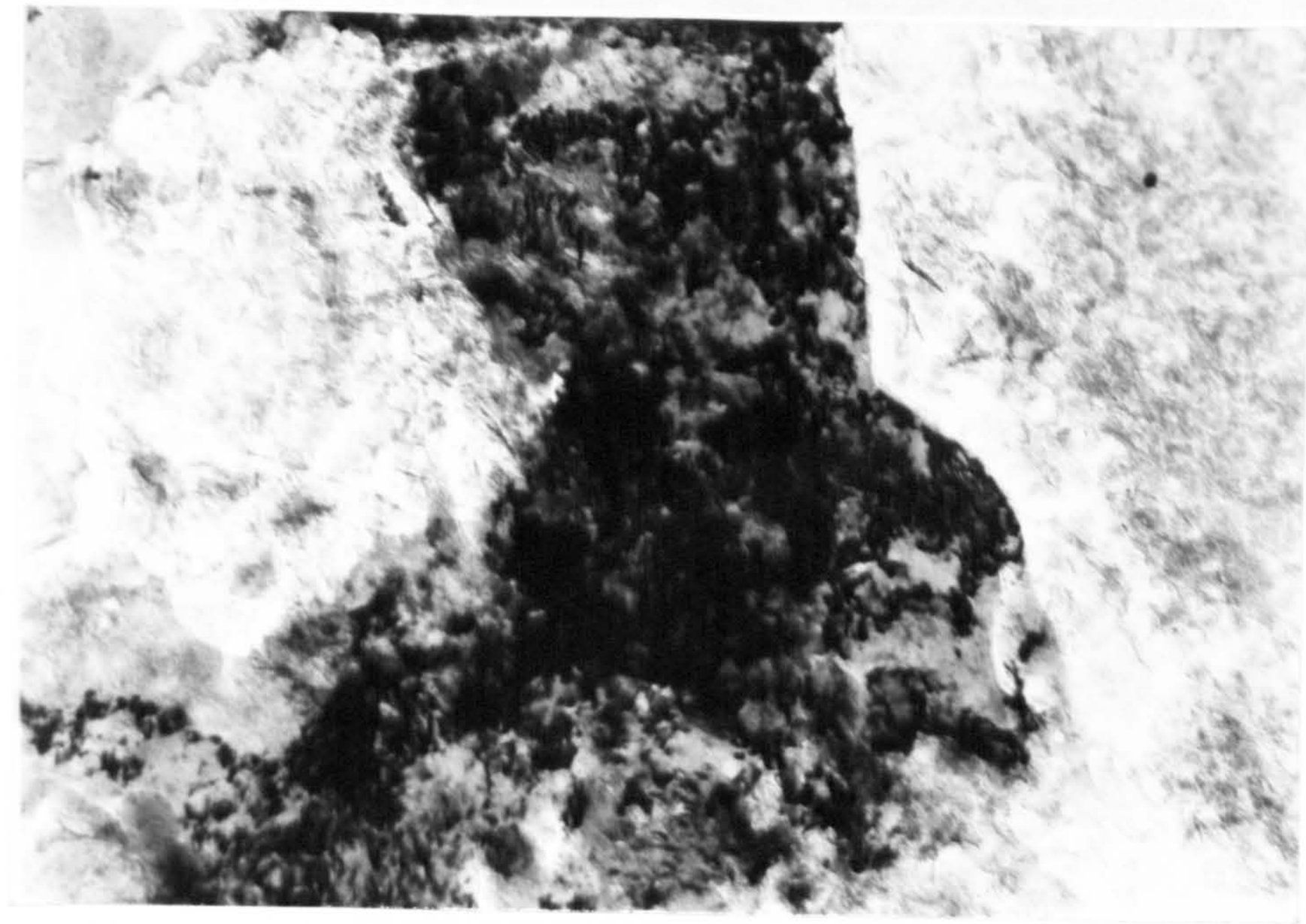

a

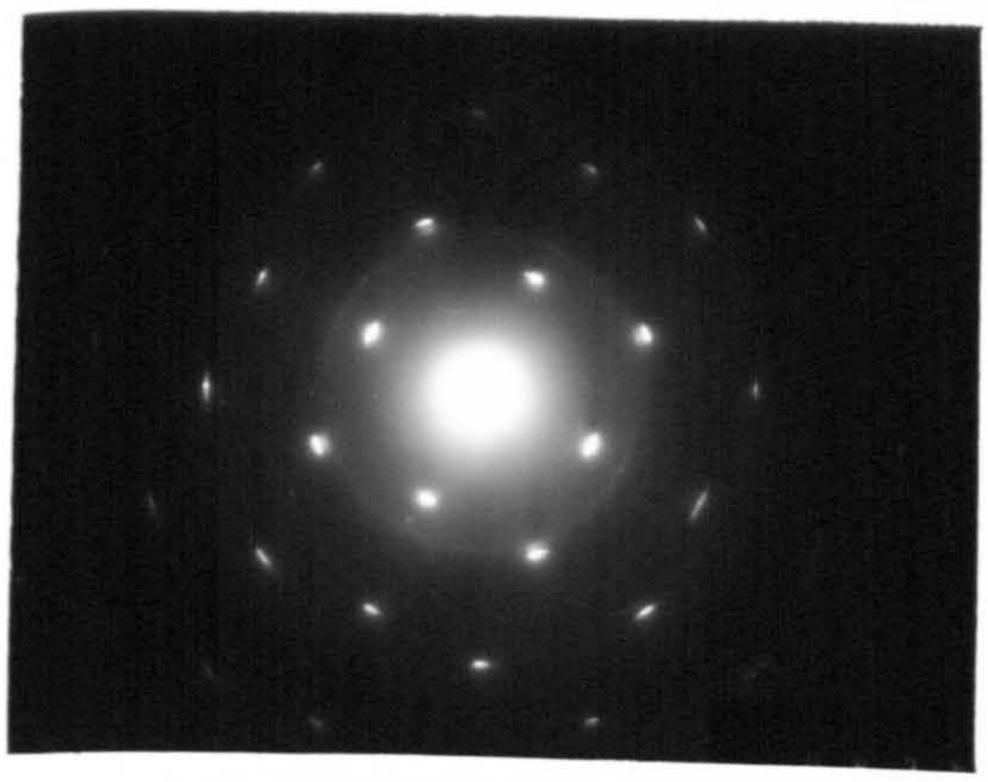

b

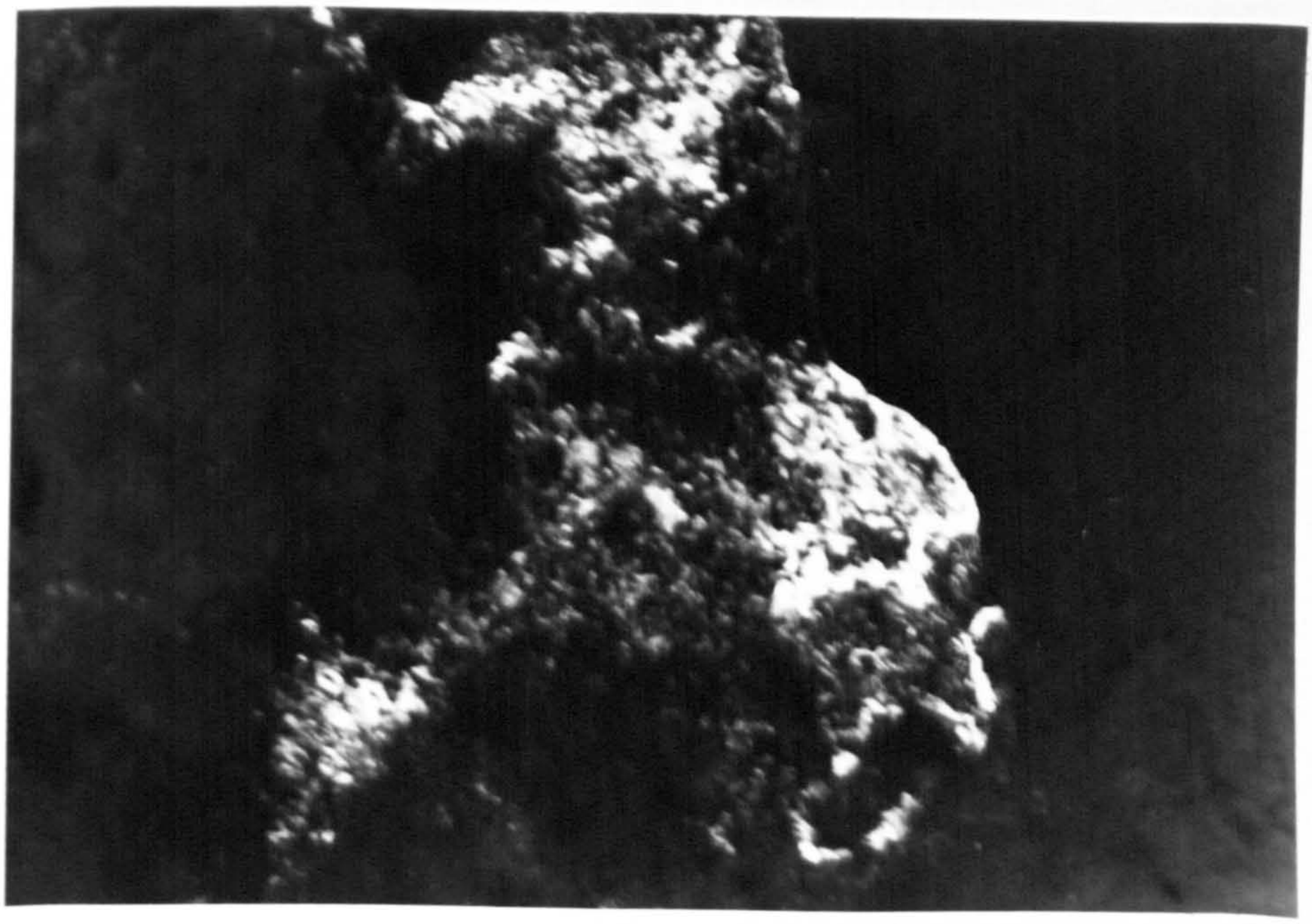

c

0.25 um

Fig.(4.13)

$d_{obs.}$ Å	$d_{cal.}$ Å	hkl
2.634	2.630	110
1.878	1.860	200
1.526	1.518	211
1.317	1.315	220
1.178	1.176	310
1.078	1.073	222
0.933	0.930	400
0.877	0.877	411
0.832	0.832	420

Table 4.11

Electron diffraction data for CaO.MnO, as observed in Fig. 4.13(b). Calculated values using a = 3.72 Å

Fig. 4.14 Electron diffraction pattern obtained from a two-stage carbon extraction of a bulk specimen of En41B steel nitrided at 570°C in 80% NH_3, showing both hexagonal AlN and "cubic AlN". Pattern (a) was obtained from the middle of the nitrided layer; pattern (b) was obtained from just under the white layer. The spotty pattern in (a) indicating a larger particle size.

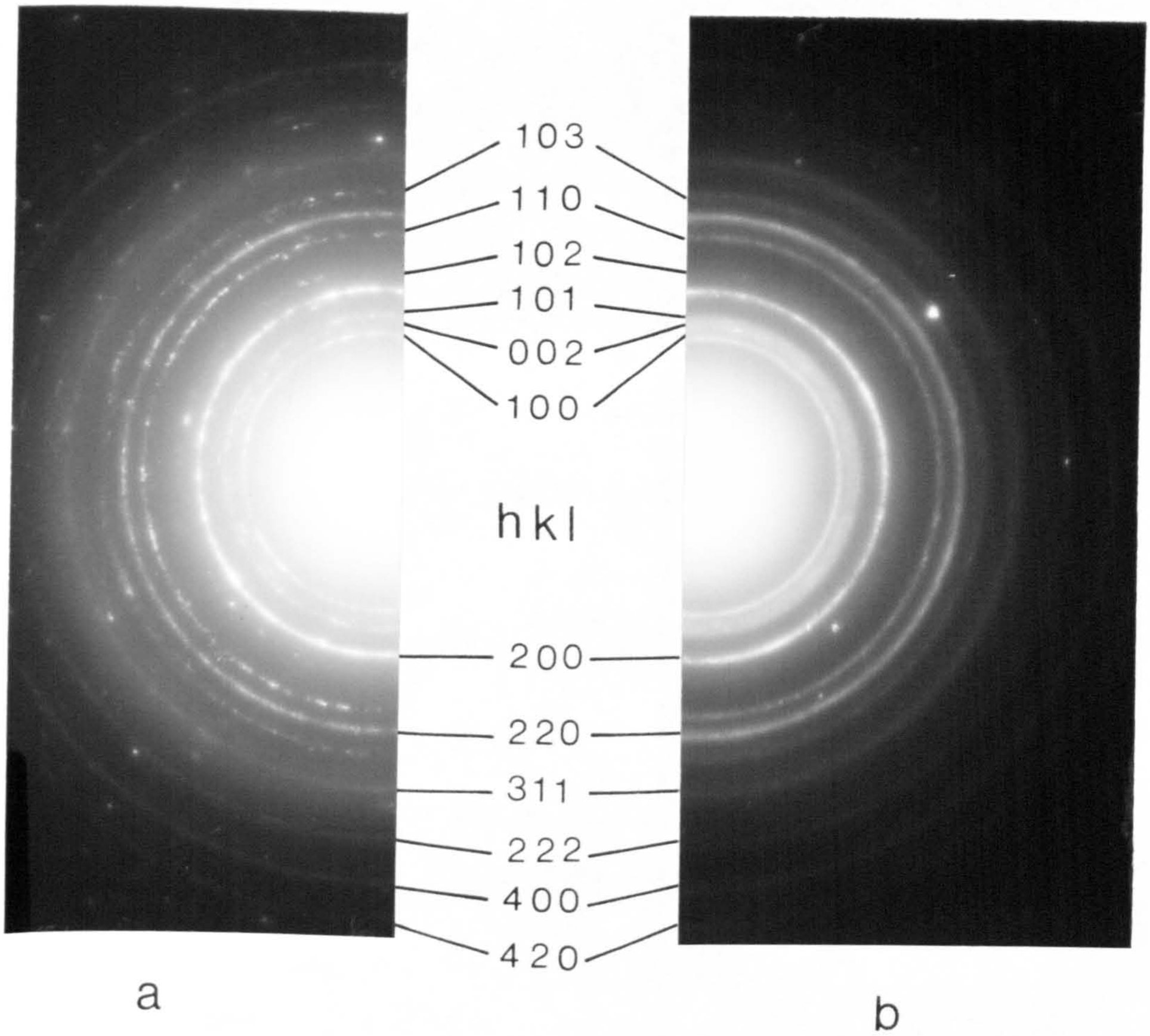
Hex. AlN
103
110
102
101
002
100
hkl
200
220
311
222
400
420
a
b
Cubic AlN

FIG. (4·14)

Hexagonal AlN		Cubic AlN	
$d_{obs.}$ Å	hkl	$d_{obs.}$ Å	hkl
2.700	100		
2.540	002		
2.367	101		
		2.057	100
1.838	102		
1.556	110		
		1.44	220
1.320	112		
		1.175	222
		1.016	400
		0.908	420
0.864	213		
		0.827	442

Table 4.12

Electron diffraction data for hexagonal and Cubic AlN as observed in Fig. 4.14

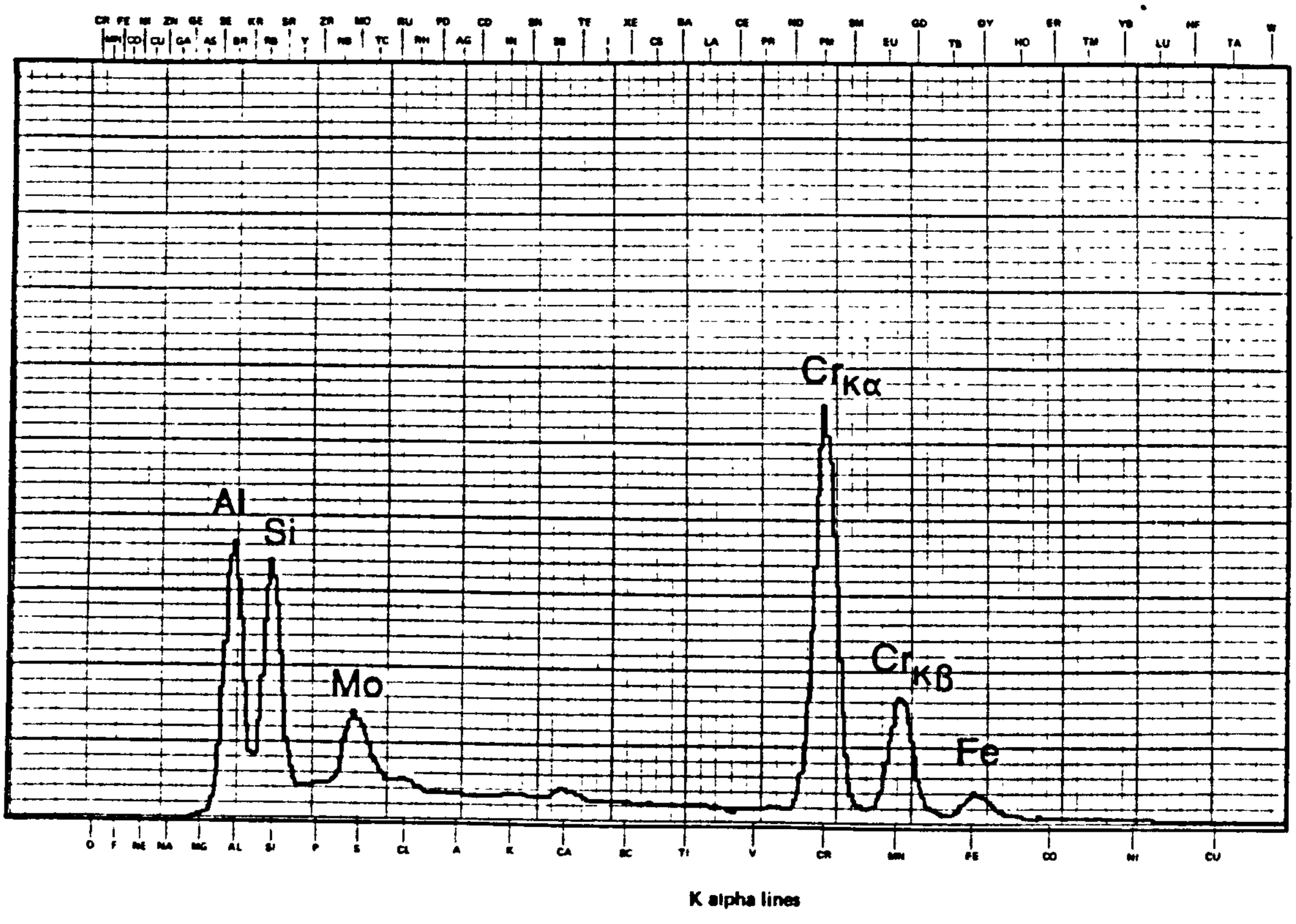

Fig. 4.15 X-ray microanalysis traces of the nitride particles extracted from a thin specimen of En41B nitrided at 570°C in 13% NH_3. Note the high peaks from Al and Si in relation to Cr, which indicates a significant proportion of the former elements.

Fig. 4.16 X-ray microanalysis traces of the extracted particles from thin specimen of En41(-Cr) steel, nitrided at 570°C in 13% NH_3. Note the close similarity in Al, Si and Mo proportions compared to those in En41B (see Fig. 4.15).

Fig. 4.17 As above with specimens nitrided first at 570°C in 13% NH_3, then annealed at 700°C. Note the increase in the Al peak in proportion to Si peak.

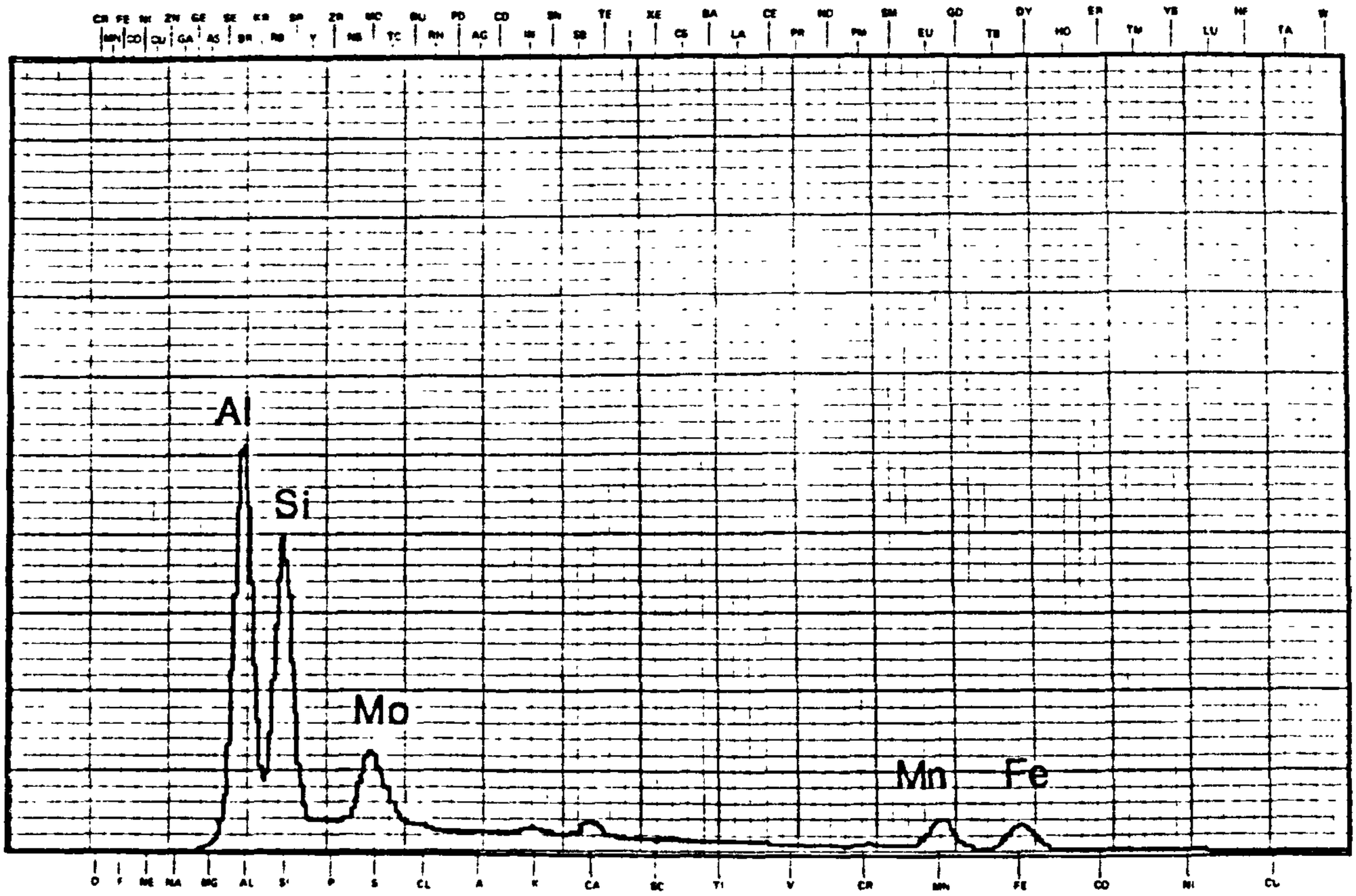

FIG. (4·16)

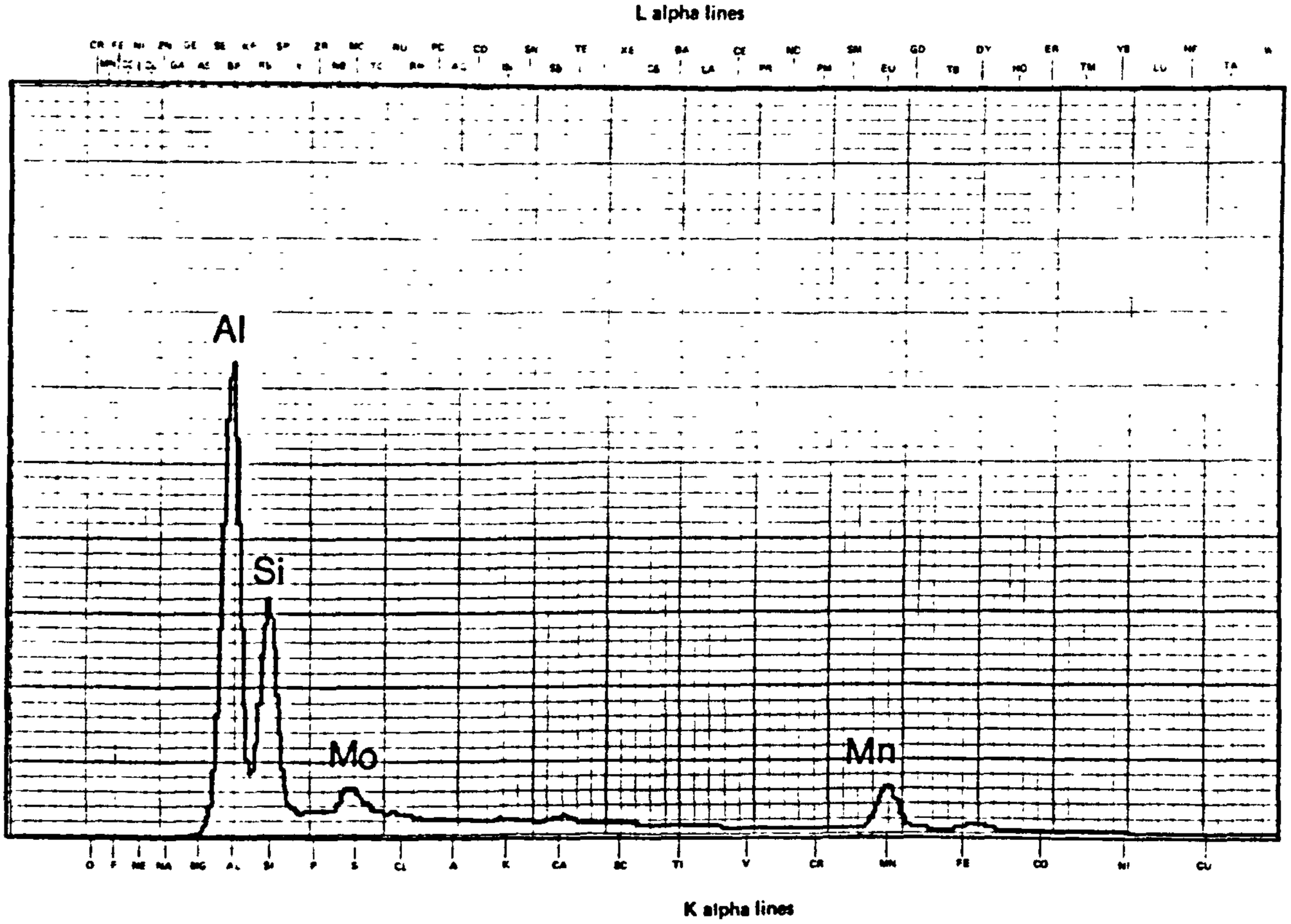

FIG. (4·17)

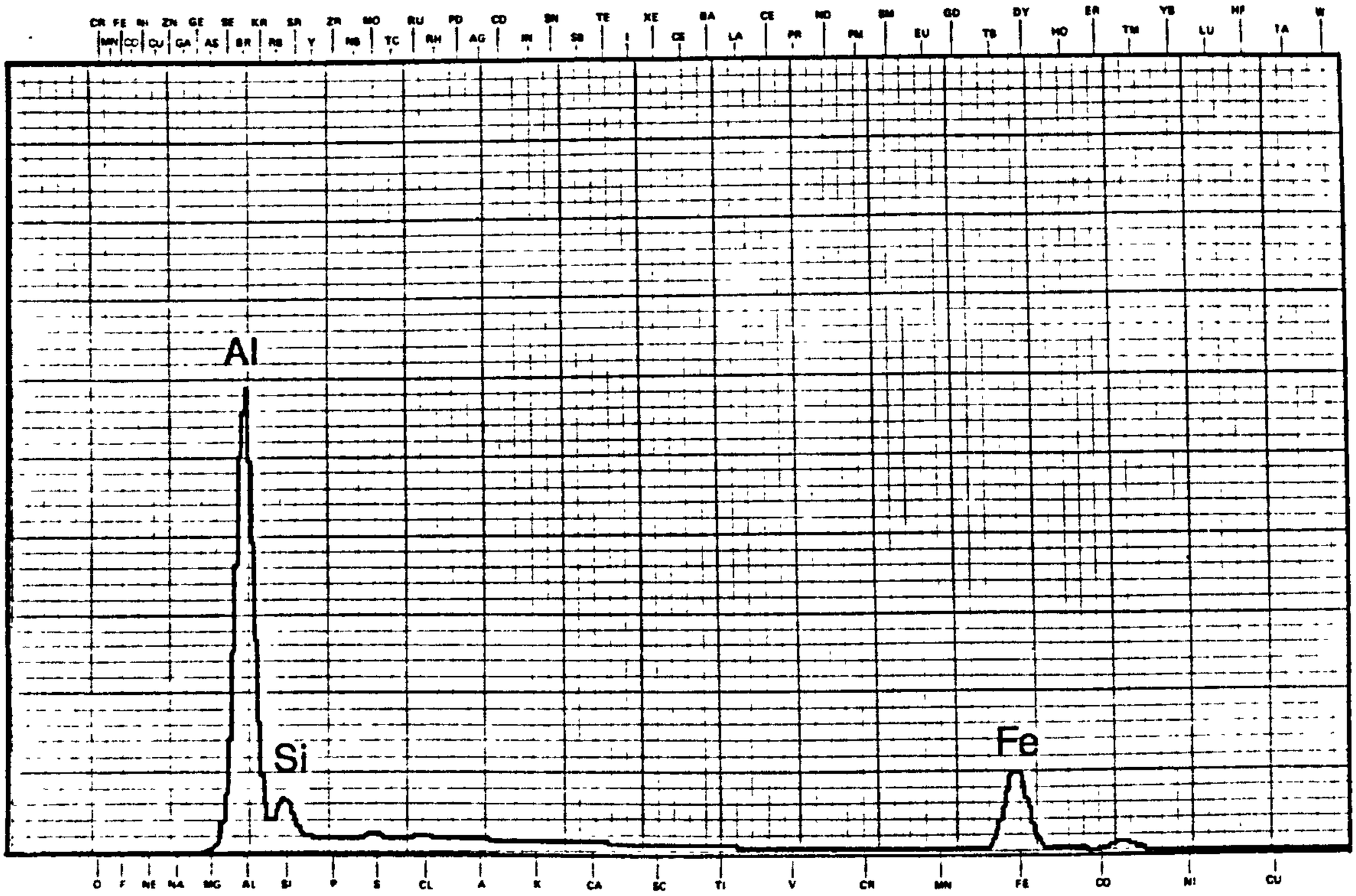

Fig. 4.18 X-ray microanalysis traces of the extracted particles from thin specimens of Fe-C-Al steel, nitrided at 570°C in 13% NH_3, showing the presence of Al and small amounts of Si and iron

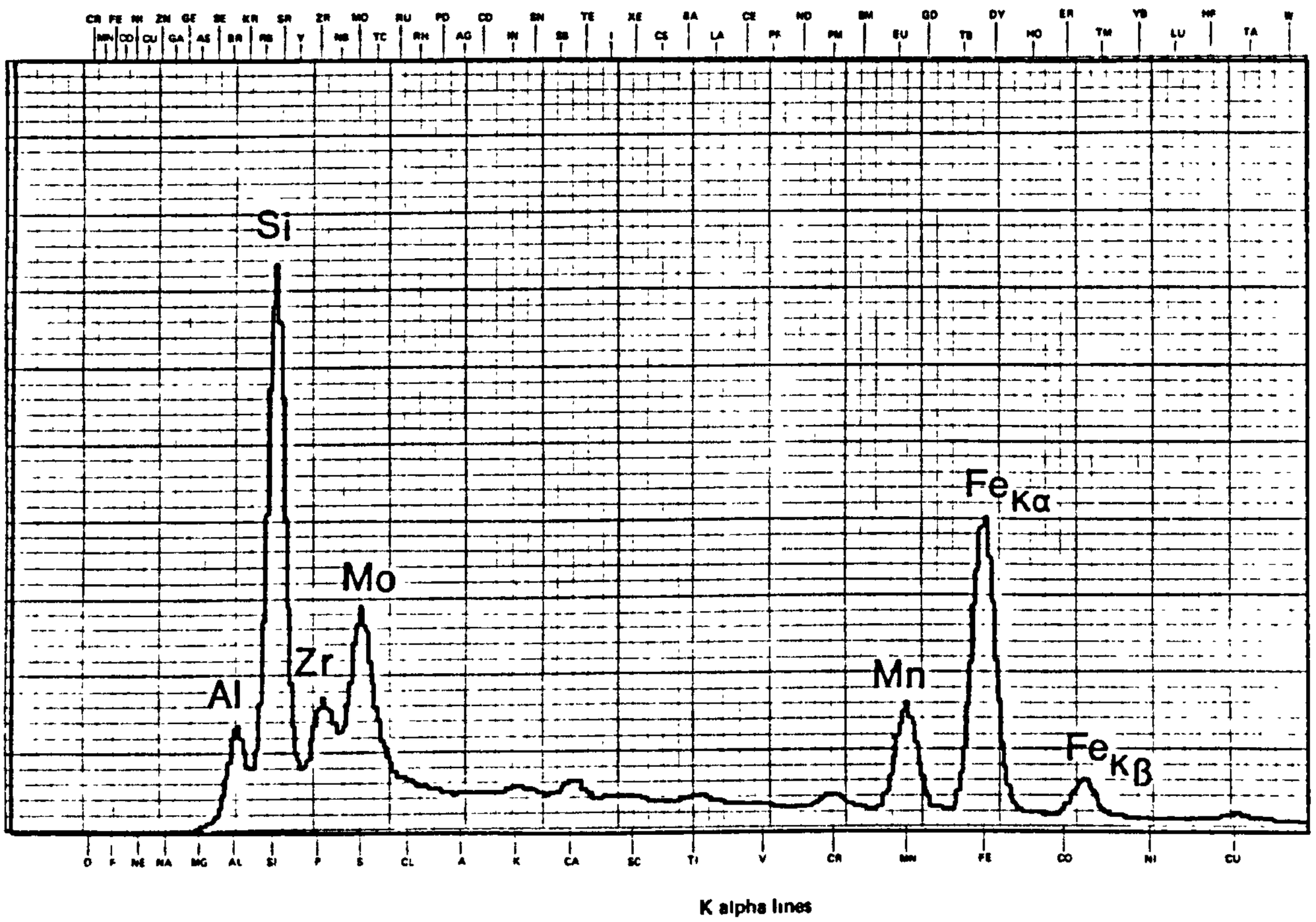

Fig. 4.19 X-ray microanalysis traces of the particles extracted from thin specimens of En41(-Cr), nitrided at 500°C in 16% NH_3, showing presence of zircomium. Note the high silicon peak. The cementite particles were removed by a magnet

Element	Al	Si	Mo	Mn	Fe
wt%	51.0	23.5	11.8	7.8	5.9

Table 4.13

Percentage of the elements in the extracted precipitate sample from En41(-Cr) nitrided at 570^{o}C in 13% NH_3 for 24 h.

Cubic AlN assumed (63) a_o = 4.047 A			Cubic AlN previous (63) observation			Cubic AlN present work obs. a = 4.05 Å		
$d_{cal.}$ Å	I/I_o	hkl	$d_{obs.}$ Å	I/I_o	hkl	$d_{obs.}$ Å	I/I_o	hkl
2.336	14	111	2.336	v.w	111	missing		111
2.023	100	200	2.036	S	200	2.027	S	200
1.431	42	220	1.431	M	220	1.430	M	220
1.220	1	311	missing		311	missing		311
1.168	11	222	1.174	M	222	1.172	W	222
1.012	4	400	1.018	v.w	400	1.013	v.w	400
0.928	0.4	331	missing		331	missing		331
0.905	10	420	0.909	W	420	0.904	W	420
0.826	6	422	0.835	W	422	0.829	W	422

Table 4.14

Lists of the d-spacing of cubic AlN observed in the present work and those calculated and observed by Hanai et al. (63).

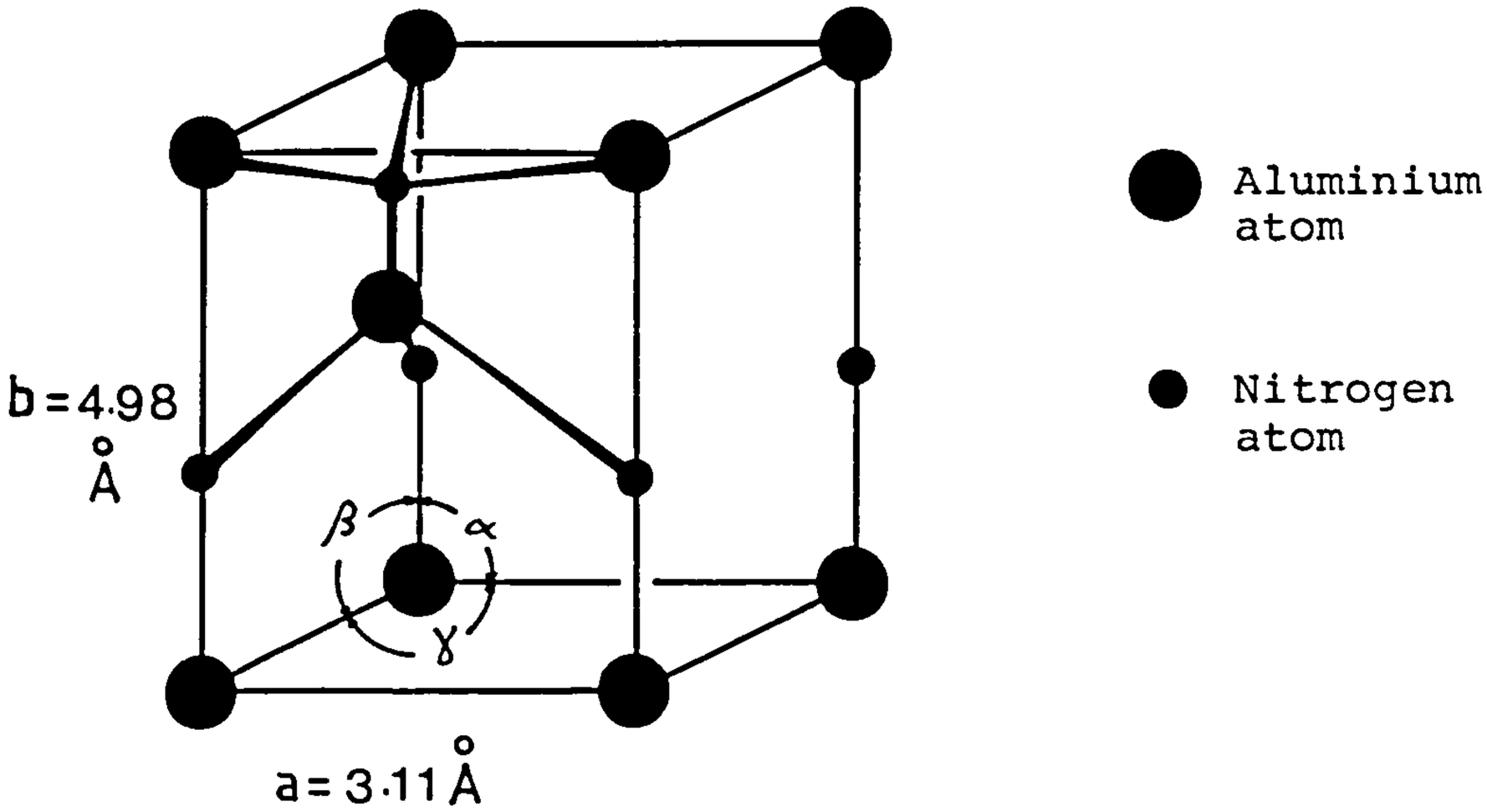

Fig. 4.20 The crystal structure of hexagonal AlN

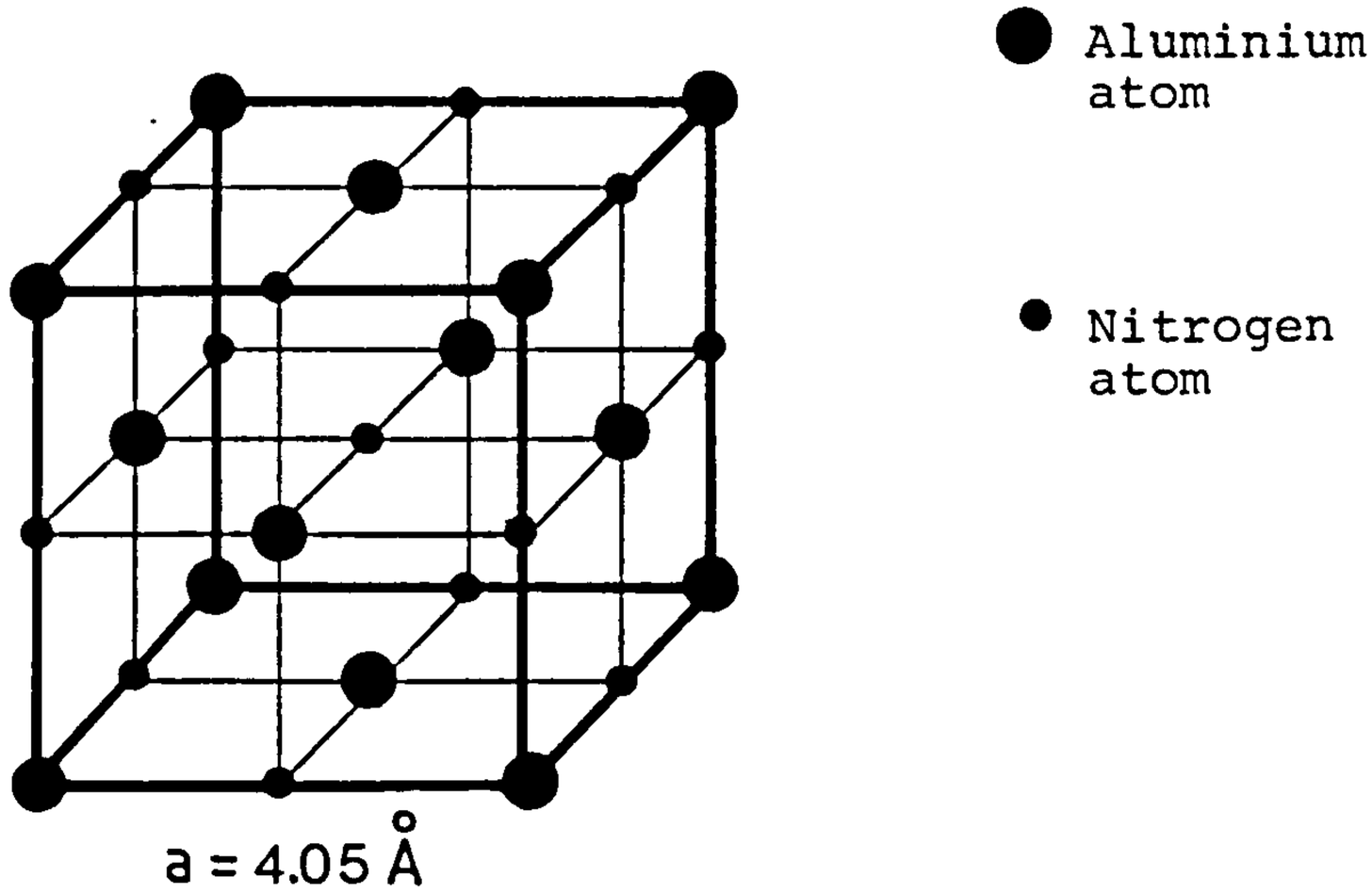

Fig. 4.21 Cubic AlN of NaCl structure

Steel	detected phases			
En41B	CrN	AlN (hexagonal)		
En41(-Cr)		AlN (hexagonal)	AlN (Cubic)	f.c.c phase $a = 4.6\text{A}^{o}$
Fe-C-Al		AlN (hexagonal)	AlN (Cubic)	

Table 4.15

The phases detected in the investigated steels

Nitrided phase	Nitriding conditions			
	$500^{o}C$		$570^{o}C$	
	16% NH_3	80% NH_3	13% NH_3	80% NH_3
CrN	Replica X-ray	Replica X-ray	Replica X-ray	Replica X-ray
AlN (hex)	- -	- -	- -	Replica -

Table 4.16

The conditions for the occurrance and detection of CrN and hexagonal AlN in En41B steel

Nitride phase	Nitriding conditions			
	500°C		570°C	
	16% NH_3	80% NH_3	13% NH_3	80% NH_3
Hex. AlN	Replica -	Replica -	Replica -	Replica -
Cubic AlN	Replica -	Replica -	Replica X-ray	Replica -
f.c.c. phase a = 4.6 Å	- X-ray	-	- X-ray	-

Table 4.17

The conditions for the occurrance and detection of Cubic AlN, hexagonal AlN and the f.c.c. phase with a = 4.60 Å in En41(-Cr)

Nitride phase	Nitriding conditions			
	500°C		570°C	
	16% NH_3	80% NH_3	13% NH_3	80% NH_3
Hex. AlN	- -	Replica	X-ray	Replica
Cubic AlN	- -	Replica	X-ray	Replica

Table 4.18

The conditions for the occurance and detection of cubic AlN and hexagonal AlN in Fe-C-Al

CHAPTER 5

STRUCTURE OF THE NITRIDED ALUMINIUM CONTAINING STEELS

5.1 Previous Work

The microstructure of nitrided iron and steel alloys has been the subject of extensive investigation during the last decade (35,36,37,62,67,68,69). Much of the recent work has been confined to aluminium-free materials, mainly chromium containing steels, some of which are commercially known, such as the En40 and En19 types (47,48), therefore very little is known still about the structure of nitrided Al-containing steels.

The work carried out by Podgursky et al. (39) described some aspects of the behaviour of aluminium in nitrided dilute Fe-Al alloys. The main microstructural features of the nitrided Fe-Al alloys were the high increase in the dislocation density and the fact that the AlN particles were indistinguishable even at high magnifications. However, careful examination of their transmission electron micrographs suggested that these particles may have been nucleated, and grown in an aligned manner on dislocation. To confirm these observations, the authors nitrided three different Fe-Al alloys with 0.16%, 0.5% and 2.0% Al. These were nitrided between 500^{o} and 575^{o}C in a variety of NH_3/H_2 gas mixtures. The results of these experiments showed that as the aluminium content of the alloy increases the dislocation density tends to increase as well, making it even more difficult to

distinguish structural details such as dislocation networks and particle size and shape.

Phillips et al. (62) also examined some binary Fe-Al alloys and Cr-steels with and without 1% Al. Among these alloys were Fe-1% Al, Fe-1% Cr-1.2% Al-0.4%C and Fe-1% Cr-0.4%C. Binary Fe-1% Al was ion nitrided in the annealed condition at 550°C and the precipitation was shown to occur as groups of small particles clustered around a "stem". It was suggested that dislocations were produced as a result of the high mismatch strains around the precipitates which form initially and then serve to nucleate small precipitates around the initial particles. The particles were concluded to be hexagonal AlN. A cold rolled Fe-1% Al foil was ion nitrided at 550°C, then annealed for 1h at 650°C in N_2-1% H_2 in an attempt to coarsen the particles for easier examination. The resulting structure was finer but otherwise similar to the one obtained by nitriding annealed foil. There were many more "chains of particles" per unit volume, and the typical chain thickness was reduced from about 150 A to about 50 A. This was attributed to the presence of dislocations in the cold rolled strip, which helped to nucleate many more particles during nitriding, as a result of which the particles produced were smaller in size.

The microstructure of the nitrided steel containing 1.2% Al was different to the one without Al, and it strongly resembled the nitrided Fe-1% Al alloy. In addition there were fairly equiaxed particles apparently preserved from the pre-

nitriding structure, taken as being chromium carbides. Therefore it was concluded that these carbides had little or no effect on the nucleation of nitrides. Nitrided low-alloy ausformable steels containing Al, Si, Mn and Mo were examined by Jack et al. (70). The microstructure was found to consist of nitride precipitates with the metal atoms arranged on f.c.c lattice with a Bain (38) relation with the matrix i.e. $(010)_{\alpha}//(010)_{pp}$, $[001]_{\alpha}||[101]_{pp}$, $[101]_{\alpha}||[0101]_{pp}$, and a unit cell of 4.1 Å, but the individual particles were indistinguishable in bright field. However, the dark field image shows strong reflexions of plate-like precipitates. No hexagonal AlN was reported as being present in the alloys.

5.2 Nitriding of chromium containing steel

The En40B steel is a chromium containing Al-free steel of a commercial quality, widely known and used for nitriding. Mridha (48), thoroughly investigated the structure of the nitrided layer, and characterized the different zones in this steel, using several different etching reagents. Four microconstituents were clearly observed and identified, namely: a compound zone or "white layer", an internally nitrided layer, a grain boundary phase within the nitrided layer, and a carburized zone ahead of the nitrided layer. The compound zone of the nitrided En40B steel was found to be a mixture of ε-Fe_3N and γ'-Fe_4N, or γ'-Fe_4N alone depending on the nitriding conditions. The outermost region of the compound zone was quite porous, whereas the innermost region was more compact and effectively keyed into the structure after

long nitriding times by virtue of extensive penetration down the prior-austenite grain boundaries. The nitrided layer was found to contain f.c.c CrN, which confirms earlier findings (46)(47). These precipitates were plate shaped and very fine. No carbide particles were found within this layer except those at prior austenite grain boundaries, which constitute the grain boundary phase observed by etching. It was established that the phase is cementite, and forms not as a continuous film, but as linked globular particles approximately 0.3 μm across. The carburized zone, which had already been observed before (71,72,73,46,47) was confirmed and revealed very clearly, by etching in oberhoffer's reagent, which stains the zone black. It was suggested that the formation of this layer depends on the development of the residual compressive stress in the nitrided layer case, which causes the dissociation of the carbides, the free carbon then being pushed ahead of the nitrided layer and reprecipitated again causing a carbide rich layer.

5.3 Structure of the nitrided aluminium containing steel

The internally nitrided zone can be defined as the nitrided part of the specimen between the white layer and the nitride free core/case interface. Some authors (48) prefer to define it as the region between the white layer and the carburized zone, but such definition has limitations due to the fact that in carbon-free alloys there will be no carbon-rich layer, and more over the layer does not form in all steels. This is the case for the Fe-C-Al steel, as will be shown later in this chapter. Also nitride precipitates can

occur within and beyond the carburized zone.

5.3.1 Material and techniques

The investigation was carried out using En41B, En41(-Cr) and Fe-C-Al steels. Also an alloy* with chemical composition 0.29%C, 1.25%Cr and 0.62%Al was used for thin foil purposes only, where clear evidence of plate-like CrN was produced.

Two different types of specimens were prepared from each steel, bulk specimens approximately 5mm thick and thin specimens with thickness of 100-150 μm. The bulk specimens were nitrided under two different nitriding conditions, i.e. 500°C with 80% NH_3 for 72 h and 570°C with 80% NH_3 for 48h. The nitrided specimens were then ground so that a cross-section of the nitrided case and the core of the specimen was revealed. Carbon extraction replicas were prepared for transmission electron microscopy, and the etched surface was examined by scanning electron microscopy and optical microscopy.

The thin specimens were nitrided in two different conditions: 570°C in 13% NH_3 for 24h and 500°C in 16% NH_3 for 24h. By using a low NH_3 concentration in the nitriding gas mixture, the formation of surface iron nitrides was prevented. These specimens were used to prepare thin foils for transmission electron microscopy.

---

* This alloy was prepared for experimental purposes to resemble the C, Cr and Al contents of En41B steel but it was not used for the rest of the work because of the large deviation from the intended composition.

5.3.2 Results

5.3.2.1 Fe-C-Al Steel

Fig. 5.1 is an electron micrograph of a thin foil nitrided at 500°C in 16% NH_3 for 24h. The cementite particles do not appear to have been affected by the nitriding, and can be clearly seen. They also seem to retain their original shape and size. Also a needle like precipitate was observed, which is taken to be α''-$Fe_{16}N_2$. This phase has a fully ordered nitrogen atom arrangement in a slightly distorted b.c.c iron atom array (see Fig. 1.5), and forms during the cooling of the nitrided specimen.

The microstructure produced by nitriding at 570°C in 13% NH_3 was found to be completely different from that found in the specimen nitrided at 500°C. Firstly, there was no sign of any cementite particles left in the matrix, and it appears that the carbides have completely dissolved, and the free carbon diffused through the specimen to the furnace atmosphere. Secondly, large needle-like precipitates were observed within the grains, some of which had grown closely adjacent to each other along the same direction in relation to the matrix, see Fig. 5.2, also the grain boundaries were found to contain particles smaller than those observed within the grains. Fig. 5.3(a) is a bright field micrograph showing the whole matrix is dominated by needle-like precipitates. The diffraction pattern shown in Fig. 5.3(b) was obtained from the same specimen, and consists of three different sets of reflections. The interpretation of the pattern is illustrated in Fig. 5.3(d). The large spots are shown to be

from the matrix, while the faint spots are consistent with hexagonal AlN, see Fig. 5.3(d1) and Table 5.1(a). The streaked set in the diffraction pattern can be interpreted in terms of an f.c.c phase with a = 4.05 $\mathring{A}$, see Fig. 5.3(d2) and Table 5.1(b). The streaks in the pattern indicate that f.c.c AlN particles are very thin plates.

Fig. 5.4(a) is a bright field micrograph of a carbon extraction replica taken from a thick specimen nitrided at 570^{o}C in 80% NH_3 for 48h. The electron diffraction pattern shown in Fig. 5.5(b) indicates the presence of both hexagonal and cubic AlN, see Table 5.2, but it is not possible to distinguish between the two. However, close examination of the bright field micrograph shows that the "needles" are actually made of small particles linked to give what is overall a needle shaped precipitate.

5.3.2.2 En41(-Cr) steel

Fig. 5.5 is a thin foil micrograph obtained from a specimen nitrided at 500^{o}C in 16% NH_3. It does not show any basic changes in the tempered structure and the cementite particles are unaffected by nitriding. The only change that can be observed is a mottling of the matrix. No diffraction pattern of either form of AlN was observed.

When nitriding was carried out at 570^{o}C in 13% NH_3, the tempered structure became totally indistinct and the cementite dissociation appeared to be complete. Fig. 5.6(a) is a bright field micrograph of a thin foil, and clearly shows the matrix to contain very fine needle-like precipitates.

These precipitates become more visible in the dark field image, Fig. 5.6(b), from which it can be seen that the particles also decorate the martensite lath boundaries.

In bulk specimens of En41(-Cr), nitrided at 570^{o}C and 500^{o}C in 80% NH_3, the hard subscale was found to contain fine precipitates of hexagonal AlN and f.c.c AlN, which were finer near the surface. The hexagonal AlN particles produced at 570^{o}C appeared to be finer than those found at 500^{o}C.

5.3.2.3 <u>En41B steel</u>

Tempered thin specimens nitrided at 500^{o}C in 16% NH_3 for 24h, show that the tempered martensite structure is preserved, and what appear to be carbide particles are still clearly visible. Fig. 5.7(a) is a bright field micrograph of a thin foil, nitrided at 500^{o}C. It shows large particles at lath boundaries. The dark field image of the same area, Fig. 5.9(b), shows a fine precipitate dispersion, which consists of a f.c.c CrN particles. It is clear from the micrograph that some of the lath boundary carbides have been transformed to nitride by an in situ mechanism. When nitriding at 570^{o}C, all of the carbides appeared to have been dissociated, apart from this however, the structure was generally similar to that found at 500^{o}C. Fig. 5.8(a) and (b) are the bright field and dark field images taken from the same area, showing some large CrN particles in which the original shape of the carbides are preserved after they have transformed to nitrides. This behaviour also occurs in bulk specimens nitrided in high NH_3 contents. Fig. 5.9(a) is a bright field micrograph of a

carbon extraction replica obtained from a bulk specimens nitrided at 570°C in 80% NH_3. It shows that the microstructure consists of large particles, and the background appears to be decorated with fine scale precipitates. The spotty ring pattern of CrN, Fig. 5.9(b) indicates the presence of large CrN particles. These particles are clearly shown in the dark field image, Fig. 5.9(c), which also shows finer CrN particles in the background. The micrographs were taken from an area just under the white layer. In general, the CrN particles produced at 570°C are coarser than those found at 500°C.

A clear example of fine CrN plate-like particles is illustrated in Fig. 5.10. The individual particles are not clearly resolved in bright field image (a), but the dark field image (c) clearly shows that the particles are plate shaped. These micrographs were obtained from a thin foil, which was prepared from an a lloy with chemical composition 0.29% C - 1.2% Cr - 0.6% Al.

5.4 Carbon displacement during nitriding

5.4.1 Introduction

Earlier in this chapter it was shown that when thin alloy steel specimens were nitrided at 570°C in 13% NH_3, the specimens were totally decarburized (see Figs. 5.3, 5.6(a) and 5.8(a). The dissociation of carbides in nitrided steel has been reported before. Levy et al. (74) showed that cementite was dissolved when they nitrided a series of plain carbon steels, with carbon contents varying from 0.28 - 0.74 wt% C in NH_3/H_2 mixtures at 500°C. To explain this behaviour

the authors suggested that as both nitrogen and carbon occupy the same octahedral sites, and with nitrogen being far more soluble in α-iron, the introduction of large numbers of nitrogen atoms into a lattice already saturated with carbon would lower the interstitial carbon content and thus would make the cementite particles dissolve. Lightfoot (46) observed similar behaviour in Fe-5 wt% Cr - 0.8% C nitrided at 575^{o}C in 18% NH_3, but disagreed with this explanation and suggested that since nitrogen is far more reactive with chromium than it is with nitrogen, it is quite likely that the carbides were destabilised as chromium transferred from the carbides to the nitrides which begin to nucleate at the surface of the carbides. Decarburization then occurs due to diffusion to the surface, and there reacting with hydrogen to form methane.

When a bulk specimen is partially nitrided it appears that carbon from the dissociated carbides diffuses ahead of the nitriding front to form a carburized layer. The formation of carbon rich layer in chromium steel has been observed by several authors. Sumarokov (71), Lakhtin et al. (72) and Minkevich (73), all reported the presence of such a layer. Their results were based on layer by layer X-ray and chemical phase analysis of the nitrided layer. Lightfoot (46) presented evidence for the formation of the carburized layer at the case/core interface, by measuring the carbon profile through the nitrided case of the Fe - 5 wt% Cr - 0.8-wt% C alloy. This was done by direct emission spectroscopy on various layers within the case. Also carbon extraction

replicas from the case/core interface were examined. The precipitation was so dense in this region that the identification of the precipitates was only possible using the 1 MeV electron microscope. The precipitates were found to be a mixture of Cr_7C_3 and Fe_3C. The presence of the latter carbide was regarded as proof that caruburization is taking place, because the carbides in this material after long tempering at 575^{o}C would transfer to $(Fe, Cr)_7C_3$.

More recently the presence of the carburized layer was further examined and confirmed. Mridha (48) nitrided specimens of En40B steel under different conditions. The specimens were then etched in oberhoffer's reagent and it was found that all these specimens revealed a black band at the case/core interface irrespective of their treatment conditions.

Regarding the formation of the carburized layer, Lightfoot proposed that carbon moves into a chromium rich area ahead of the nitriding front, where it has a greater tendency to form chromium-containing cementite than in the chromium depleted area behind the nitriding front. The dissociation of carbides during nitriding was attributed to the removal of the chromium from the solid solution due to the formation of chromium nitride which makes the carbides unstable with respect to the chromium rich carbides ahead of the nitriding front.

When nitriding is carried out at a high temperature and in low ammonia, so that no surface iron-nitride is permitted to form, then the nitrided specimen will suffer surface decarburization, but if nitriding is carried out in

a gas mixture with enough ammonia to form surface-iron nitride then a carbide "pile-up" will take place just under the white layer. This was particularly the case in chromium free materials. So, carbon dissociation during nitriding may cause any of the following effects:

a) carburized layer ahead of the nitriding front

b) grain boundary cementite

c) carbide "pile-up" under the white layer

d) surface decarburization.

All these effects were observed in the present investigation.

5.4.2 Material and techniques

The materials used were En41B, En41(-Cr) and Fe-C-Al steels.

The nitrided bulk specimens were ground and carefully polished to 0.5 mm on diamond impregnated cloth wheel. Three different etching reagents were used. Oberhoffer's reagent was used to reveal the carburized layer. Etching was carried out by immersing the specimens in the reagent at room temperature for about 20 S. Ferricyanide solution was used to reveal the grain boundary phase and any carbide pile-up under the white layer; this solution gives the carbides a dark stain. Nital solution was used to reveal the surface decarburization, which is distinguished by its lighter etch.

5.4.3 Carburized layer

This layer was found to occur in En41B and En41(-Cr) steels, both materials giving a clear etching response in

oberhoffer's reagent. A dark thick line was revealed along the case/core interface where the carburized layer occurs. The character of the "dark line" was found to be different to that previously found in En40B (48). Fig. 5.11(a) and (b) shows that the dark line along the case/core interface contains non-etched or lighter etched intervals. This was obtained from En41B steel specimens nitrided at 570°C in 80% NH_3. It may be that the etching is influenced by the orientation of the grains.

In the chromium free steels the results were inconsistent. In En41(-Cr), nitrided at 570°C in 80 NH_3 for 48 h, etching experiments revealed the presence of a carbon rich layer, Fig. 5.12(a), but when specimens of Fe-C-Al were nitrided under the same conditions they did not show any indication of the presence of a carbon rich layer, see Fig. 5.12(a). Since both steels are chromium free, and chemical analysis of the cementite extracted from tempered En41(-Cr) steel appeared to be free from any nitride forming element, then the removal of aluminium from solid solution in the matrix, due to precipitation of AlN, would not affect the stability of the carbides. This may lead to the conclusion that the formation of the carburized layer, at least in this case, depends on the compressive stress in the nitrided case which causes the dissolution of cementite, and not due solely to chemical effects.

The absence of the carburized layer in Fe-C-Al steel can be attributed to the large carbide size in this material, and moreover the hardness level of the nitrided layer is lower than that in En41(-Cr). This would mean that the compressive stress is too low to induce any effect on the larger and more stable carbides in the Fe-C-Al.

5.4.4 Carbide "pile-up" under the white layer

Examination of carbon extraction replicas, taken from nitrided bulk steel specimens containing a white layer, revealed a layer containing high density of carbides just under the white layer. This was particularly noticeable in the chromium-free steels En41(-Cr) and Fe-C-Al.

Since no such layer had previously been reported, further investigation was carried out.

5.4.4.1 Material and techniques

The alloys used in this part of the investigation were En41B, En41(-Cr) and Fe-C-Al steel.

A carefully prepared carbon extraction replica was examined by transmission electron microscopy. For optical microscopy, the nitrided bulk specimens were polished and then etched in ferricyanide solution at 90^{o}C for 60 seconds. This etch revealed the carbides by giving them a black stain.

5.4.4.2 Observation of the carbide "pile-up"

Fig. 5.13 is an electron micrograph of a carbon extraction replica taken from Fe-C-Al steel nitrided at 570^{o}C in 80% NH_3. The micrograph was taken from an area just under the white layer. It clearly shows dense carbide precipitation, some of which are rod-shaped. This type of carbide was not observed in the as-tempered material. Also it was noticed that the favoured sites for the carbide precipitation were around the martensite lath boundaries and the prior austenite grain boundaries.

Figs. 5.14(a), (b) and (c) are optical micrographs from nitrided En41B, En41(-Cr) and Fe-C-Al steels respectively. They all indicate the presence of a carbide "pile-up" just under the white layer as well as grain boundary cementite within the nitrided layer. Fig. 5.15 is a higher magnification micrograph of the same specimen used in Fig. 5.16(c). It shows in more detail the carbide concentration under the white layer.

The formation of the carbide "pile-up" just under the white layer, most likely occurs because of the formation of the white layer itself. Nitriding at high temperature and ammonia levels i.e. 570^{o}C in 80% NH_3, leads to the rapid formation of the surface iron nitrides, so the carbides at the surface which did not dissolve before the formation of the white layer, will dissolve, and the carbon then will be pushed ahead of the white layer and will reprecipitate on the grain and sub-grain boundaries.

5.4.5 Surface decarburization

It has been shown in section 5.4.4 that when nitriding is carried out at high temperatures with high enough ammonia concentration to form a white layer on the surface of a bulk specimen, carbide "pile-up" will take place just under the white layer. But when nitriding was carried out with a low enough ammonia concentration to prevent the formation of the white layer, the surface of the nitrided specimens were found to be decarburized. This was observed in Fe-C-Al steel.

The degree of the surface decarburization was found to be greatly influenced by tempering temperature prior to nitriding. Maximum decarburization was found to occur in

specimens tempered at 500°C, Fig. 5.16(a), the specimens tempered at 600° and 700°C showed far less of a decarburization effect, see Fig. 5.16(b) and (c).

The surface decarburization appeared to be influenced by two factors; carbide size and internal compressive stress due to the precipitation of AlN. Prior tempering treatment at 500°C, produces small size carbides embedded in a matrix which still contains a high enough dislocation density to act as nucleation sites for AlN. Precipitation of AlN creates even more dislocations, thus quickly increasing the internal compressive stress in the nitrided layer which leads to the carbide dissociation. Tempering at 600° and 700°C results in larger carbides embedded in a matrix which is largely recovered and partially recrystallized. Such a combination in the matrix reduces the amount of AlN precipitation, which leads to a lower level of internal compressive stress, which is insufficient to dissociate the larger carbides.

Figs. 5.17(a) and 5.17(b) are optical micrographs at low and high magnification which further illustrate the decarburization effect. They also indicate that the grain boundary carbides do not seem to be affected, and this behaviour may offer an explanation for the presence of grain boundary carbides in the nitrided layer.

5.4.6 Grain boundary phase

5.4.6.1 Introduction

The formation of the grain boundary phase during the nitriding of steels, within the nitrided layer, is a well known

phenomenon. The phase forms preferentially on the prior austenite boundaries parallel to the surface. It has usually been referred to as "nitride" or "carbo-nitride", but recently it has been shown (48), that the phase is in fact Fe_3C formed as linked globular particles, and not as a large continuous phase along the grain boundaries.

5.4.6.2 Structural observation of the grain boundary phase

The grain boundary phase was found to occur in En41B steel as well as in the chromium free En41(-Cr) and Fe-C-Al steel. Figs. 5.14(a),(b) and (c) are optical micrographs obtained from the above steels nitrided at 570°C in 80 NH_3 and etched in ferricyanide solution. It is clearly shown that in chromium containing En41B, the grain boundary phase tends to form preferentially on the boundaries parallel to the specimen surface, whereas in chromium free steels the phase precipitates all around the austenite grain boundaries with no preferential direction with respect to the surface. However, when nitriding was carried out at 500°C in 80 for 72 h. The grain boundary phase in En41(-Cr) also appeared to be parallel to the surface. See Fig. 5.18. This change in behaviour may confirm the belief that the compressive stress in the nitrided layer prevents the grain boundary phase from growing along the boundaries perpendicular to the growth direction of nitrided layer. This is clearly demonstrated in Fig. 5.19, the grain boundary which runs perpendicular towards the surface contains no grain boundary phase.

Further beneath the white layer of the specimen shown in Fig. 5.14(b), there are bands parallel to the surface, which are sub-grain boundary carbides, these grow in a similar manner to those on the original austenite grain boundaries.

Attempts were made to extract the grain boundary phase using the conventional method of carbon extraction without success. However, a large portion of the phase was successfully extracted by using the technique described in Section 2.4.3.2(b) Fig. 5.20 is a transmission electron micrograph of an extraction carbon replica obtained from nitrided Fe-C-Al steel. It clearly shows the phase along the austenite grain boundary. Although it is not possible to see the details of the phase, the general appearance indicates that it consists of large particles which are closely adjacent and may even be linked together. It was not possible to obtain a diffraction pattern because the particles were too thick.

Regarding the formation of the grain boundary phase it was shown (48) that the phase forms firstly away from the surface of the nitrided specimen near the interface between the nitrided layer and the carburized zone, and it was suggested that it may actually form in the carburized layer, and as the carburized layer pushes ahead of the nitrided front the phase stays behind.

But since the phase also forms in Fe-C-Al steel, which did not show the presence of carburized zone, any connection between the g.b phase and the carburized layer may be ruled out.

A possible explanation for the formation of the grain boundary phase is that, as the carbide starts to dissolve under the internal compressive stress, a large proportion of the carbon will migrate into the grain boundaries to reprecipitate as cementite. These particles become very stable as they grow larger.

5.5. Structure of the white-layer

5.5.1. Material and techniques

The materials used were En41B, En41(-Cr), Fe-C-Al and an Fe-0.52% Al alloy. Specimens from these alloys were nitrided under two different nitriding conditions, i.e. 570^{o}C in 80% NH_3 for 48 h and at 500^{o}C in 80% NH_3 for 72h. Optical and scanning electron microscopy were used to examine the microstructure and the general features of the white layer. Nital solution was used to reveal the white layer. The depth and hardness of the white layer was measured using a Reichert microhardness tester.

An attempt was made to extract the surface iron nitride form a nitrided bulk specimen by using potentiostatic etching technique. Part of the white layer was successfully extracted, and the phases present were determined by X-ray diffraction.

All specimens were subjected to the standard heat treatment before nitriding i.e. oil quenched from 900^{o}C and tempered at 600^{o}C for 1 h.

5.5.2. Microstructure of the white layer

Three main features of the white layer were observed in the nitrided steels. They were, a thin porous layer at the outermost region, beneath it a more compact layer finally a net-like interface linking the white layer with the bulk of the specimen. Fig. 5.21 is a scanning electron micrograph obtained from an En41B specimen nitrided at 570^{o}C in 80% NH_3 for 48 h, and shows the main features of the white layer. The porous feature of the outermost part of the white layer was reported previously (47,48,75). It appears that the porous region consists of ε - Fe_3N and that the compact region is γ'-Fe_4N.

The penetration of γ'-Fe_4N appeared to take place preferentially down the austenite grain boundaries, and around the lath boundaries close to the advancing edge of the white layer. This forms a network of γ'-Fe_4N, and as nitriding continues these penetrations widen and the gaps between them gradually close to form a compact layer, while further penetration occurs further on. Fig. 5.22 is a transmission electron micrograph of a carbon replica obtained from En41B nitrided at 570^{o}C in 80% NH_3, in which the intergranular and transgranular penetration is clearly shown. A similar penetration mechanism was observed in En41(-Cr) and Fe-C-Al steel. Previous investigations (47,48) on En40B steel showed that Fe_4N penetration occurs mainly down the grain boundaries, and the transgranular penetration is very much less than that found in En41B steel. Such a difference in the penetration mechanism in different steels is not well recognised. However

there is a belief that the carbide size in the steels may be an influencing factor on the way the white layer penetrates into the matrix. This is probably best demonstrated when En40B steel is compared with other steels like En41B, En41(-Cr) and Fe-C-Al. In all these latter steels there is an extensive transgranular penetration of γ'-Fe_4N into the matrix, Figs. 5.23 and 5.24, despite the difference in chemical composition, but the carbide sizes in En40B steel are very much smaller than in the other steels.

In Fe-0.52% Al the white layer was also found to be porous at the outer region and compact at the innermost region. Unlike in the steels, the interface between the white layer and the nitrided layer is defined by a clear borderline, which is interrupted at some grain boundaries where Fe_4N penetration has taken place. A needle like growth of Fe_4N through the grain was also observed, see Fig. 5.25(a).

The growth rate of the white layer can be different in different grains. Fig. 5.25(b) shows an abrupt change in the thickness of the white layer at the grain boundary between grains A and B. This indicates that an orientation effect may be influencing the growth of Fe_4N into the iron matrix.

The surface iron nitride which was extracted from a bulk specimen of En41(-Cr) nitrided at 570°C in 80% NH_3 for 48 h, was a mixture of Fe_3N and Fe_4N. Fig. 5.26 is the X-ray diffraction pattern from these particles, and the d-spacings are listed in the adjacent Table 5.2.

The extracted powder was chemically analysed to see whether there are any other elements incorporated in the

surface iron nitride, but the analysis results showed the particles contain only iron, Fig. 5.27 is an X-ray micro-analysis trace of the extracted particles.

5.5.3 Thickness and hardness of the white-layer

The investigation was carried out using En41B, En41(-Cr) and Fe-C-Al steels.

The specimens were nitrided in 80% NH_3 at two different nitriding temperatures i.e. 500° and 570°C, and two different nitriding periods at each temperature i.e. 24 and 72h at 500°C, and 24 and 48h at 570°C.

The averages of the thickness and hardness measurements of the white layer for each steel are given in Table 5.3. The thickness of the white layer appeared to be greatly influenced by the nitriding temperature and time and to a lesser extent by the alloying element. The thickness increases for each steel with the increase in the nitriding time and temperature. When the nitriding time increased from 24h to 72h, at 500°C, the thickness almost doubled. The effect of time at 570°C is slightly less significant than at 500°C.

The effect of the alloying element on the thickness of the white layer seems to vary with the nitriding temperature and time. At 500°C and after a period of 24h, the chromium free En41(-Cr) and Fe-C-Al steels have the same thickness, while En41B has a slightly thicker white layer. But after a longer period i.e. 72h, the thickness decreases steadily with the decrease in alloying elements. At 570°C

the thickness always decreases with the decrease in the alloying elements.

The microhardness results given in Table 5.3 suggest that the outer zone $\varepsilon - Fe_3N$ phase is softer than the inner zone $\gamma'-Fe_4N$. At 570°C, the hardness of the $\varepsilon - Fe_3N$ phase appears to be the same for the three steels, with an average value of 900 $\pm$ 20 VHN regardless of the nitriding time.

The variations in the maximum hardness for each steel, after nitriding in different conditions are small, but higher hardness is achieved in En41B with 1130 $\pm$ 50 VHN compared to En41(-Cr) with 1050 $\pm$ 50 VHN, and Fe-C-Al with 950 $\pm$ 50 VHN. The lower hardness in Fe-C-Al may suggest that the proportion of the $\varepsilon - Fe_3N$ phase in the white layer is greater than that in En41B.

5.6 Summary and Conclusions

1. The structure of the nitrided En41B contains fine precipitates of f.c.c CrN on {001} ferrite planes. The particles produced at 570°C are coarser than those produced at 500°C.

2. The structure of the nitrided chromium-free En41(-Cr) and Fe-C-Al steels consists of fine needle-like precipitates with a f.c.c. lattice structure with a $\sim$ 4.05 A. These were regarded as f.c.c. AlN. The particles produced at 570°C are finer than those produced at 500°C.

3. In En41B, transformation of the chromium-rich carbides into nitrides can occur by an in situ mechanism. This is more significant at 570°C than at 500°C.

4. The formation of the carburized layer in nitrided bulk steel specimens depends on the internal compressive stress of the nitrided layer, and is not solely due to chemical effects. The size of the carbides is an important factor in the formation of the layer.

5. In bulk specimens, nitriding at 570°C in low NH_3 content of the gas mixture results in a surface decarburization. The magnitude of the decarburization depends on the tempering temperature prior to nitriding.

6. In bulk specimens nitrided in high NH_3 content so as to form white layer on the surface, carbide "pile-ups" take place under the white layer.

7. The thickness of the white layer decreases with the decrease in the alloying elements.

8. The hardness of the outermost part of the white layer, which consists of Fe_3N, is constant in different steels and it is softer than the innermost part which consists of Fe_4N.

9. The penetration of the γ'-Fe_4N into the matrix occurs preferentially down the austenite grain boundaries and around the lath boundaries close to the advancing edge of the white layer.

10. In Fe-0.42 Al alloy, the growth of the white layer seems to be related to the grain orientation.

Fig. 5.1 Thin foil micrograph of Fe-C-Al steel specimen, nitrided at 500^{o}C in 16% NH_3, showing the tempered structure is unchanged and the carbides have retained their morphology.

Fig. 5.2 Thin foil micrograph of Fe-C-Al steel specimen, nitrided at 570^{o}C in 13% NH_3. Note the needle like precipitates.

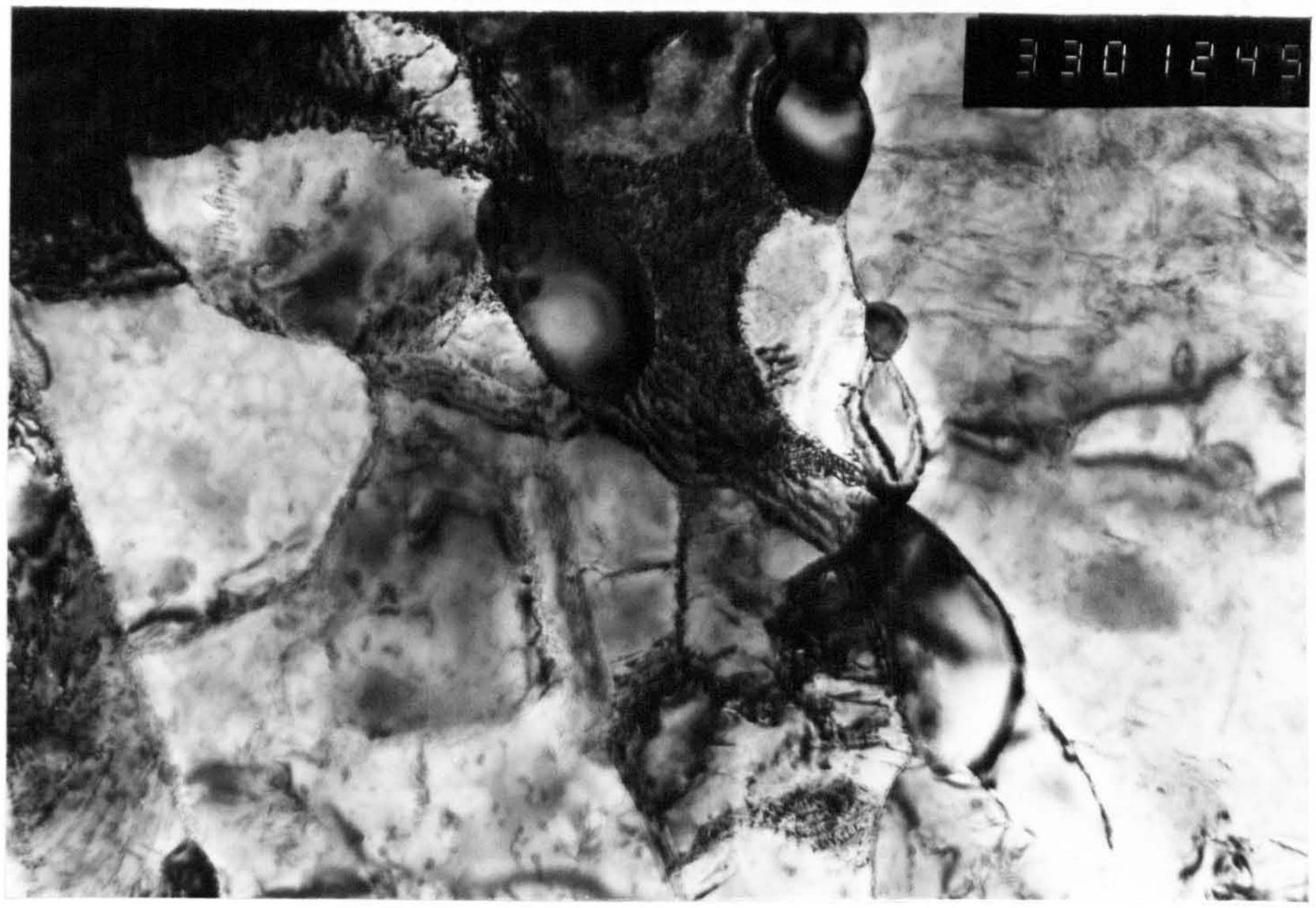

Fig. (5.1)

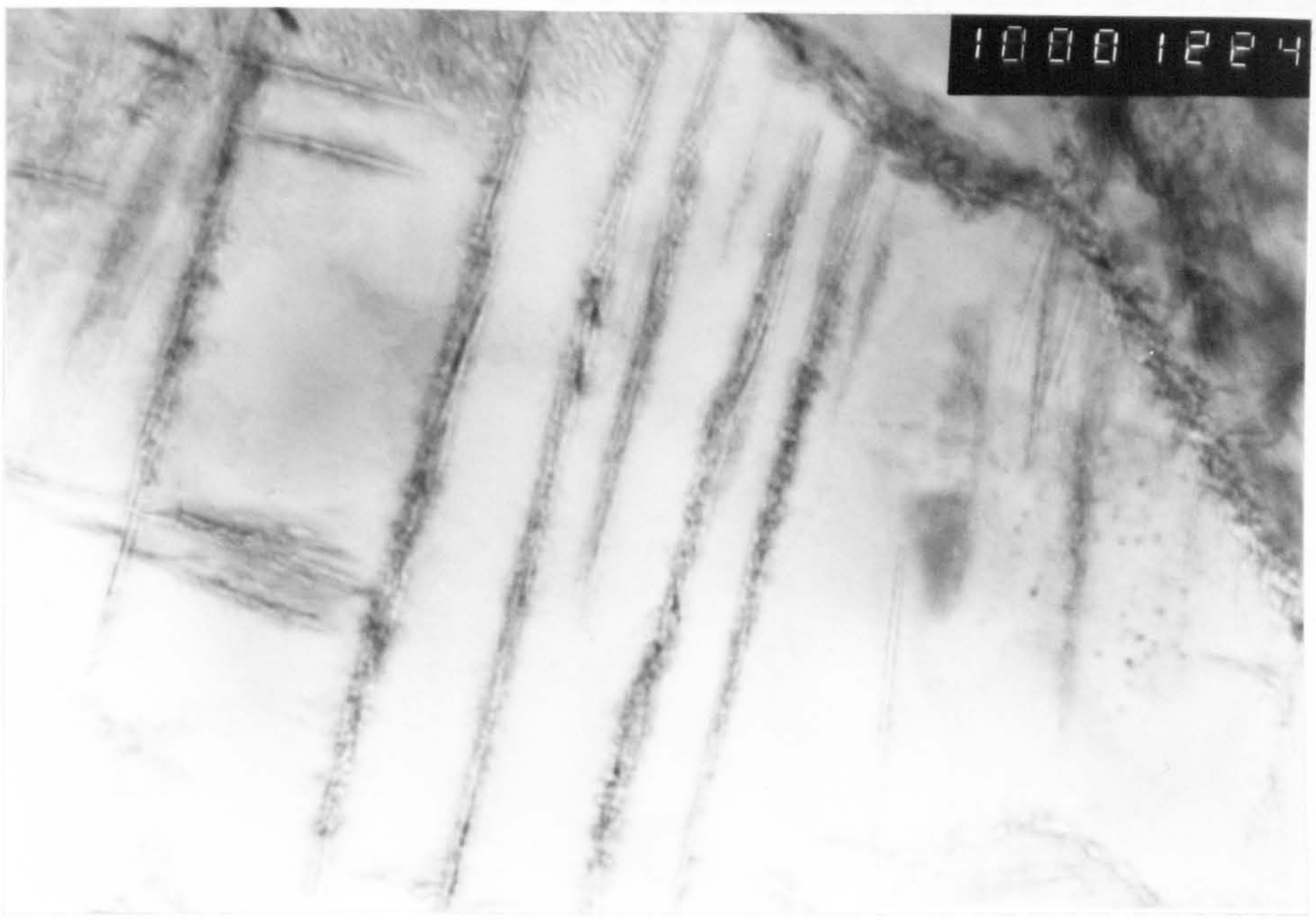

Fig. (5.2)

Fig. 5.3 Thin foil micrographs obtained from a nitrided thin specimen of Fe-C-Al. Nitrided at 570°C in 13% NH_3

a - Bright field showing fine needle-like precipitates of cubic AlN

b - Electron diffraction pattern showing presence of both hexagonal AlN (spots) and cubic AlN (streaks)

c - Dark field immage of (a) showing cubic AlN needles (200 precipita relfexion)

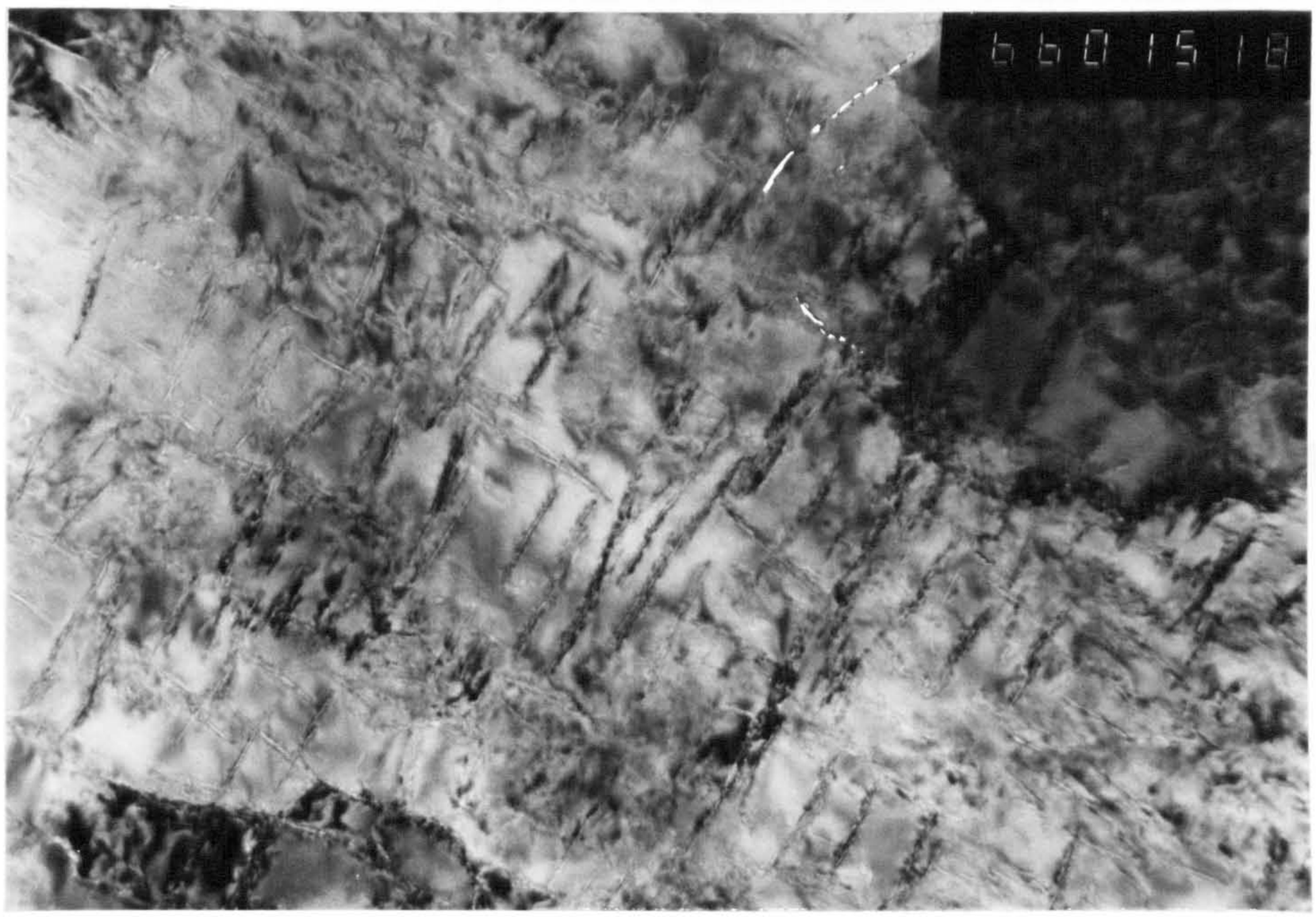

a

0.25 um

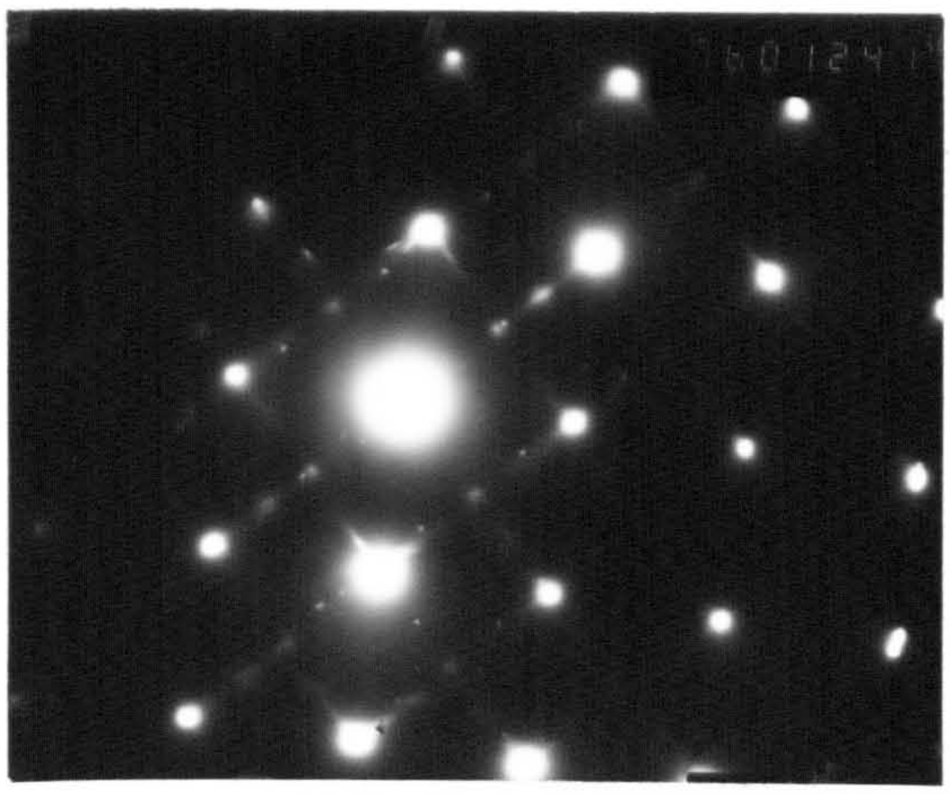

b

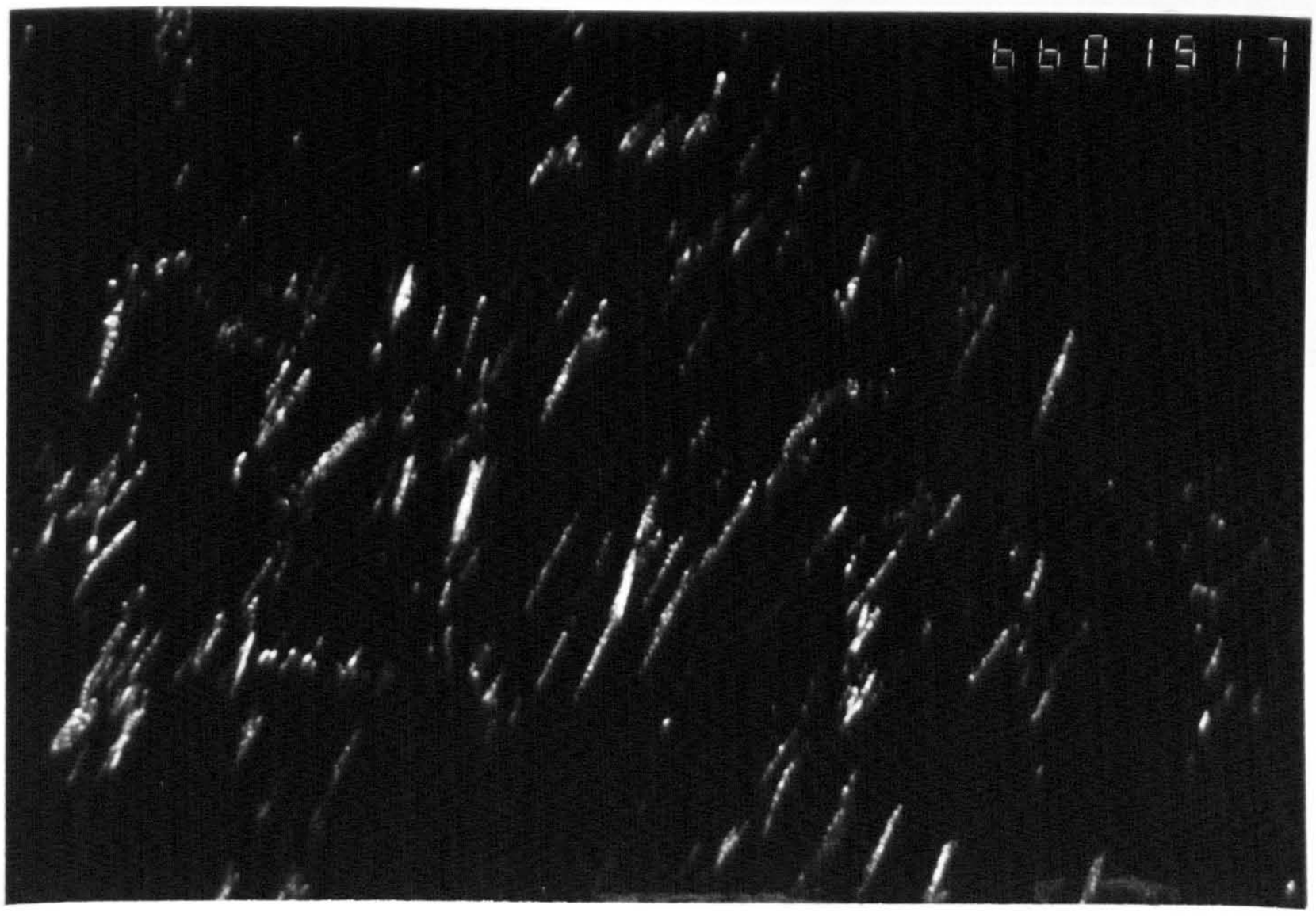

C

Fig. (5.3)

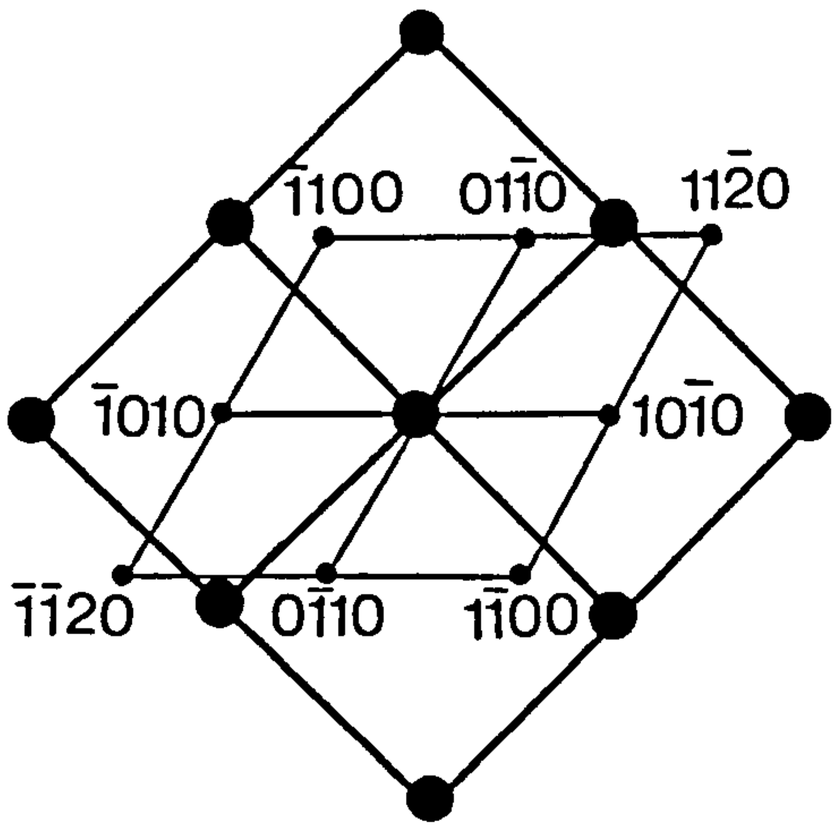

d_1

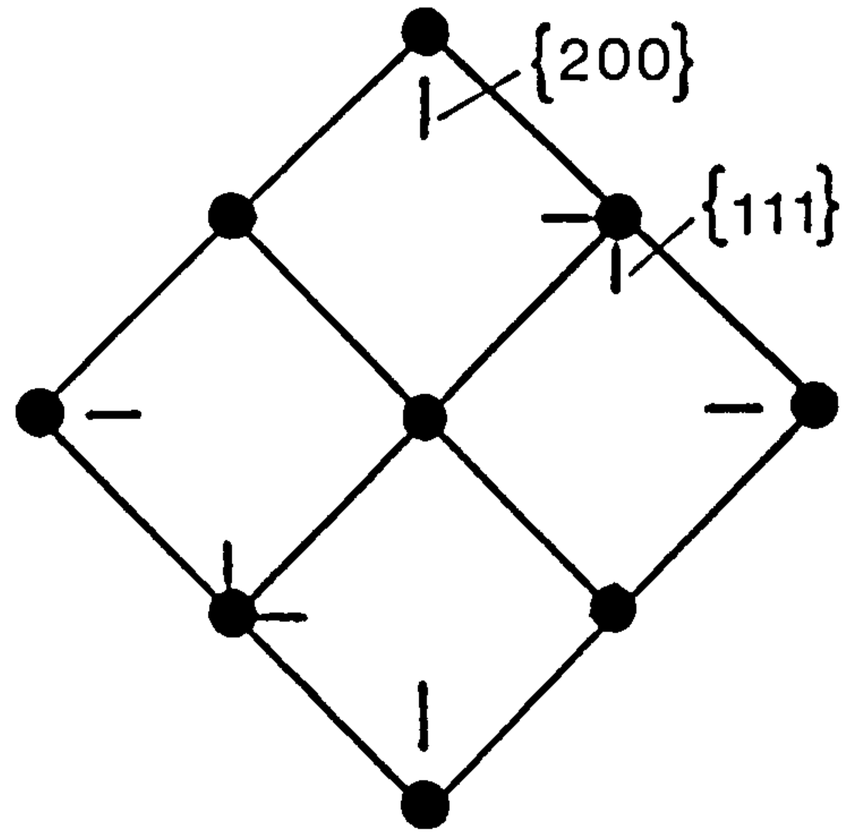

d_2

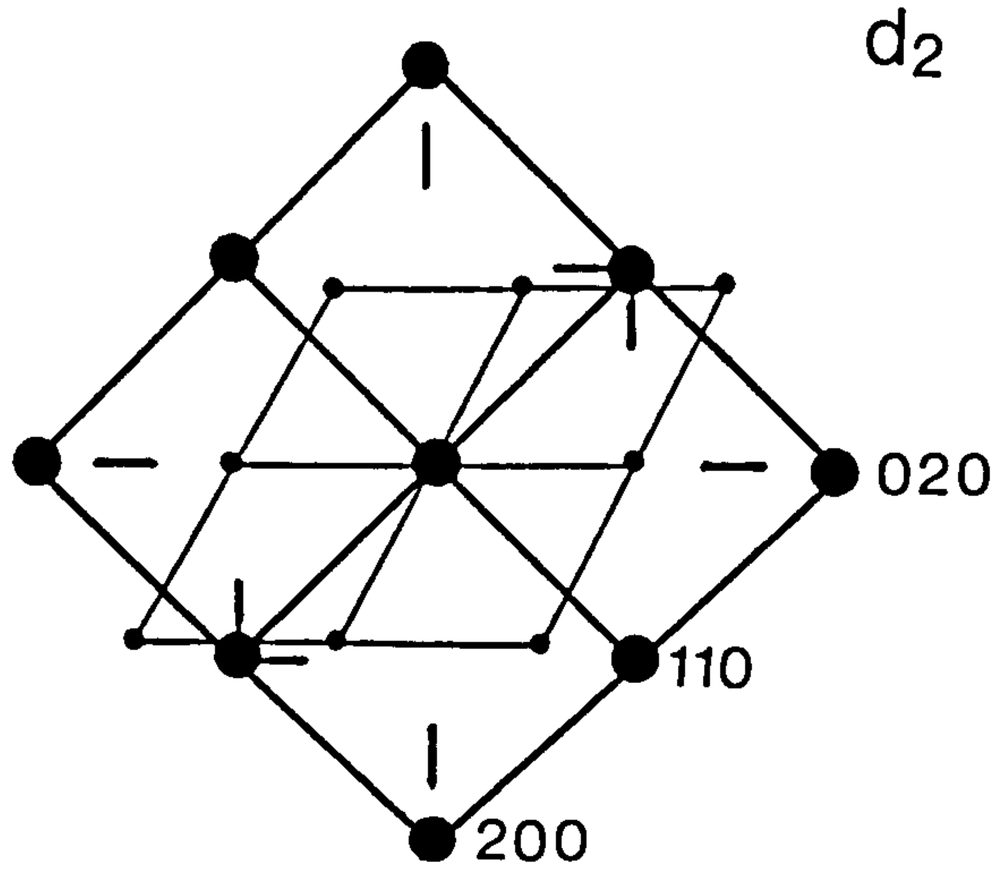

$d_1 + d_2$

d_1 - Hexagonal AlN spots + α-Fe spots

d_2 - f.c.c AlN streaks + α-Fe spots

$d_1 + d_2$ is the actual pattern

Fig. 5.3(d) Interpretation of the diffraction pattern shown in Fig. 5.3(b)

a)

$d_{obs.}$ Å	$d_{cal.}$ Å	hkl
2.686	2.693	100
1.852	1.825	102
1.552	1.555	110
1.436	1.413	103

Calculated values using

$a_o = 3.11$ Å

$b_o = 4.98$ Å

b)

$d_{obs.}$ Å	$d_{cal.}$ Å	hkl
2.335	2.338	111
2.027	2.025	200

Calculated values using

$a_o = 4.05$ Å

Table 5.1

Electron diffraction pattern data for

a) hexagonal AlN

b) Cubic AlN

[As observed in Fig. 5.3(b)]

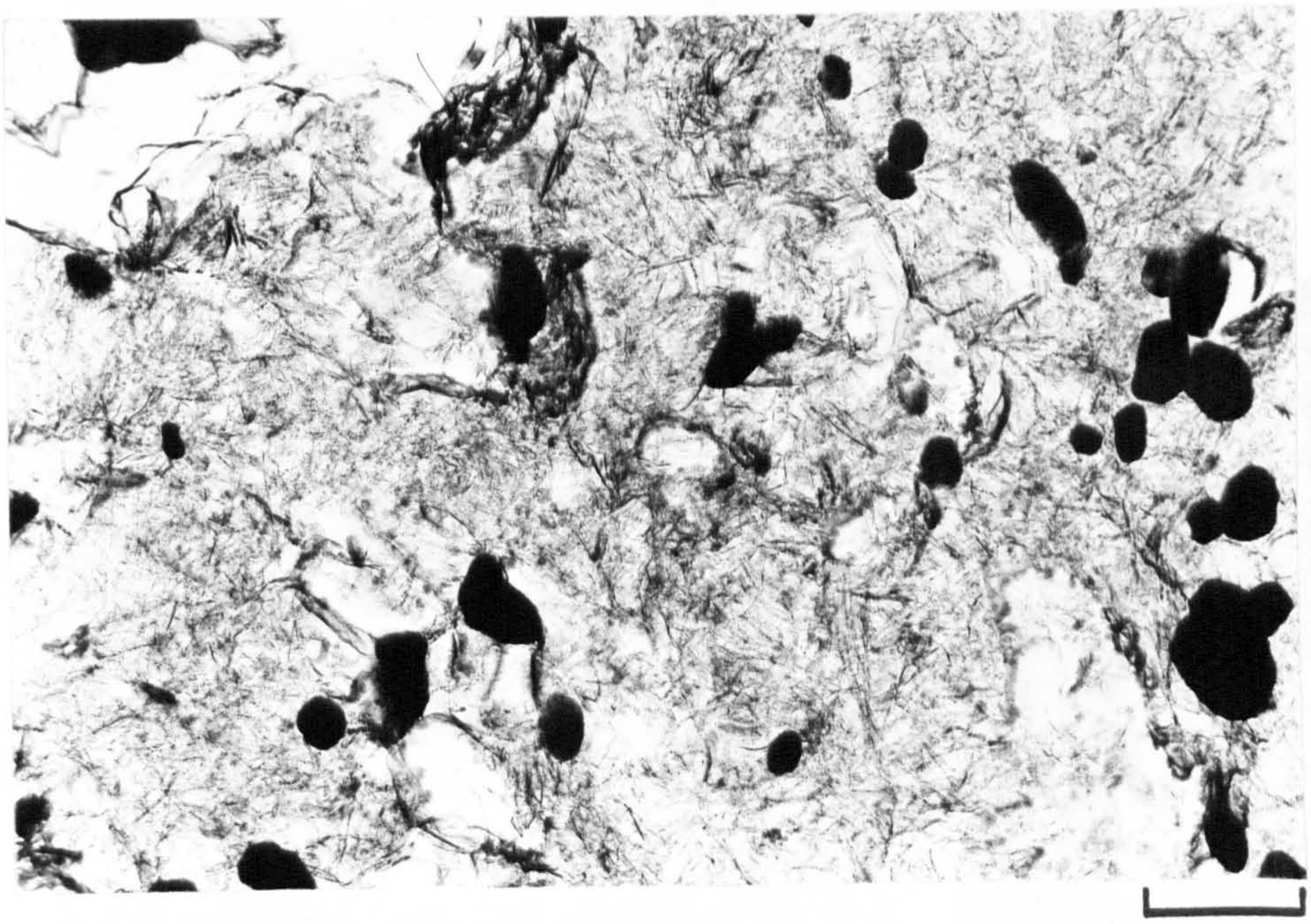

a

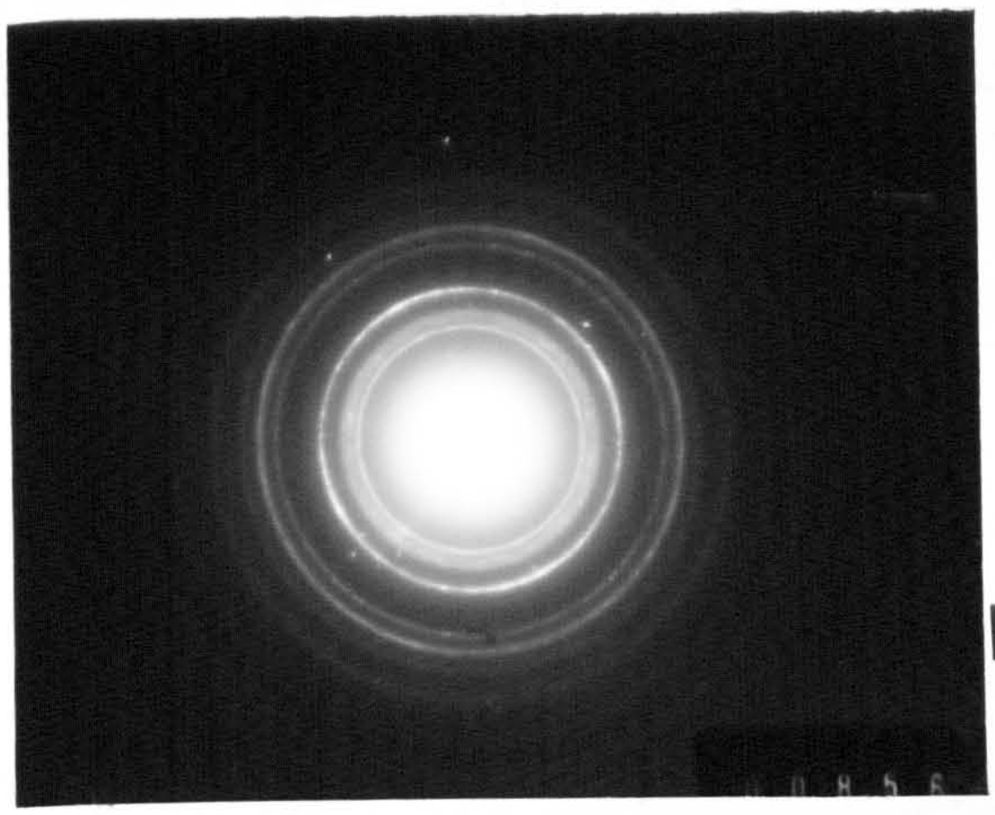

b

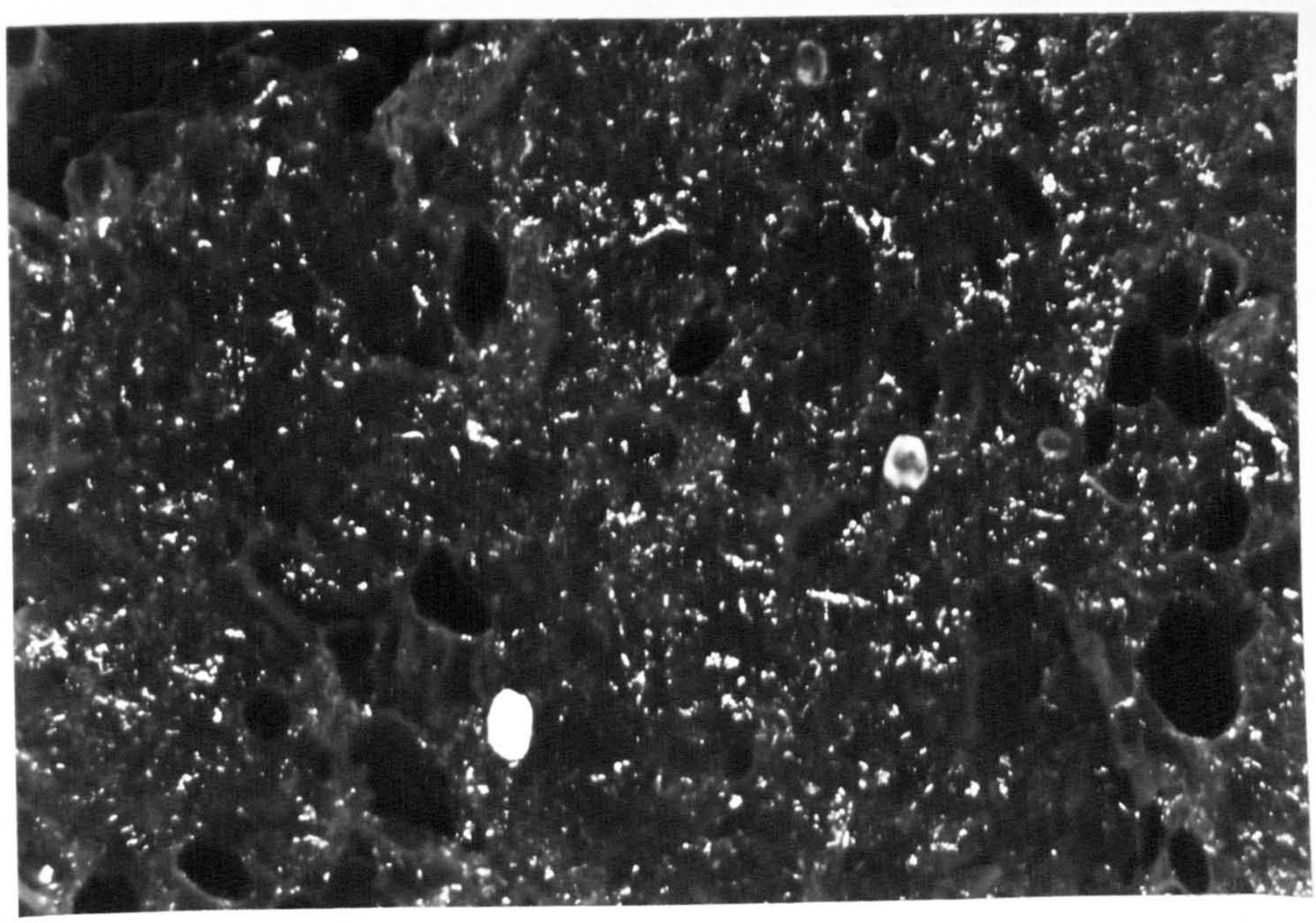

C

Fig. (5.4)

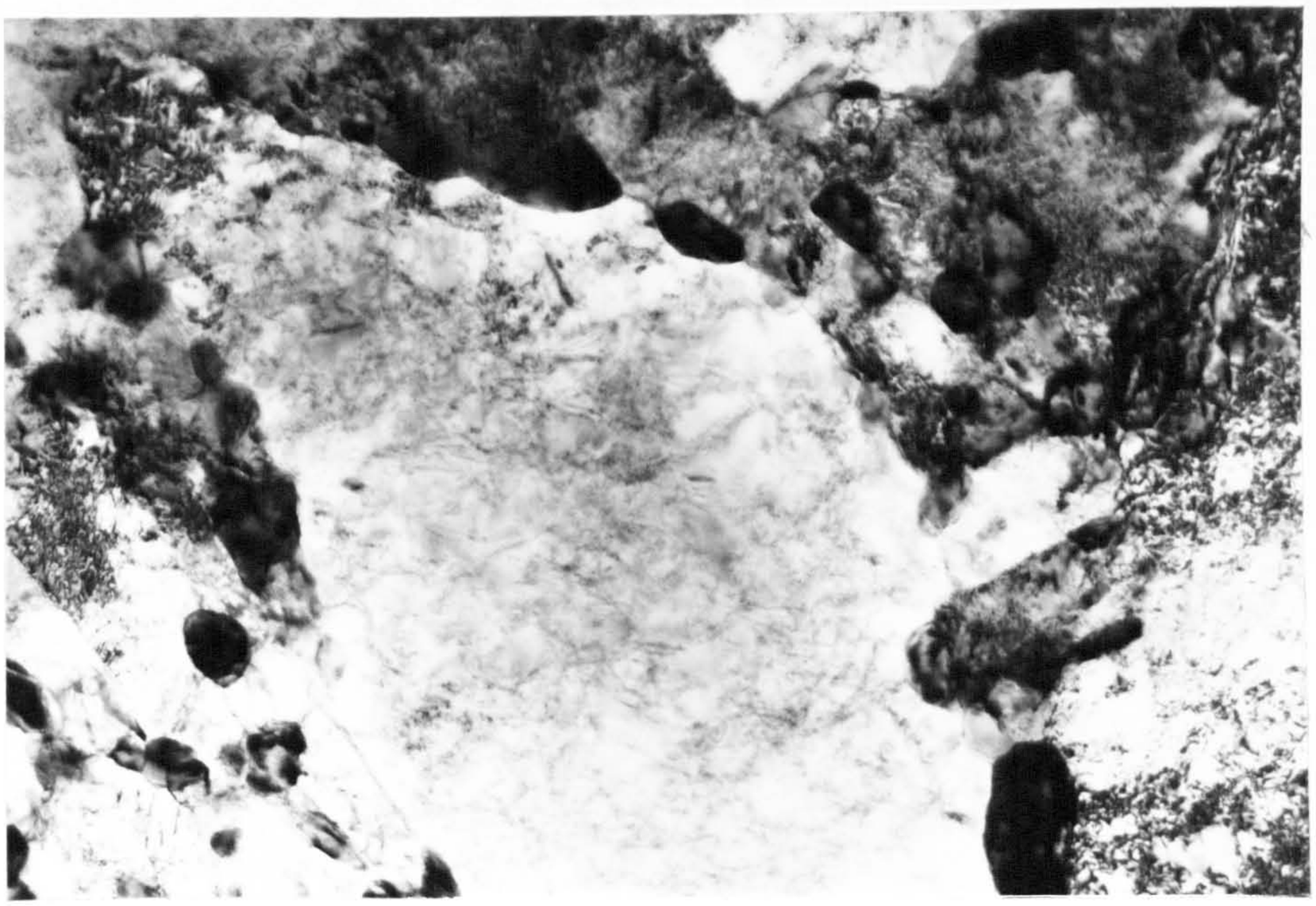

Fig. 5.5 Thin foil micrograph of a thin specimen of En41(-Cr), nitrided at 500°C in 16% NH_3, showing presence of carbides and a mottled matrix

Fig. 5.6 Thin foil micrograph of a nitrided thin specimen of En41(-Cr), nitrided at 570°C in 13% NH_3

a - Bright field image showing fine particles of cubic AlN

b - Dark field image of (a) from a 200 precipitate reflextion

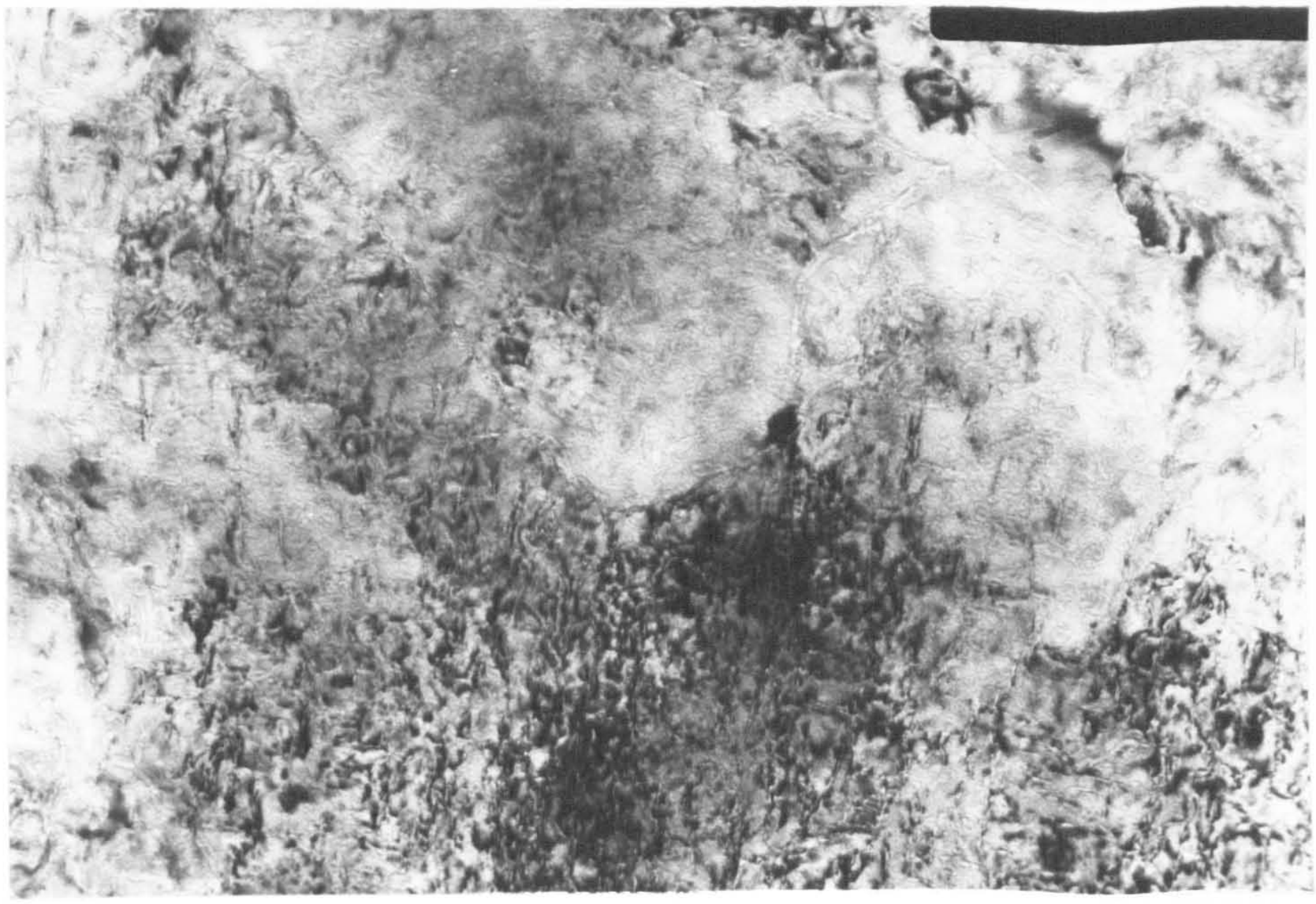

a

0.25 µm

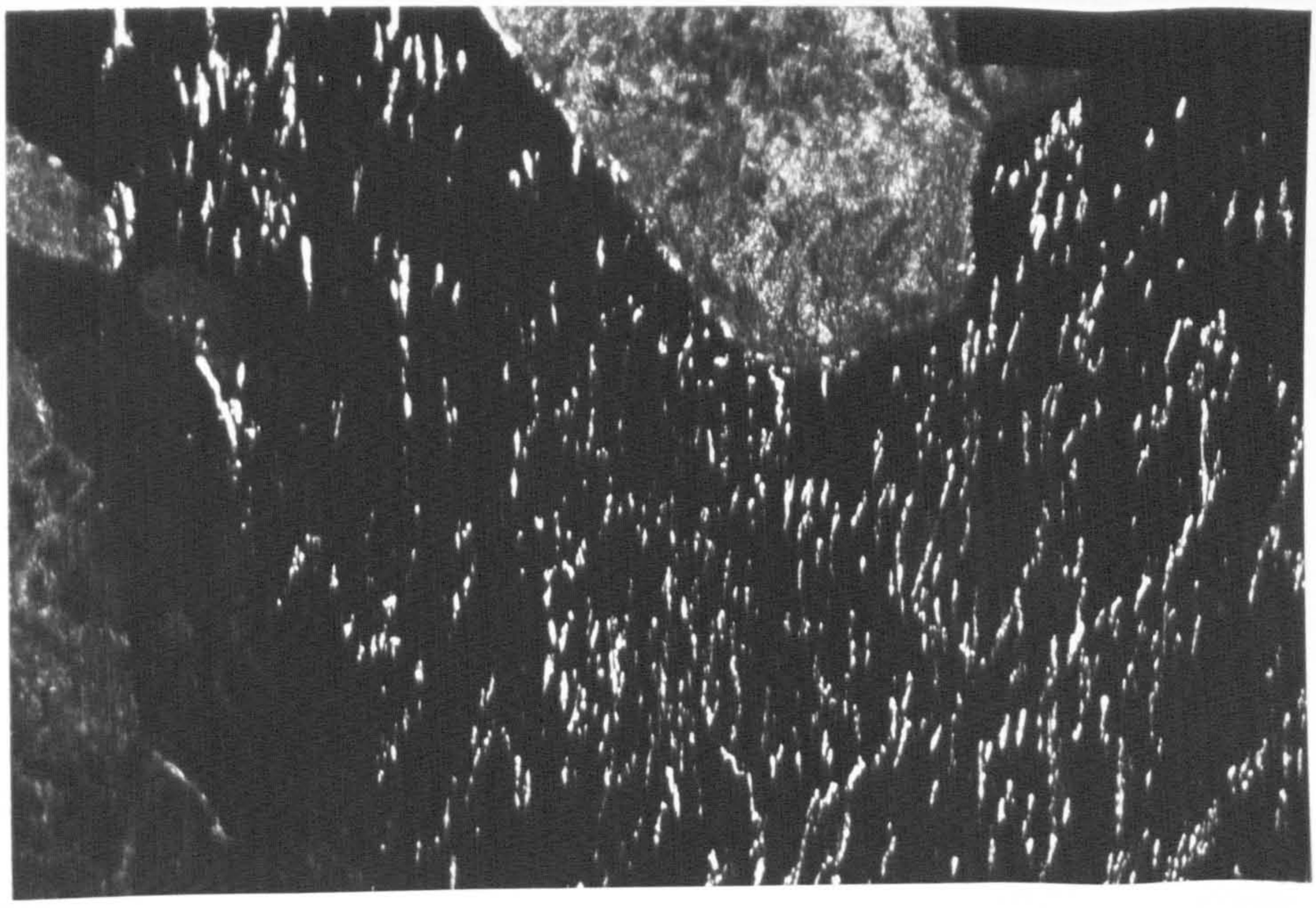

b

Fig. (5.6)

Fig. 5.7 Thin foil micrographs of a thin specimen of En41B, nitrided at 500°C in 16% NH_3

a - Bright field image showing undissolved carbides on the lath boundaries, and fine particles of CrN in the background

b - Dark field image of (a) showing finely dispersed CrN particles

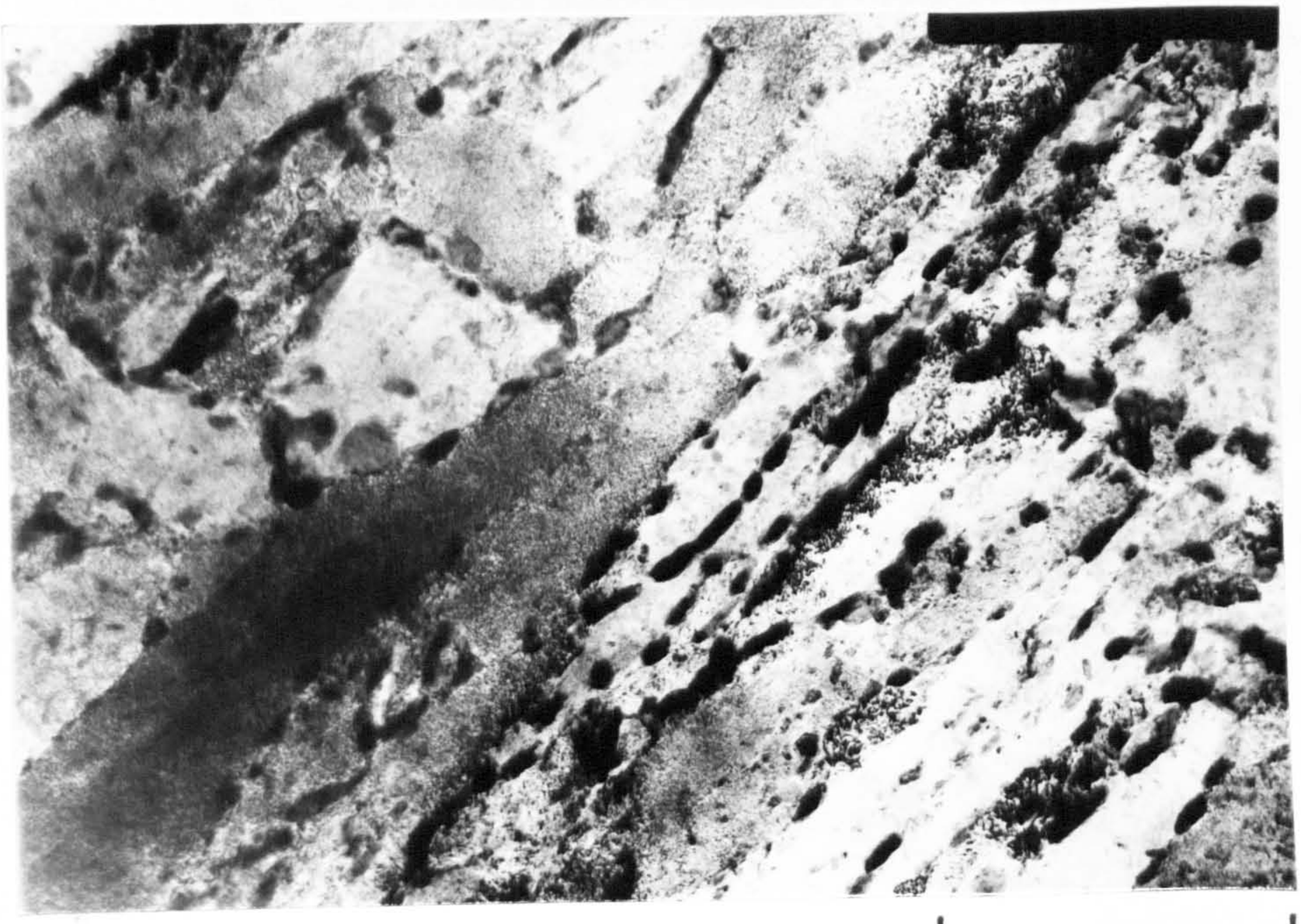

a

1 um

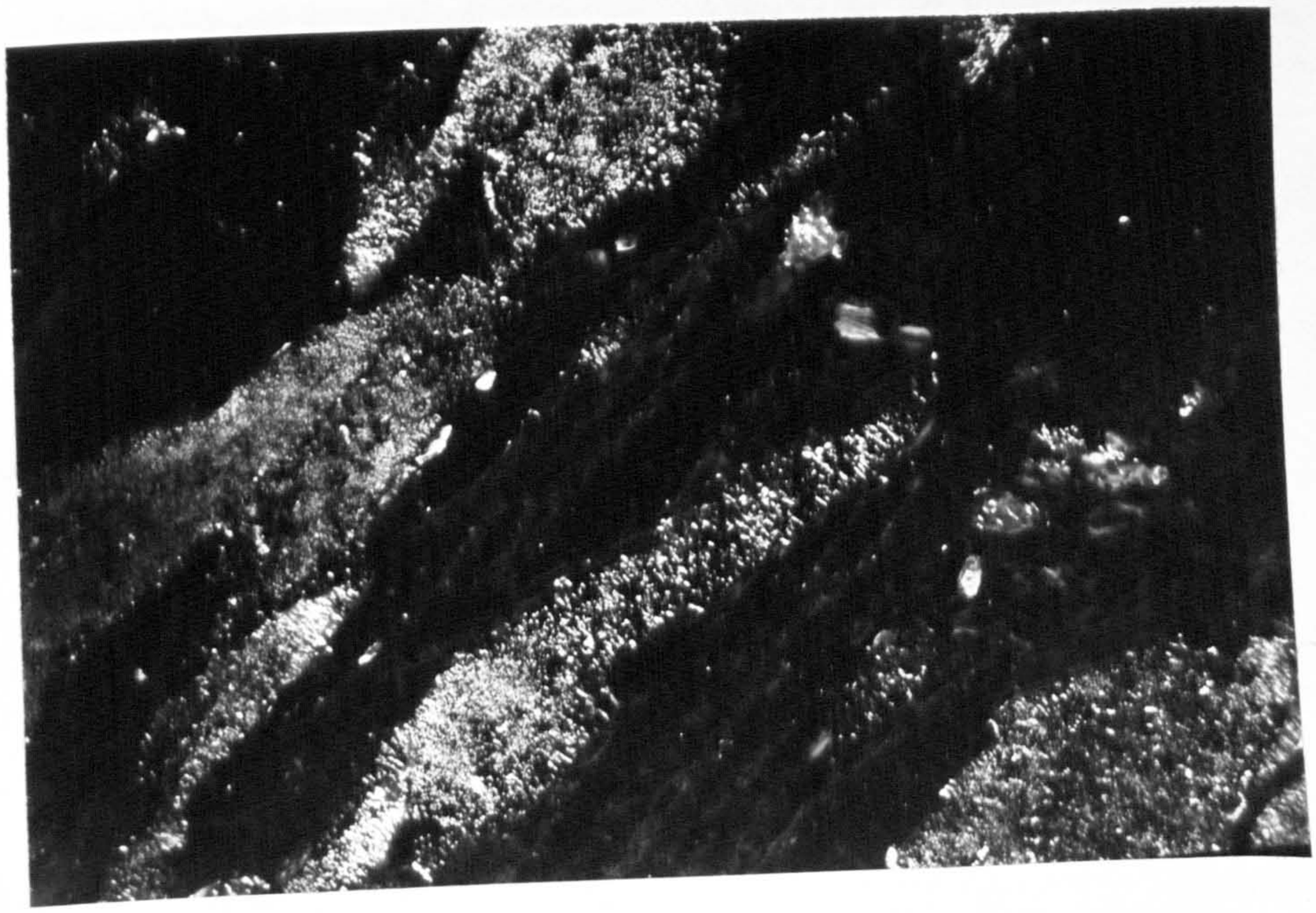

b

Fig. (5.7)

Fig. 5.8 Thin foil micrographs of thin specimen of En41B, nitrided at 570^{o}C in 13% NH_3

a - Bright field image showing large and fine particles

b - Dark field image showing both types of particles are CrN, indicating that the carbides have transformed into nitrides

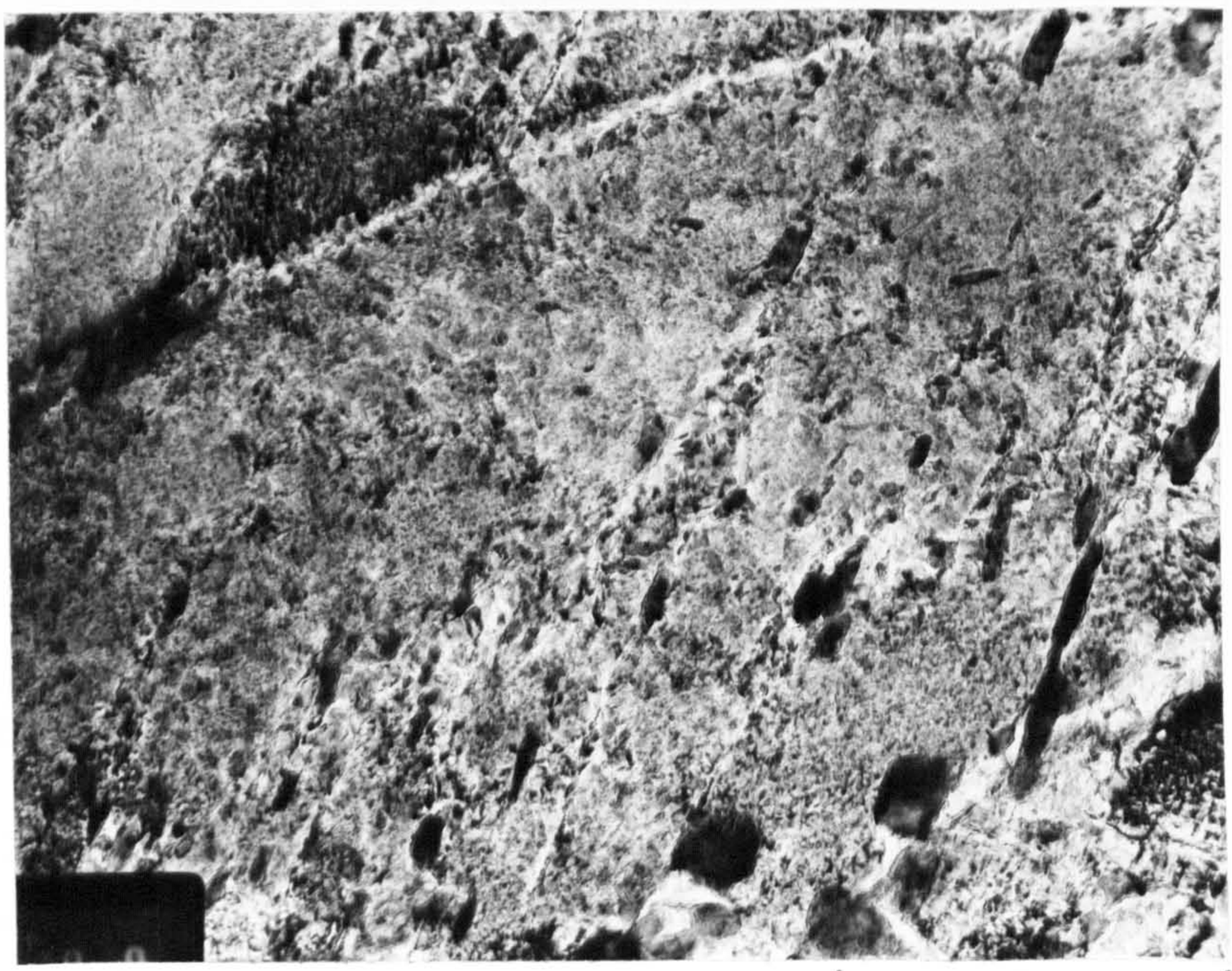

a

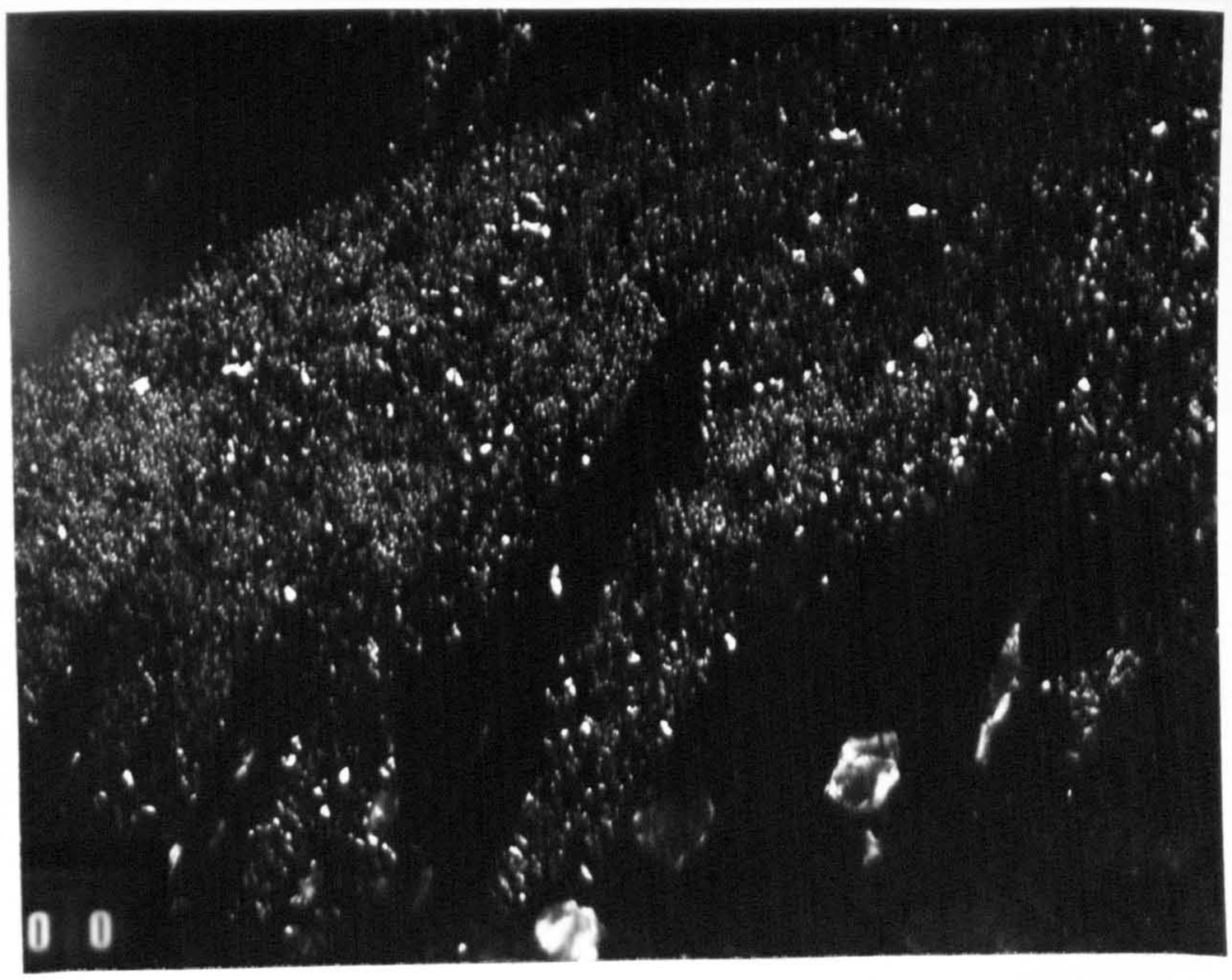

b

Fig. (5.8)

Fig. 5.9 Transmission electron micrographs from a two-stage carbon extraction replica of a bulk specimen of En41B, nitrided at 500°C in 80% NH_3

a - Bright field image showing large and fine particles

b - Diffraction pattern of CrN

c - Dark field image of a. Note the large CrN particles

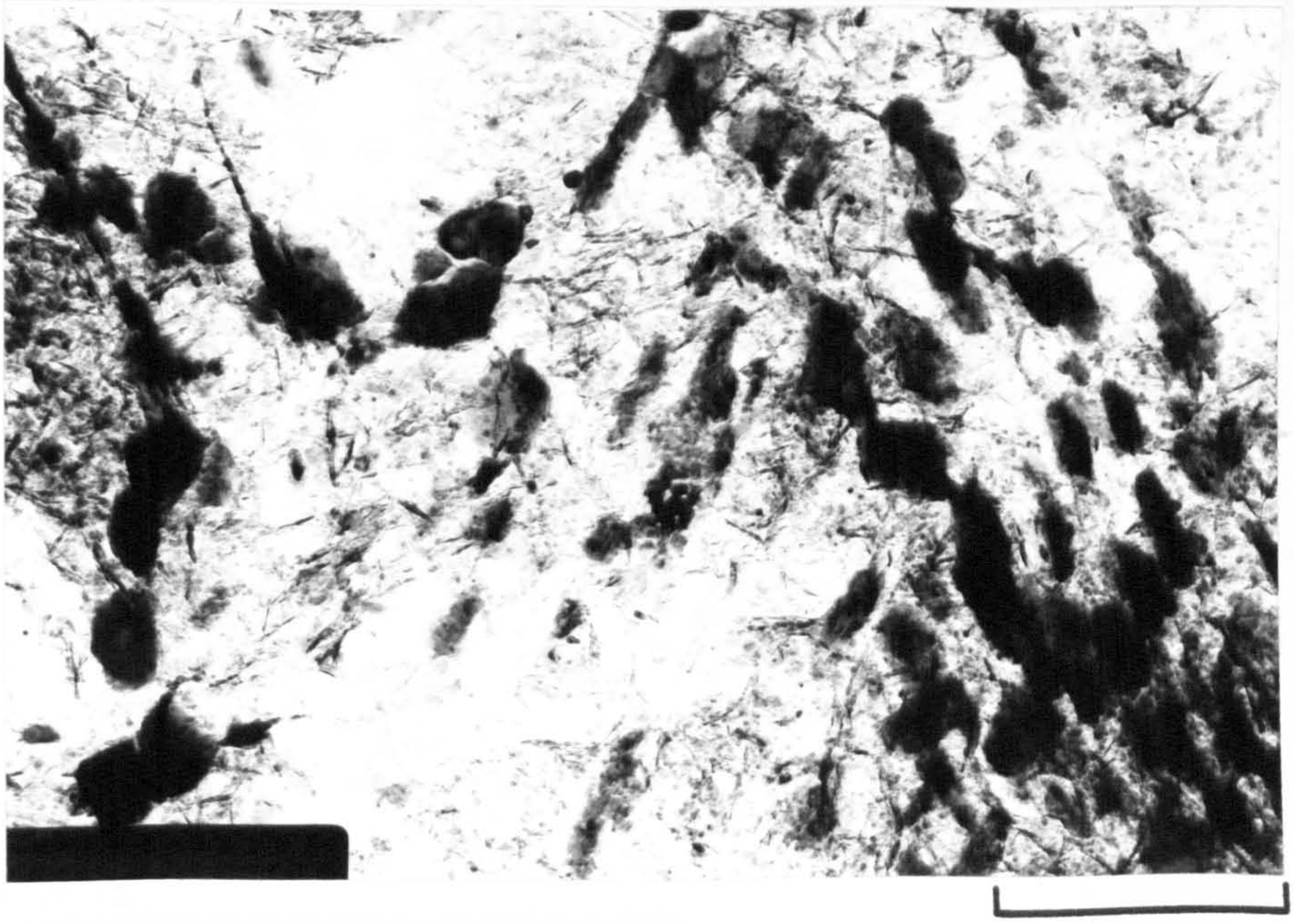

a

0.5 um

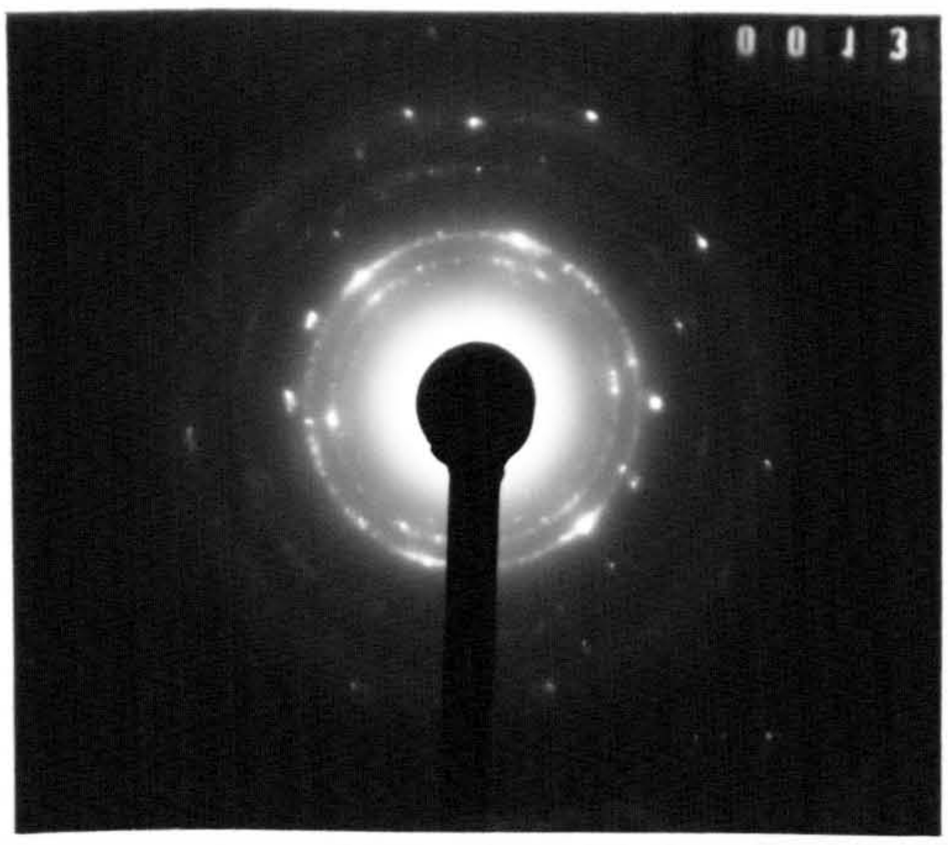

b

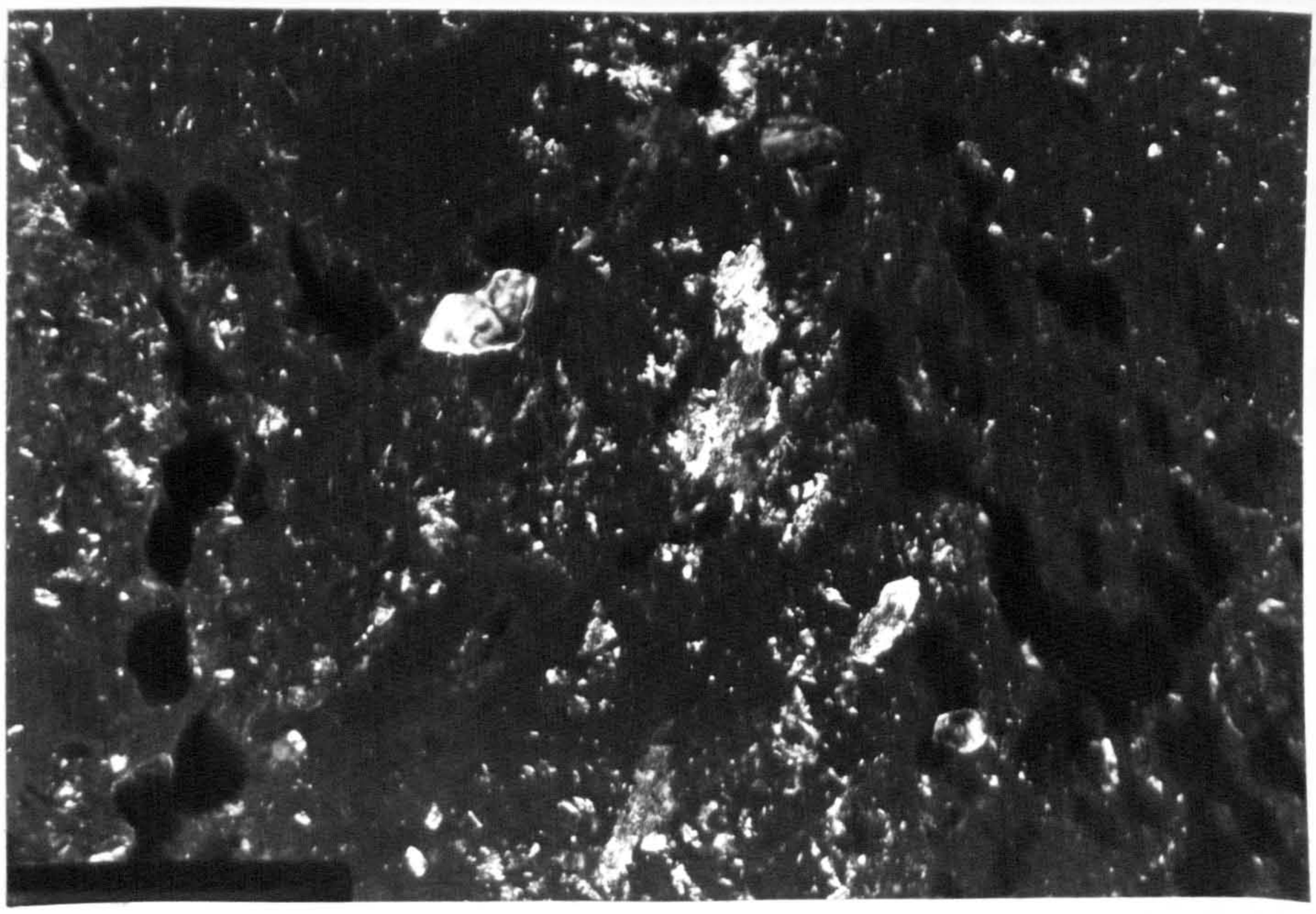

c

Fig. (5.9)

Fig. 5.10 Thin foil micrographs of a nitrided thin specimen of Fe-Cr-Al-C alloy

a - Bright field image showing fine CrN particles

b - Diffraction pattern containing streaks of CrN reflections

d - Dark field image showing fine plates of CrN.

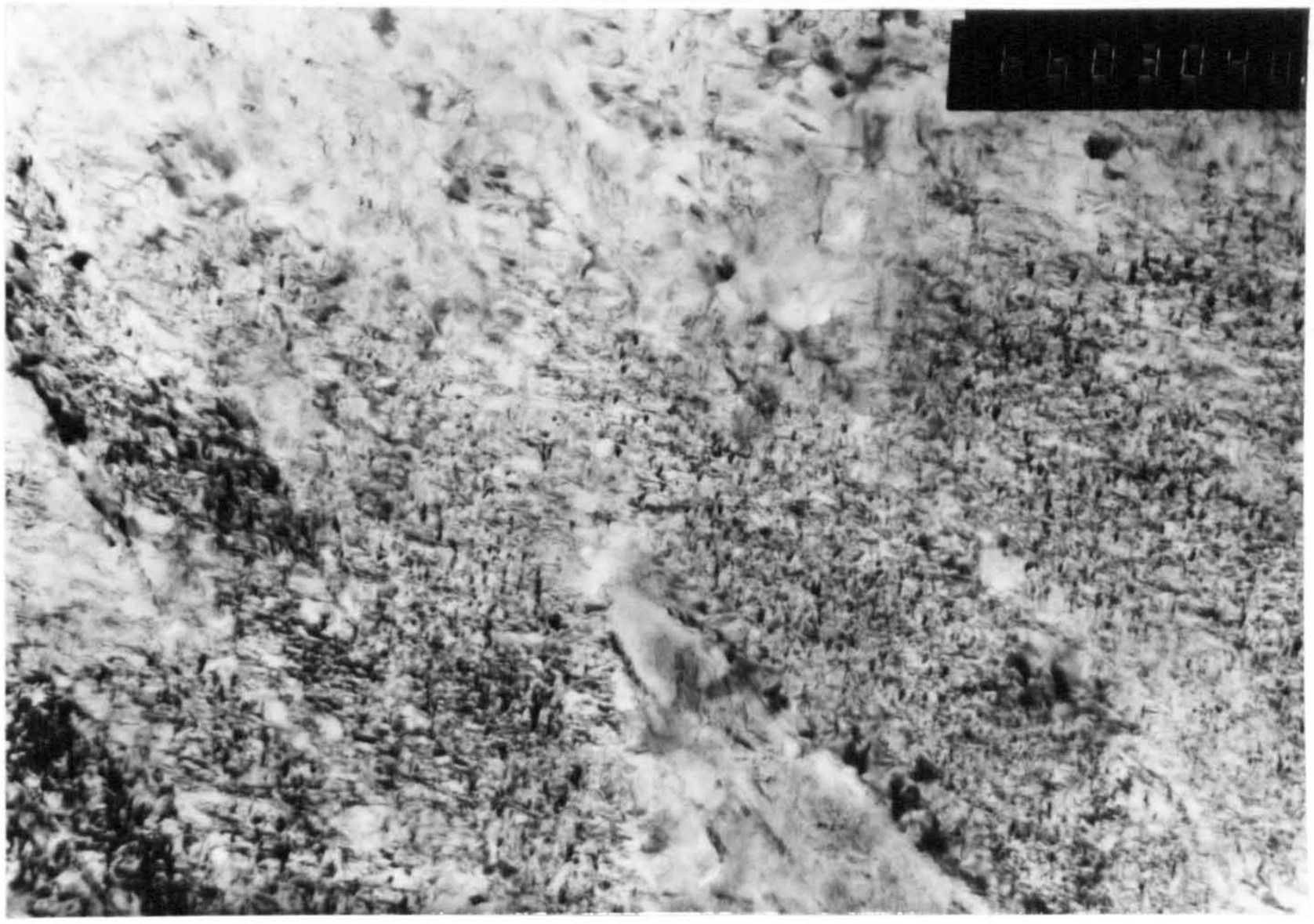

a

0.5 um

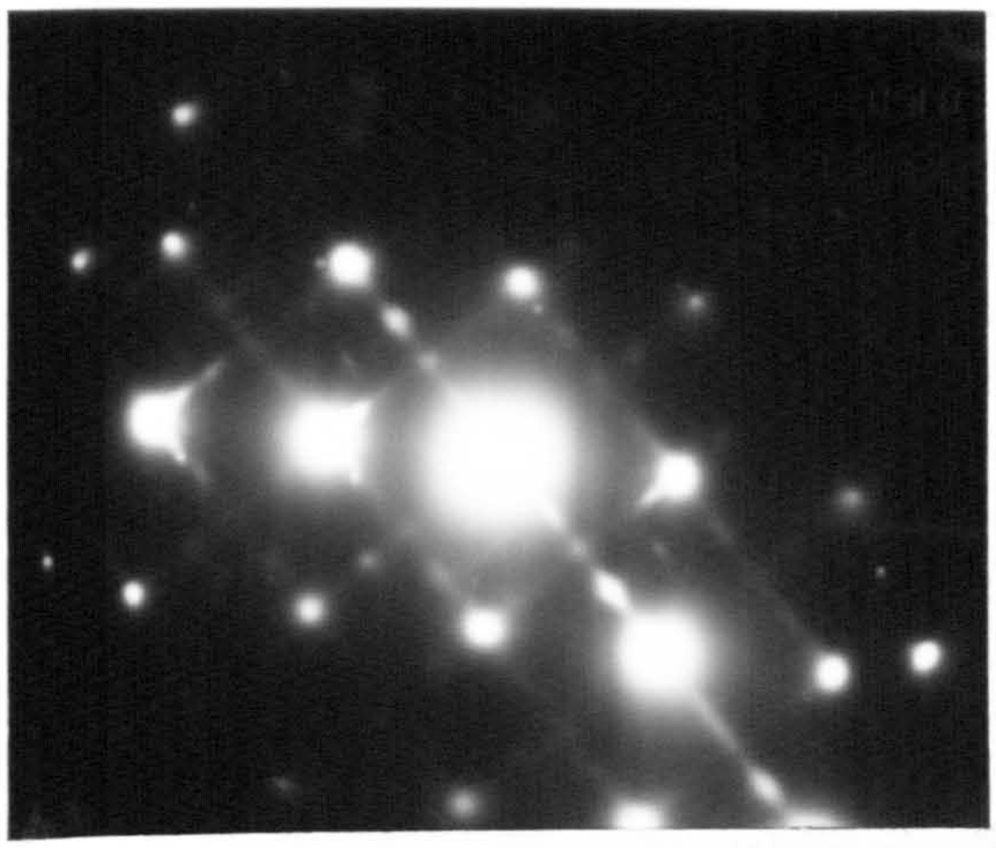

b

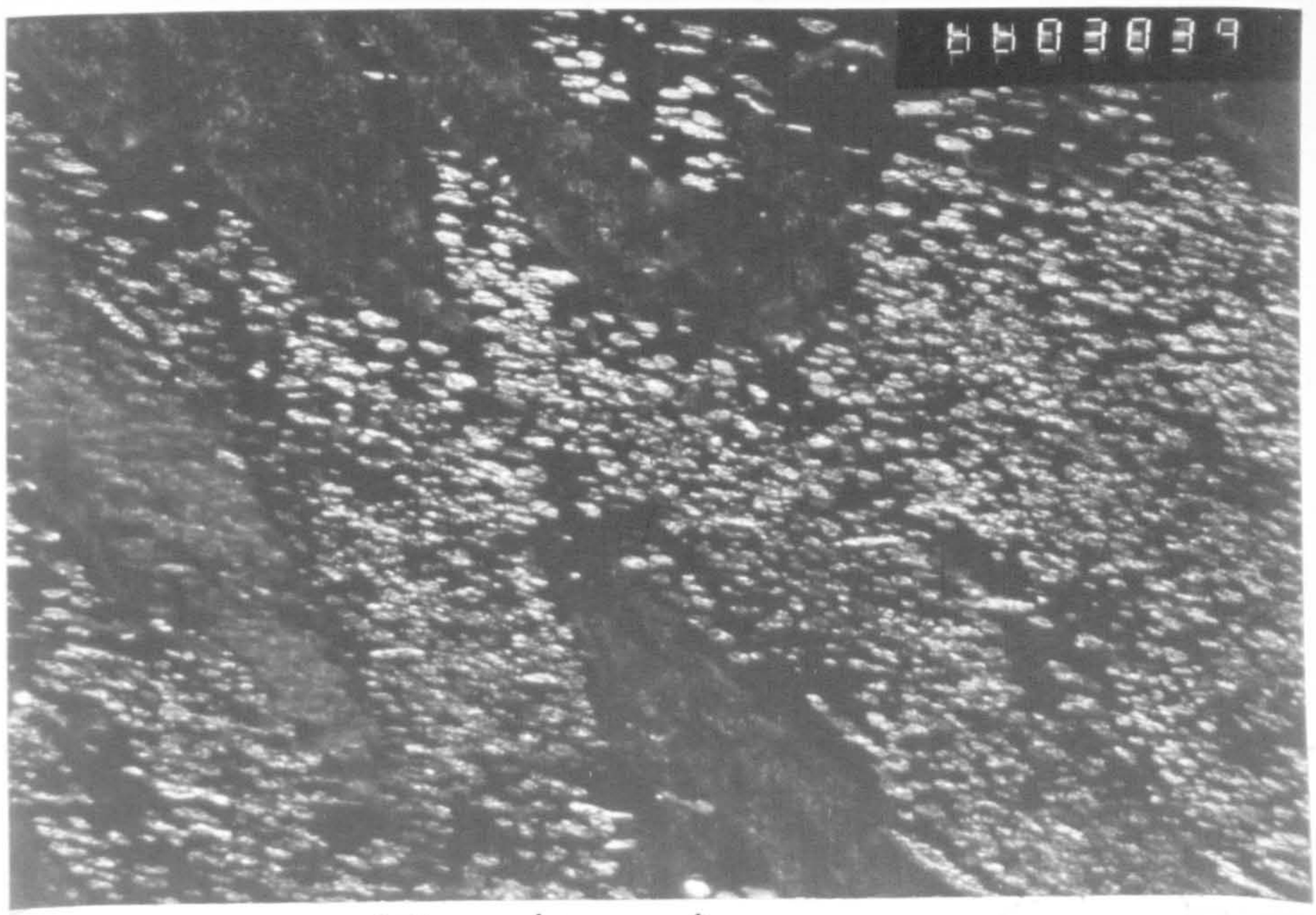

c

Fig. (5.9)

Fig. 5.11 Optical micrographs of nitrided En41B, etched in Oberhoffer's reagent, showing a dark stain at the case/core interface, probably indicating the presence of a carbon-rich layer

a - Nitrided at 570^{o}C in 80% NH_3 for 48h.

b - Nitrided at 500^{o}C in 80% NH_3 for 72h.

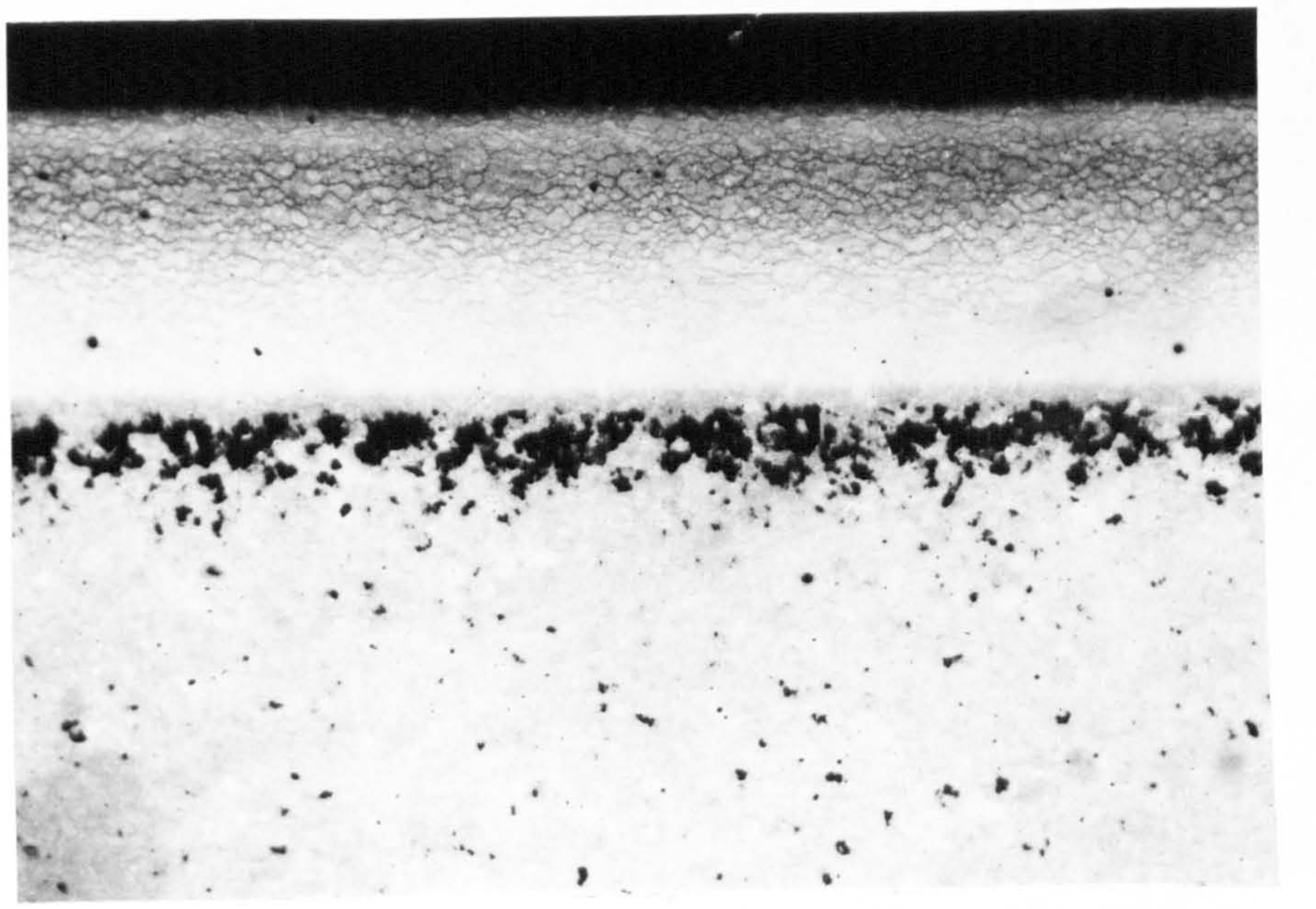

a

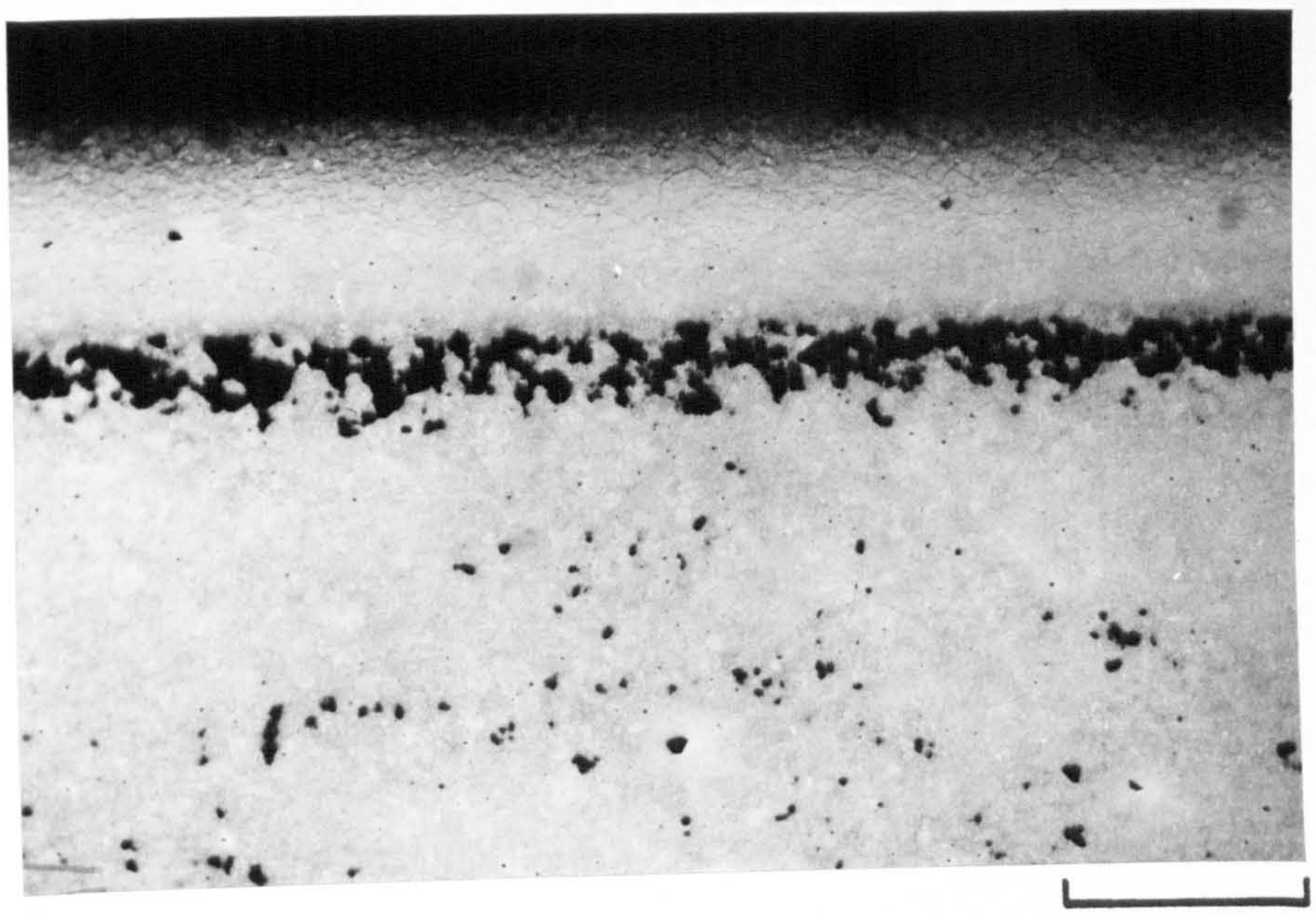

b

500 um

FIG. (5.11)

Fig. 5.12 Optical micrographs of the chromium-free steels, nitrided at 570°C in 80% NH_3 for 48h etched in Oberhoffer's reagent

a - En41(-Cr) steel, showing the presence of a carbon rich layer

b - Fe-C-Al steel, showing the absence of a carbon rich layer

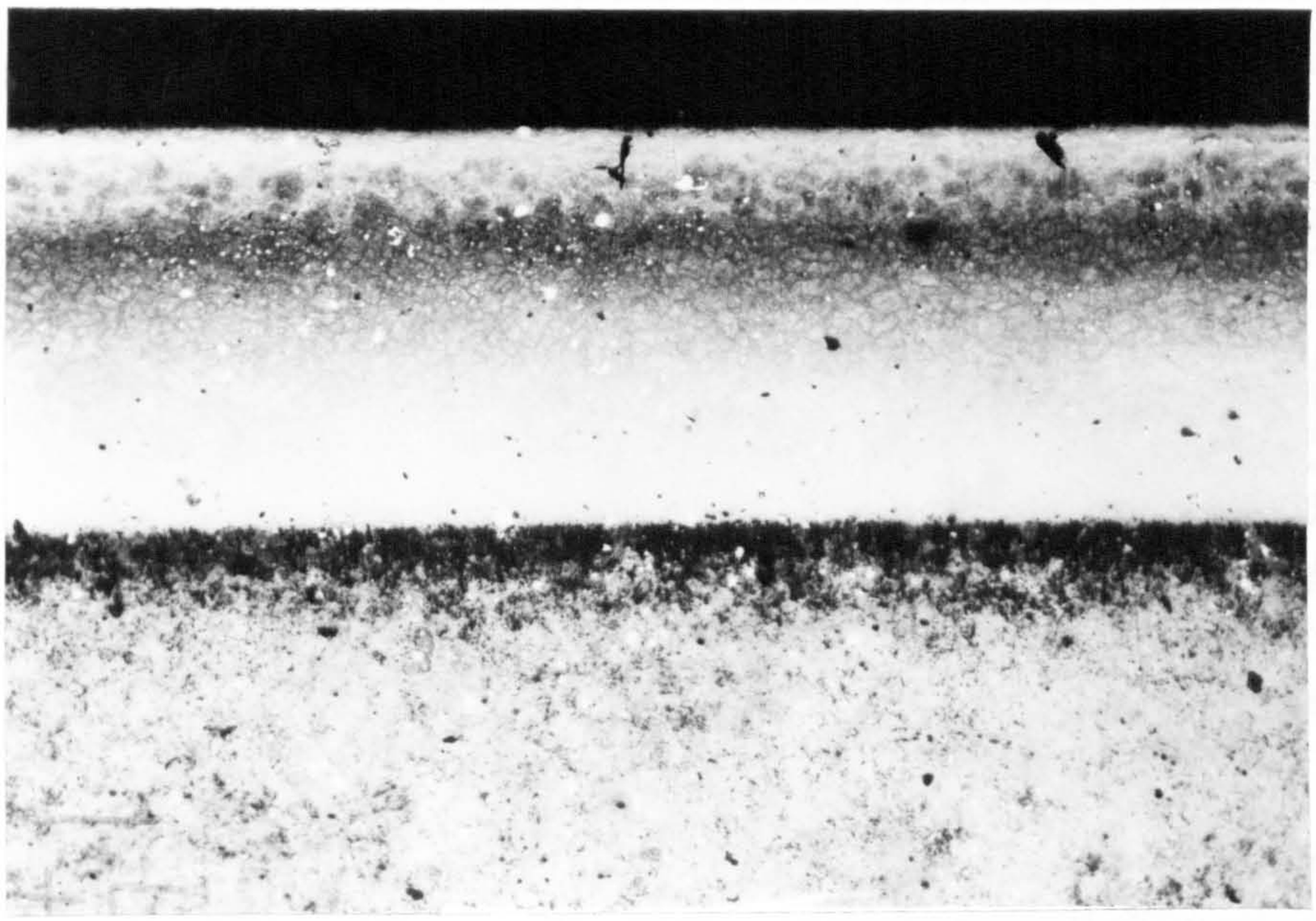

a

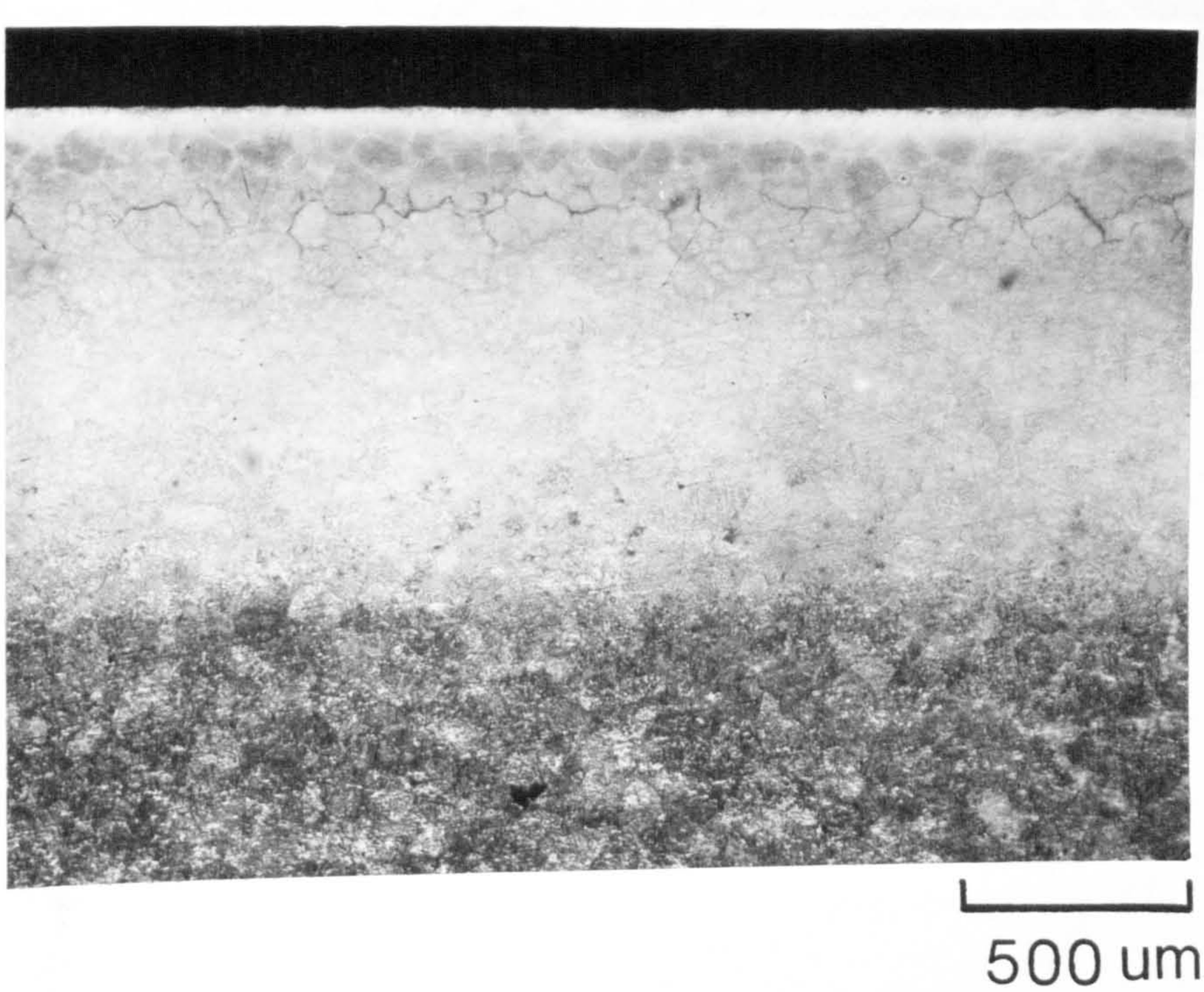

b

500 um

FIG. (5.12)

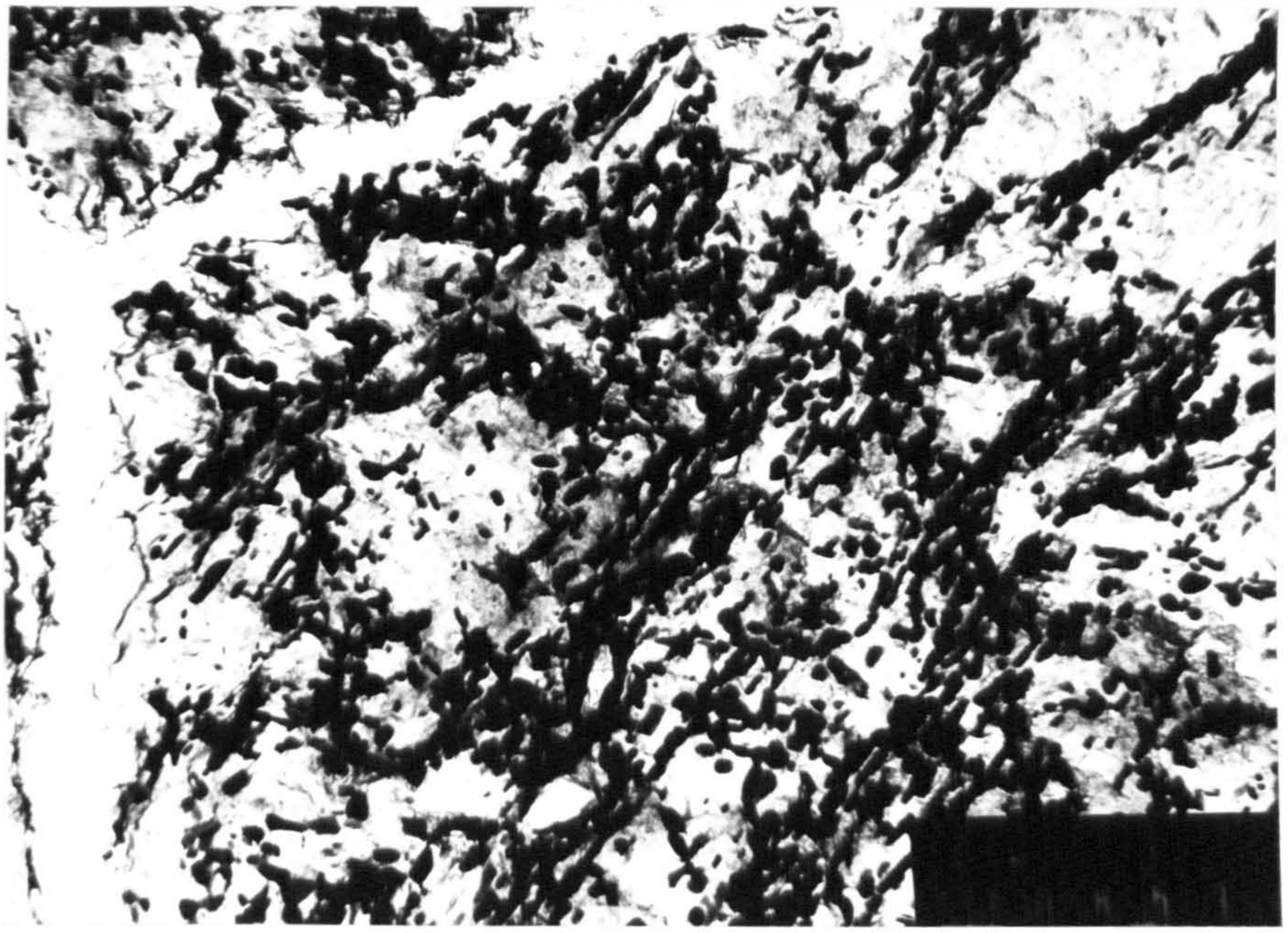

Fig. 5.13 Transmission electron micrograph of an extraction carbon replica taken from a bulk specimen of Fe-C-Al, nitrided at 570^{o}C in 80% NH_3. The micrograph is from an area just under the white layer, showing a high carbide concentration.

Fig. 5.14 Optical micrographs of a) En41B, b) En41(-Cr) and c) Fe-C-Al, nitrided at 570°C in 80% NH_3 and etched in ferricyanide solution. The micrographs show the presence of a carbide pile-up just under the white layer as well as the grain boundary phase (Fe_3C). Note the dark "bands" parallel to the surface in (b), these are carbides within the grains, probably along the lath boundaries.

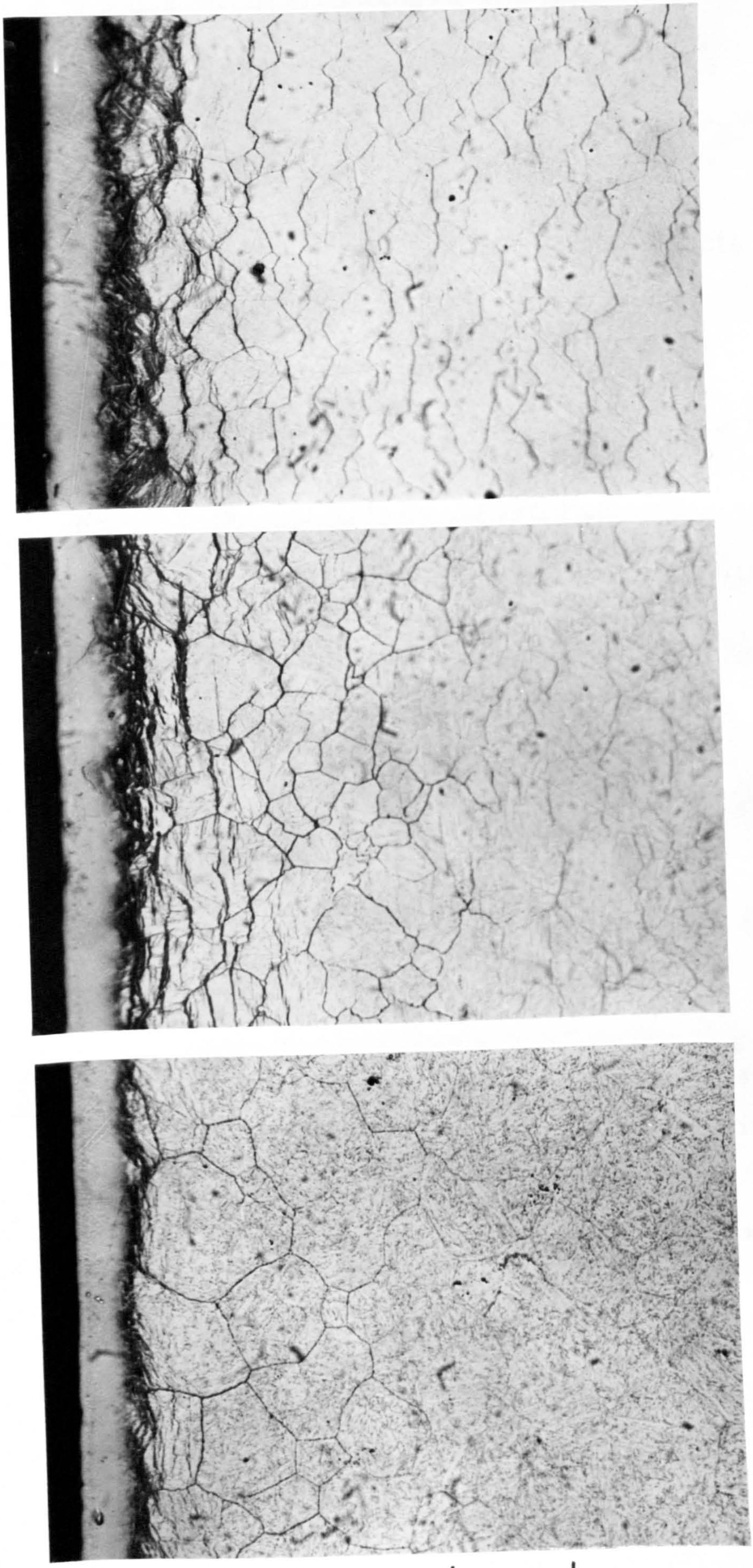

a

b

c

50 um

Fig. (5.14)

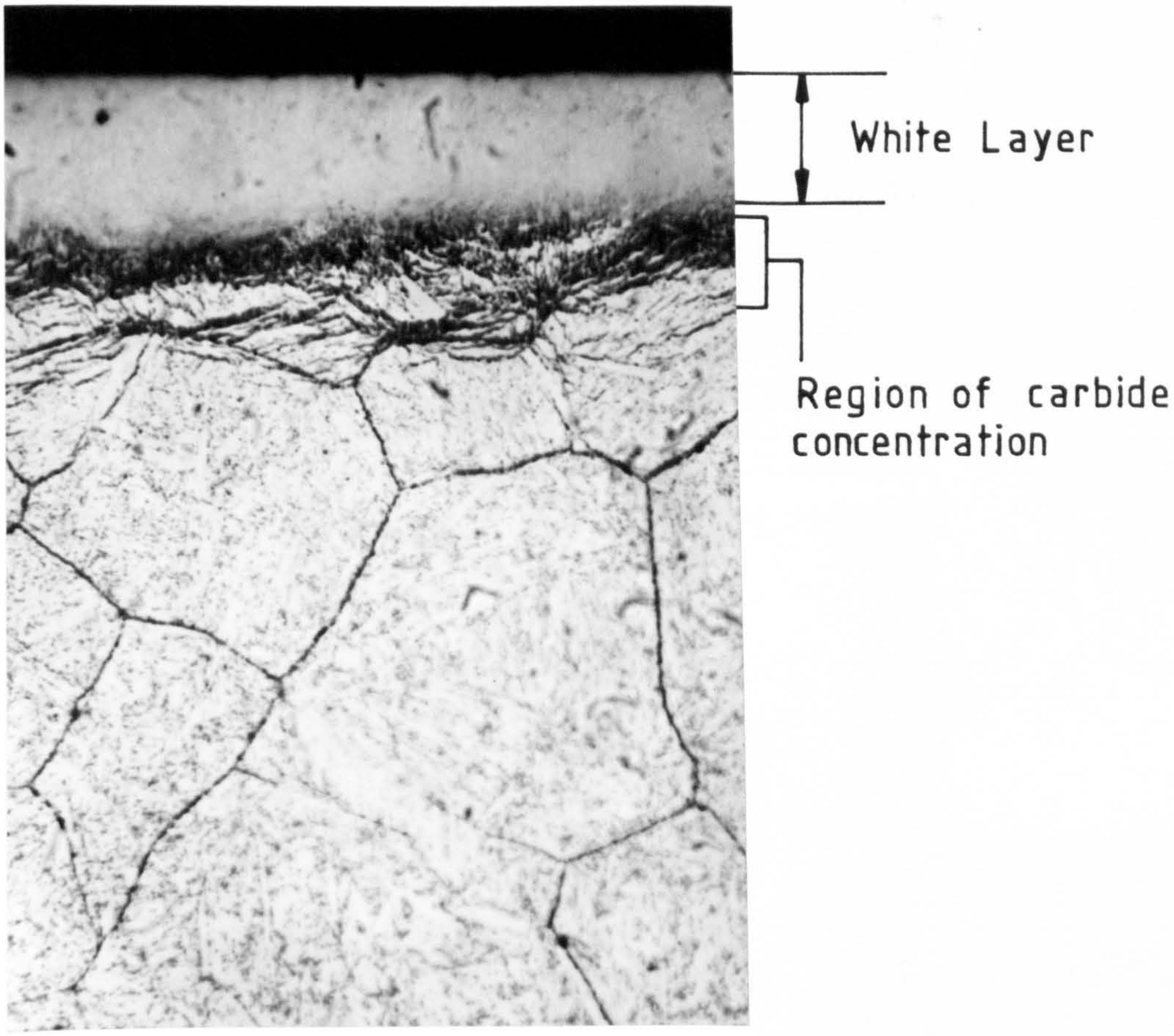

Fig. 5.15 Optical micrograph of F-C-Al steel, nitrided at 570^{o}C in 80% NH_3, and etched in ferricyanide solution, showing carbide concentration just under the white layer and the grain boundary phase (Fe_3C).

Fig. 5.16 Optical micrographs of Fe-C-Al nitrided at 570°C in 20% NH_3, showing the effect of tempering temperature prior to nitriding on decarburization during nitriding

a) Tempered at 500°C 1h

b) Tempered at 600°C 1h

c) Tempered at 700°C 1h

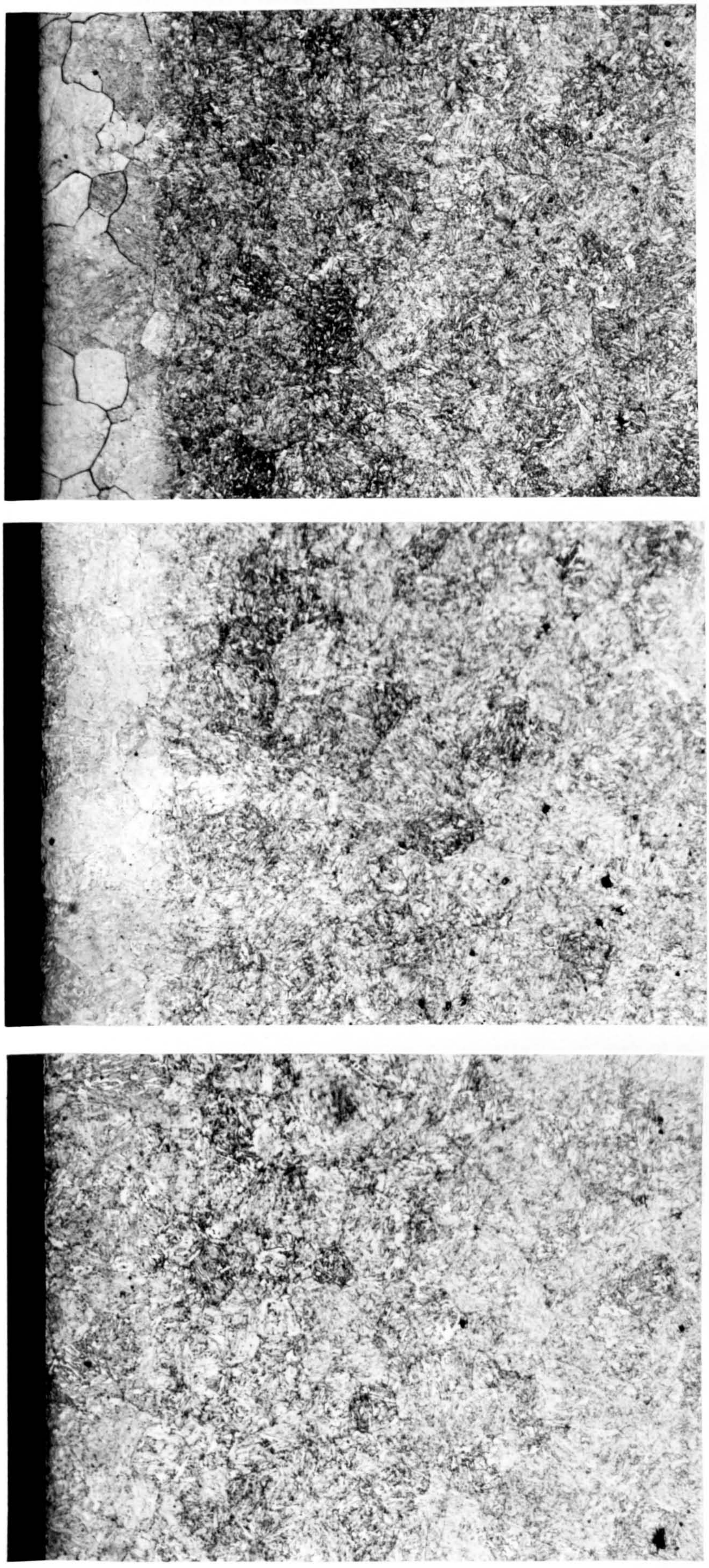

a

b

C

200 um

Fig. (5.16)

Fig. 5.17

a) Lower magnification of Fig. 5.16(a) showing the decarburized and the "nitrided" layers

b) Higher magnification of (a), clearly showing the carbides in the non-decarburized region. Note the unaffected grain boundary cementite

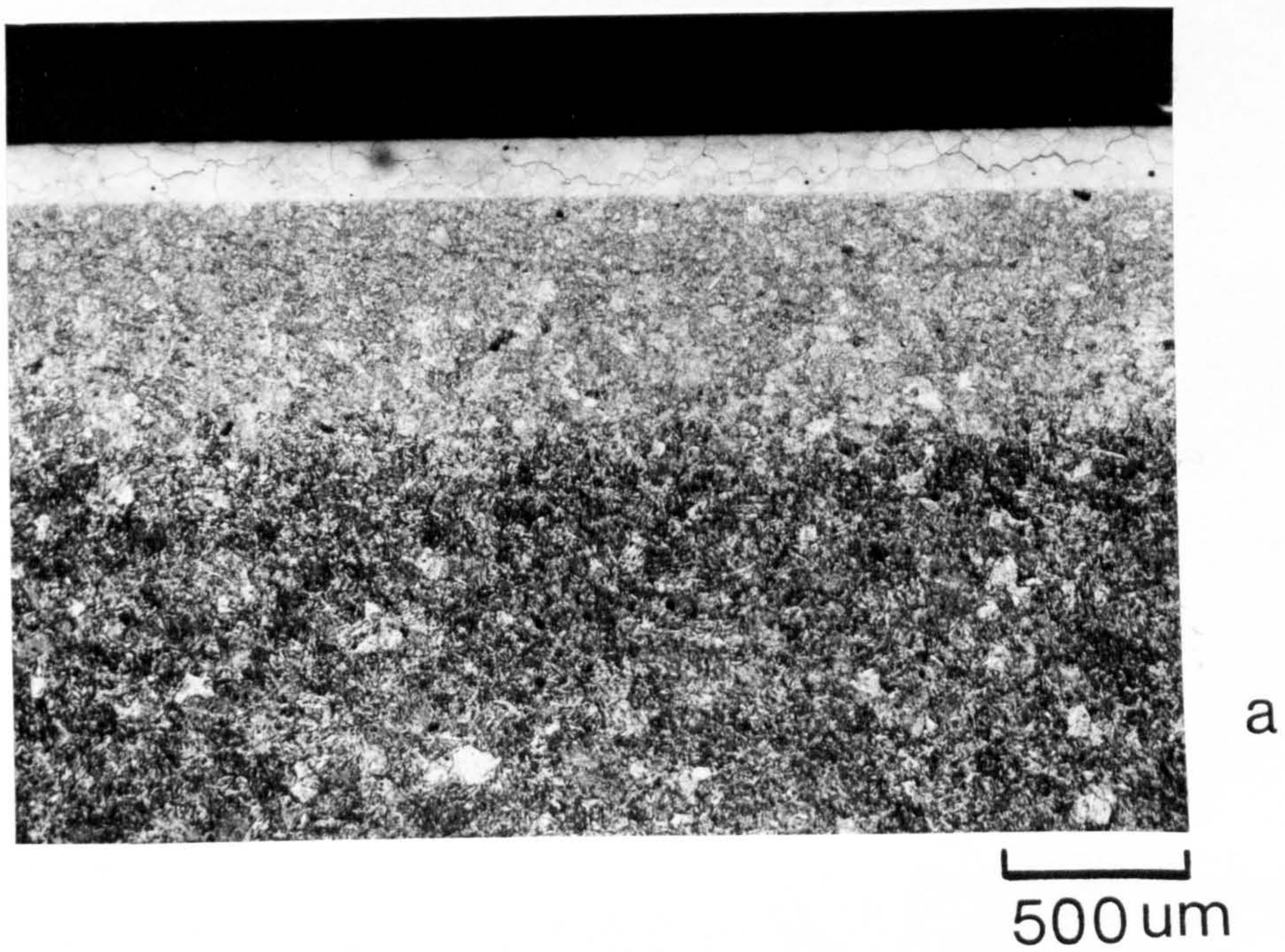

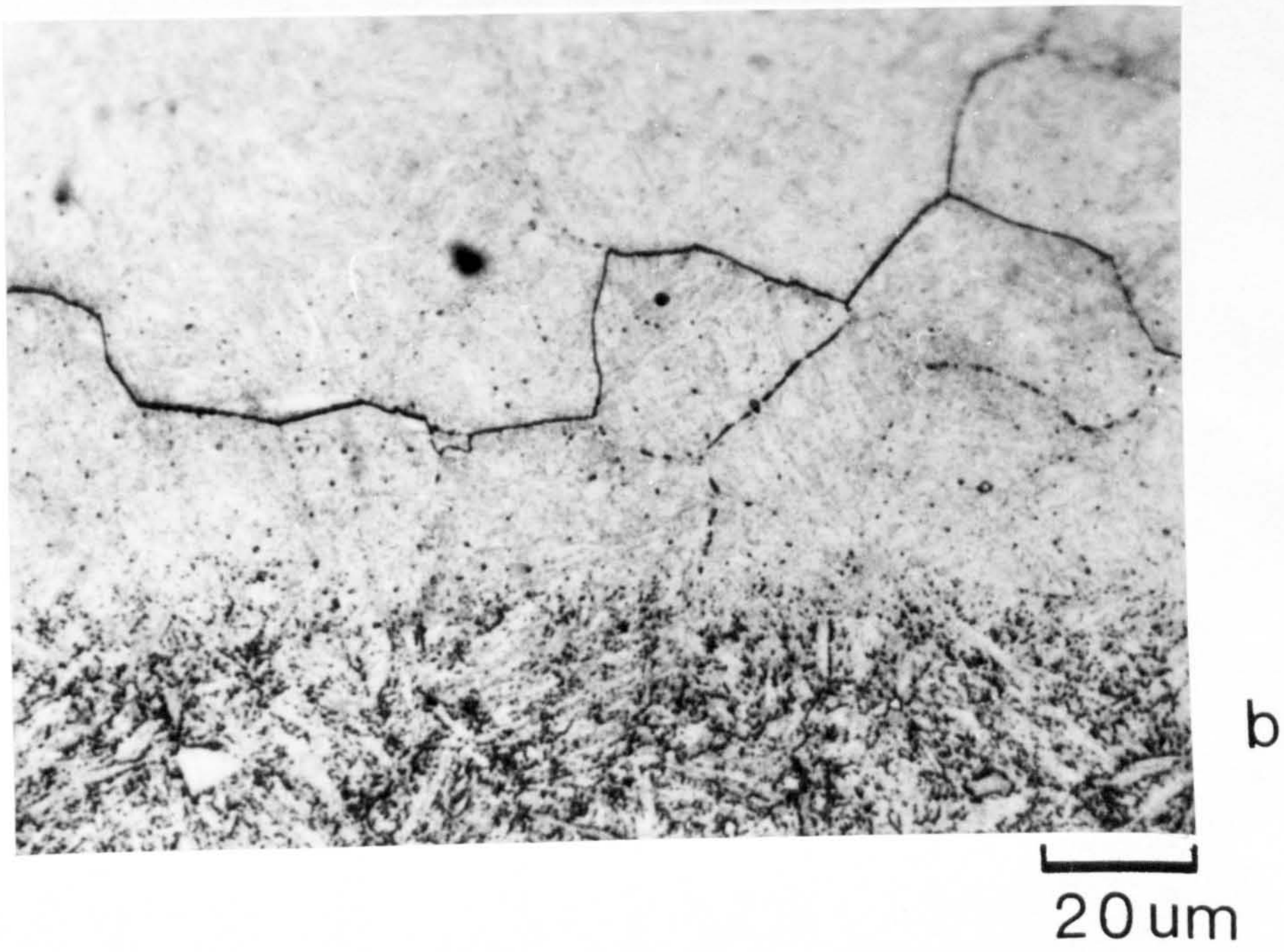

FIG. (5.17)

Fig. 5.18 Optical micrograph of En41(-Cr) nitrided at 500°C in 80% NH_3, etched in ferricyanide solution. Note the grain boundary phase which is more parallel to the surface than that observed in Fig. 5.14(b), which was from En41(-Cr) nitrided at 570°C.

Fig. 5.19 Transmission electron micrograph from a two-stage carbon replica of nitrided En41B steel, indicating that the formation of the grain boundary phase is influenced by the grain boundary inclination. Note the grain boundary perpendicular to the surface is free of grain boundary phase.

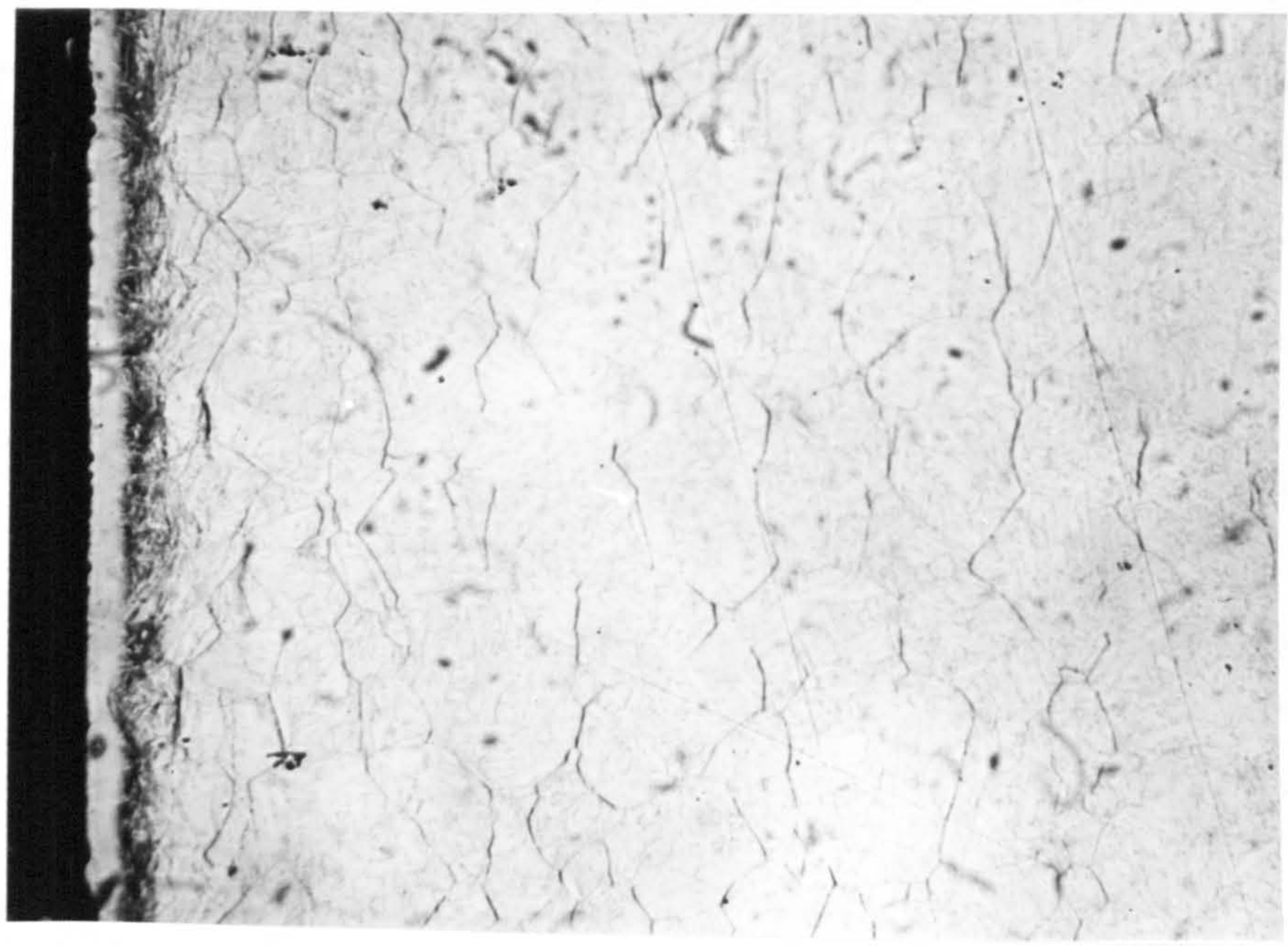

100 um

FIG. (5.18)

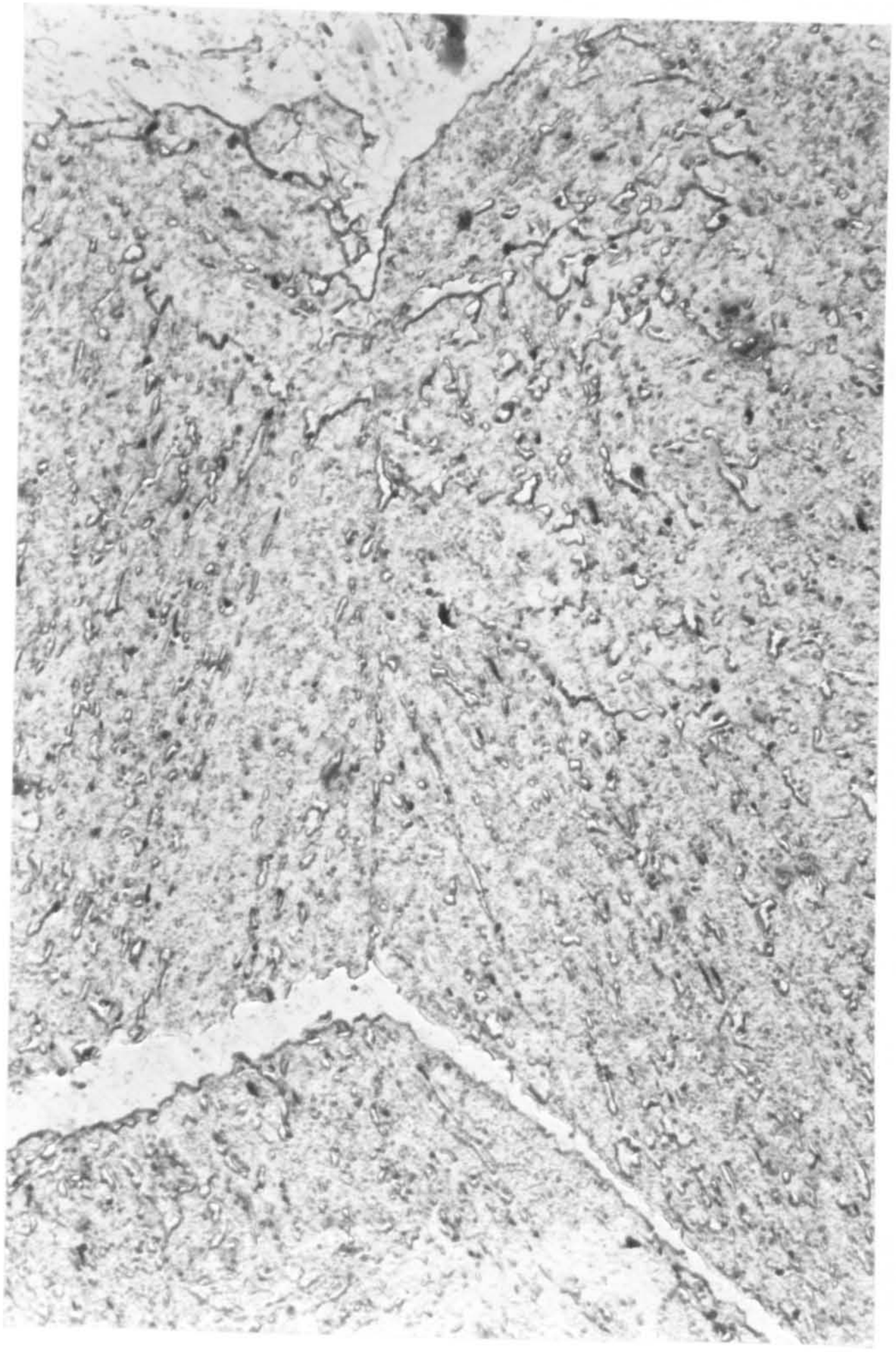

1 um

FIG. (5.19)

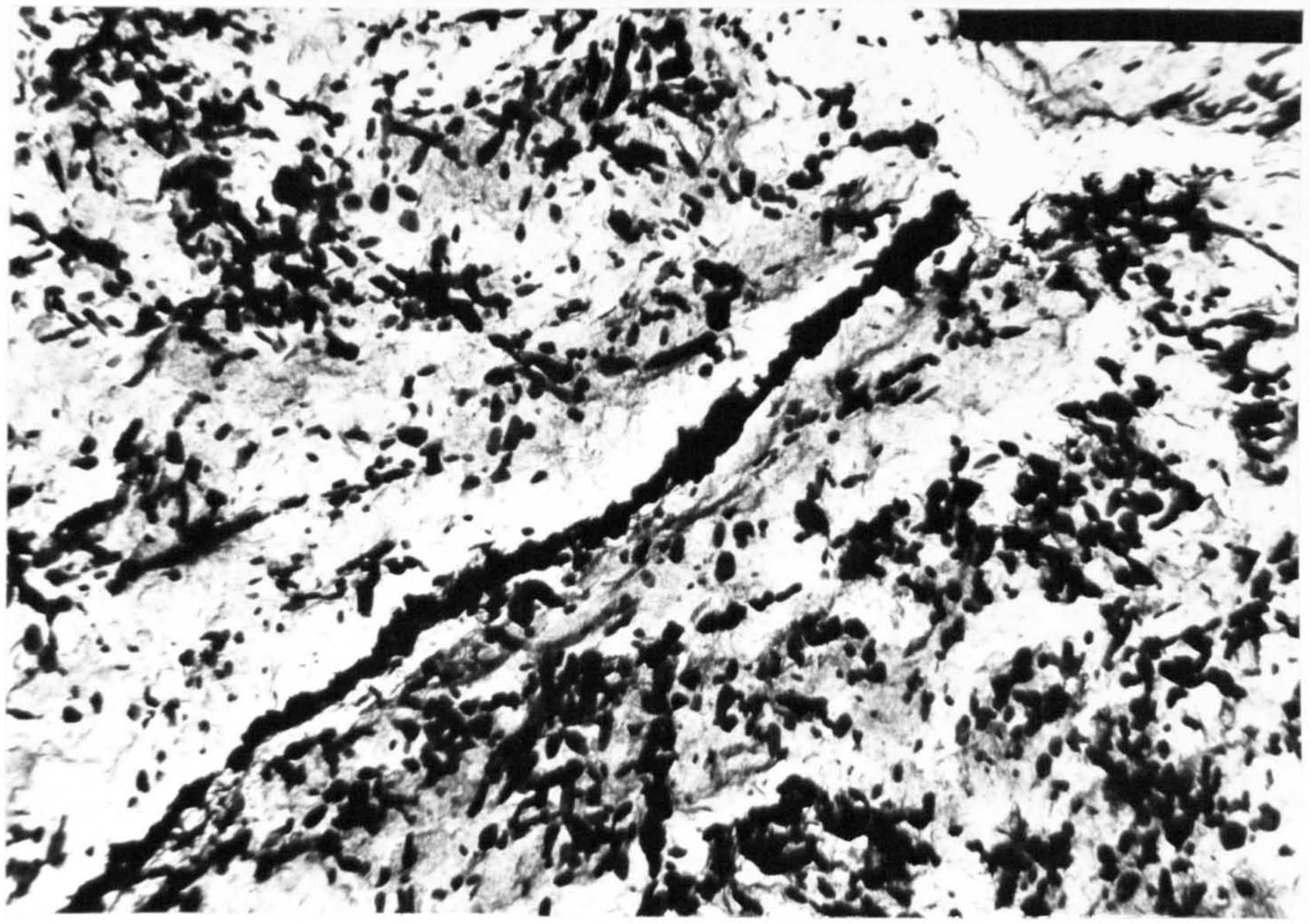

Fig. 5.20 Transmission electron micrograph of a two-stage extraction carbon replica, showing large portion of the grain boundary cementite formed as large carbides linked together

Fig. 5.21 Scanning electron micrograph of nitrided En41B, showing the porous nature of the white layer. Note the penetration down the austenite grain boundaries and through the grains.

Fig. 5.22 Transmission electron micrograph from a two-stage carbon replica of a nitrided EN41B, showing net-like penetration at the edge of the white layer.

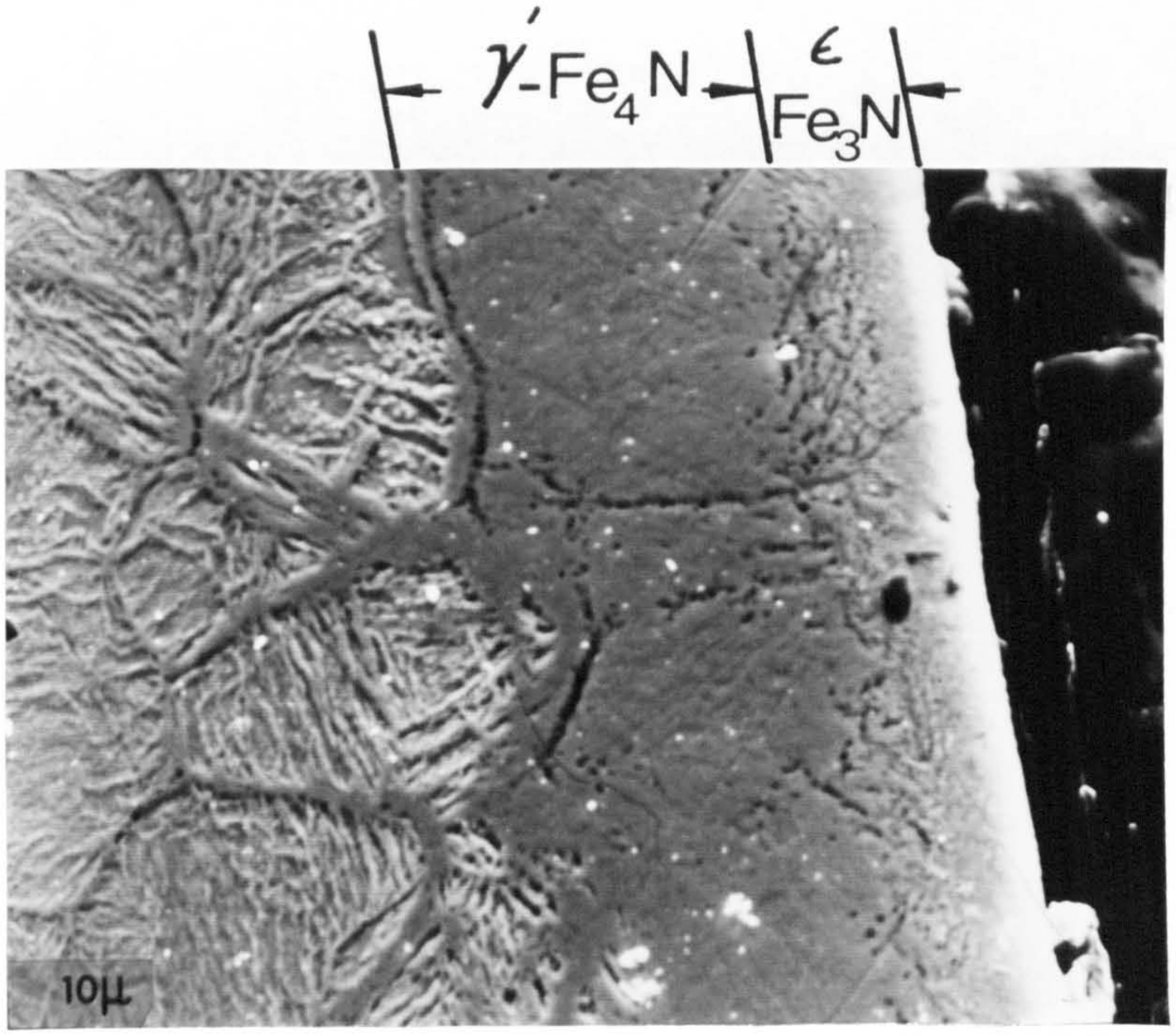

FIG. (5.21)

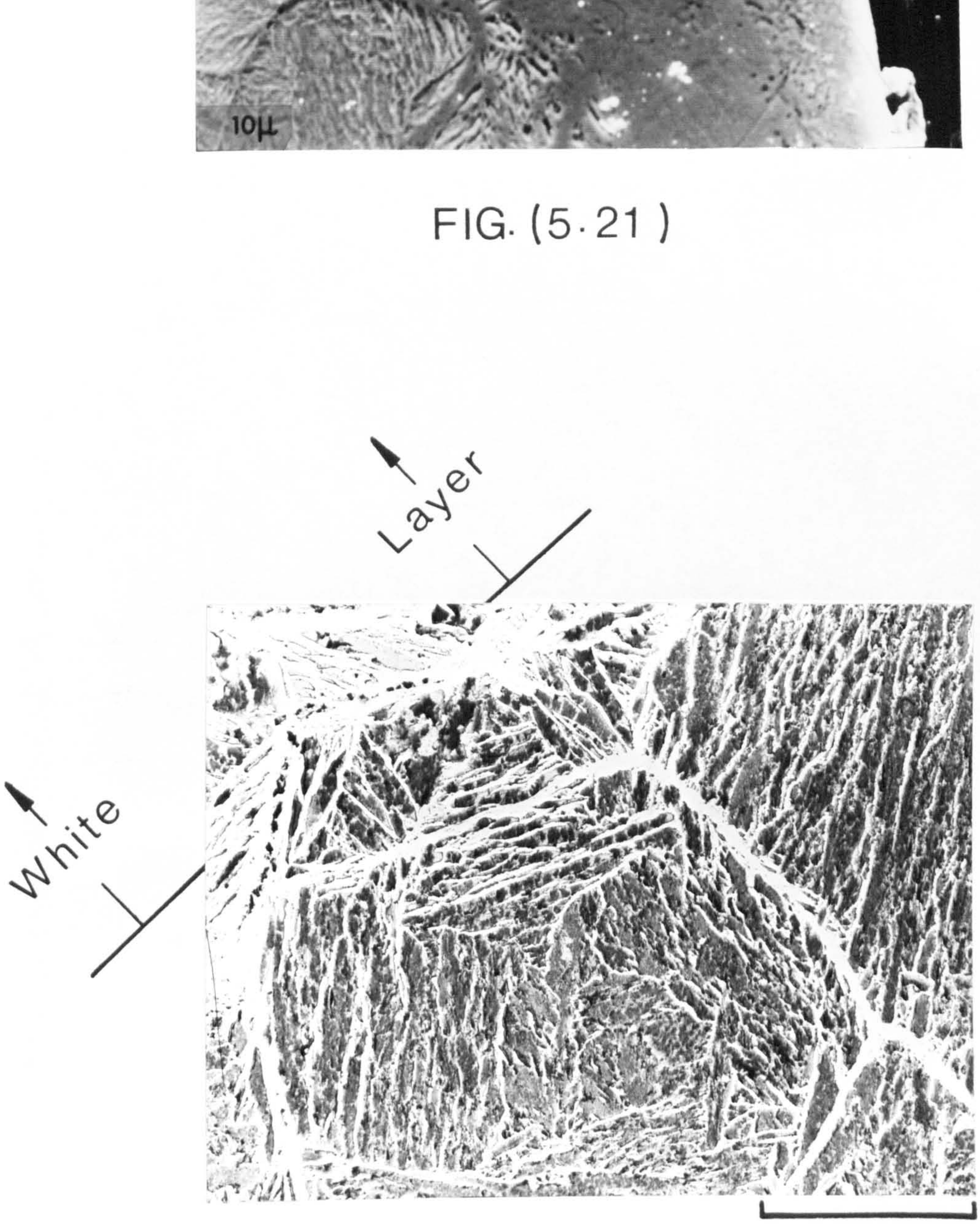

FIG. (5.22)

Fig. 5.23 Scanning electron micrographs showing the nature of the white layer in different materials nitrided at 500°C in 80% NH_3

a) En41B steel

b) En41(-Cr) steel

c) Fe-C-Al steel

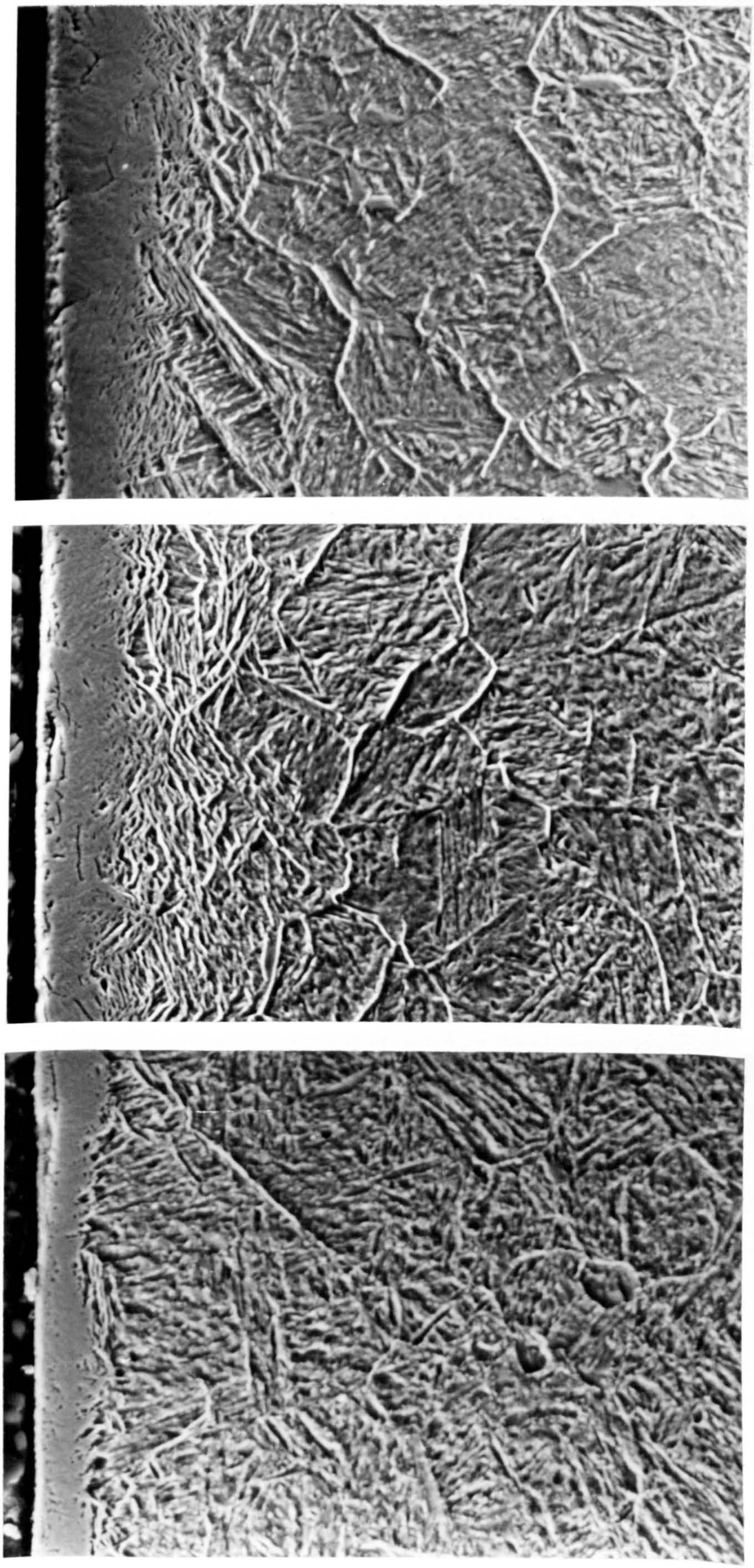

FIG.(5.23)

Fig. 5.24 Scanning electron micrographs showing the different nature of the white layer in different materials, nitrided at 570^{o}C in 80% NH_3.

a) En41B steel

b) En41(-Cr) steel

c) Fe-C-Al steel

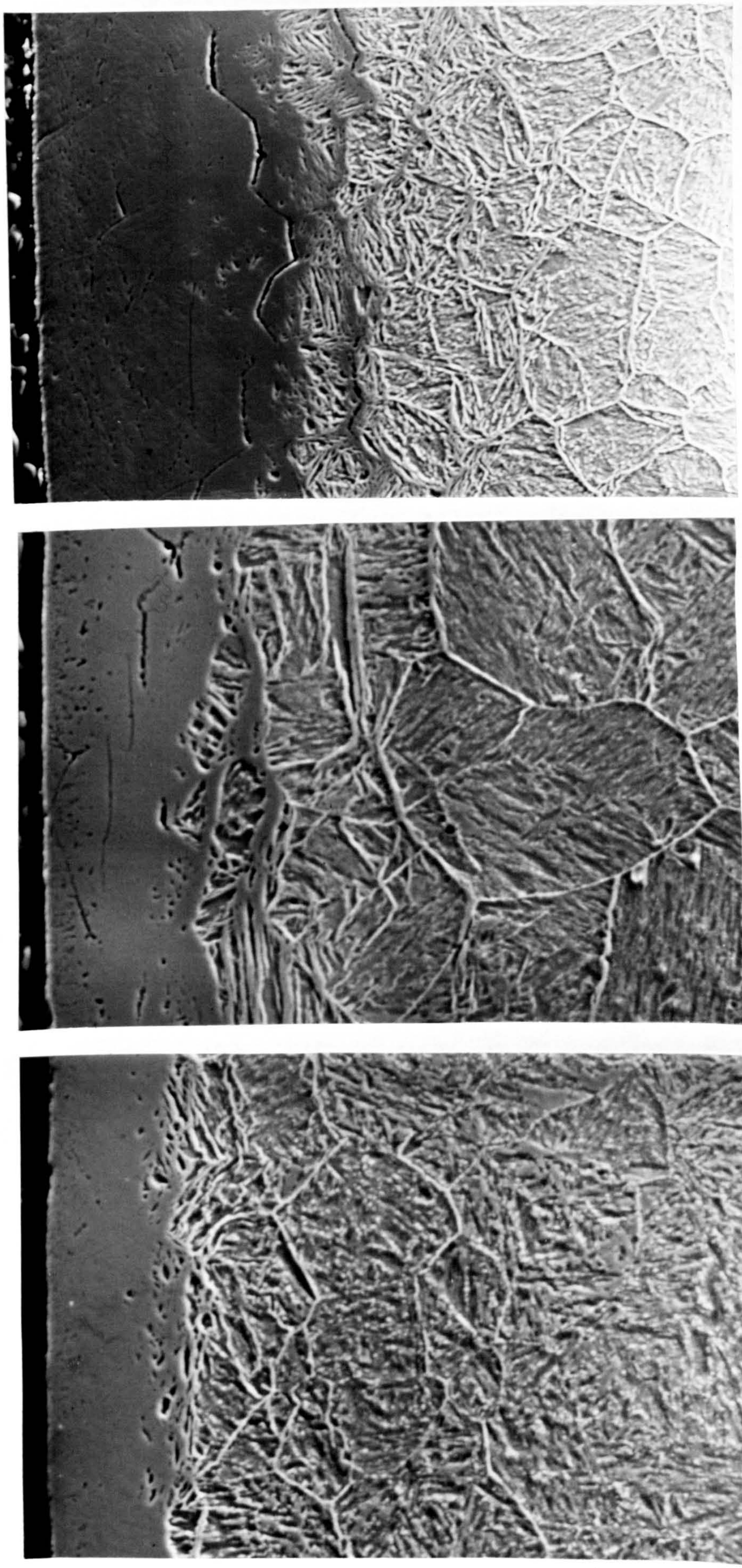

FIG. (5.24)

Fig. 5.25 Optical micrographs of nitrided Fe 0.52 Al alloy

a) showing iron nitride penetration down a grain boundary

b) showing different growth rates of the white layer in different grains

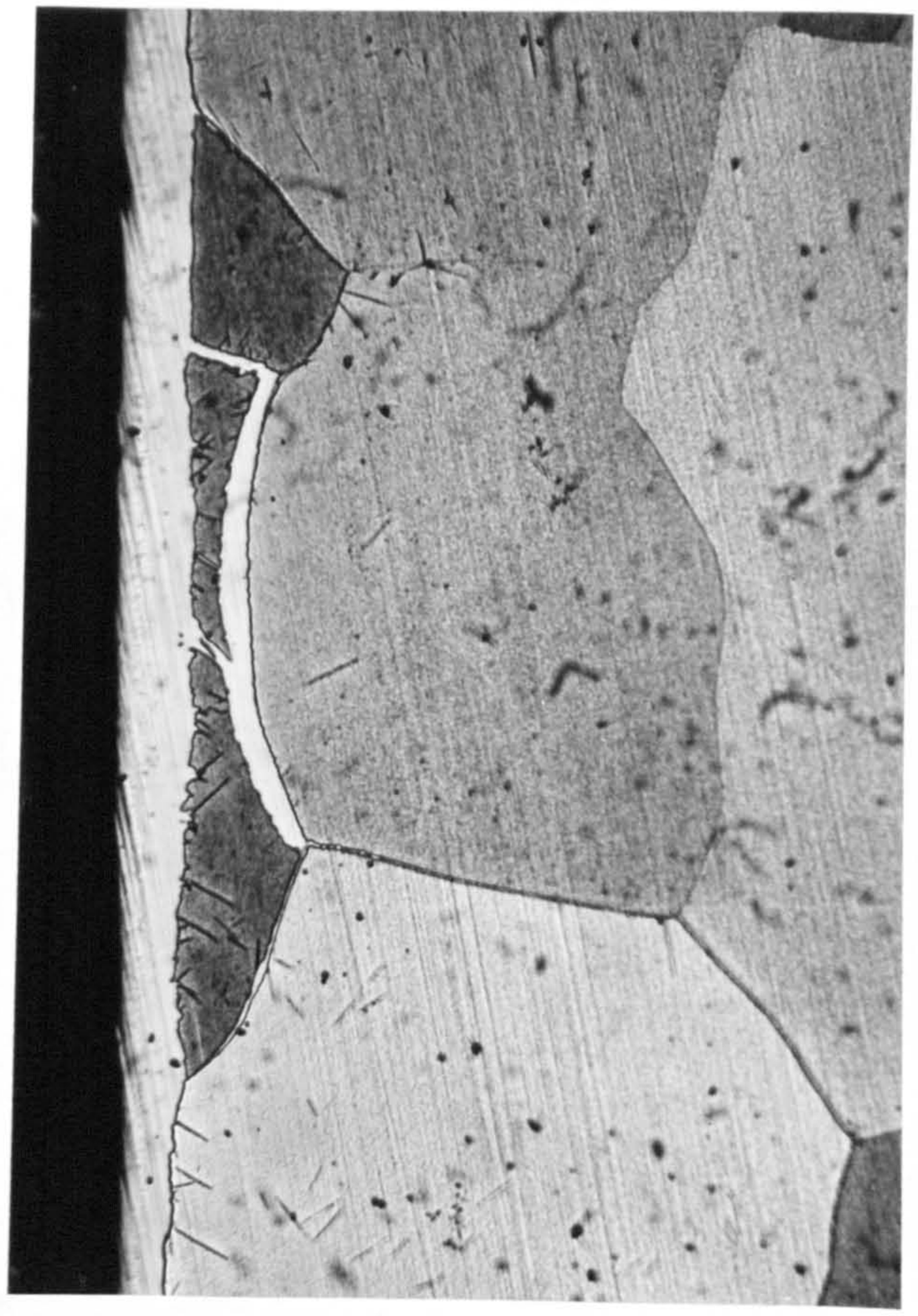

a

50um

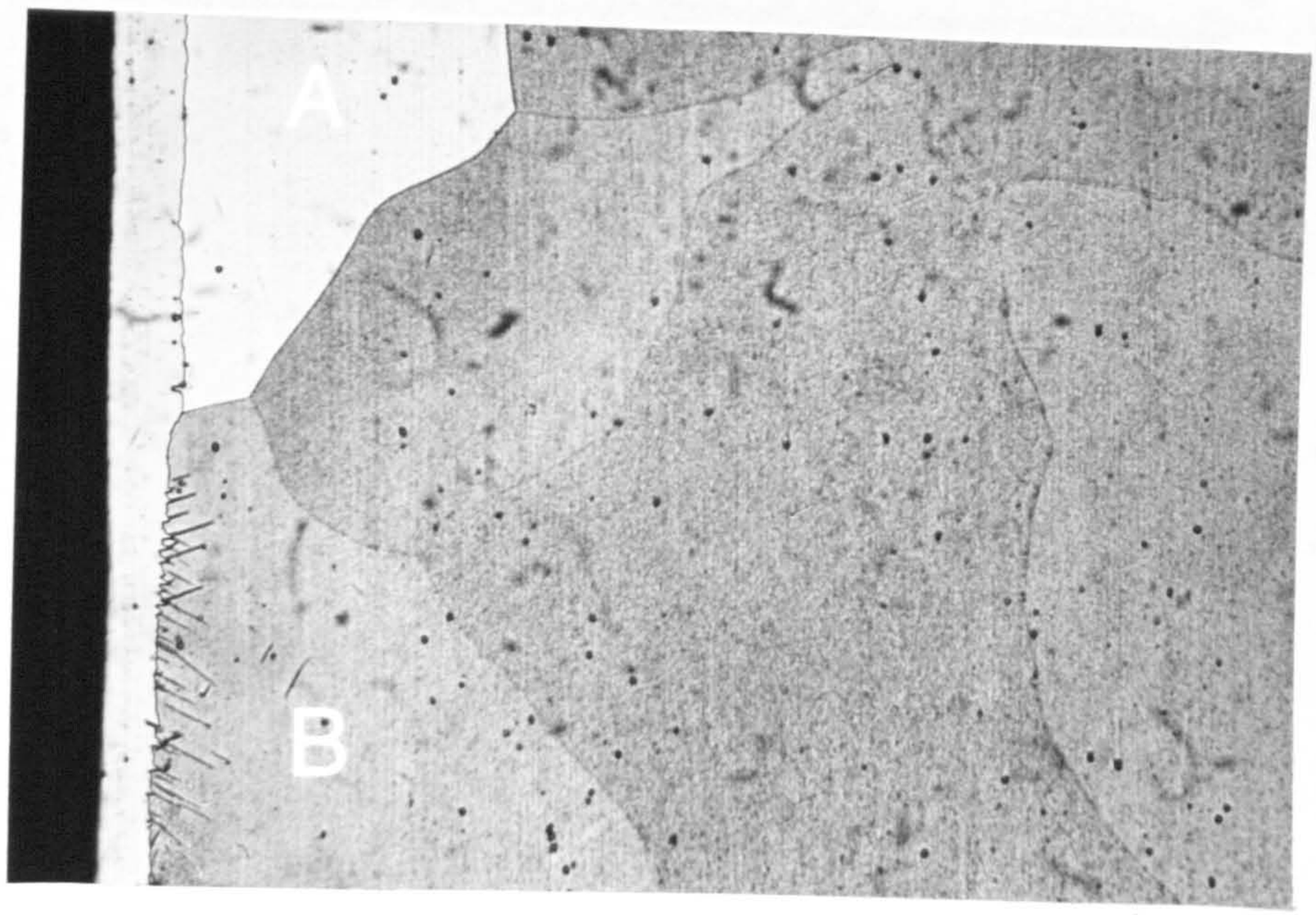

b

50um

FIG.(5.25)

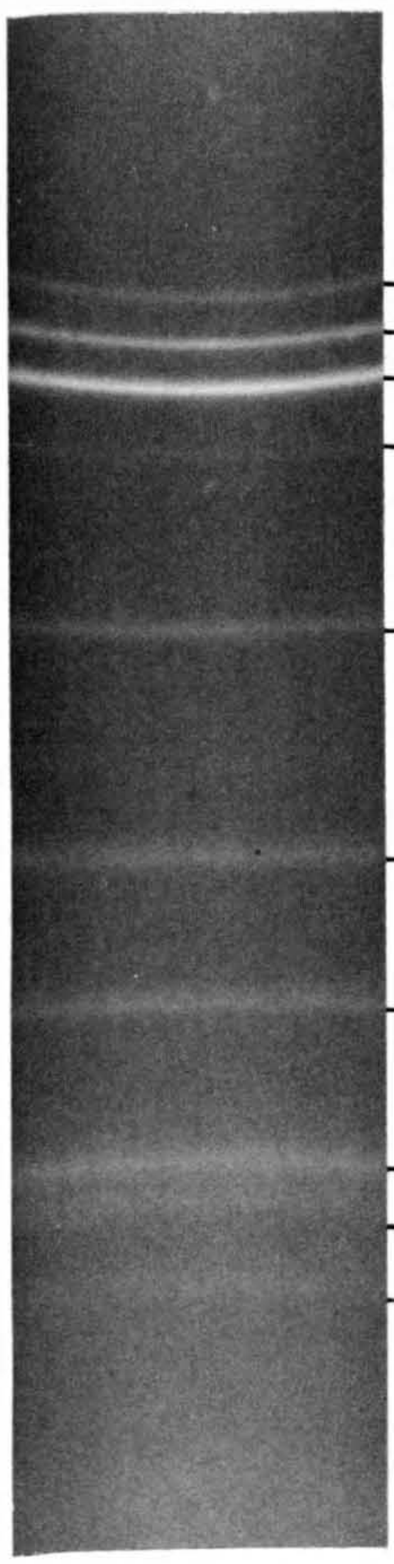

$d_{obs.}$ Å	hkl	
	Fe_3N	Fe_4N
2.35	100	
2.175	002	111
2.042	100	
1.902		200
1.596	102	
1.346	110	220
1.355	103	
1.147	200	311
1.128	112	311
1.107		222

Table 5.2

X-ray data for Fe_3N and Fe_4N

Fig. 5.26

X-ray powder pattern of Fe_3N and Fe_4N. The particles were extracted from the surface of a nitrided bulk specimen of En41(-Cr)

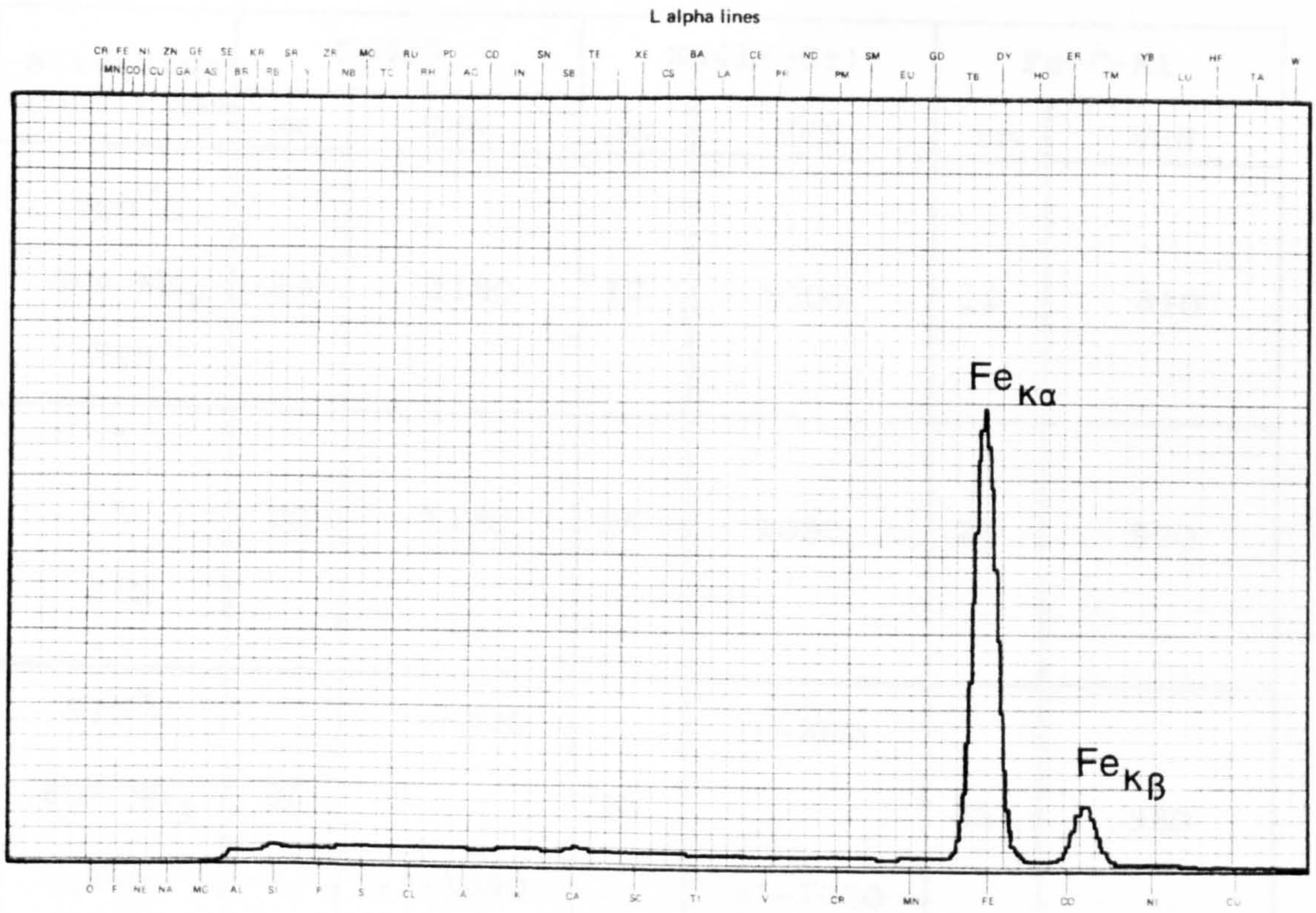

Fig. 5.27 X-ray microanalysis of the particles extracted from the white layer of a nitrided En41(-Cr) specimen showing presence of iron only

Nitriding conditions	En41B		En41(-Cr)		Fe-C-Al	
	µm	VHN	µm	VHN	µm	VHN
500°C 80% NH_3 24h	15	1180	12	1000	12	810
" " 72h	30	1130	25	1080	20	950
570°C 80% NH_3 24h	38	ϵ-920 γ'-1090	30	ϵ-880 γ'-1090	25	980
" " 48 h	50	ϵ-920 γ'-1090	40	ϵ-890 γ'-1080	30	ϵ-920 γ'-1000

Table 5.3

The averages of the thicknesses and hardnesses of the white layer for each steel nitrided under different conditions

CHAPTER 6

CHARACTERISTICS OF THE NITRIDED ALUMINIUM CONTAINING STEELS

6.1 Introduction

Previous work (46,47,48) carried out on chromium containing steels has shown that the characteristics of the nitrided steel were influenced by several process variables, such as: the nitriding temperature, NH_3 content of the gas mixture, heat treatment prior to nitriding, and the chromium and carbon contents of the steel. It has been concluded that the maximum case depth can be achieved by nitriding at a high temperature and a high NH_3 gas mixture, but higher nitriding temperatures produce a shallower hardness profile. On the other hand a steeper hardness profile can be achieved by nitriding at lower temperatures in a high NH_3 gas mixture.

In the present investigation, the nitriding process was carried out in a controlled ammonia-hydrogen mixture under different nitriding conditions for different times.

The variables affecting the nitriding characteristics were considered in this investigation. The results of the nitriding experiments were divided into two main categories namely depth and hardness of the nitrided layer. The hardness was explicitly discussed according to the effect of the process variables on the bases of maximum hardness, the level and depth of hardening, the hardness profiles.

6.2 Material and Methods

The work has been carried out on three different aluminium-containing steels, commercial En41B, experimental chromium-free En(-Cr) and Fe-C-Al. The quality differences in terms of alloying elements between these steels provided a basis for comparison.

The specimens were oil quenched from 900°C and tempered at the required tempering temperature (500°C, 600°C or 700°C) for 1h. Two nitriding temperatures were employed i.e. 500°C and 570°C throughout the investigation. An 80% NH_3 gas mixture was used except when it was necessary to avoid the formation of the white layer, in which case 20% NH_3 and 14% NH_3 were used at temperatures of 500°C and 570°C respectively. Three different nitriding times were used, 72h, 48h and 24h.

Hardness measurements were carried out using a Reichert microhardness tester and a 50g load was used throughout the test.

6.3 Nitriding depth

In any nitrided material, the effective case depth, which is defined as the depth reached at a specific minimum hardness value does not necessarily correspond to the total nitrided case depth. Mridha (48), has defined the "nitrided case depth" as the depth from the surface up to the beginning of the carburized zone. This definition was based on the etching depth revealed by oberhoffer's reagent, which corresponds to the point at which the hardness drops to within 100 VHN of the matrix value.

S. Winnik (47) had previously carried out etching experiments on En4OB without using Oberhoffer's reagent, and he regarded a 2% Nital solution as the most accurate and reproducible measure of total case depth, but admitted that a wide degree of error is possible even if a single etching reagent is used, and variables such as time of etching and the temperature should be standardized. Therefore it has been concluded that it is very difficult to strictly define the "nitrided case depth". However, the real case depth can be regarded as the limit of the alloy nitride formation, which can only be detected by electron microscopy, and not the limit of nitrogen penetration.

In commercial practice, the nitrided case depth is measured directly from the hardness profile of the nitrided material.

In this investigation the limiting value of hardness above the core hardness was regarded as the "nitrided case depth" for the purposes of comparison.

6.3.1 Effect of nitriding temperature

Fig. 6.1 represent the hardness profiles of two specimens of En41B, nitrided at different temperatures, but keeping both time and the NH_3 gas mixture content fixed in both cases i.e. 80% NH_3 for 24 h. The nitrided case depth of the specimen nitrided at 500^{o}C, profile (a), is less than that of the specimen nitrided at 570^{o}C, profile (b). The difference in the case depth as measured from the hardness profiles is approximately 0.18 mm. The same experiment was

carried on En41(-Cr) steel. Fig. 6.2 indicates that the specimen nitrided at 570°C, profile (b), has a case depth increase of about 0.18 mm over that nitrided at 500°C, profile (b). In Fe-C-Al steel, the situation was quite different. The hardness profile of the specimen nitrided at 500°C which is illustrated in Fig. 6.3 profile (a), shows in clear change in the hardness at the interface between the nitrided and non-nitrided part of the specimen, so the "case depth" had to be measured direct from the specimen after being etched in oberhoffer's reagent, and the etching limit in this case was regarded as the nitrided case depth, which was approximately 0.45 mm. The same procedure was adopted for the specimen nitrided at 570°C, and the depth revealed by etching was approximately 0.7 mm. This value is very close to that measured from profile (b).

These results confirm the previous finding, that an increase in nitriding temperature leads to an increase in the nitrided depth.

The diffusivity of nitrogen is temperature dependent and increases with temperature, so at a given time and fixed NH_3 content in the gas mixture the nitrogen diffusion rate is higher at higher temperature, which leads to a deeper nitrided case.

6.3.2 Effect of NH_3 gas mixture content

The nitriding experiments were carried out at 500°C using 80% NH_3 and 20% NH_3, and at 570°C using 80% NH_3 and 14% NH_3, or in other words with and without white layer

formation. IN all cases the nitriding period was 24h. At 500°C, the experiment was performed on En41B only, and the reason for not presenting the results for En41(-Cr) and Fe-C-Al steels, is because at such a low nitriding potential the hardness profile are so shallow that it would be very difficult to measure or even to estimate the case depths in these steels.

The results are represented in Figs. 6.4 and 6.5 illustrate the hardness profiles of En41B nitrided at 500°C and 570°C. In both cases the hardness profiles indicate an increase in the case depth of the specimens nitrided in 80% NH_3 over to those nitrided in 20% NH_3 and 14% NH_3.

In chromium-free steels i.e. En41(-Cr) and Fe-C-Al, the nitrided case depth does not seem to be affected by the concentration of NH_3. Figs. 5.6 and 5.7 clearly show the similarity of the case depth in both steels.

6.3.3 Effect of prior heat treatment

The investigation was carried out using commercial En41B steel and experimental Fe-C-Al steel. After quench hardening specimens were tempered at 500°, 600° and 700°C for 1h. For En41B nitriding was carried out at 500°C and 570°C for 72h and 48h respectively, and for Fe-C-Al nitriding was carried out at 570°C for 24h. 80% NH_3 was used in cases.

The results from both steels show very little or no effect of prior tempering treatment and the nitrided depth. En41B results show little, but steady, increase in depth with

increasing tempering temperature especially when the specimens were nitrided at 570°C, see Fig. 6.8. However, specimens tempered at 500° and 600°C showed no depth difference when nitriding was carried out at 500°C, but specimens tempered at 700°C show some depth increase, but in this case, the case hardness was lower, see Fig. 6.9. The experimental Fe-C-Al steel shows no such effects of prior tempering treatment on depth of nitriding, and this is clearly shown in Fig. 6.10.

Previous work has shown that different steels behave differently, in respect of the effect of prior tempering temperature on the nitrided depth. En19 steel (48,57) behaved in a similar way to En41B, while En40B (48) showed behaviour closer to Fe-C-Al. Such similarities and differences in behaviour between different steels in their response to nitriding, as a result of prior tempering treatment, can be attributed to the amount of the alloying element and carbon in the steel and the degree of interaction between them. In the case of chromium containing steels, the effect of tempering temperature is more pronounced in En41B and En19, than in En40B. This is because both steels have higher carbon and lower chromium contents than En40B. So on tempering the matrix in the En41B and En19 steels will be left with much less free chromium than in the latter steel. Also higher tempering temperatures increases the carbide size, and since larger carbides are more difficult to dissociate, there will be even less chromium available for nitriding, hence variations in the nitrided depth occurs. Both En41B and En19 steels have a much larger carbide size than En40B, and this explains

why tempering temperatures do not influence the nitrided depth in En40B.

In the chromium free Fe-C-Al steel, tempering temperatures have no effect on the nitriding depth. This is because aluminium does not interact with carbon, so the amount of the aluminium available for nitriding remains the same, at any tempering temperature.

6.3.4 Effect of nitriding time

The investigation was carried out using En41B, En41(-Cr) and Fe-C-Al steels. The specimens were subjected to the standard prenitriding treatment (Quenched from 900^{o}C and tempered for 1h at 600^{o}C), except in one case the specimens used were as-quenched. The nitriding was carried out at 500^{o}C in 80% NH_3 for periods of 24 and 72h, and at 570^{o}C in 80% NH_3 for periods of 24 and 48h.

The results shown in Figs. 6.11, 6.12, 6.13 and 6.14. demonstrate clearly that a longer nitriding time increases the nitrided depth, and this is seen to be the case under most nitriding conditions except in En41B when nitriding is carried out at 500^{o}C in a 20% NH_3 (specimens were in the quenched condition before nitriding). Though the hardness profiles are different, the nitrided case depths are very close in both cases. However, if the nitriding is carried out at 570^{o}C in a 14% NH_3, the results indicate that the specimen subjected to a longer nitriding period has a greater case depth, as shown in Fig. 6.15. Previous work carried out on En19 and En41B led to similar conclusions.

6.3.5 Effect of alloying elements

The materials used in this investigation were En41B, En41(-Cr) and Fe-C-Al steels. All specimens were subjected to the standard heat treatment prior to nitriding.

The results indicate that steels with different chemical compositions respond variably under different nitriding conditions. Fig. 6.16 shows super-imposed hardness profiles of the steels nitrided at 500°C in 80% NH_3 for 72h. It shows that En41B and En41(-Cr) steels have a very similar case depth; but Fe-C-Al, although it has a very shallow hardness profile, has a greater case depth. Nitriding for a short time under the above conditions gave the same results, see Fig. 6.17.

Nitriding at 570°C with 80% NH_3, shows that En41(-Cr) has a greater case depth than En41B and Fe-C-Al has an even greater one. A shorter nitriding time gave similar results, see Figs. 6.18 and 6.19. Nitriding in low NH_3 gas mixture content i.e. 14% NH_3 which does not induce surface nitride formation, results in an even greater case depth difference between En41B and En41(-Cr). Fig. 6.20 shows a similarity in the hardness profiles between the two steels, but En41B has a higher hardness at the surface, and a shallower depth.

These results suggest that the nitriding behaviour of aluminium containing steels (with and without chromium) is compatable with the simple models of sub scale growth only when nitriding is carried out at high temperature (570°C). The likely explanation for such behaviour is that at higher nitriding temperature, chromium, aluminium and silicon react

readily with nitrogen to form nitrides, even in a low ammonia gas mixture. So, a high proportion of the above elements would precipitate. This has already been demonstrated in Chapter 4, where particles extracted from specimens of En41B nitrided at 570^{o}C shows the presence of a high proportion of chromium, aluminium and silicon. The same applied to En41(-Cr) where a high proportion of both aluminium and silicon precipitated as nitrides, but the absence of chromium in the latter steel gives a more rapid nitriding response.

At a lower nitriding temperature (500^{o}C), precipitate extracted from nitrided En41B contains mainly chromium (as nitride), and very low proportion of aluminium and silicon, which implies that only a small percentage of aluminium and silicon took part in the reaction. Diffraction patterns and micrographs obtained from extraction replicas of a bulk specimen of En41(-Cr) nitrided at 500^{o}C in 80% NH_3, show a dense precipitation of AlN, which is rich in silicon. Because aluminium and silicon did not take part in the nitriding reaction of En41B at 500^{o}C, this behaviour may have influenced the nitriding rate and brought it closer to that of En41(-Cr), hence a more similar nitrided depth has resulted in the two steels.

6.4 Hardness of the nitrided aluminium containing steels

6.4.1 Introduction

The main aim of the nitriding process is to produce a stable structure of extreme hardness at the surface of the

nitrided components. The high hardness of the nitrided layer is caused by the precipitation of very fine nitride.

There are several factors that may influence the hardness development, and they are mainly, the nitriding temperature, the NH_3 content of the gas mixture, the prior tempering temperature, period of nitriding, concentration and nature of the nitride forming elements and the carbon content in the steel.

6.4.2 Development of hardness

6.4.2.1 Effect of nitriding temperature

Figs. 6.1, 6.2 and 6.3 illustrate the hardness profiles of En41B, En41(-Cr) and Fe-C-Al respectively. Profile (a) is from specimens nitrided at 500°C, and profile (b) from those nitrided at 570°C. In both cases nitriding was carried out in 80% NH_3 for 24h. The hardness was measured from the nearest possible point to the surface, so the hardness of the white layer is included for the specimens with white layer.

In Fe-C-Al, the maximum hardness at the surface is greatly increased with increasing nitriding temperature, and the general level of the hardness is also increased. This considerable difference in the hardness due to the effect of nitriding temperature can be explained in terms of nucleation and growth phenomena. In Fe-C-Al, the hardening effect depends on the precipitation of aluminium nitride only. The nucleation of aluminium nitride at 500°C is much more difficult than at 570°C. Consequently nitriding at 570°C

produces fine aluminium nitride in larger quantities, whereas a larger size and smaller quantity of aluminium nitride is produced at 500°C (see Chapter 4), so higher hardness is achieved at 570°C.

Fig. 6.2 illustrates the hardness profiles of En41(-Cr), nitrided in 80% NH_3 for 24h at (a) 500°C and (b) 570°C. In this case the nitriding temperature does not seem to influence the maximum hardness surface hardness, but the general hardness level and the depth of hardening are both increased with increasing nitriding temperature.

Comparing the hardness profiles of En41(-Cr) (Fig. 6.2) with those of Fe-C-Al (Fig. 6.3), the effect of the nitriding temperature on the hardening behaviour is not the same. In Fe-C-Al the hardness decreases steadily, whereas in En41(-Cr) there is a rapid decrease just below the surface, then a much shallower decline, and finally a drop to the core hardness level.

The hardening capability of aluminium seems to be enhanced by the addition of silicon in En41(-Cr). The evidence of chapter 4 suggests that aluminium and silicon react with nitrogen in a co-operative way to form an (Al,Si)N phase similar suggestions have been made before. Jack et al. (65) nitrided a low alloy ausformable steel and found that only a combination of Al, Si and Mn would give a high hardening response. So, in En41(-Cr), the severe nucleation difficulties of AlN are partially overcome, and the most influential factor controlling the development of hardness in this case is the diffusivity of nitrogen. Hence

higher temperatures give a greater hardening depth.

The hardening behaviour of En41B steel illustrated in Fig. 6.1, shows that a higher nitriding temperature leads to a decrease in the maximum hardness at the surface and an increase in the depth of hardening. The presence of chromium in this steel has greatly influenced the hardening response, since chromium reacts readily with nitrogen to form fine nitrides at both temperatures (500^{o} and 570^{o}C), and the major factor dictating the hardening behaviour is the diffusivity of nitrogen and chromium in the matrix. Higher nitriding temperatures increase the diffusivity which leads to an increase in hardening depth, but also leads to a lower hardness level due to the reduction of the hardening effect of fine nitride precipitates due to coarsening. Also see Fig. 6.21.

6.4.2.2 Effect of the NH_3 content of the gas mixture

The effect of NH_3 content on the nitriding response of En41B is shown in Figs. 6.4 and 6.5. The hardness level and the depth of hardening are both increased with increase in NH_3. In low ammonia contents, the hardness build up is very slow due to a low flux of nitrogen which limits the precipitation of nitrides, but at higher ammonia contents the activity of nitrogen will be higher leading to a rapid reaction between nitrogen and solute atoms to form fine nitrides, and hence higher hardnesses.

The effect of NH_3 content on the hardening of En41(-Cr) is shown in Fig. 6.6, and can be seen to be qualitatively similar to the situation in the case of En41B,

although the difference in profiles is less pronounced.

In Fe-C-Al, Fig. 6.7, the hardness profile in 14% NH_3 is shallower than in 80% NH_3, and the maximum surface hardness is very much less. Again, the behaviour is explicable in terms of higher nitrogen fluxes increasing the nucleation frequency of the AlN.

6.4.2.3 Effect of tempering temperature

Figs. 6.8 and 6.9 show the hardness profiles of En41B steel nitrided at 570°C for 48h and 500°C for 72h respectively in 80% NH_3. The prior tempering temperature does not appear to have much effect on the hardening behaviour of this steel under these nitriding conditions. But if nitriding is carried out for a shorter time using the same nitriding conditions, the effect of tempering temperature is more apparent. Fig. 6.22 illustrates the hardness profile after nitriding for 24h at 500°C. The maximum hardness and the hardness level decreases with increasing tempering temperature. This occurs because tempering at higher temperature increases the size of the carbides, and since larger carbides are more difficult to dissociate, especially at low nitriding temperatures, less chromium will be available for precipitation as fine nitrides.

Nitriding for shorter at 570°C, Fig. 6.23, produces profiles which are similar for samples tempered at 500° and 600°C, but there is a lower hardness profile after tempering at 700°C, which is attributed to the fact that the size of the carbides produced at this temperature are much too large

to be dissociated easily. Moreover after tempering at 700°C the matrix will be largely recovered and recrystallized, which effectively reduces the dislocation density, and as a result less AlN would precipitate. So, the combination of large carbides and a lower dislocation density reduces the hardness level and the effect is more apparent at lower nitriding temperatures and short times.

Hardening of Fe-C-Al is not influenced by varying the tempering temperature if nitriding is carried out at high temperature. This is clearly demonstrated in Fig. 6.10, in which nitriding was carried out at 570°C. At lower nitriding temperatures, the prior tempering temperature does have a significant effect, see Fig. 6.24. The hardness level decreases as the prior tempering temperature increases.

This sort of behaviour occurs in Fe-C-Al because nucleation of AlN is more difficult at 500°C and requires dislocations as nucleating sites. As has been earlier explained the dislocation density decreases with the increase in tempering temperature, and the precipitation of AlN is effectively reduced. However, AlN precipitates easily at 570°C, so the influence of dislocations as a vital factor in the precipitation process would not be significant when the nitriding was carried at this temperature.

Since aluminium does not react with the carbides, the size of the cementite particles is not relevant to the nitriding response.

6.4.2.4 Effect of nitriding time

Figs. 6.25, 6.26 and 6.13 illustrate the hardness profiles of En41B, En41(-Cr) and Fe-C-Al after nitriding at 570^{o}C in 80% NH_3. They show very clearly that nitriding for longer periods at 570^{o}C does not affect the maximum hardness nor the hardness level, but it does significantly increase the hardening depth in En41B and En41(-Cr).

At a lower nitriding temperature (500^{o}C), the effect of time on the hardening of the above steels is different. In En41B, the maximum hardness remains the same, but the depth and the level of hardness both increased when the nitriding time was increased from 24h to 72h, see Fig. 6.11. In En41(-Cr), there is an overall increase in the hardness if nitriding is carried on for a longer period (72h). Although the hardness is the same at the surface, it falls very sharply immediately under the white layer for the shorter nitriding period, see Fig. 6.12. Similar effects were observed in Fe-C-Al, but with very different hardness profiles, as demonstrated in Fig. 6.27. Profile (a), after a 24h nitriding period, shows a sharp drop in the hardness just under the white layer, and the level of hardness is very low. Profile (b) after 72h nitriding shows some increase in the hardness level nearer to the surface then drops to the low level closer to profile (a).

6.4.5.2 Effect of alloying elements

Since the nitride forming elements are the decisive factor in the hardening behaviour of the steels, then steels

with different chemical compositions would be expected to behave differently when nitrided under the same nitriding conditions. The investigated steels En41B, En41(-Cr) and Fe-C-Al provided a basis for comparison and evaluation of the effect of alloying elements.

Fig. 6.16 represents the hardness profiles of the above steels nitrided at 500^{o}C in 80% NH_3 for 72h. It shows that the hardness profile becomes more shallow each time one or more alloying elements are removed from the steel. The absence of chromium in En41(-Cr) caused a decrease in the hardness level, but did not effect the hardening depth. Removing the rest of alloying elements except aluminium and carbon, as in Fe-C-Al, result in a very shallow hardness profile.

The pesence of silicon and perhaps the other alloying elements in En41(-Cr) greatly improves the hardening response of this steel. However, if nitriding is carried out for a short time i.e. 24h, then the hardening response of En41(-Cr) is significantly reduced. Fig. 6.17 shows that the maximum hardness and the hardness level are much lower than those of En41B, but nevertheless they are very much higher than those of Fe-C-Al.

At higher nitriding temperature (570^{o}C) the presence or absence of chromium in En41B and En41(-Cr) respectively does not seem to affect the maximum hardness at the surface nor the general level of hardness, but it does reduce the hardening depth in En41B. Fig. 6.18 illustrates the hardness profile of the above steels together with that of Fe-C-Al,

after nitriding at 570°C in 80% NH_3 for 48h. The hardness profile of Fe-C-Al is much shallower in comparison with the other two steels. When nitriding was carried out under the same conditions as above, but for shorter period i.e. 24h, the hardness level decreased in En41(-Cr), but the hardening depth was still greater than that of En41B, as is shown in Fig. 6.19.

An explanation for this kind of behaviour is that when nitriding at a higher temperature in a high ammonia concentration, AlN precipitates more easily, and in the case of En41(-Cr) the presence of alloying elements, especially silicon, further assists the process and increases the hardness. At shorter nitriding times, given the same nitrogen flux, the hardness develops more quickly in En41B than En41(-Cr) because chromium nitride precipitates more easily than AlN, even in the presence of silicon in the latter steel, so nearer to the surface the hardness is higher in En41B than in En41(-Cr), but as nitriding is carried on over a longer period the hardness level does not change in En41B, whereas in En41(-Cr) the hardness level increase until it becomes equal to that in En41B.

6.5 Discussion

6.5.1 Hardness profiles in aluminium-containing steels

5.6.1.1 Introduction

The hardness profiles of the nitrided materials largely depend on the concentration and nature of the alloy-

ing elements that react with nitrogen to form fine nitride precipitates.

The main features that shape the hardness profile are; the maximum surface hardness, the general hardness level and the hardening depth. The development of these features are influenced by several factors, principally:

a) The nitriding temperature

b) The activity of the nitrogen in the NH_3/H_2 gas mixture (nitriding potential).

c) The period of nitriding

d) The ease of nucleation of the nitride precipitate

e) The strength of the solute-nitrogen interaction

f) Alloy element concentration in the alloy

g) Prior tempering treatment.

Previous work (46) carried out on chromium-containing irons and steels showed that the form of the hardness profile developed during nitriding depends upon the strength of the interaction between the alloying element and nitrogen and upon the ease of nucleation of a nitride phase. The different types of interaction are described in sections 1.7.1 - 1.7.3.

6.5.1.2 Hardness profile of En41B

The hardness profile curves exhibited at different nitriding temperatures and treatment times are shown in Figs. 6.1, 6.11 and 6.25. Fig. 6.1 illustrates the behaviour of En41B steel nitrided at 500°C and 570°C, represented by profiles (a) and (b) respectively. At 500°C the hardness

profile is very steep, but at 570°C the hardness profile shape is shallow with slightly lower maximum hardness at the surface. Increasing the period of nitriding does not seem to affect the shape of the hardness profile, but it increases the hardening depth. This is the case at both temperatures, see Figs. 6.11 and 6.25.

The effect of NH_3 concentration in the gas mixture are illustrated in Figs. 6.5, 6.4, 6.28 and 6.29. Nitriding at 570°C in 14% NH_3 produces a very shallow profile, with a high hardness value at the surface (950 VHN), followed by a steep decrease for short distance. When nitriding was carried out in 80% NH_3, the hardness at the surface increased to a high value (1075 VHN) then decreased more gradually and uniformly and the overall level of the hardness profile is higher with better hardening depth than when the nitriding was carried out in 14% NH_3, see Fig. 6.5.

On prolonging the nitriding period, the shape of the hardness profiles in both cases become very similar, with equal maximum hardness, but the hardening depth is better at 80% NH_3, as is shown in Fig. 6.28.

The effect of NH_3 concentration at 500°C is shown in Fig. 6.4 and Fig. 6.29. Shorter nitriding periods and a low NH_3 concentration (i.e. 24h, 14% NH_3) produces high surface hardness with hardness profile steeper than that for the specimens nitrided with 80% NH_3 (profile b). A prolonged nitriding period with low NH_3 concentration reduces the surface hardness and the whole profile becomes less steep. Fig. 6.29 shows that the hardness profile in both cases have the same gradients.

The effect of tempering temperature on the hardness profile within the temperature range of 500^{o} - 700^{o} is slight especially when nitriding is carried out in a high NH_3 concentration for long times (see Figs. 6.8 and 6.9). If nitriding is carried out for a shorter time, the depth of hardening becomes somewhat less with increase in tempering temperature, as clearly demonstrated in Fig. 6.22.

6.5.1.3 Hardness profile of En41(-Cr)

The effect of nitriding temperature and time on the shape of the hardness profile is illustrated in Figs. 6.2, 6.6, 6.12 and 6.26.

On nitriding with an 80% NH_3 concentration for 24h, the hardness profile is shallower at $500^{o}C$ than at $570^{o}C$, but when nitriding was carried out for a longer period i.e. 72h at $500^{o}C$ and 48h at $570^{o}C$, the general hardness level and hardening depth were both increased at $500^{o}C$ (Fig. 6.12), whereas at $570^{o}C$ the basic shape of the hardness profile remained the same with no change in maximum hardness or general hardness level, and the only change in the hardness profile as a result of prolonged nitriding time is an increase in hardening depth, as illustrated in Fig. 6.26.

Nitriding with low NH_3 concentration (14%) at $570^{o}C$ does not effect the basic shape of the hardness profile or hardening depth, although the maximum hardness at the surface and the general hardness level decreased. Fig. 6.6 illustrates the behaviour of En41(-Cr) at $570^{o}C$ with 14% and 80% NH_3 concentrations.

6.5.1.4 Hardness profile of Fe-C-Al

The effect of nitriding temperature on the shape of the hardness profile is shown in Fig. 6.3. At 500°C the hardness profile is very shallow. The hardness at the surface reaches maximum value of ∿ 800 VHN due to the formation of the white layer, under which the hardness drops very sharply to 450 VHN then gradually decreases to the core hardness level. At 570°C, the profile is less shallow, and the hardness at the surface is approximately 1000 VHN. This value drops sharply to 800 VHN then continues to decrease steadily in a linear fashion.

Nitriding with a 14% NH_3 concentration at 570°C (to prevent the formation of iron nitride on the surface of the specimen) greatly reduces the maximum hardness at the surface to a value of 550 VHN, which decreases gradually in a linear fashion, see Fig. 6.7 profile (a).

Tempering temperature does not have an effect on the hardness profile when nitriding is carried out at 570°C, but when nitriding is carrie d out at 500°C the hardness profile becomes shallower with increase in tempering temperature. Fig. 6.10 and Fig. 6.24 illustrate these points.

6.6 Summary and Conclusions

1. The hardening behaviour and the response of different steels toward nitriding is different.

2. Nitriding temperature has the greatest influence on the nitriding response of the steels. In chromium-containing steels En41B, nitriding at 500°C produces high surface

hardness, a steeper hardness profile and small nitrided depth, whereas nitriding at 570°C produces lower surface hardness, a shallower hardness profile and deeper case. In chromium-free steels En41(-Cr) and Fe-C-Al, nitriding at 570°C produces higher su r face hardness, a higher general hardness level and better hardening depth than at 500°C.

3. In En41B, nitriding in a high NH_3 contents in the gas mixture (enough to form white layer) produces higher surface hardness, a better hardening depth and higher hardness level than nitriding with low NH_3 content (not enough to for white layer). In En41(-Cr) and Fe-C-Al the only significant difference is the higher surface hardness if nitriding is carried out with high NH_3 contents in the gas mixture. There is a small increase in the general hardness level but the nitrided depth remains the same.

4. In En41B and Fe-C-Al steels the effect of tempering treatment prior to nitriding at 570°C has a very little or no effect on the hardness profile.

5. At high temperature and high NH_3 content in the NH_3/H_2 gas mixture, increasing the nitriding time always increases the nitrided case depth, but does not affect the maximum hardness at the surface or the level of hardness. At a lower nitriding temperature, a longer nitriding period increases the general level of hardness and the nitrided case depth . In En41B this increase in the hardness level occurs at some distance from the surface, whereas in En41(-Cr) and Fe-C-Al the increase in the hardness takes place almost immediately under the white layer.

6. The hardness profile of En41(-Cr) is very similar to that of En41B, especially at 570°C in 80% NH_3. Whereas Fe-C-Al has a very shallow hardness profile under all nitriding conditions.

7. The presence of silicon together with aluminium greatly improves the hardening response. Aluminium by itself does not induce high hardness.

Fig. 6.1 Effect of nitriding temperature on the case depth of En41B

Fig. 6.2 Effect of nitriding temperature on the case depth of En41(-Cr)

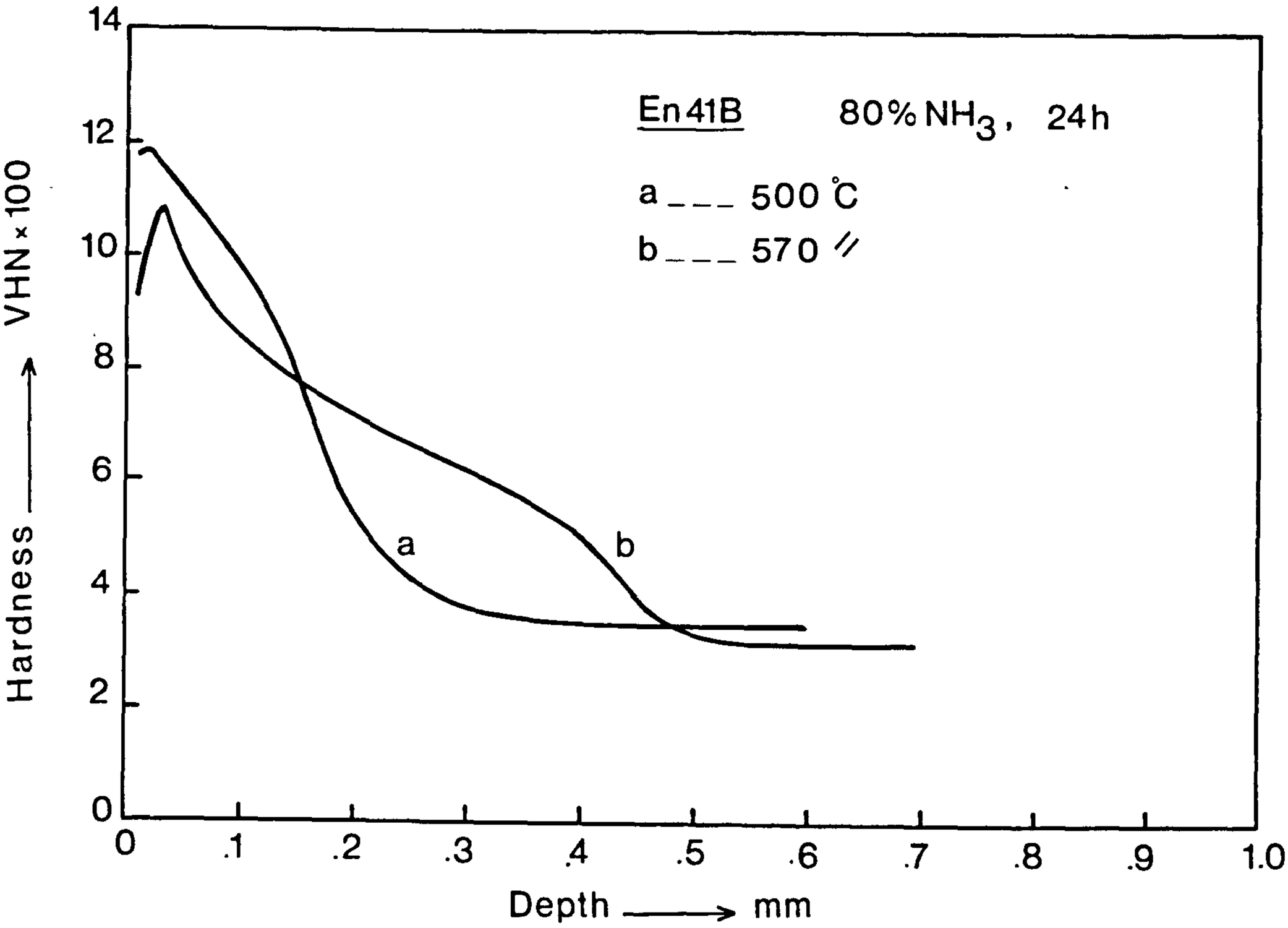
En41B 80% NH_3, 24h
a ___ 500 °C
b ___ 570 //
VHN × 100
Hardness
14
12
10
8
6
4
2
0
a
b
0
.1
.2
.3
.4
.5
.6
.7
.8
.9
1.0
Depth mm

FIG. (6.1)

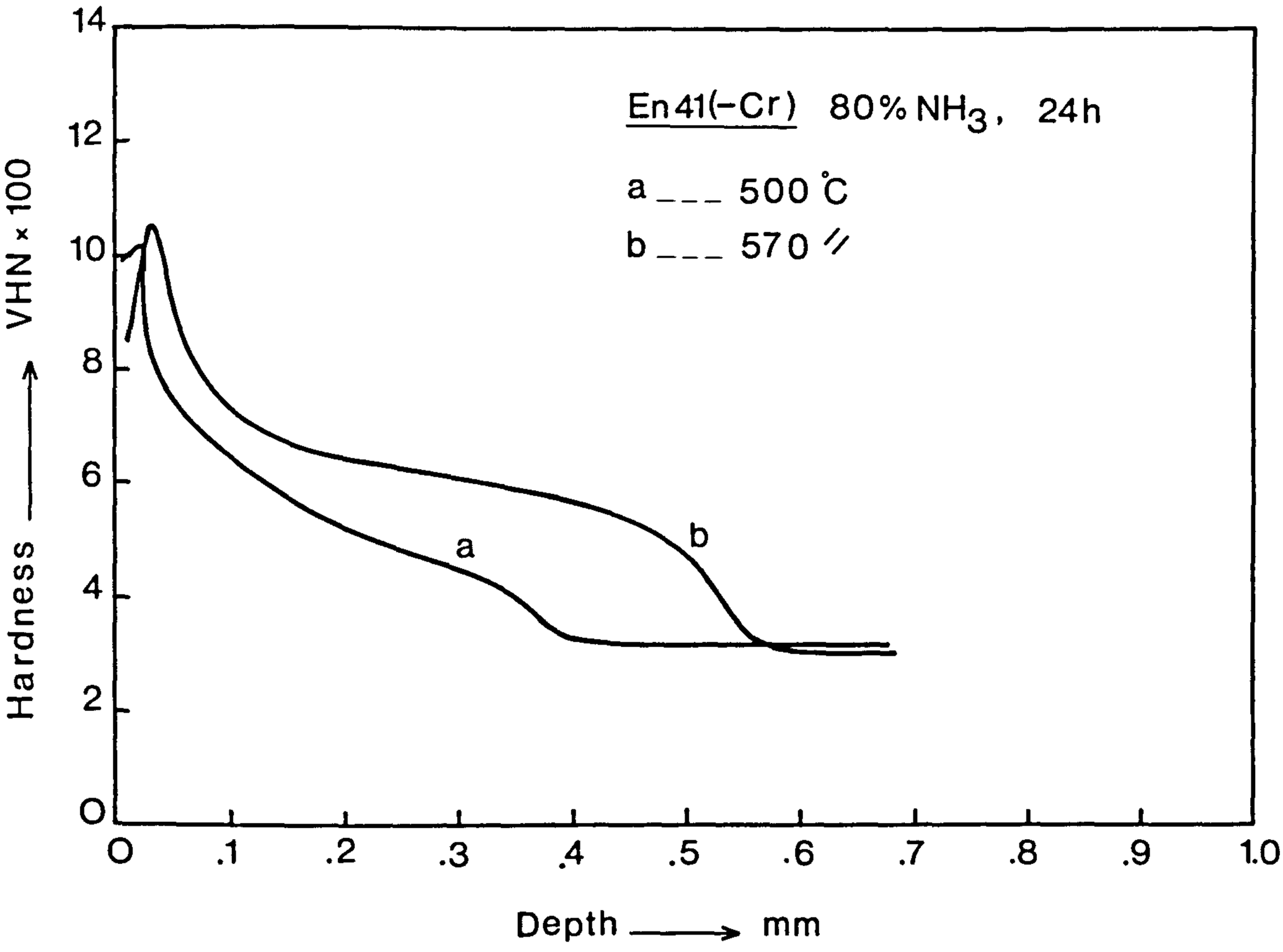
En41(-Cr) 80% NH_3, 24h
a ___ 500 °C
b ___ 570 //
VHN × 100
Hardness
14
12
10
8
6
4
2
0
a
b
0
.1
.2
.3
.4
.5
.6
.7
.8
.9
1.0
Depth mm

FIG. (6.2)

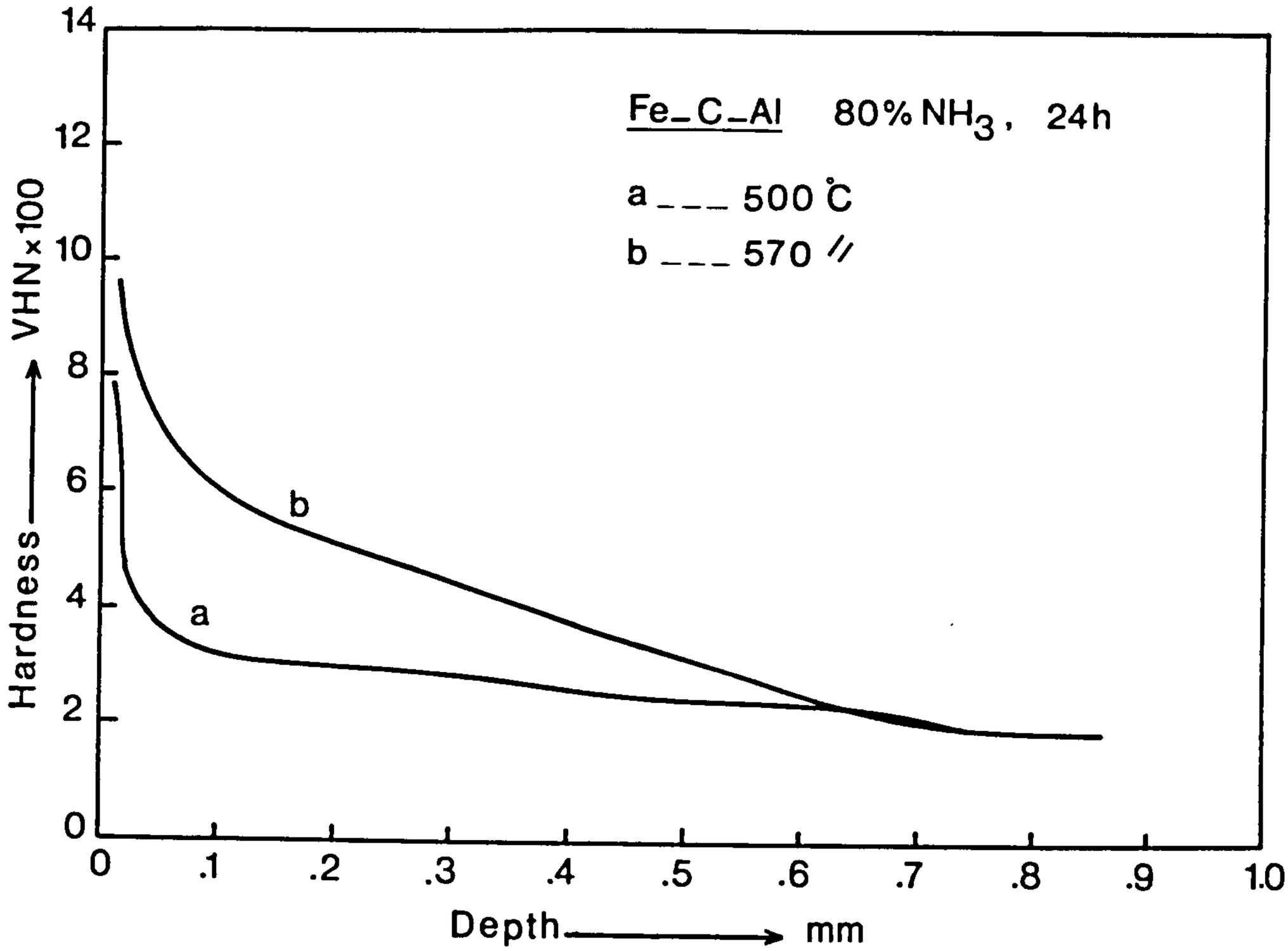

Fig. 6.3 Effect of nitriding temperature on the case depth of Fe-C-Al

Fig. 6.4 Effect of NH_3 content of the gas mixture on the case depth of En41B, nitrided at 500°C

Fig. 6.5 Effect of NH_3 content of the gas mixture on the case depth of En41B, nitrided at 570°C

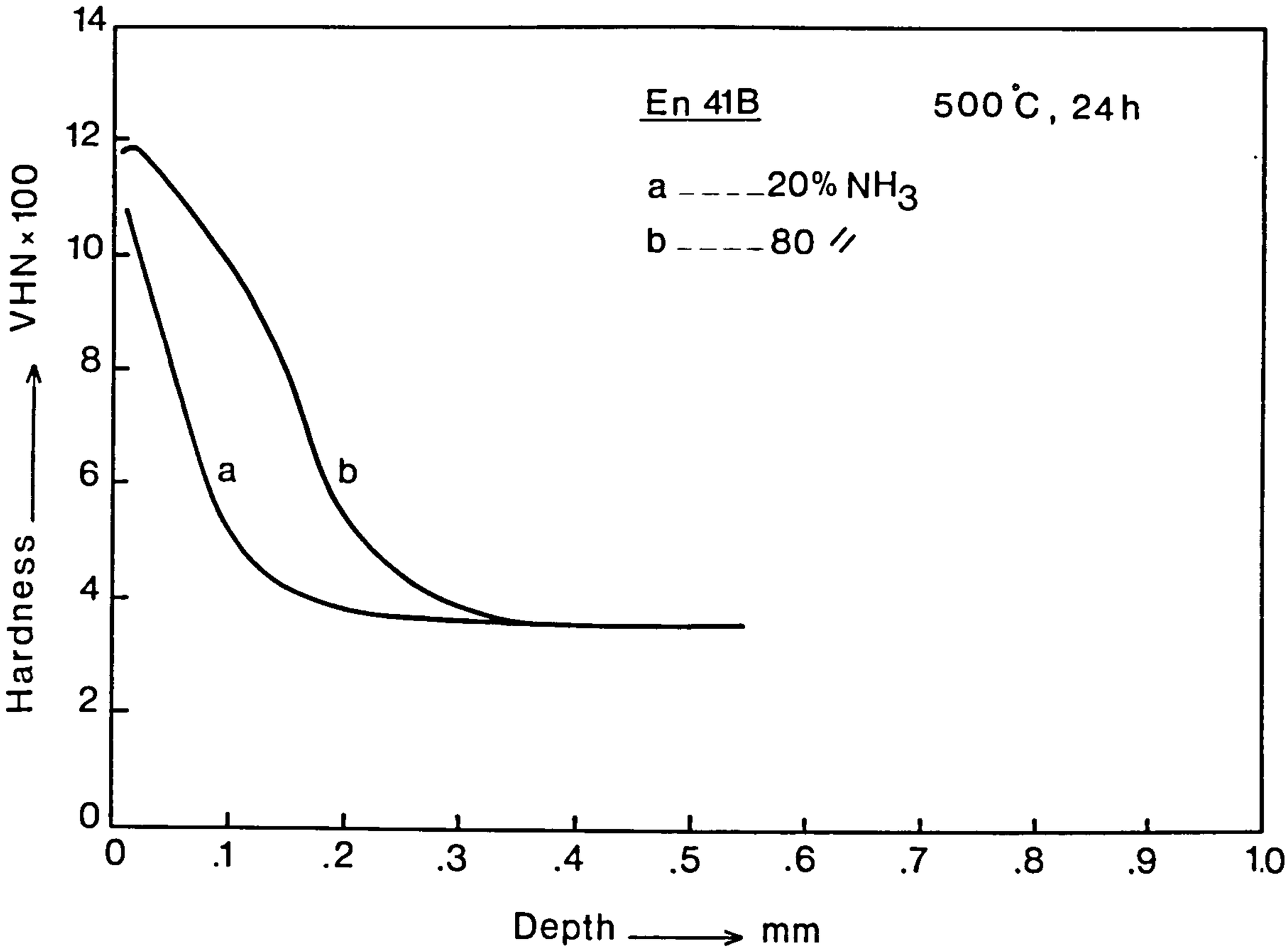
En 41B
500°C, 24h
a ____20% NH3
b ____80 //
VHN × 100
Hardness
14
12
10
8
6
4
2
0
a
b
0
.1
.2
.3
.4
.5
.6
.7
.8
.9
1.0
Depth ⟶ mm

FIG.(6·4)

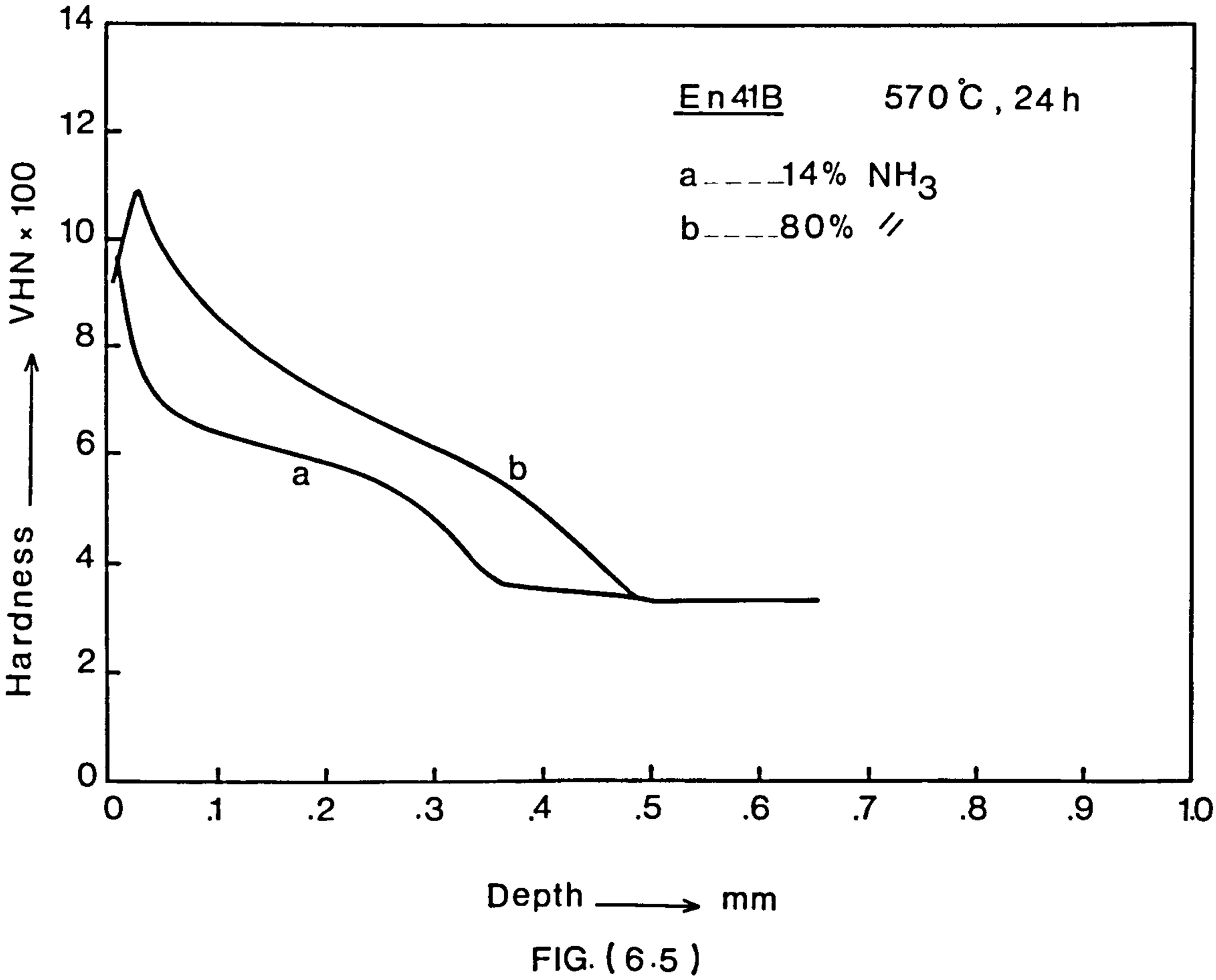
En41B
570°C, 24h
a ____14% NH3
b ____80% //
VHN × 100
Hardness
14
12
10
8
6
4
2
0
a
b
0
.1
.2
.3
.4
.5
.6
.7
.8
.9
1.0
Depth ⟶ mm

FIG. (6.5)

Fig. 6.6 Effect of NH_3 content in the gas mixture on the case depth of En41(-Cr) nitrided at 570°C

Fig. 6.7 Effect of NH_3 content in the gas mixture on the case depth of Fe-C-Al, nitrided at 570°C

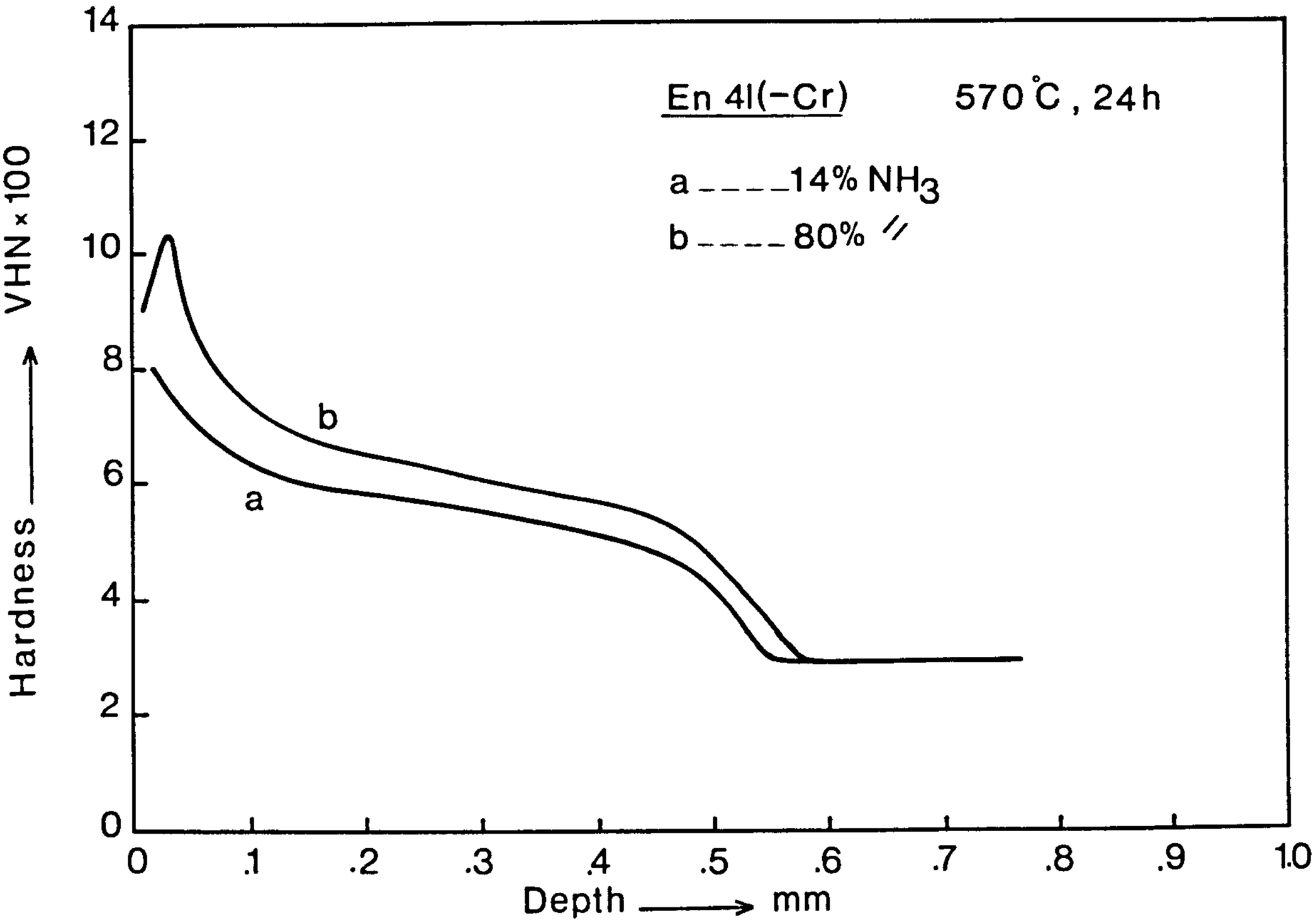
En 4l(-Cr)
570°C, 24h
a ____ 14% NH3
b ____ 80% //
VHN × 100
Hardness
14
12
10
8
6
4
2
0
a
b
0
.1
.2
.3
.4
.5
.6
.7
.8
.9
1.0
Depth → mm

FIG. (6.6)

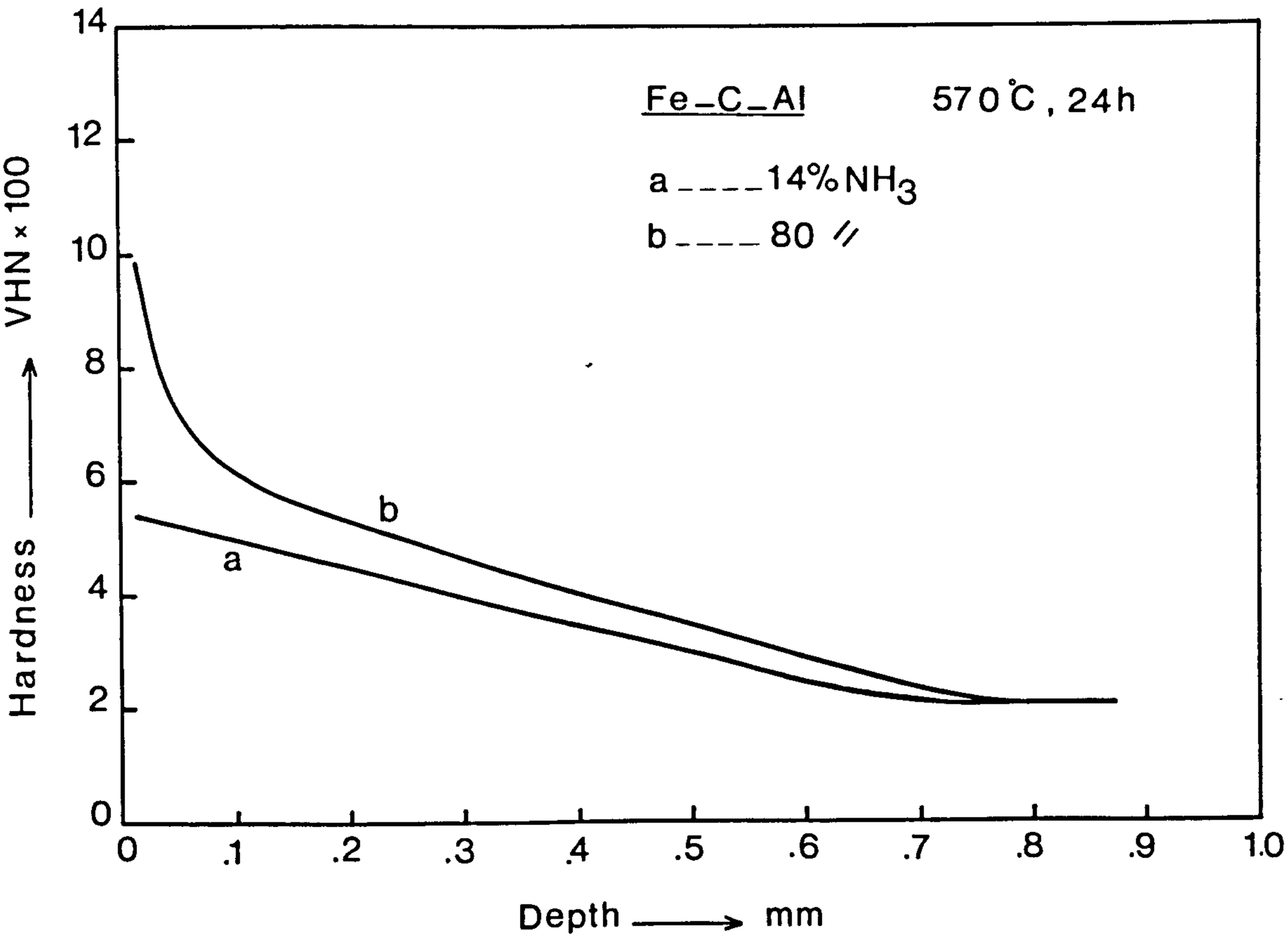
Fe-C-Al
570°C, 24h
a ____ 14% NH3
b ____ 80 //
VHN × 100
Hardness
14
12
10
8
6
4
2
0
a
b
0
.1
.2
.3
.4
.5
.6
.7
.8
.9
1.0
Depth → mm

FIG. (6.7)

Fig. 6.8 Effect of tempering temperature prior to nitriding on the case depth of En41B, nitrided at 570°C

Fig. 6.9 As in Fig. 6.8, nitrided at 500°C for 72h.

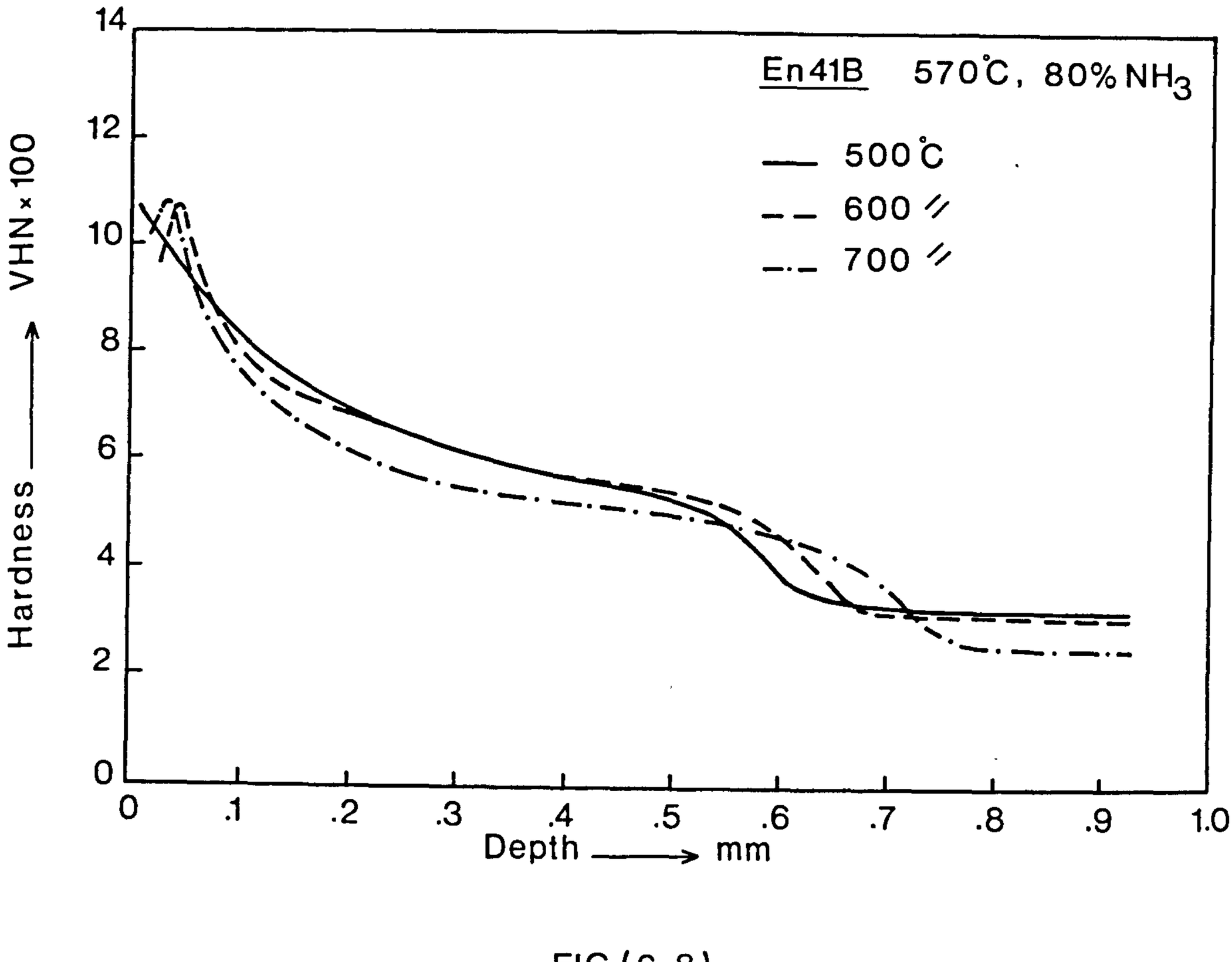
En41B 570°C, 80% NH3
500°C
600 //
700 //
VHN × 100
Hardness
14
12
10
8
6
4
2
0
0
.1
.2
.3
.4
.5
.6
.7
.8
.9
1.0
Depth mm

FIG.(6.8)

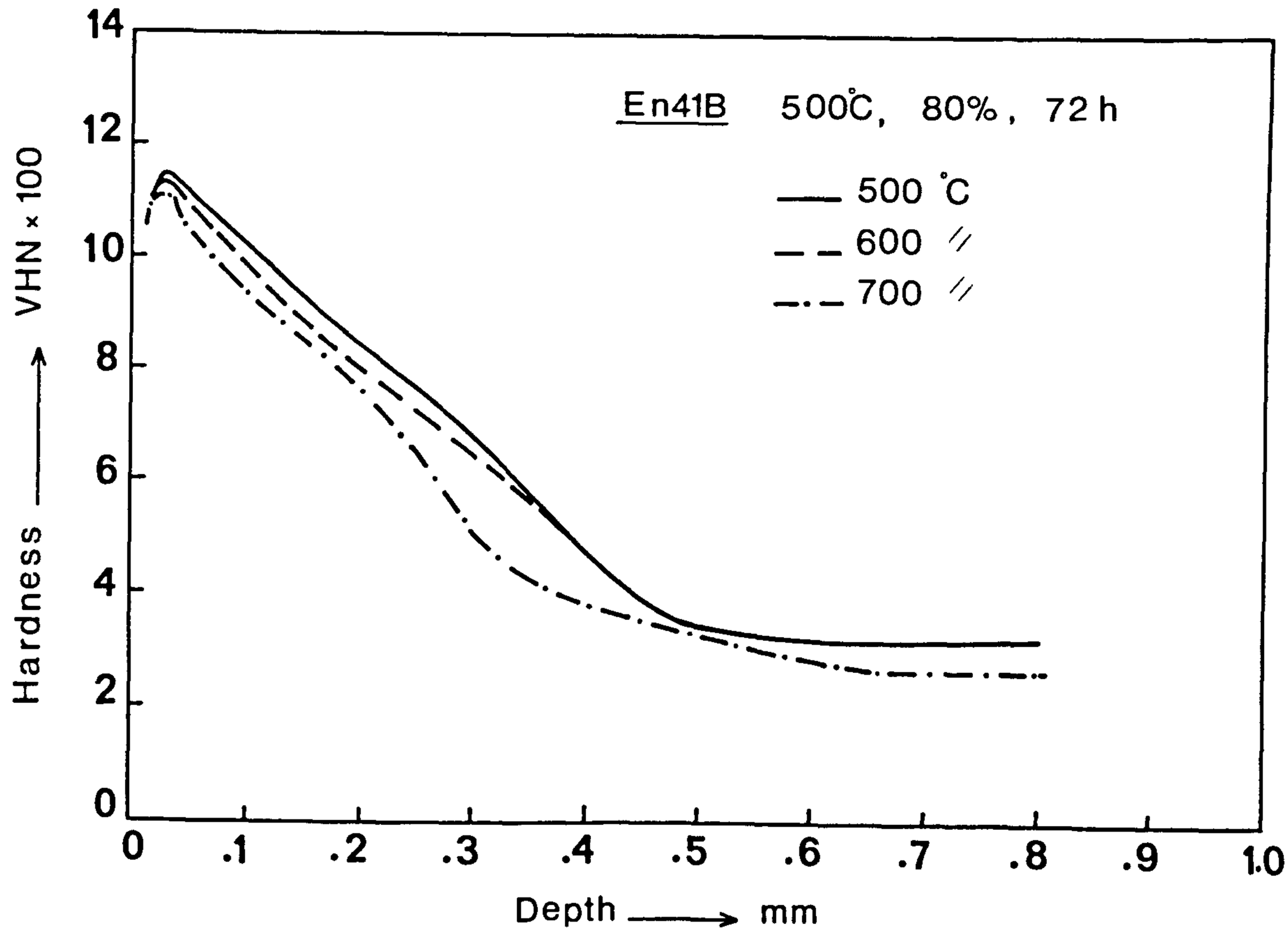
En41B 500°C, 80%, 72 h
500 °C
600 //
700 //
VHN × 100
Hardness
14
12
10
8
6
4
2
0
0
.1
.2
.3
.4
.5
.6
.7
.8
.9
1.0
Depth mm

FIG. (6·9)

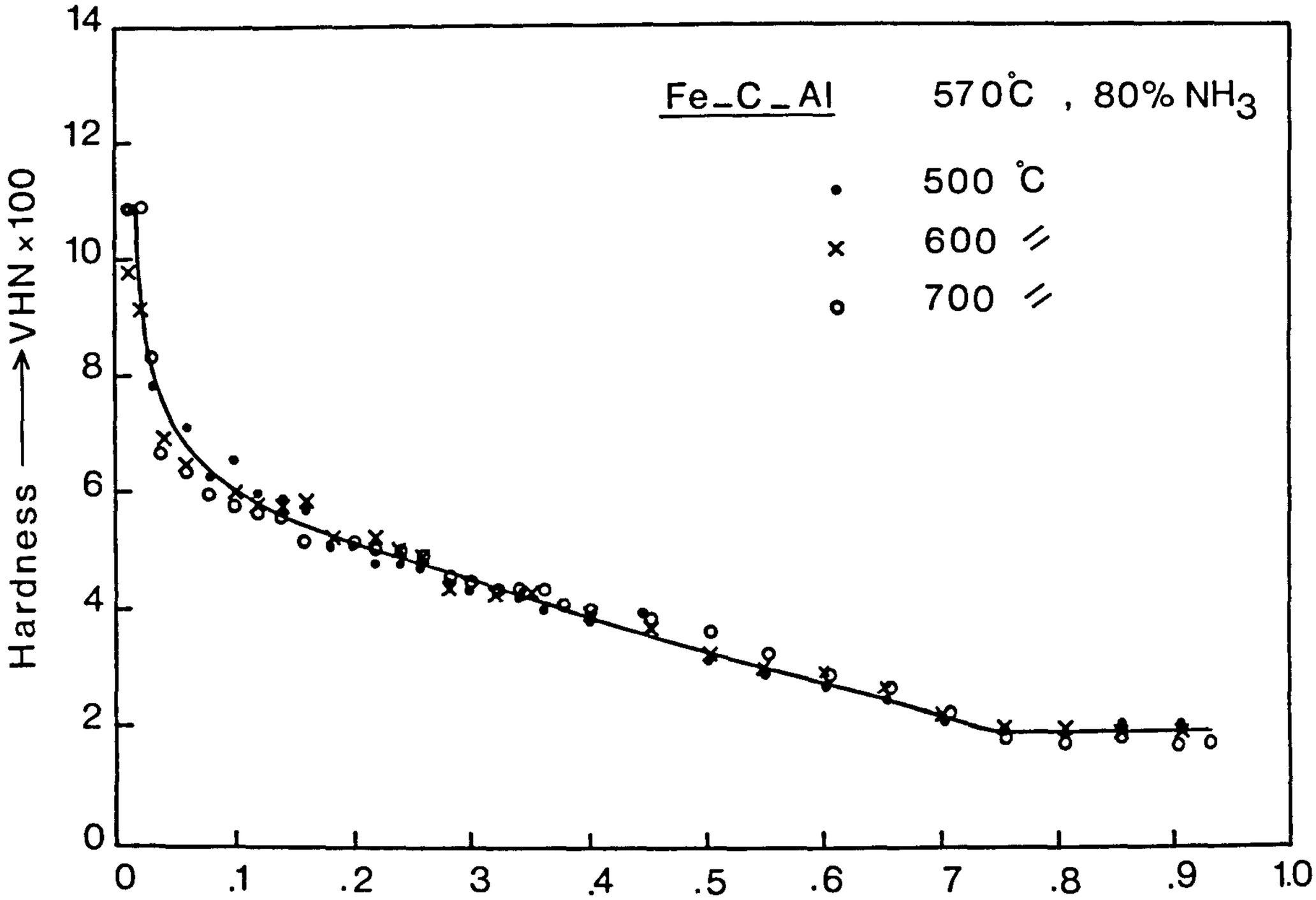

Fig. 6.10 Showing that the tempering temperature has no effect on the case depth of Fe-C-Al steel

Fig. 6.11 Effect of nitriding time on the case depth of En41B

Fig. 6.12 Effect of nitriding time on the case depth of En41(-Cr)

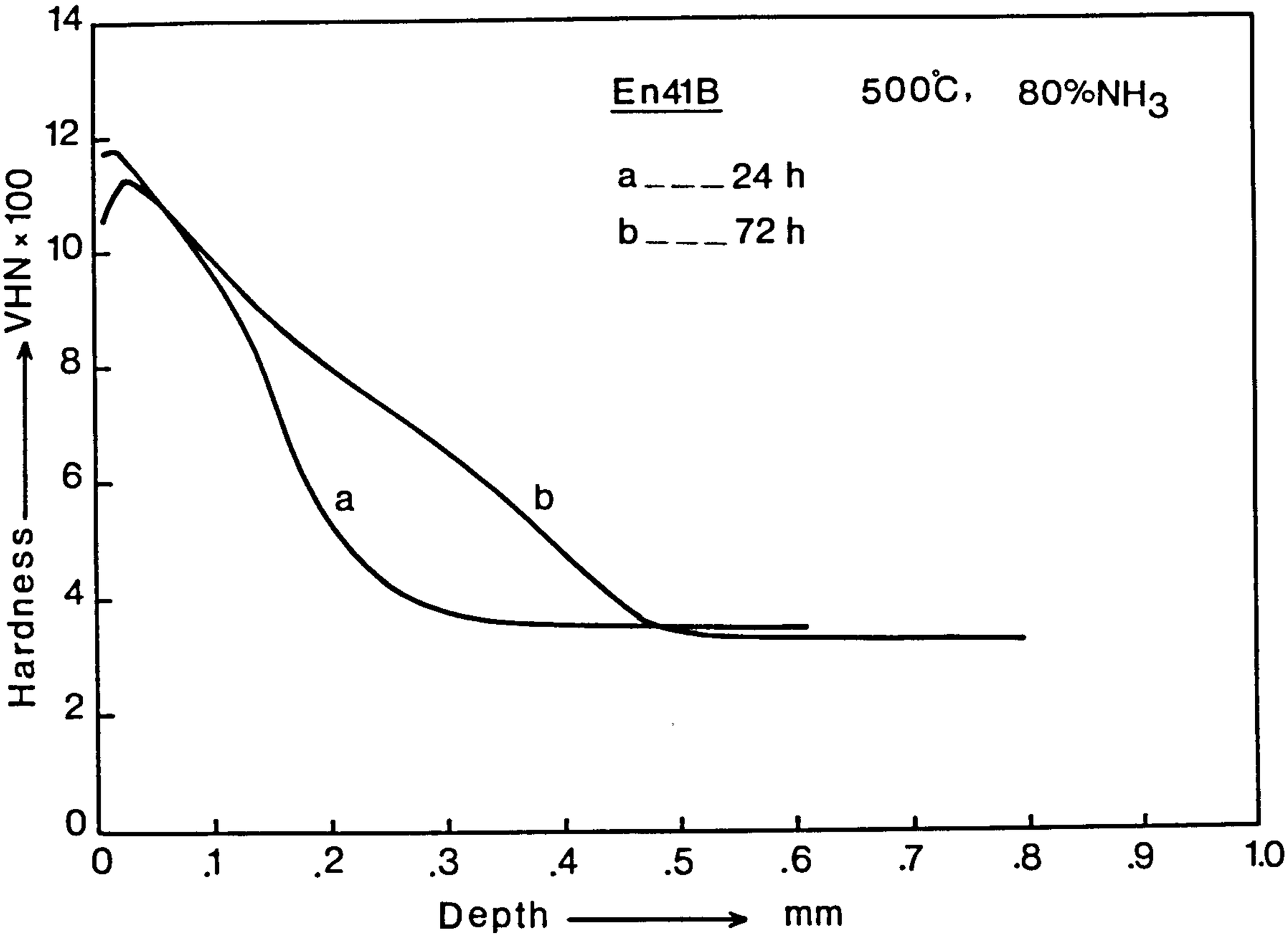

FIG. (6.11)

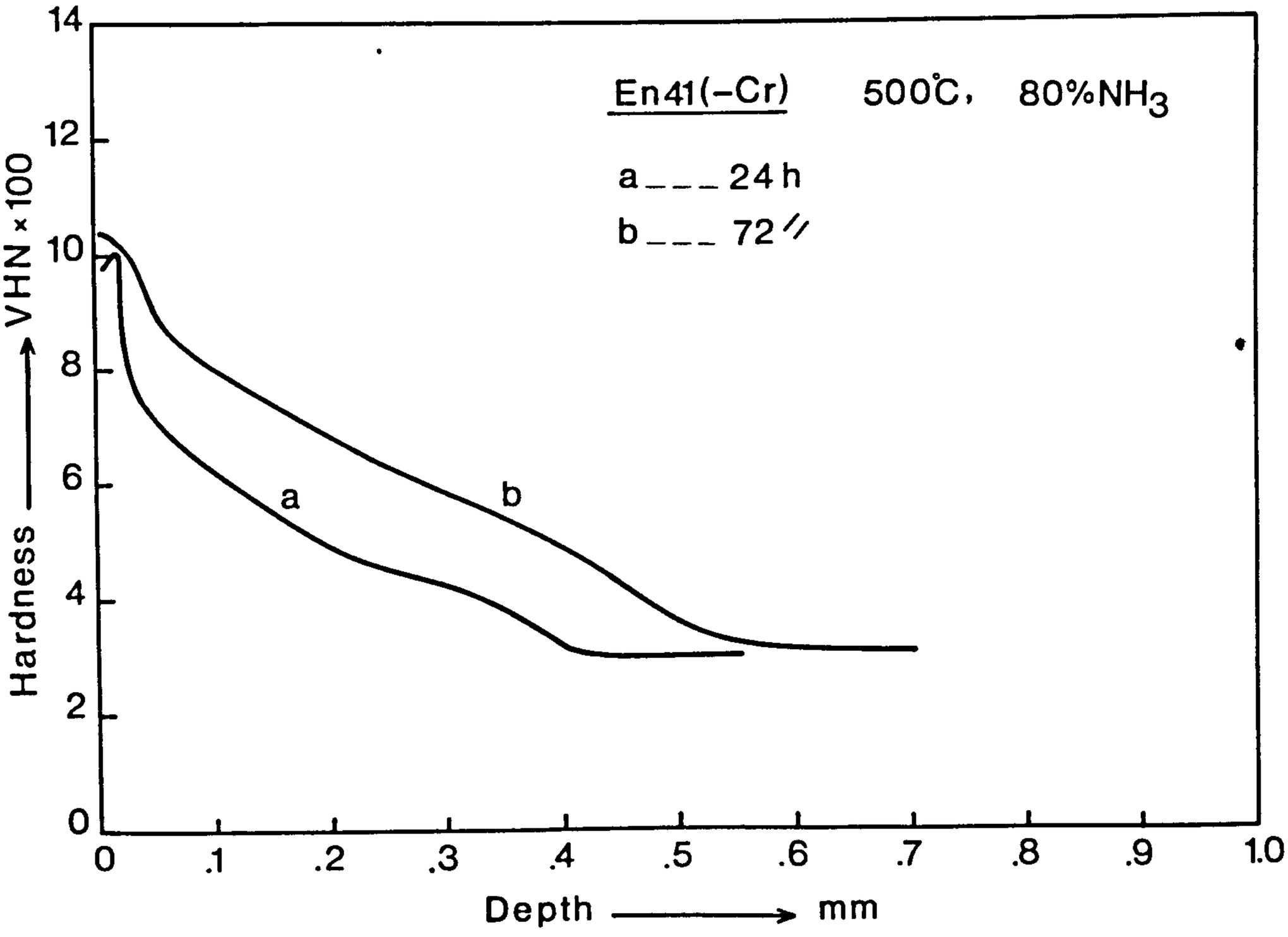

FIG. (6.12)

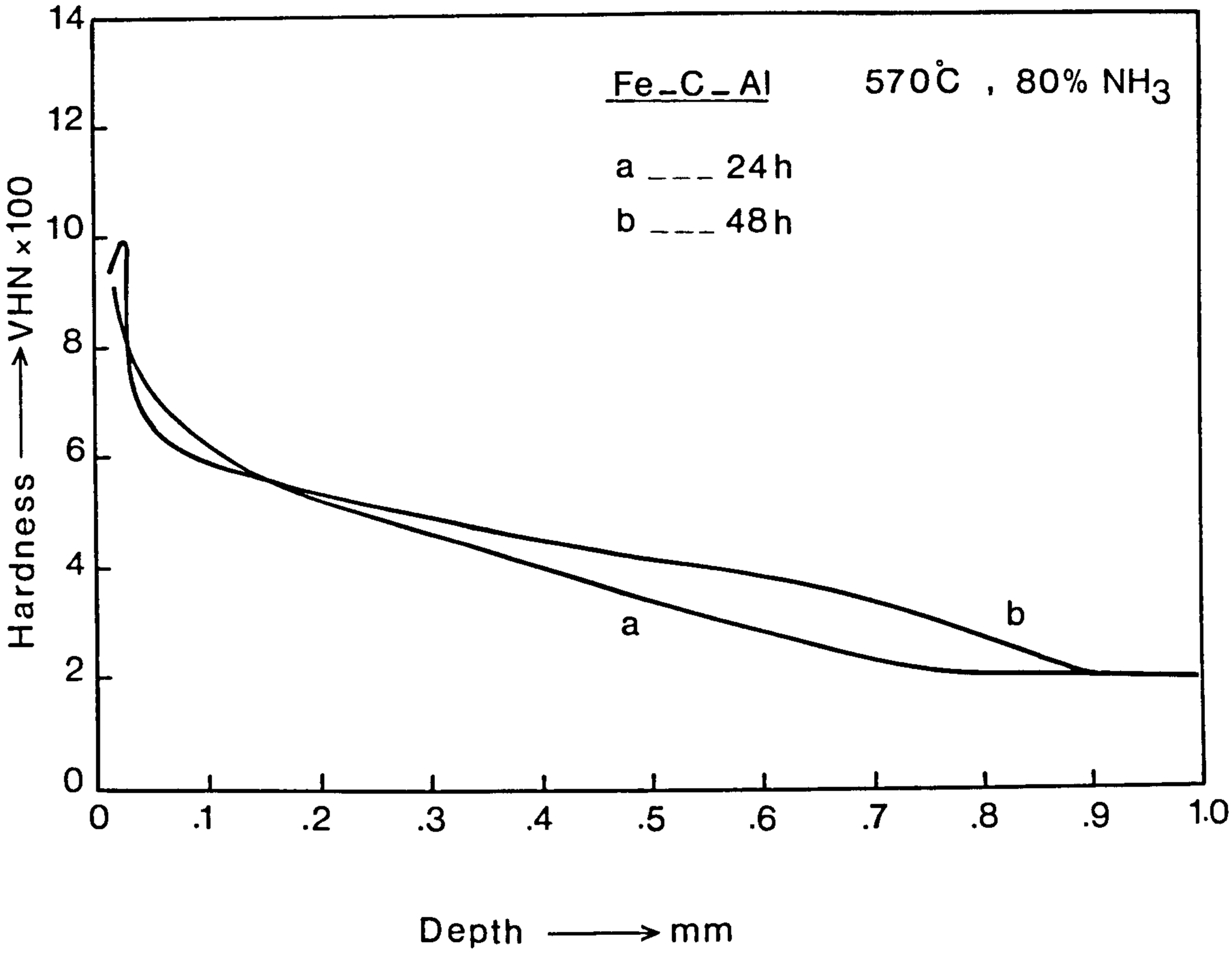

Fig. 6.13 Effect of nitriding time on the case depth of Fe-C-Al steel

Fig. 6.14 Effect of nitriding time on the case depth of En41B, nitrided at 500°C in 20% NH_3

Fig. 6.15 As in Fig. 6.14 nitrided at 570°C in 14% NH_3

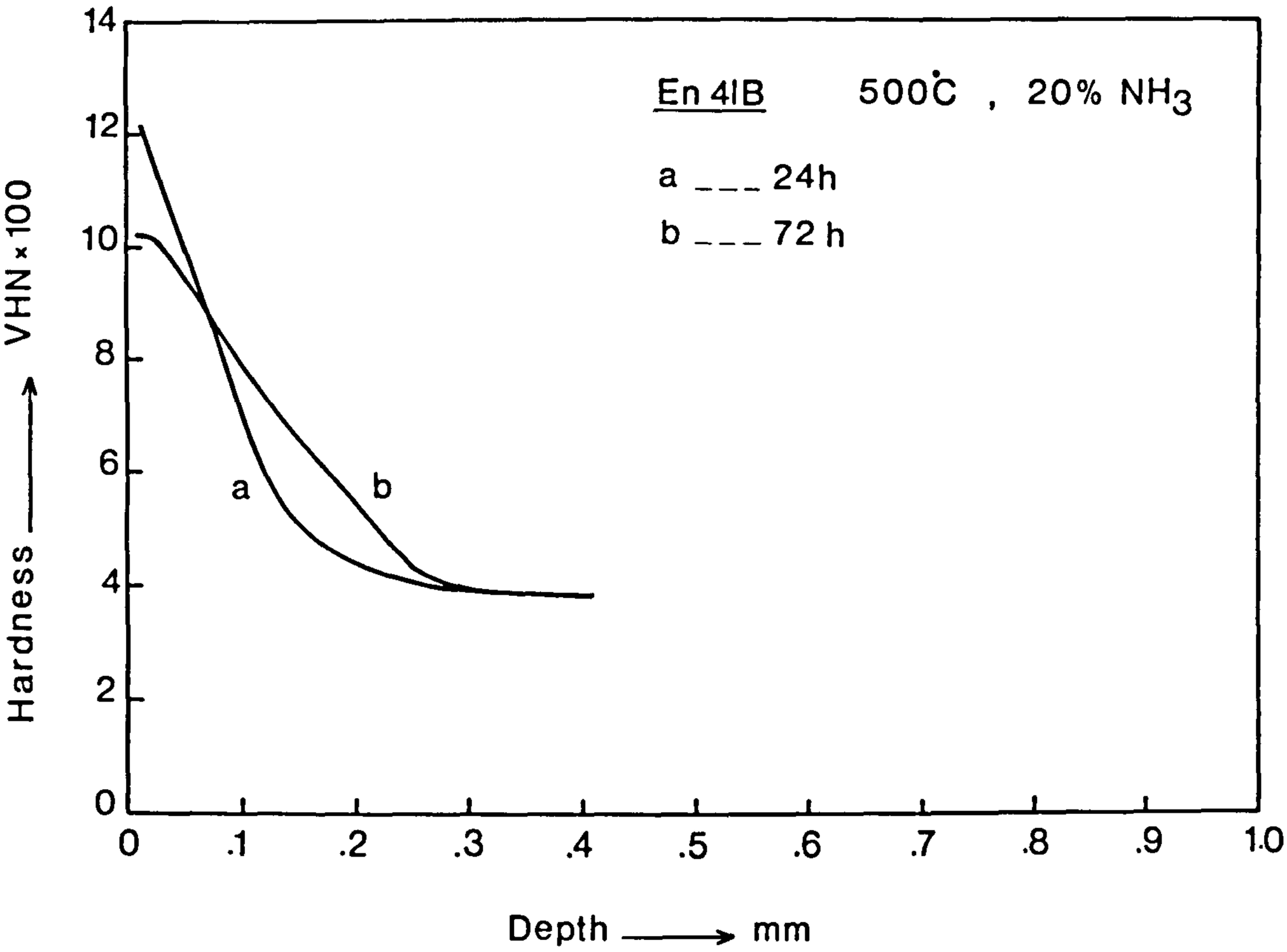

FIG. (6.14)

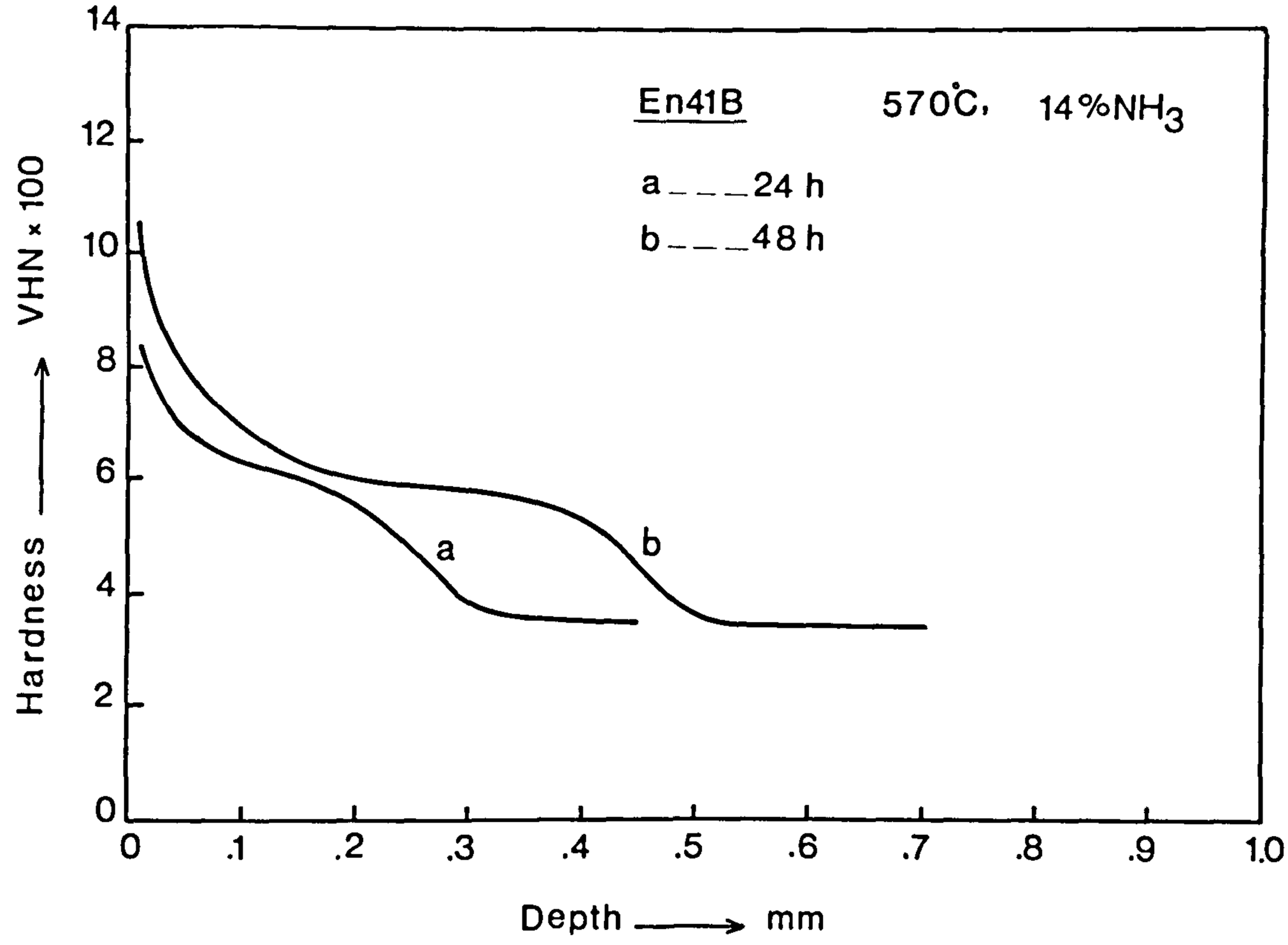

FIG. (6.15)

Fig. 6.16 Effect of the alloying elements on the case depth of the nitrided steels, nitrided for 72h at 500°C in 80% NH_3

Fig. 6.17 As in Fig. 6.16 nitrided for 24h

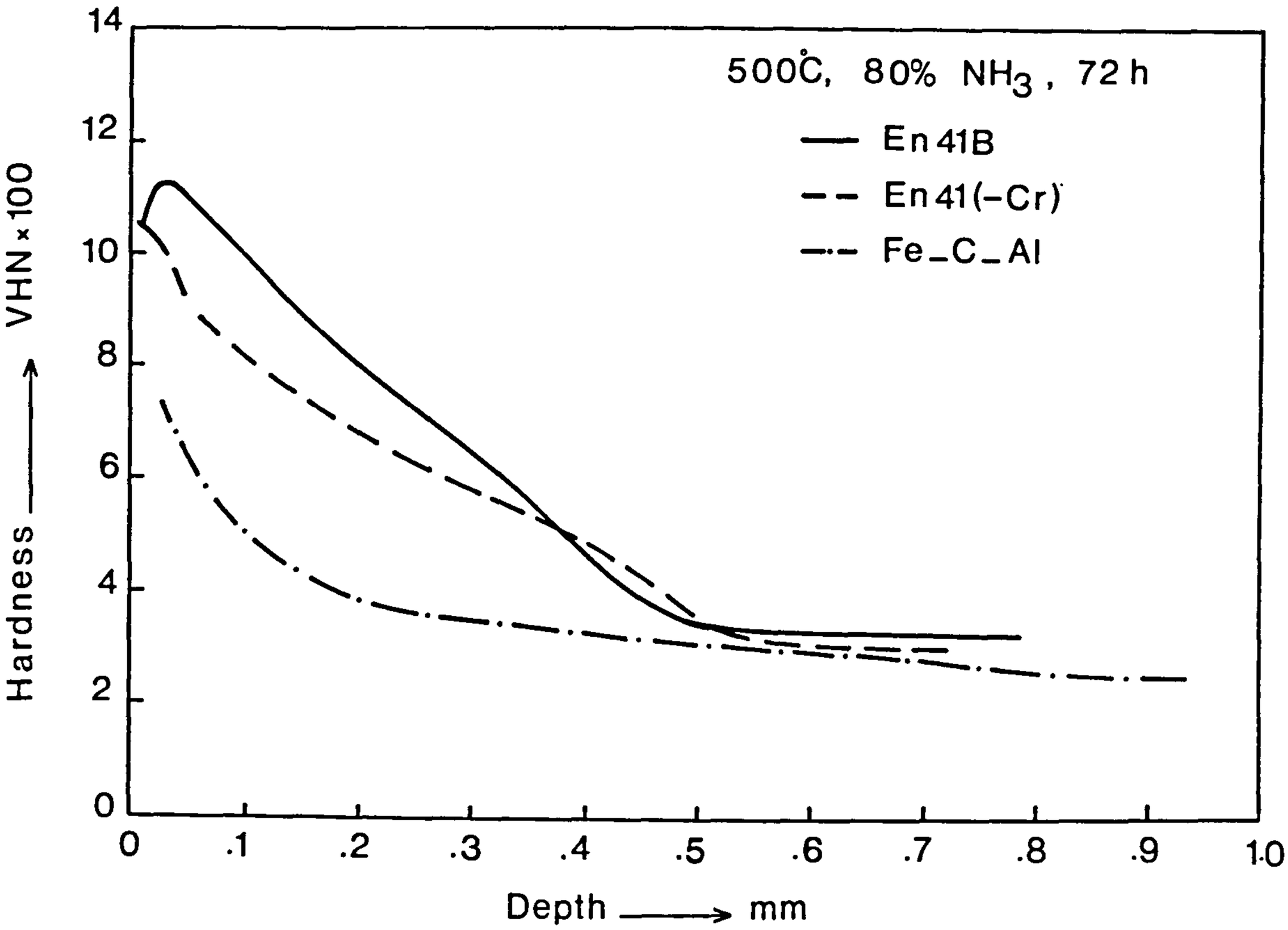

FIG.(6.16)

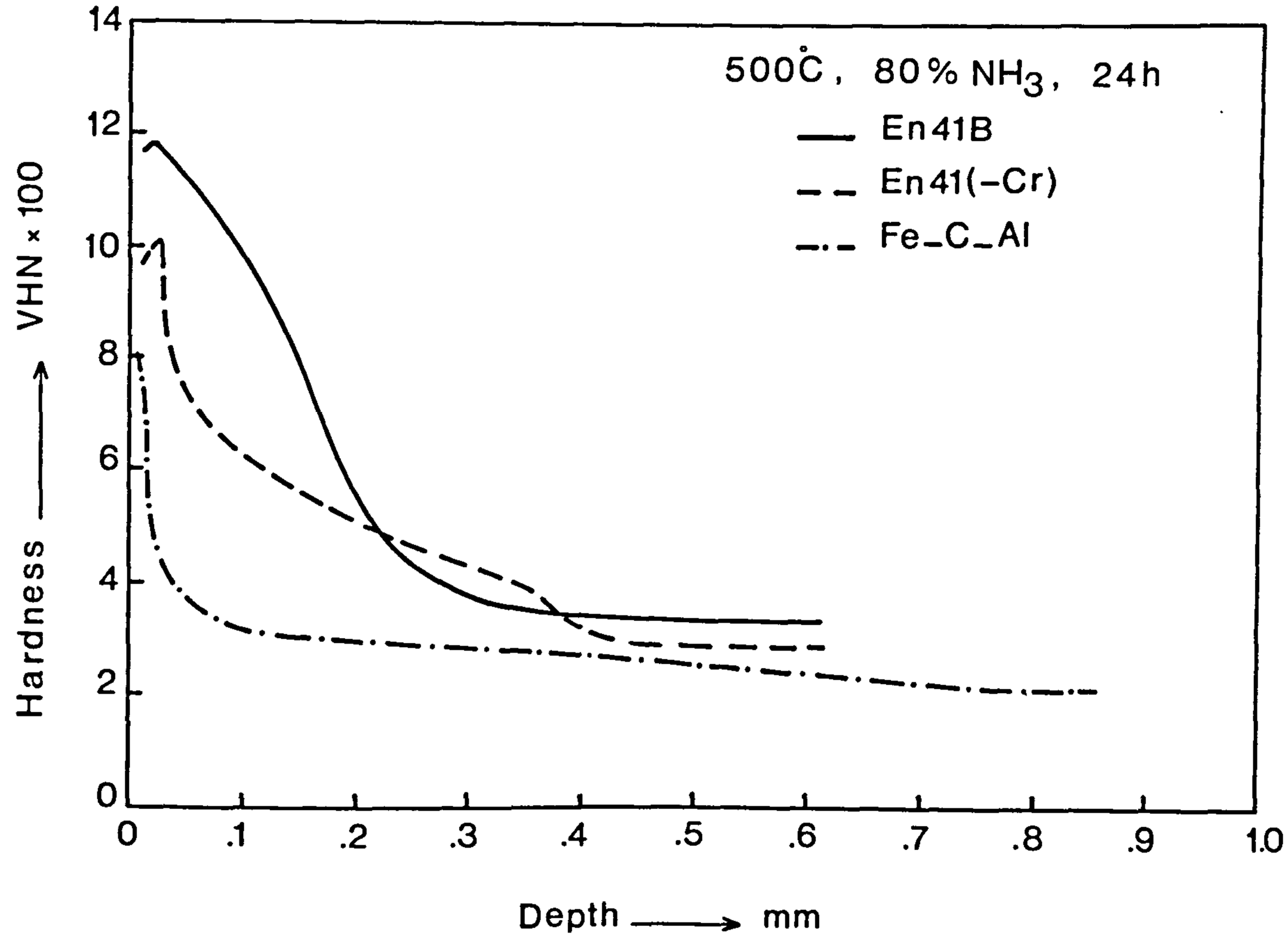

FIG.(6.17)

Fig. 6.18 Effect of the alloying elements on the case depth of nitrided for 24h at 570°C for 80% NH_3

Fig. 6.19 As in Fig. 6.18 but nitrided for 24h

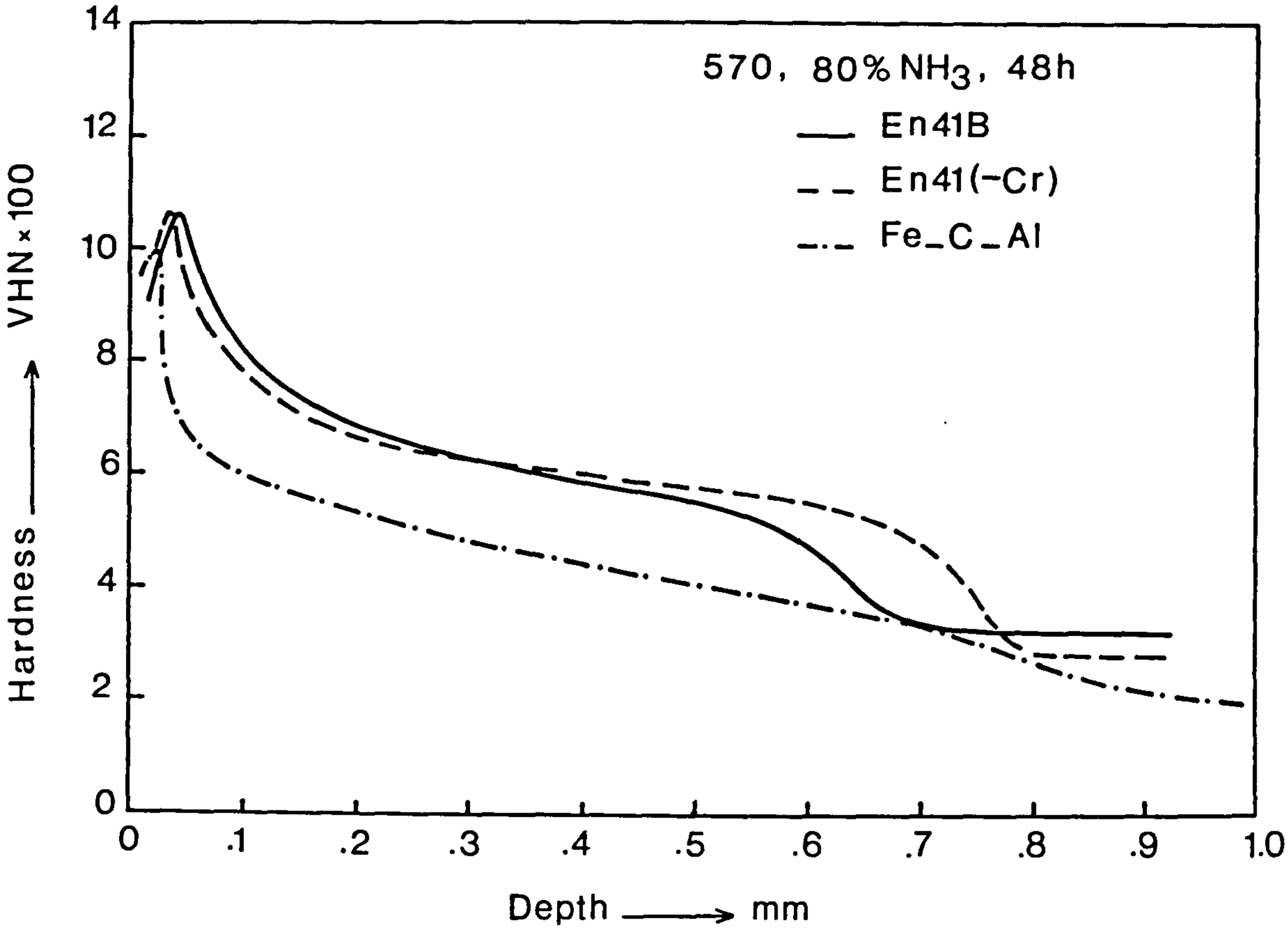

FIG.(6.18)

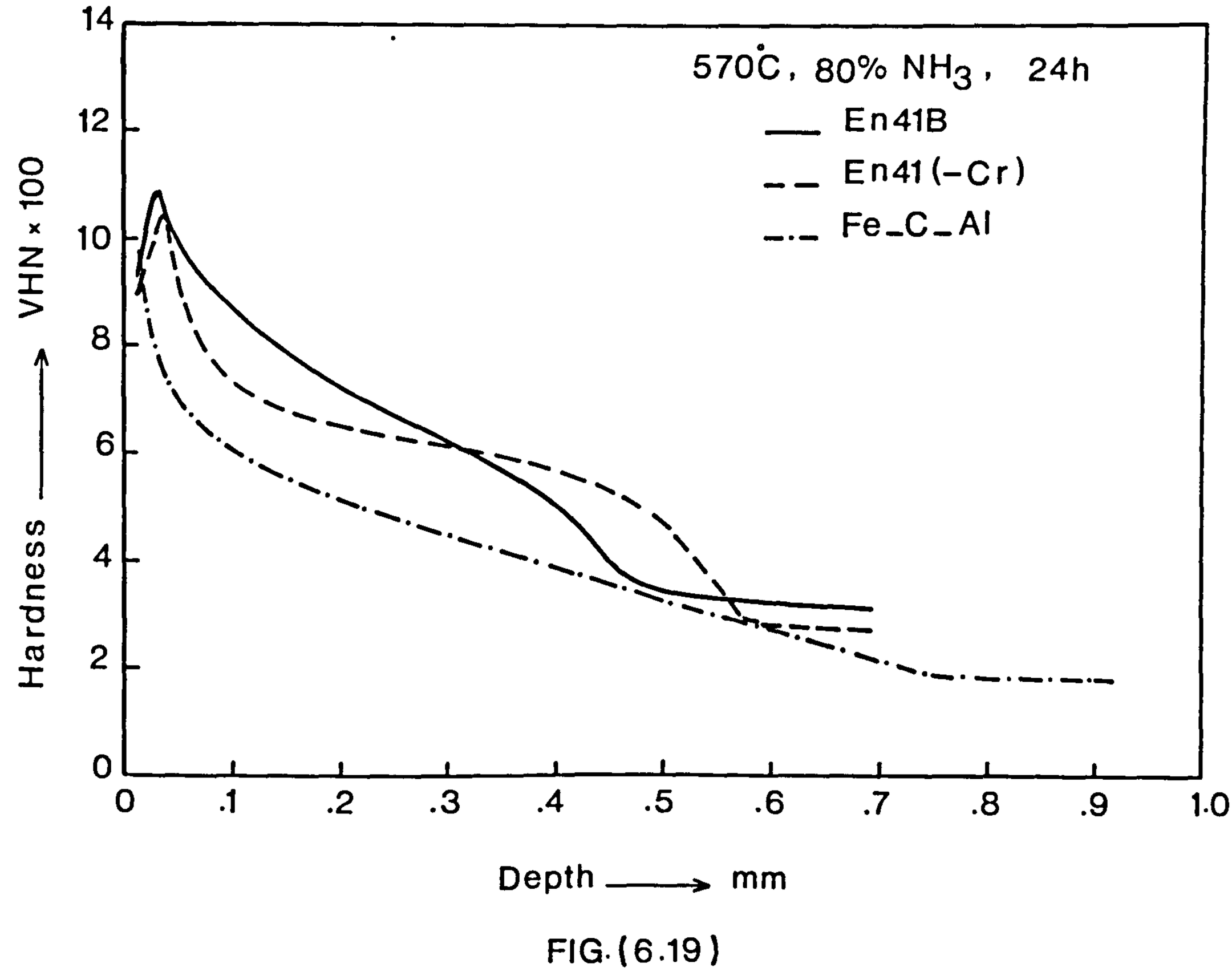

FIG.(6.19)

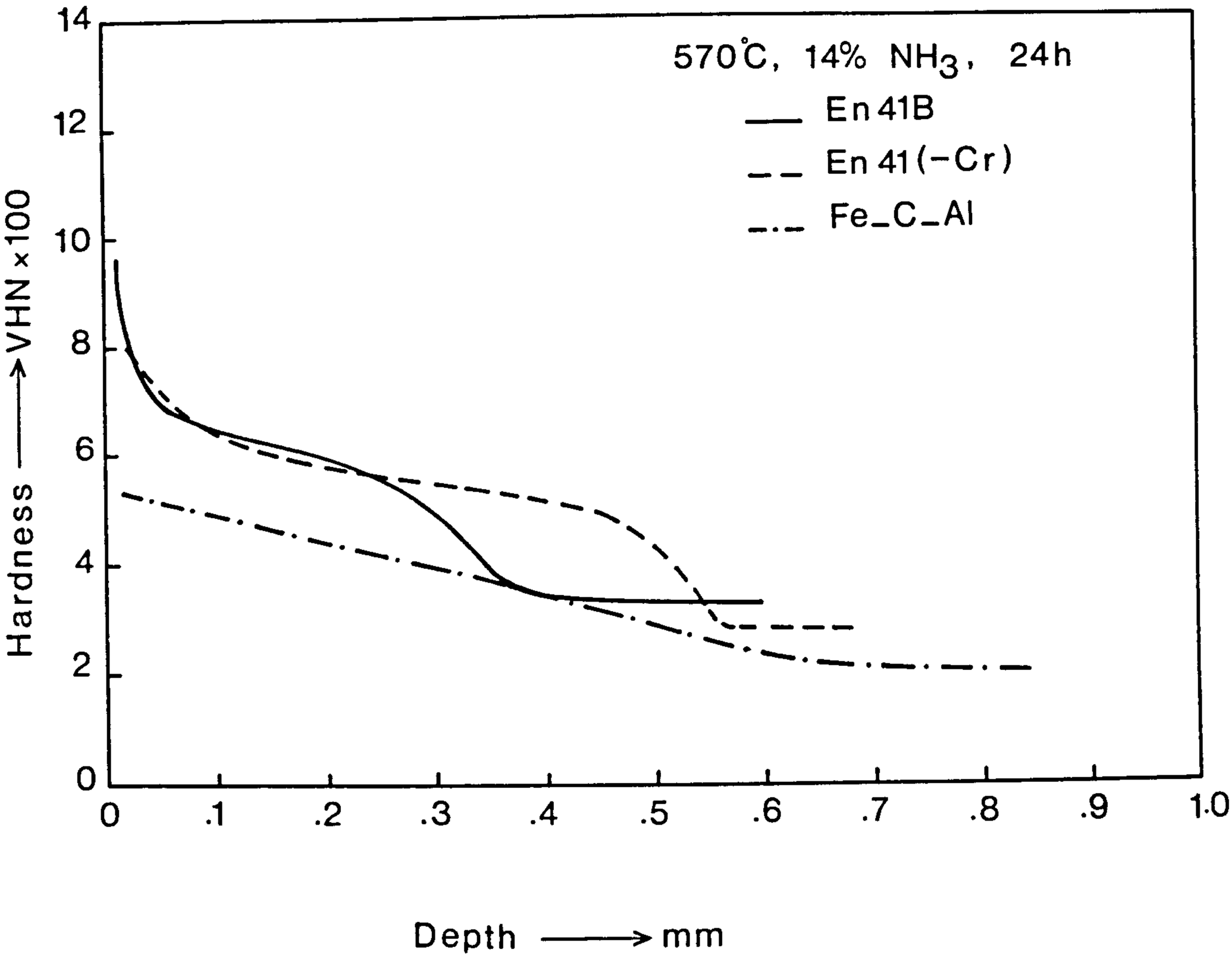

Fig. 6.20 Effect of alloying elements on the case depth, nitrided at 570°C in 14% NH_3

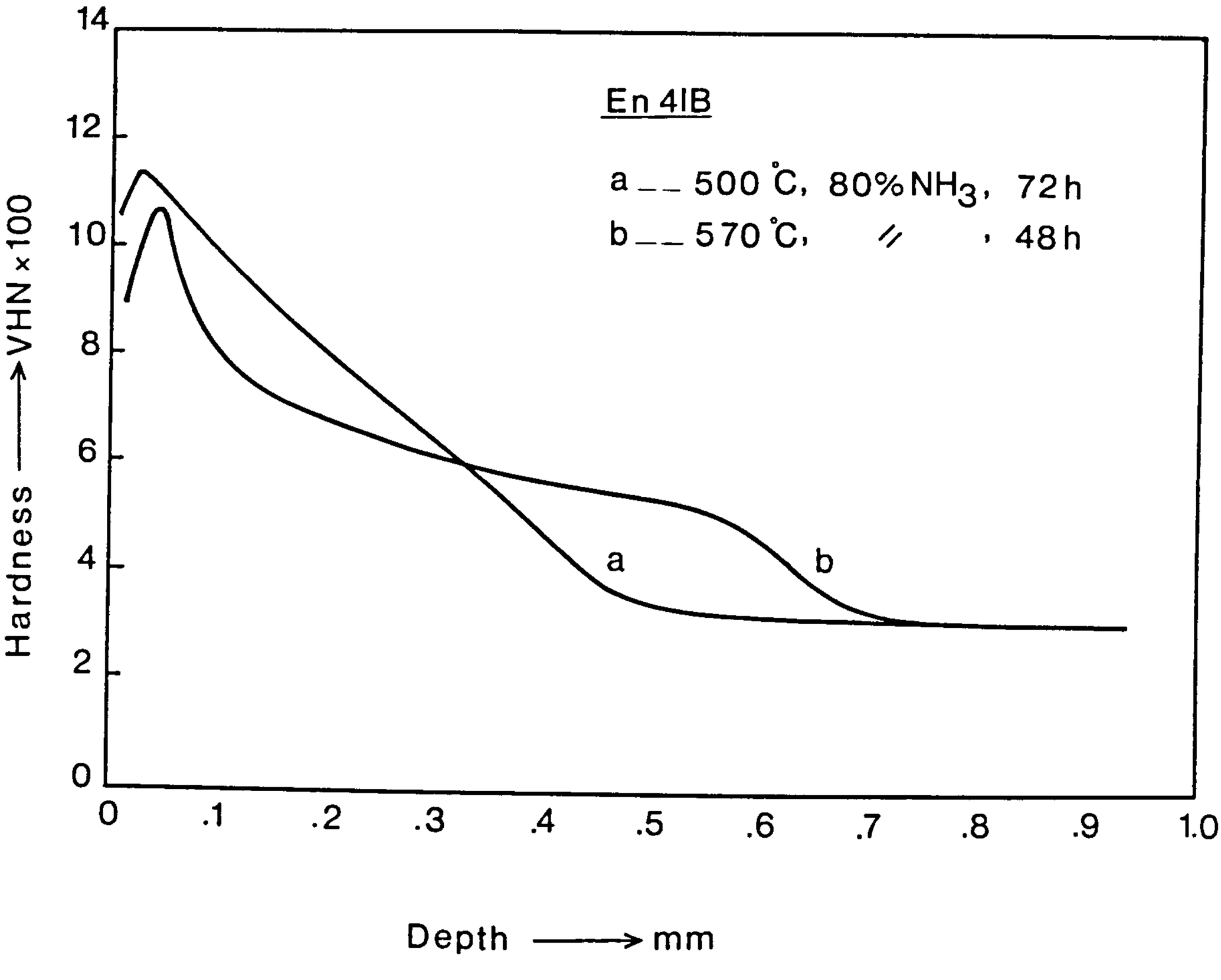

Fig. 6.21 Effect of nitriding temperature on the hardening response of En41B

Fig. 6.22 Effect of tempering temperature prior to nitriding on the hardening response of En41B, nitrided at 500°C

Fig. 6.23 As in Fig. 6.23 nitrided at 570°C

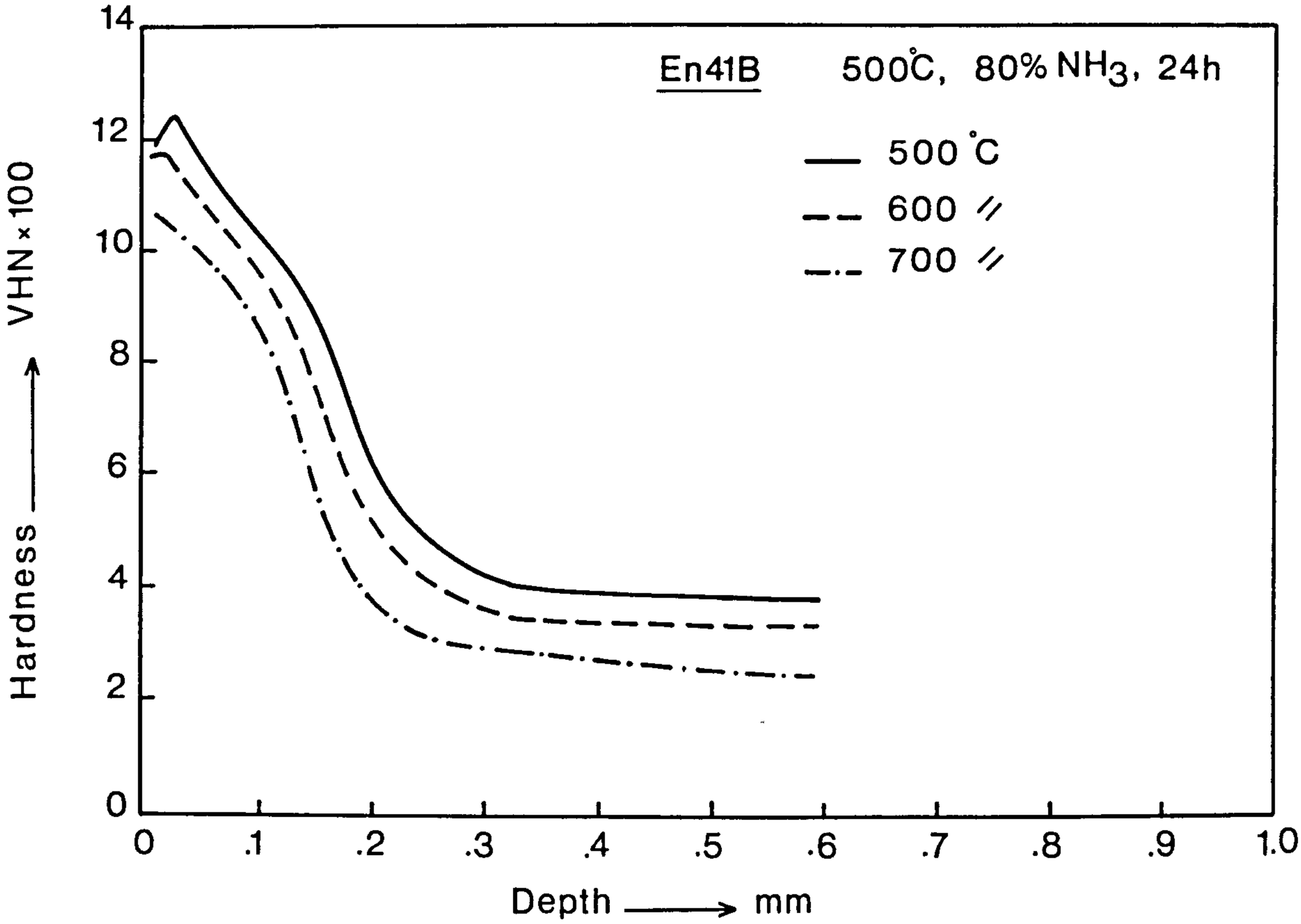

FIG. (6.22)

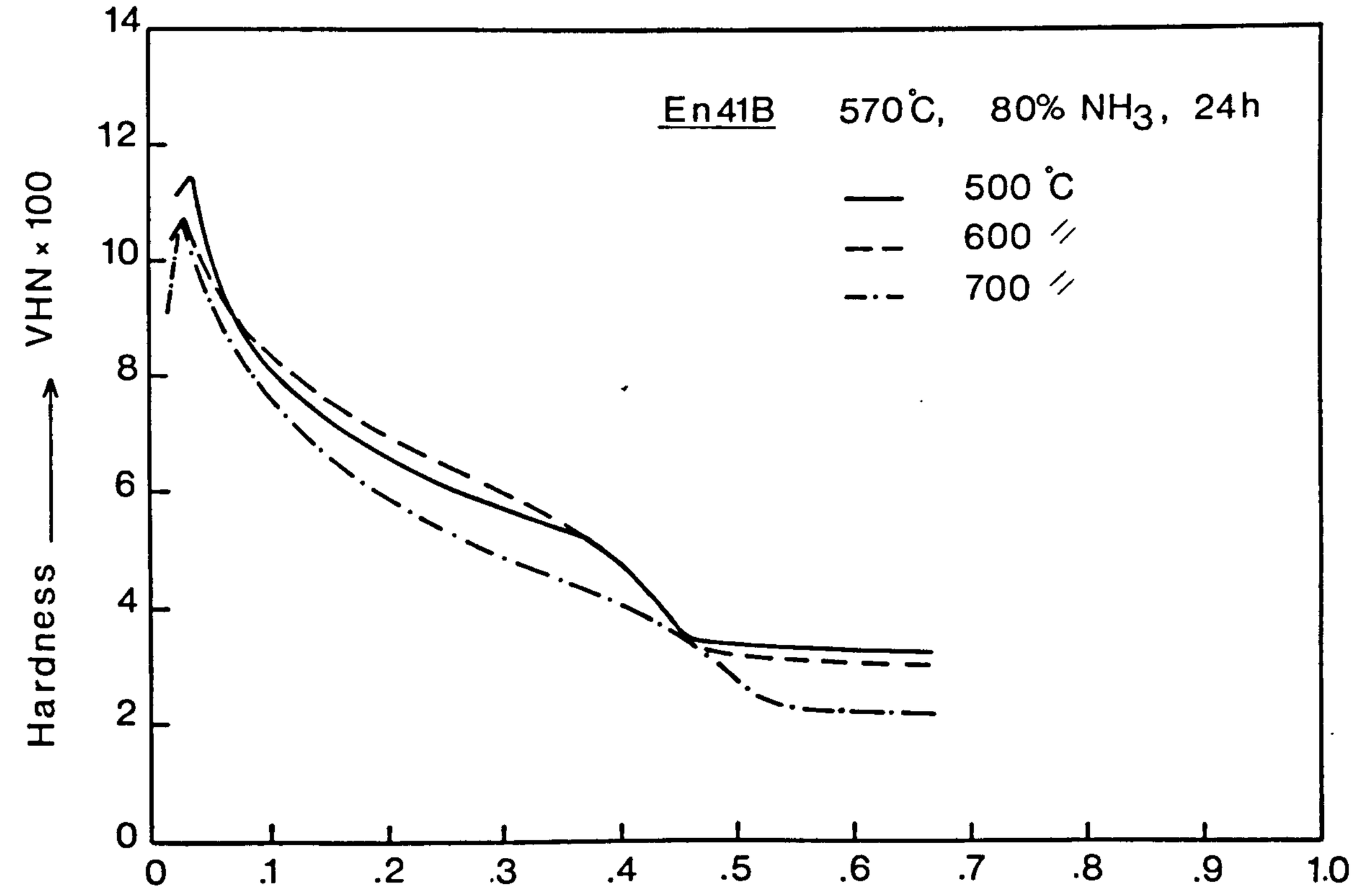

FIG. (6.23)

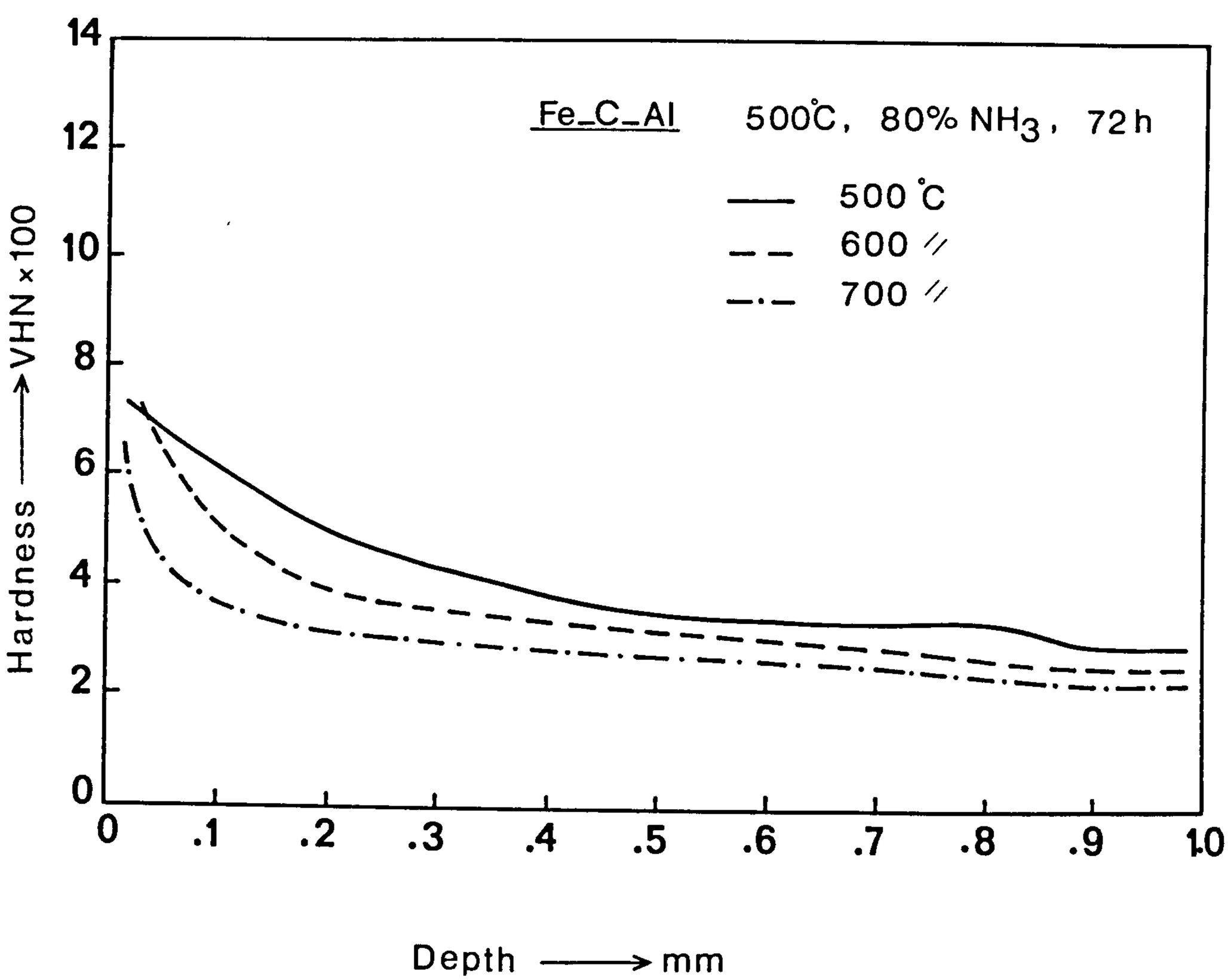

Fig. 6.24 Effect of tempering temperature prior to nitriding on the hardening response of Fe-C-Al, nitrided at 500°C

Fig. 6.25 Hardness profiles of En41B nitrided at 570°C in 80% NH_3 showing the effect of nitriding time on the hardness profile

Fig. 6.26 Hardness profiles of En41(-Cr) nitrided at 570°C in 80% NH_3, showing the effect of time on the hardness profile

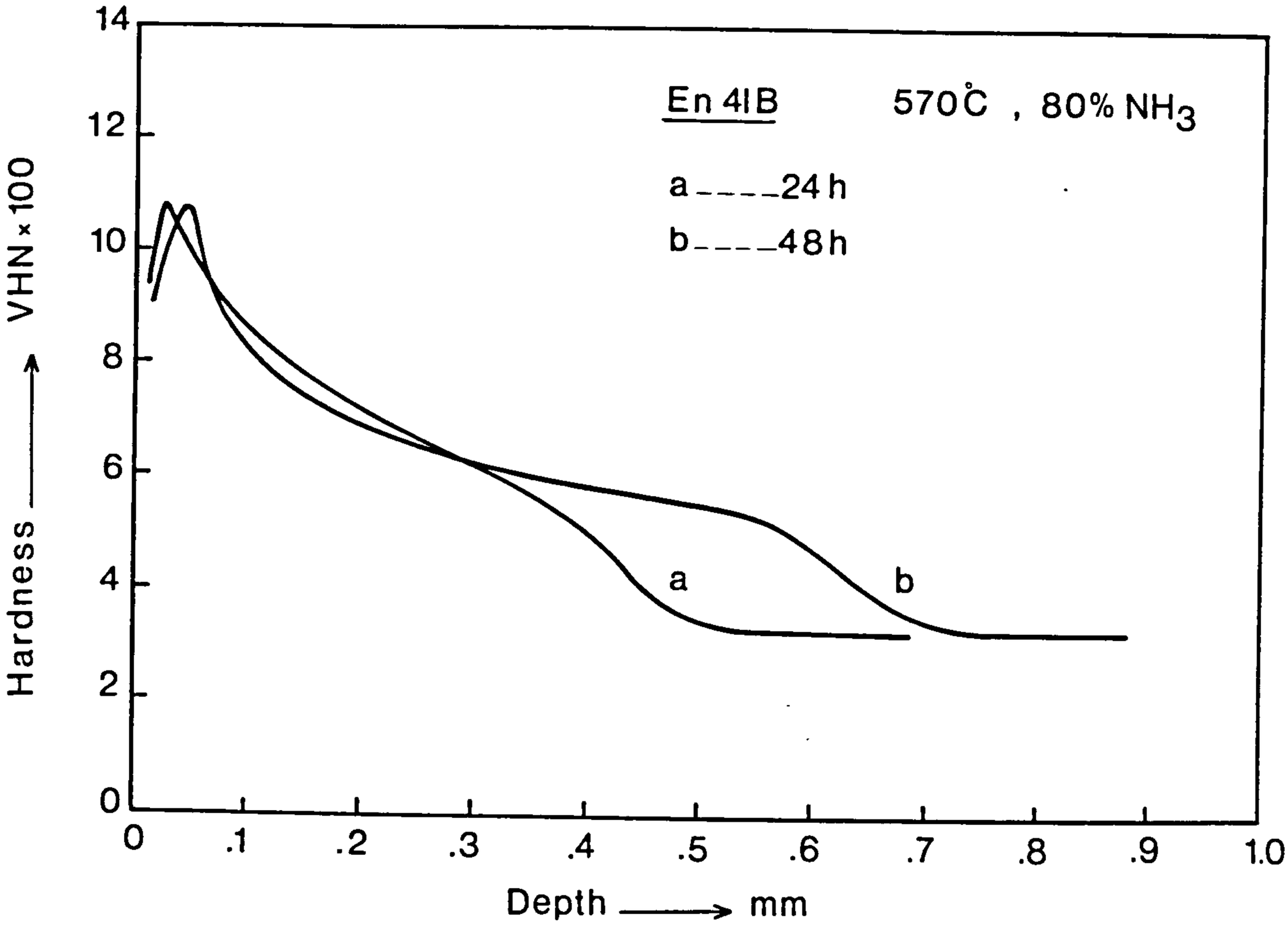

FIG. (6.25)

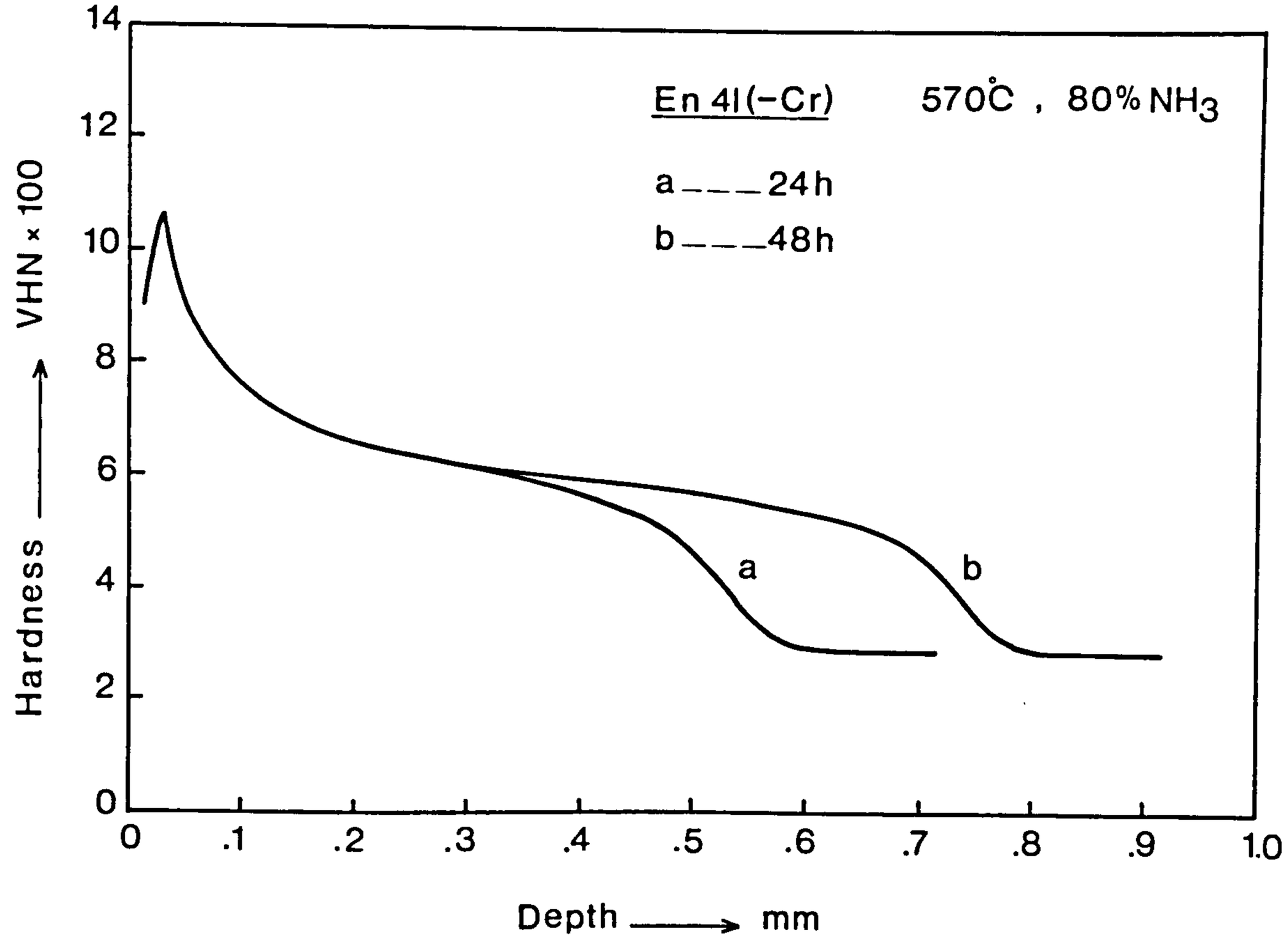

FIG. (6.26)

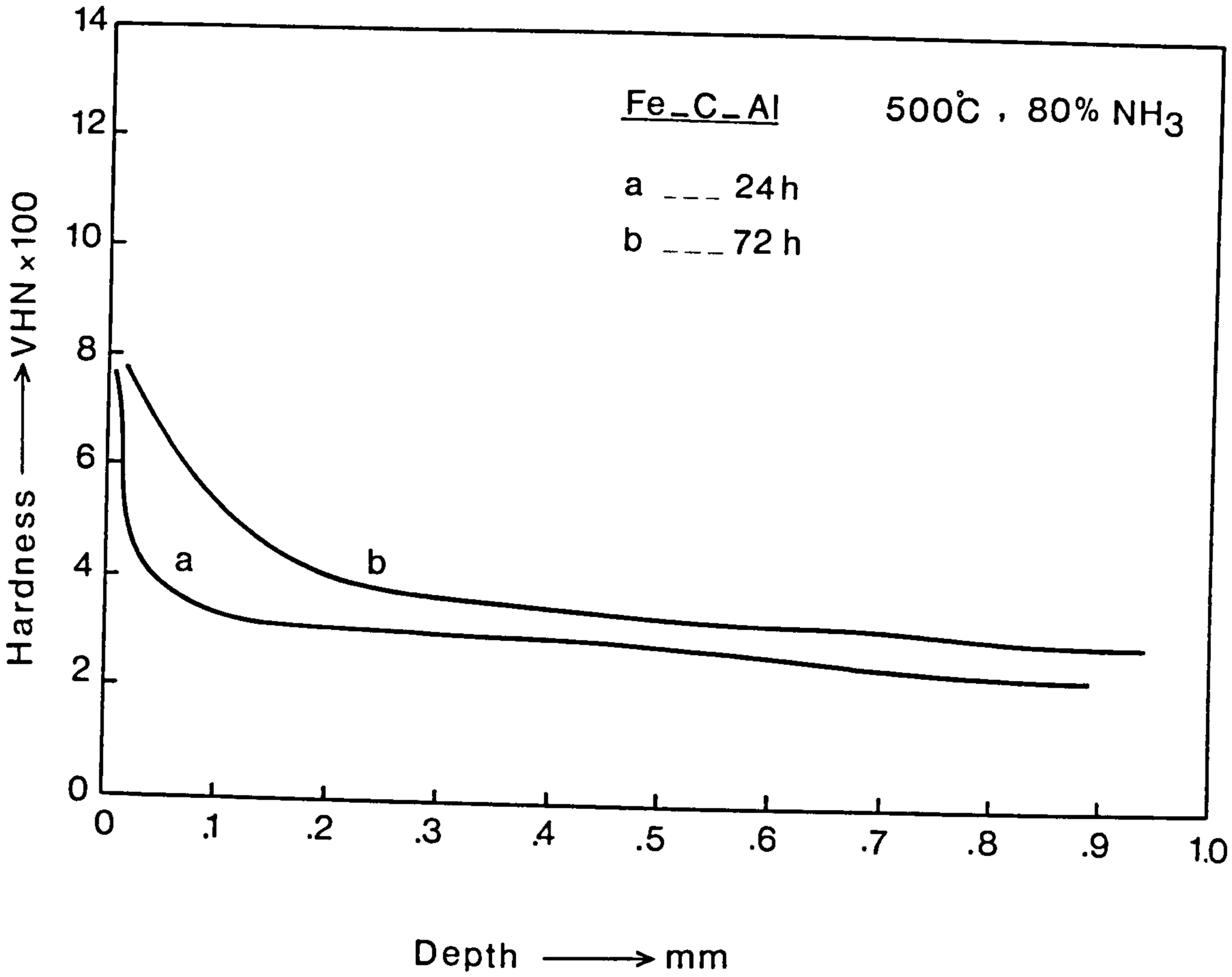

Fig. 6.27 Effect of nitriding time on the hardness profile of Fe-C-Al, nitrided at 500°C in 80% NH_3

Fig. 6.28 Effect of the NH_3 content of the gas mixture on the hardness profile of En41B nitrided at 570°C for 48h

Fig. 6.29 As in Fig. 6.28, nitrided at 500°C for 72h

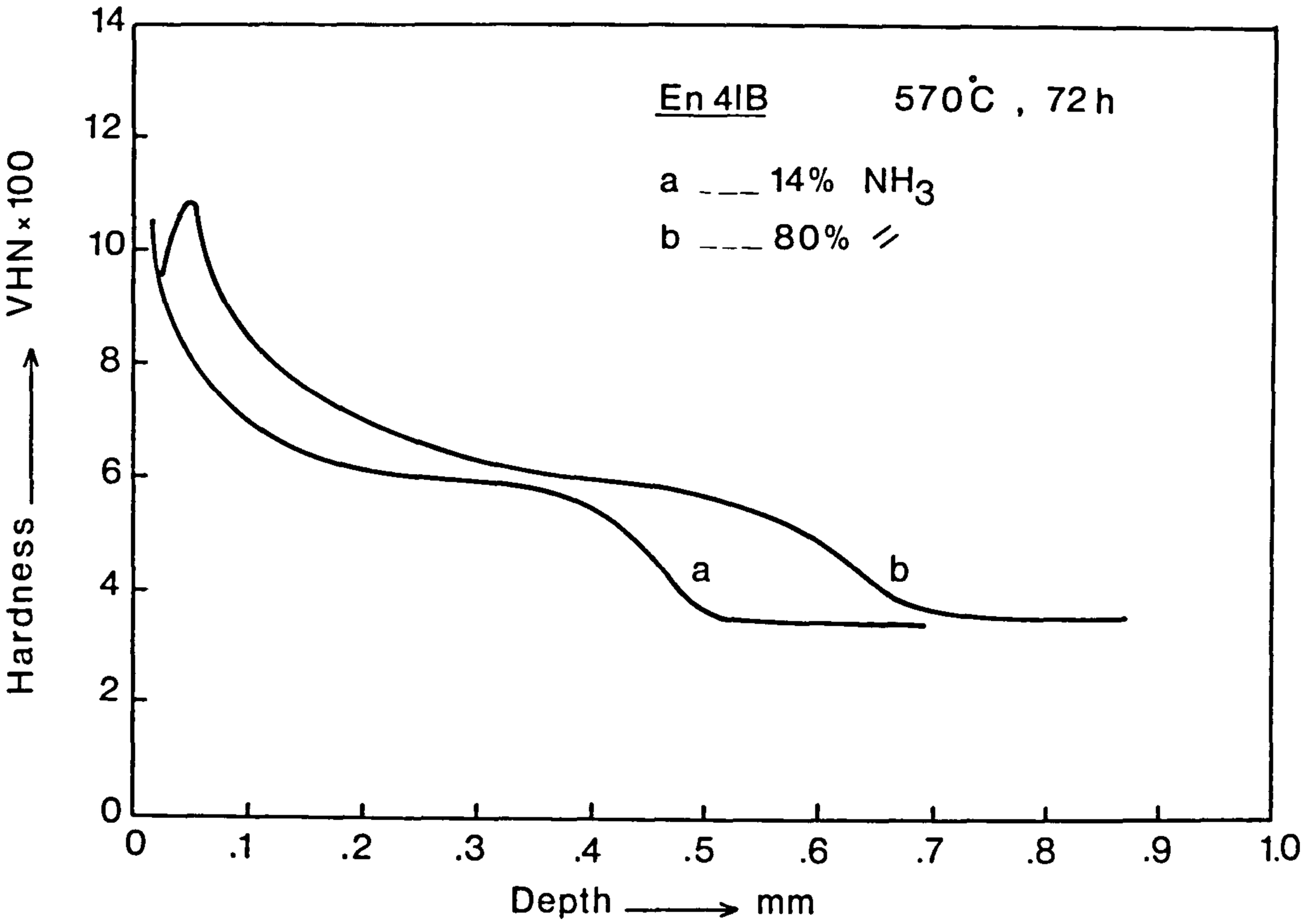

FIG. (6.28)

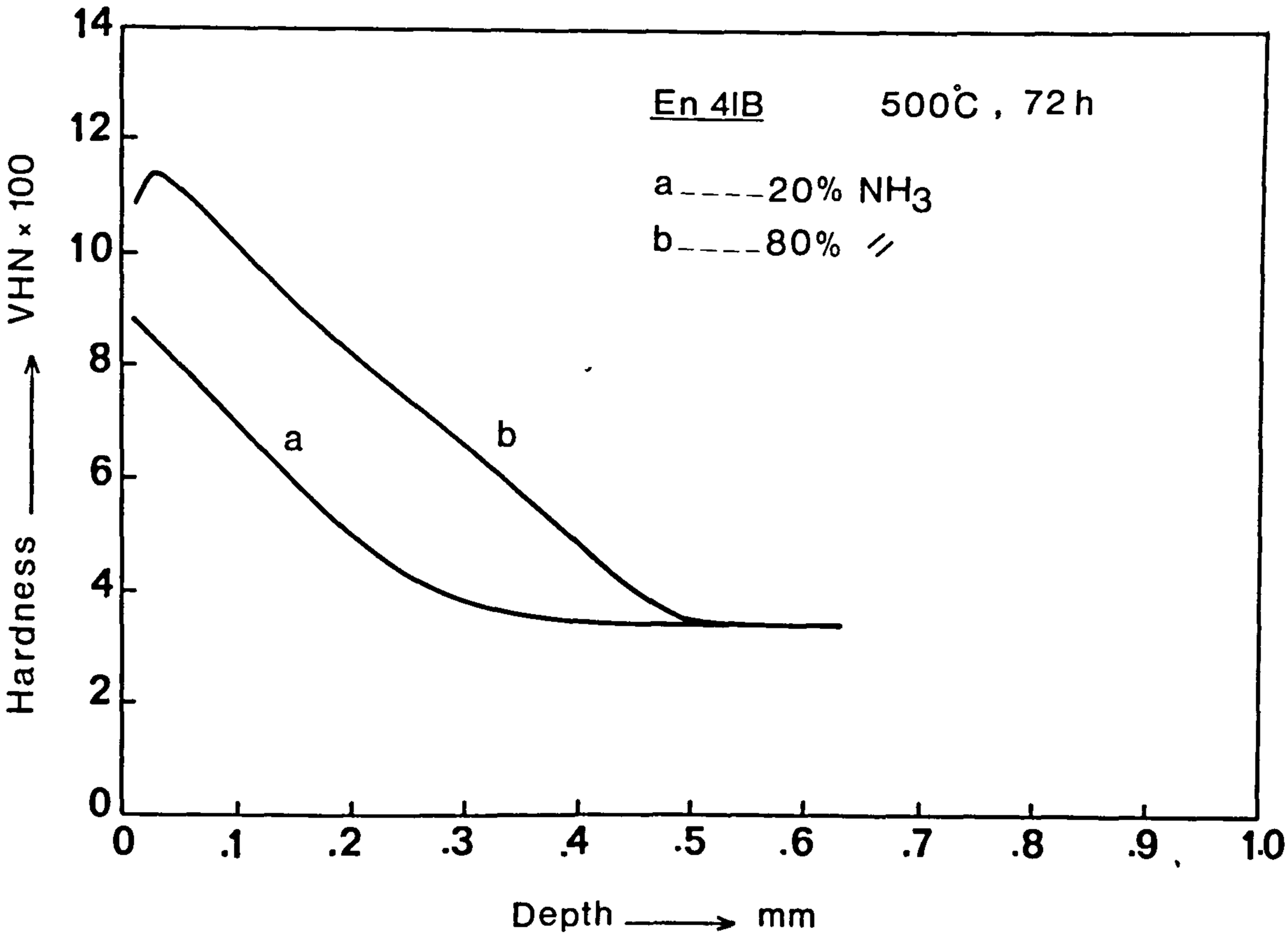

FIG. (6.29)

CHAPTER 7

FATIGUE BEHAVIOUR OF NITRIDED En41A STEEL

7.1 Previous work

It has been recognized that the fatigue properties of metals are greatly affected by the surface condition. In steel parts a marked improvement in fatigue performance can result from the formation of a hard layer on the surface. The processes commonly used for surface hardening are nitriding and carburizing. Although both treatments improve the fatigue properties, it is recognized that nitrided parts have better fatigue properties than carburized ones. Nitriding has the advantage that it is not essential to quench, so minimizing any distortion. Carburizing can give a thicker hardened case than nitriding, but the latter produces a higher surface hardness. Though both processes give rise to high surface compressive residual stress, which effectively increases the fatigue performance, nitriding has been found to give a higher compressive residual stress than carburizing (76,77,78).

Early investigations (79, 80) showed that the endurance properties of nitrided steel under an alternating stress were greatly enhanced, the major benefit becoming more apparent in specimens having stress raisers, such as notches, bores or rough machined surfaces, implying that nitrided steel parts have higher notch resistance. This is important since fatigue properties are highly sensitive

towards notches and surface finish. However, regarding the effect of nitriding on the direct stress fatigue behaviour there has been some conflicting reports. Sutton (81), Bardgett (76), Cazaud (82) and Tauscher et al. (83), all reported that nitriding has little effect on the direct stress fatigue limit, whereas more recent investigations by Jones and Martin (84), carried out on En41B indicate that nitriding does significantly improve the direct stress fatigue limit. It has been shown however that the fatigue limit increases with increasing case/core area ratio, and the increase in fatigue limit was reduced with increasing nitriding time. Jack and Winnik (85) investigated the fatigue behaviour of nitrided En40B steel, using Rolls-Royce type rotating-bending fatigue specimens. It was concluded that fatigue resistance depends on residual stress in the case, and not on the microstructure of the case or the presence of surface iron nitrides.

7.2 Material and experimental methods

The material used for this work was En41A steel whose composition is given in Table 2.1. Specimens were machined from material which had been oil quenched from 900^{o}C then annealed at 600^{o}C for 1h. All specimens were smoothly hand polished then electropolished to remove the fine scratches from the surface. The tests were carried out using Rolls-Royce type rotating-bending fatigue specimens, and it was performed on a Wohler rotary bending machine at a speed of

2800 r.p.m. The fatigue specimen dimensions and schematic drawing of the fatigue test machine are shown in Figs. 2.7 and 2.8 respectively.

Five sets of specimens were tested, three of which were nitrided at different conditions for different times. The aim being to achieve the same case depth in the three nitriding conditions, but with different hardness profiles, and with or without surface iron nitride. Table 7.1 summarises the data for each nitriding condition.

The other two sets of specimens were tested in the annealed condition, one set was first annealed at 600°C for 1h then aged at 570°C for 48h to simulate the core condition of the specimens nitrided at 570°C for 48h.

The fracture surfaces were examined by both optical and electron microscopy.

7.3 Hardness and depth of the nitrided case

The microhardness profiles obtained for the different nitriding conditions are given in Fig. 7.1. At 520° a steep profile and a maximum hardness of ~ 1100 VHN was achieved in 80% NH_3. In 30% NH_3 for 48h the profile is less steep with a greater hardening depth, but the maximum hardness remains the same. However nitriding at 570°C in 10% NH_3 for 48h produced a shallow hardness profile and a maximum hardness of ~ 900 VHN.

The difference in core hardness between specimens nitrided at 570°C and those nitrided at 520°C is very small (approximately 30 VHN), see Table 7.1.

The specimens nitrided at 570°C in 10% NH_3 and 520°C in 30% NH_3 are both free of surface iron nitride, and the specimens nitrided at 520°C in 80% NH_3 contain white layer of thickness approximately 25 μm.

7.4 Fatigue test and S-N curves

The fatigue properties of a given material can be conventionally expressed in the form of S-N curves, where S is the amplitude of stress to produce fatigue failure after N cycles. The rotating bending fatigue test (Wohler test) is a common method used for cylindrical specimens.

The procedure used for determining the S-N curves was to test the first specimen at a high stress (about 2/3 of static tensile strength) where failure is expected to occur after a fairly short number of cycles. The test stress was then decreased for each succeeding specimen.

The applied stress was calculated using the maximum bending moment (86)

$$\sigma = my/I \qquad 5.1$$

where m = force applied (varies with moment WL)

y = displacement from the central axis (varies between 0 and d/2

I = second moment of area

from which

$$\sigma = \frac{32\ WL}{\pi\ d^3} \qquad 5.2$$

where W = Load applied

L = distance between the applied load and the middle of the specimen curvature

d = specimen diameter (~ 4.0 mm)

The S-N curves were obtained from tests using a minimum of 8 specimens for each condition (plain and nitrided). Owing to the statistical nature of the fatigue process and the consequent scatter of results, the number of the tests carried out in the present investigation was considered small, and as a result considerable deviation from an average curve in each condition is to be expected. However, S-N curves really represent some kind of average for the specimens tested.

7.4.1 Fatigue test results

The result from the fatigue testing programme are shown in Figs. 7.2 and 7.3 for the non-nitrided and nitrided specimens respectively. For the nitrided specimens, it is apparent that the improvement of the fatigue properties are very much dependent on the nitriding conditions. Nitriding at 520^{o}C in 30% and 80% NH_3 improves both fatigue life and fatigue limit. The fatigue life at 900 MPa increased from 4×10^4 cycles to between 6×10^5 - 10^6 MPa, and the fatigue limit was raised from 625 MPa to between 800-850 MPa, approximately a 25% increase. Also the fatigue strength improved by an average of 30%, a value which is close to that previously reported in larger cross section specimens (87).

The fatigue properties of specimens nitrided in 30% NH_3 for 48h are slightly better than those nitrided in 80% NH_3 for 24h. The specimens in both cases have the same maximum surface hardness and the same core hardness with similar hardness profiles, but the hardening depth is greater in the former condition by about 20%, and this could be the reason for the small improvement in the fatigue performance, because the extent and the magnitude of the compressive stress would be better in this case.

On the other hand, the fatigue properties of the specimen nitrided at 570°C in 10% NH_3 are inferior to those produced by nitriding at 520°C in 30% or 80% NH_3. If compared with the performance of the as-tempered material, see Fig. 7.4, the fatigue limit on nitriding at 570°C in 10% NH_3 is unchanged, but the endurance limit is very much lower specially at high stresses.

The nitriding temperature appears to be a major influencing factor on the fatigue properties. Nitriding at 570°C in 10% NH_3 for a long period is assumed to produce modest compressive stress at the surface and a reduced core strength. To confirm the effect of nitriding temperature and time on the fatigue properties, a fatigue test was carried out using specimens that were first tempered at 600°C for 1h, and then retempered at 570°C for 48h. The latter treatment was used to simulate the nitriding temperature and time. The S-N curves for the above treatment and the standard tempering treatment are shown in Fig. 7.5. There is no apparent effect on the fatigue limit, but the endurance

limit decreased significantly. Comparing the fatigue curves of 570°C nitrided specimens with the non-nitrided specimens, the nitrided ones have a lower endurance limit, see Fig. 7.6.

The inferior fatigue behaviour due to nitriding at a high temperature in a low NH_3 concentration is attributed to a combination of effects. Nitriding at 570°C produces a softer core with lower tensile strength, and due to the deeper nitrided case the core is smaller. This leads to an increase in the residual tensile stress of the core to counter balance the residual compressive stress in the case. This would adversely affect the fatigue performance, especially at high stress levels. Whereas nitriding at 520°C does not soften the core and produces very high residual compressive stresses at the surface, a combination which is favourable in terms of improving fatigue properties.

7.5 Fractography of the fatigue samples

The surfaces of a fatigue fracture can be divided into two main parts with distinctly different macroscopic appearances. The fatigue area is comparatively smooth because at this stage the crack propagation is low, and the final failure area is rougher in texture when failure is by ductile microvoid coalescence. Other features that are usually found in the area corresponding to the slow propagation of the fatigue crack are ring-shaped marking, which give the surfaces a "clamshell" appearance. These marks can be traced back toward a common point which is the crack origin or origins. It is realised however that no two fatigue

fractures are identical but they all have certain common features.

Fig. (7.7) illustrates typical optical micrographs of the fracture surfaces taken from representative non-nitrided and nitrided samples. There are clear differences in the features of the fatigue fracture between the tempered and the nitrided specimens.

The fracture surfaces of the as-tempered specimen always indicated that crack initiation occurred at the surface and in some specimens occured at more than one place at the surface. Fig. 7.7(a) shows at least two origins, at the bottom and left hand side of the cross-section. Final failure has occurred due to microvoid coalescence. Fig. 7.8(a) and (b) are scanning electron micrographs corresponding to regions of fatigue crack growth and microvoid coalescence.

No sub-surface cracks were observed in any fatigue fracture of the tempered specimens.

Unlike tempered material, the fracture surface topography of the nitrided samples was always flat and perpendicular to the longitudinal axis of the specimen. The macrostructure of the fracture surface is characterised by the presence of three distinct regions. The outer ring corresponds to the brittle fracture of the nitrided case. The annulus corresponds to the part of the core that failed by fatigue, and the central circular region corresponds to the final failure of the core (see Fig. 7.7).

The nitrided case fracture of specimens nitrided at 520^{o}C, both in 80% and 30% NH_3, showed a pure transgranular

fracture at all stress levels. The scanning electron micrographs in Fig. 7.9 are taken from the case area showing transgranular cracking with characteristic tearing. In all specimens the outermost region of the nitrided case is smoother than the interior indicating that the fractures were initiated at the surface, see Fig. 7.10.

At the limit of the nitrided case i.e. at the case/core interface, there is a change in fracture mode from pure transgranular cracking to mixture of transgranular and intergranular faceting, the latter mode of fracture is so dominant that a clear ring at the case/core interface is clearly visible, see Fig. 7.11. This behaviour does not seem to be influenced by the level of the applied stress.

In specimens that were nitrided at 570^{o}C in 10% NH_3, the case fracture is different to that observed in specimens nitrided at 520^{o}C. A combination of both transgranular and intergranular fracture modes occurs, which is clearly illustrated in Fig. 7.12. Again there is no apparent effect on the appearance of the fracture surfaces as a function of applied stress.

The depth of the brittle case fracture is constant at all stress levels, and in each nitriding condition the brittle fracture is approximately equal to the nitrided depth revealed by etching, and not the hardening depth. Table 7.2 lists the average depths revealed by microhardness readings and by etching in Oberhoffer's reagent, compared with the depth of brittle fracture under each nitriding condition.

The fatigue fracture of the annulus region is

characterised by striations and cracks. Fig. 7.13 is a scanning electron micrograph showing striations and microcracks associated with them. Similar observations were reported before; Winnk (47) investigated nitrided En40B steel, in which striations were also observed to occur in the annular region, and their spacing was found to increase in going from the end of brittle region to the edge of the final failure.

The typical microstructure of the final failure region of the core, in which the fracture occured by microvoid coalescence, is in all cases similar to that shown in Fig. 7.8(b). The area of the final fracture decreases with decreasing applied stress whilst the annular area increases. In many cases the position of this area is not located in the centre of the fracture. If the area is shifted to one side, it implies that crack propagation has started from the opposite side. A typical example is shown in Fig. 7.14. In this particular case the fracture seems to have been initiated on the surface at the region opposite to the sub-surface crack. Once the surface crack reaches the sub-surface crack, initiated by intermetalic inclusions, then crack propagation jumps into the core, whereas at the other regions of the surface the crack has not yet reached the case/core interface. In fracture surfaces that contain sub-surface cracks, the final failure area was always shifted from the centre to the side opposite to the sub-surface crack. This meant that the latter aided crack propagation within the core area.

The sub-surface cracks that are initiated by inclusions immediately below the nitrided case region were only

observed in specimens nitrided at 520 in 30% or 80% NH_3. Such cracks were not observed in any specimen nitrided at 570°C in 10% NH_3. The position of the inclusions that initiated the cracks, are always a similar distance from the surface in specimens that are nitrided under the same conditions irrespective of the applied stress. The measured figures are approximately ∿ 0.6 mm for test pieces nitrided at 520°C in 30% NH_3 for 48h, and ∿ 0.45mm for those nitrided at 520°C in 80% NH_3 for 24h. The figures are slightly greater than the limit of hardening depth in both conditions (see Table 7.2) and in this region the tensile stress is maximum, and it appears to be high enough to promote sub-surface cracks (s.s.c) at intermetalic inclusions in which the latter act as stress raisers.

It appears that the fatigue life may be affected by the size of the "s.s.c." As an example, in Table 7.3, by comparing specimen (2) which has longer fatigue life at 1010 MPa than specimen (3) with shorter fatigue life at 950 mpa, the s.s.c diameter in the latter specimen is 0.73 mm, which is much larger than that of the former specimen with diameter of 0.49 mm. The same thing occurs with specimens (3) and (4) in Table 7.4. However, it is well known that non-metallic inclusions impair the fatigue strength of steel. The reduction in strength arises from the stress concentration introduced by inclusions. The influence of inclusions on the fatigue strength depends primarily on their size, shape and their resistance to deformation and on their orientation to the stress acting on the metal. The influence of inclusions in reducing the fatigue strength is more significant in high

strength steel (88), than in low strength steel (89).

The presence of sub-surface fatigue crakcs in nitrided material has been reported previously by several authors (76, 84,90,91). Bardgett (76) reported that fatigue life of the nitrided steel was found to be shorter in material containing a high inclusion count. Jones and Martin (84) found that failure of nitrided EN41B steel, in the region of fatigue limit can be controlled by cracks propagating from non-metallic sub-surface, inclusions, when subjected to direct stress.

Fig. 7.15 illustrates the different modes of fracture that can occur in nitrided fatigue specimens.

7.6 Discussion

In order to compare various fatigue curves Fig. 7.16 shows the S-N curves for the different nitriding conditions plus the tempered non-nitrided ones.

The nitriding temperature appears to be the most influencial factor in determining the fatigue properties of the nitrided steel. Nitriding at 520^{o}C improves both fatigue limit and endurance limit, whereas nitriding at 570^{o}C resulted in inferior fatigue properties even to the tempered ones.

The structural changes produced by nitriding at 570^{o}C in 10% NH_3, has also affected the fracture mode of the case, in which brittle intergranular fracture dominated. This behaviour can be attributed to the precipitation of carbides on the grain boundaries during nitriding, especially at high temperatures. As a result the case region will be embrittled,

and would aid fatigue crack propagation and consequently lower the endurance limit.

Nitriding improves the fatigue properties of steel by producing a very hard case with high residual compressive stress, Fig. 7.17 illustrate the schematic stress distribution across the rotating bending fatigue specimens before and after applying an external load. The applied stress plus the residual stress in the case produce a total stress that has a minimum value of either tensile or compressive stress at the surface and a maximum tensile value at the case/core interface. Jones and Martin (94) measured the residual stress distribution across nitrided specimens of En41B steel by the sachs boring technique. The maximum compressive stress was found at the surface with value of (-1060) MNm^{-2} in the longitudinal direction and (-1100) MNm^{-2} in the tangential direction. Any applied stress less than these values would still leave the surface in a compressive state, which is favourable for fatigue resistance.

The presence of sub-surface cracks in all the fracture surfaces that failed beyond 10^5 cycles suggests that these cracks could effect the fatigue behaviour by acting as a stress raiser near enough to the surface to cause a stress concentration at the area between the surface and the advancing edge of the s.s.c. This would in turn help to initiate cracks at this particular area of the surface. This effect is illustrated in Fig. 7.18.

There has been no evidence of crack initiation at the case/core interface other than those initiated locally by inclusions.

7.7 Summary and conclusions

1. The fatigue behaviour of the nitrided En41A depends on the quality of the nitrided case in terms of hardness, depth and microstructure.

2. Nitriding at 520^{o}C, with and without white layer formation, improves fatigue properties due to the high residual stress level of the nitrided layer.

3. The inferior fatigue properties at 570^{o}C are due to the low residual stress level and due to the embrittlement effect.

4. The sub-surface cracks initiated by inclusions can reduce the fatigue life of the nitrided steel.

nitriding conditions	case depth mm	white layer depthmm	Maximum hardness VHN	core hardness VHN
520°C, 80% NH_3, 24h	0.425	25	1130	300
520°C, 30% NH_3, 48h	0.550	-	1100	290
570°C, 10% NH_3, 48h	0.450	-	920	270

Table 7.1 Data for nitrided En41A fatigue specimens

nitriding conditions	Hardness depth mm	Etching depth mm	Fatigue depth mm
520°C, 80% NH_3, 24h	0.425	0.35	0.32
520°C, 30% NH_3, 48h	0.55	0.45	0.45
570°C, 10% NH_3, 24h	0.45	0.63	0.66

Table 7.2 showing the nitrided case depth revealed by fatigue fracture is similar to that revealed by etching

No	S MPa	N Cycles	s.s.c diameter mm
1	1100	216,000	0.43
2*	1010	647,400	0.49
3*	950	425,900	0.73
4	950	602,100	0.60
5	885	3,503,500	0.67

Table 7.3

Fatigue data and sub-surface fatigue crack dimensions for specimens nitrided at 520°C in 30% NH_3 for 48h

No	S MPa	N Cycles	s.s.c. diameter mm
1	1100	124,100	0.41
2	1025	191,300	0.63
3*	950	314,000	0.47
4*	900	271,000	0.77
5	850	1,569,100	0.69

Table 7.4

Fatigue data and sub-surface fatigue crack dimensions for specimens nitrided at 520°C in 80% NH_3 for 24h

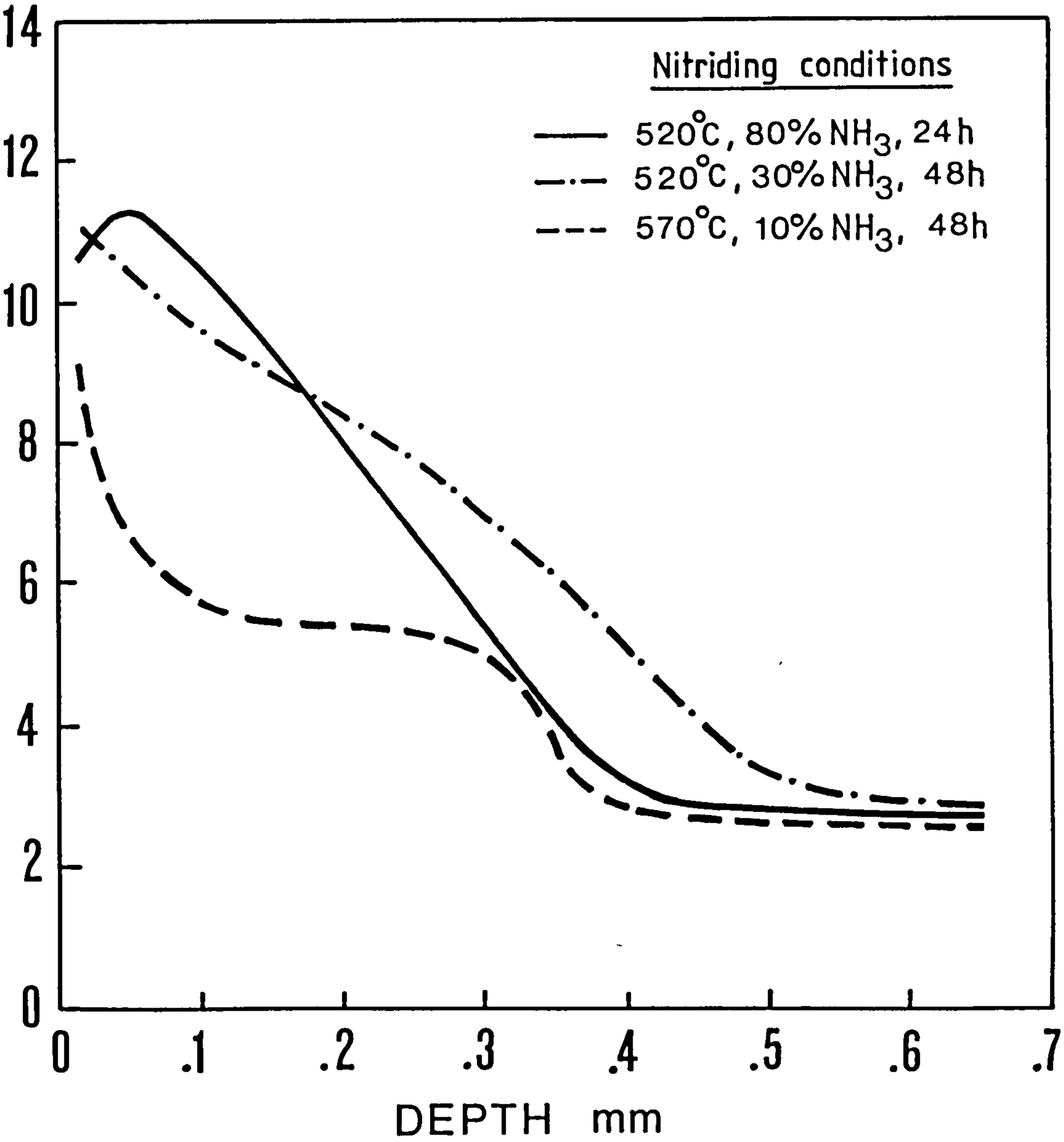

Fig. 7.1 Hardness profiles of the nitrided fatigue specimens for the conditions shown above

Fig. 7.2 S-N curve for as-tempered material

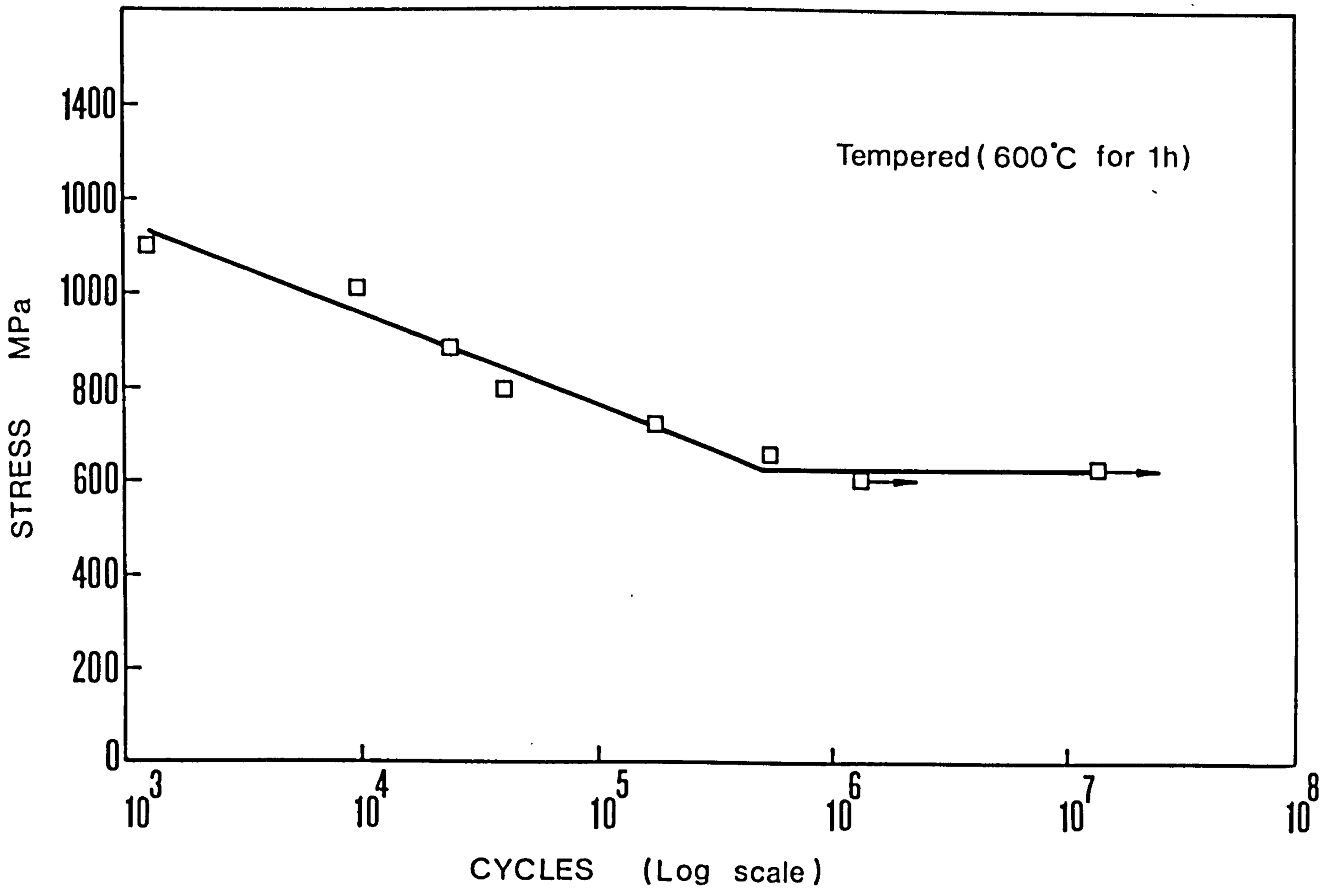

Fig. 7.3 S-N curves for the nitrided materials

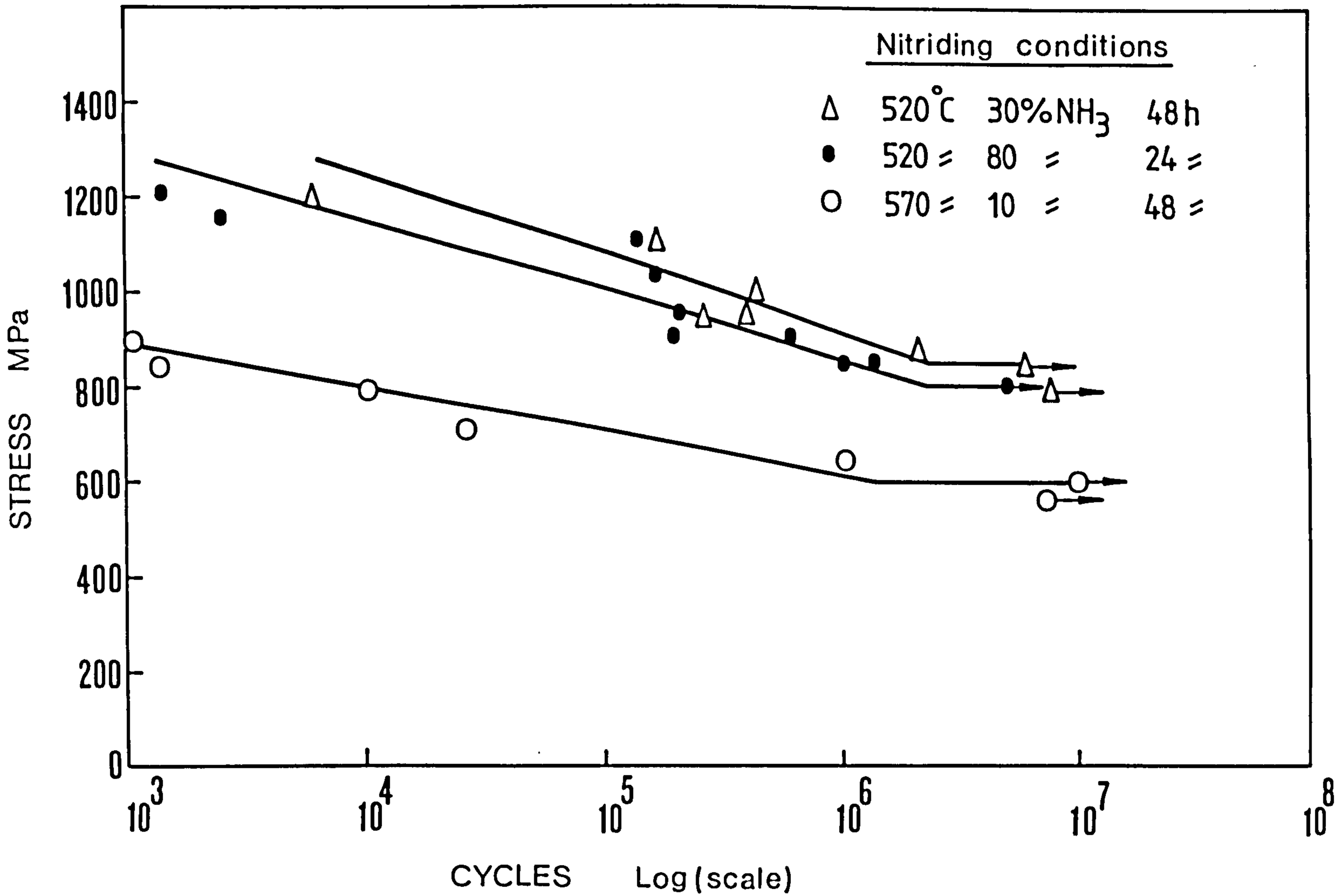

Fig. 7.4 S-N curves for the nitrided and as-tempered specimens

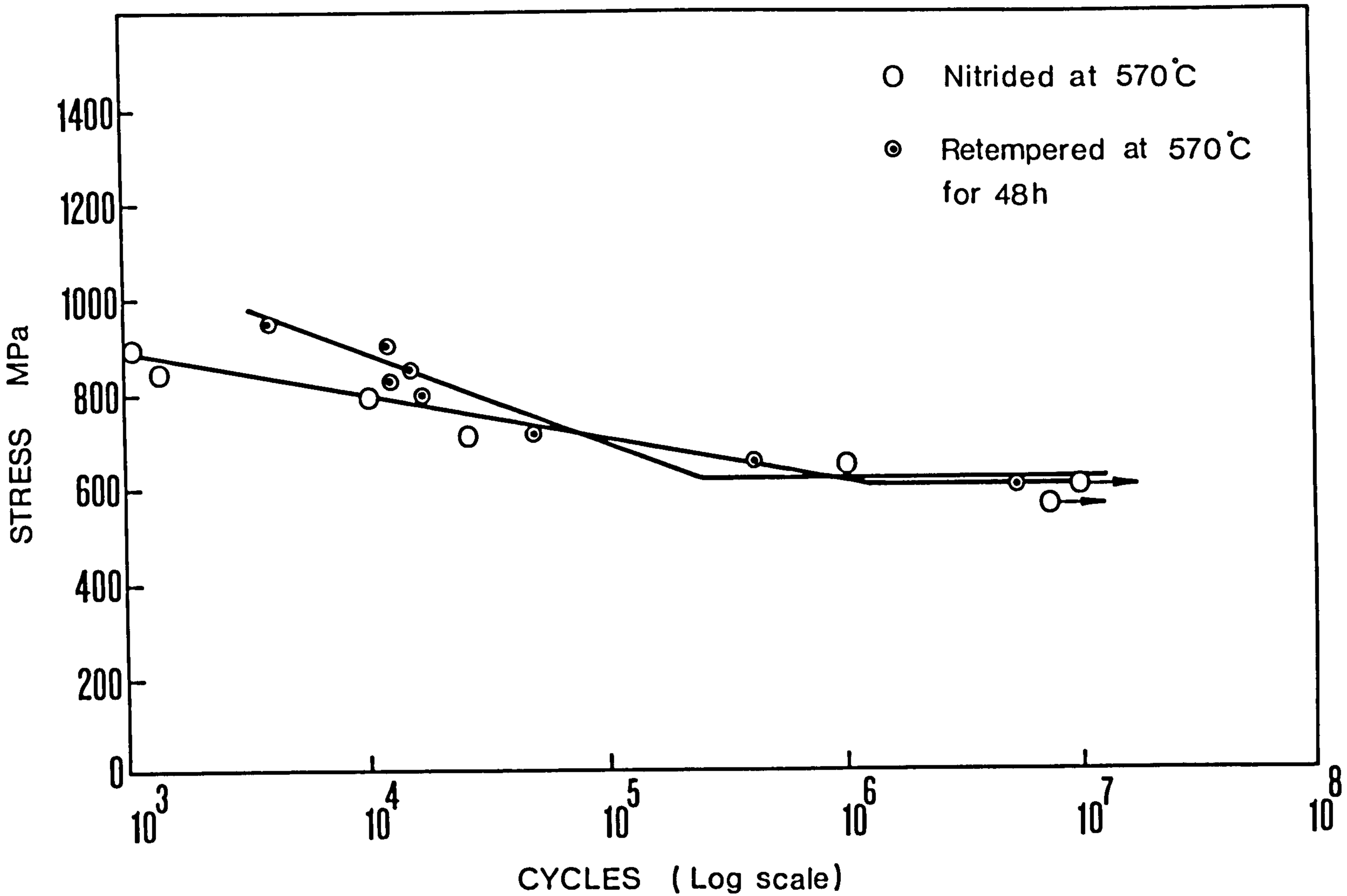

Fig. 7.5 S-N curves of non-nitrided tempered specimens showing the effect of prolonged tempering at 570°C

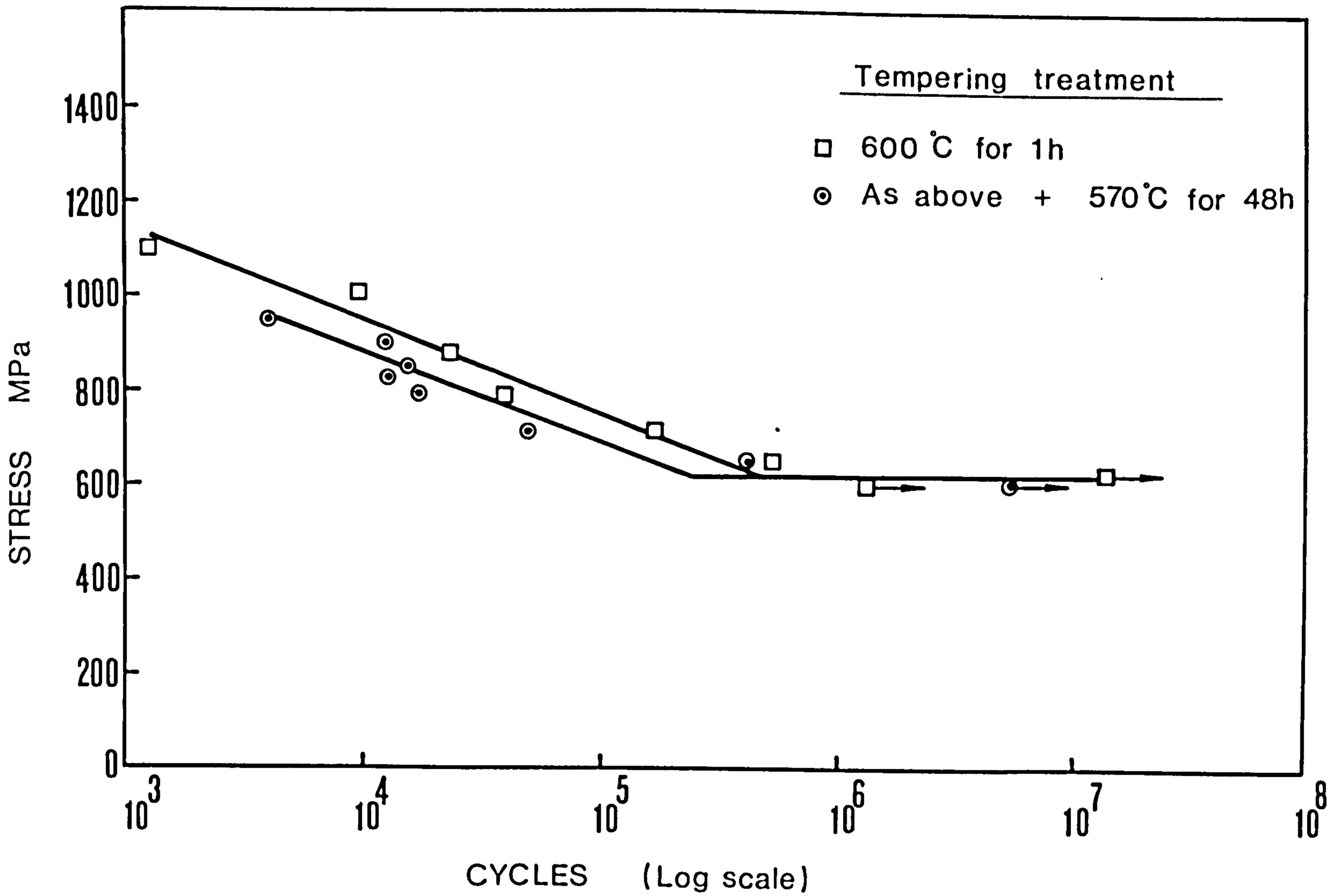

Fig. 7.6 Showing the inferior fatigue properties of the specimens nitrided at 570°C in comparison to the non-nitrided ones.

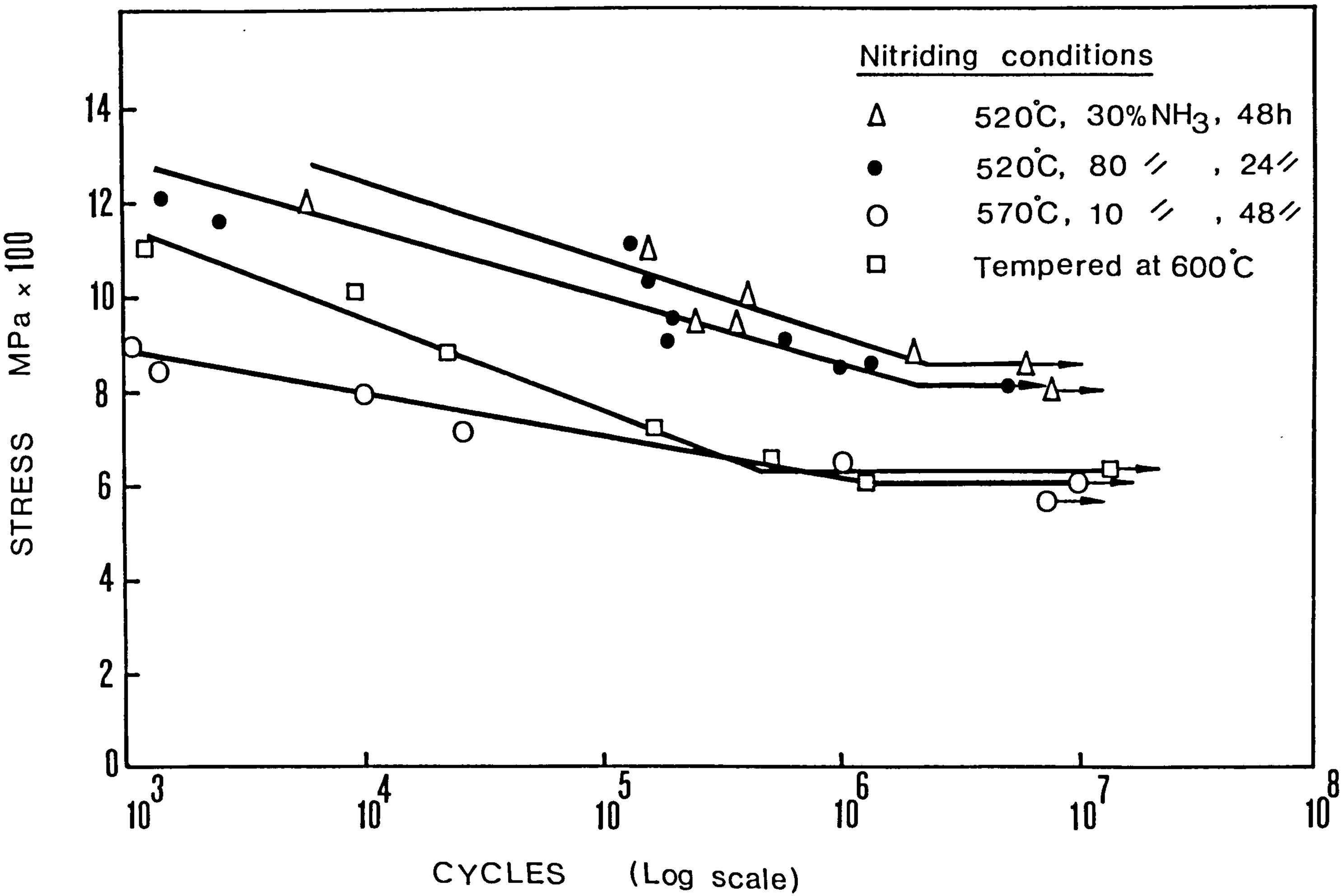

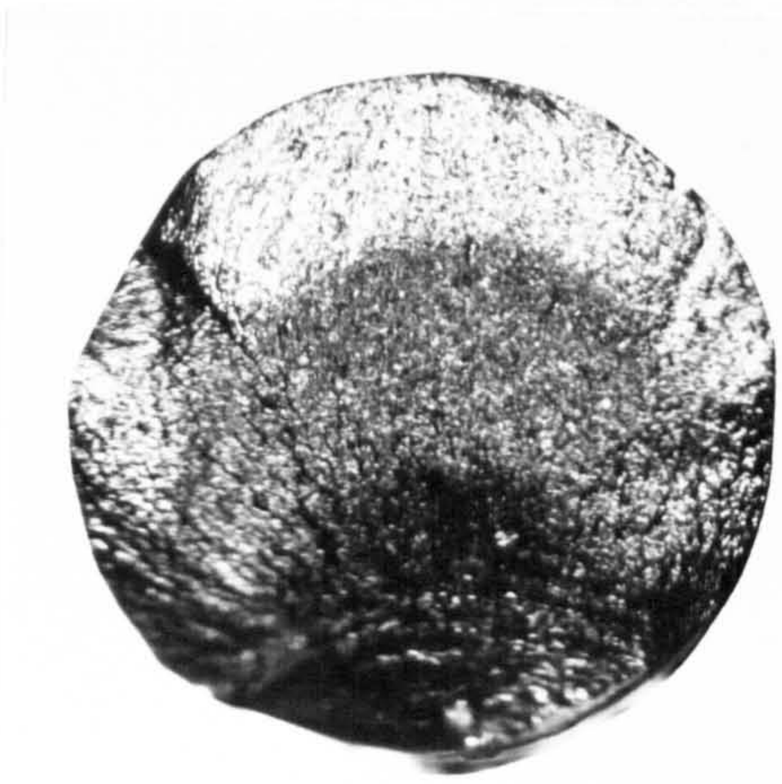

a) Tempered
600 °C, 1h

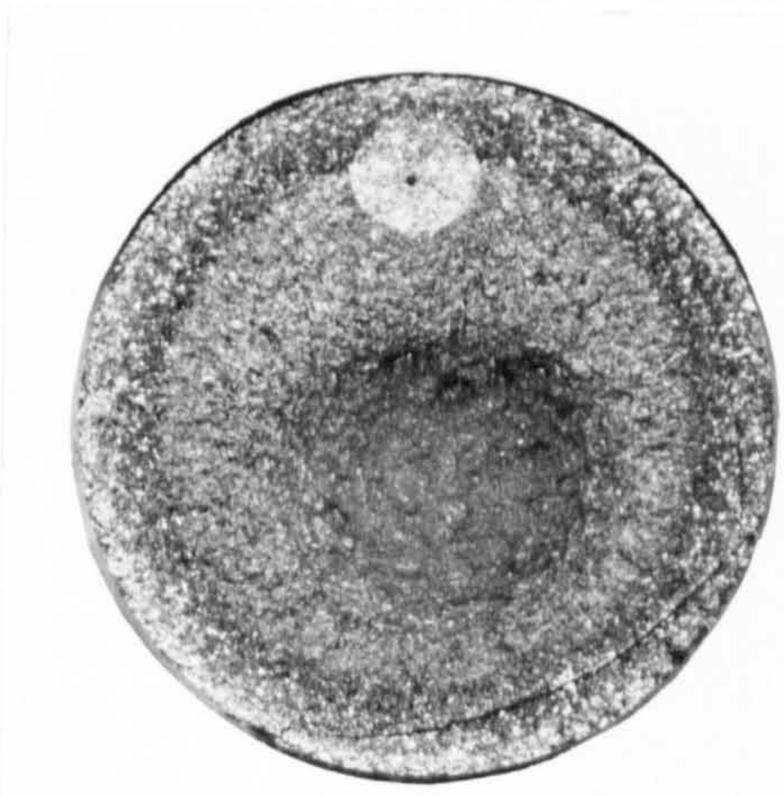

b) Nitrided
520 °C, 30% NH_3, 48h

1000 µm

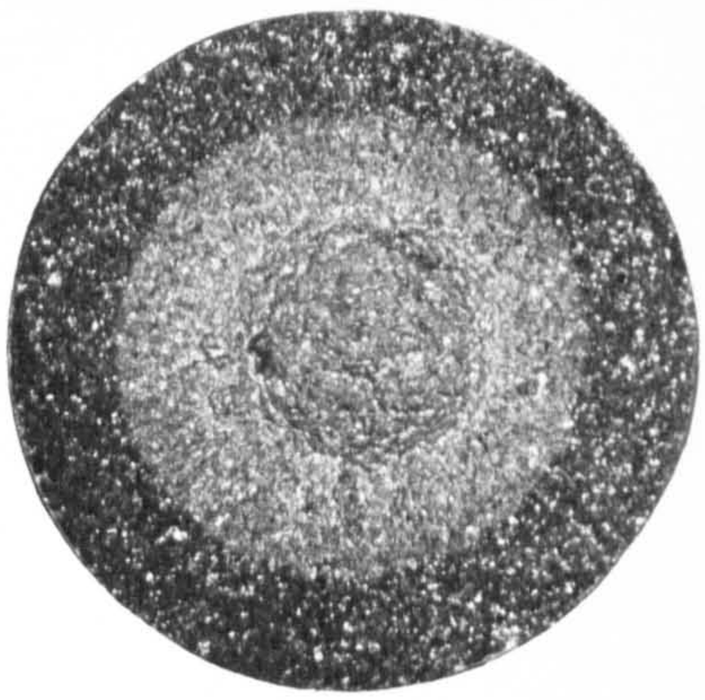

c) Nitrided
570 °C, 10% NH_3, 48h

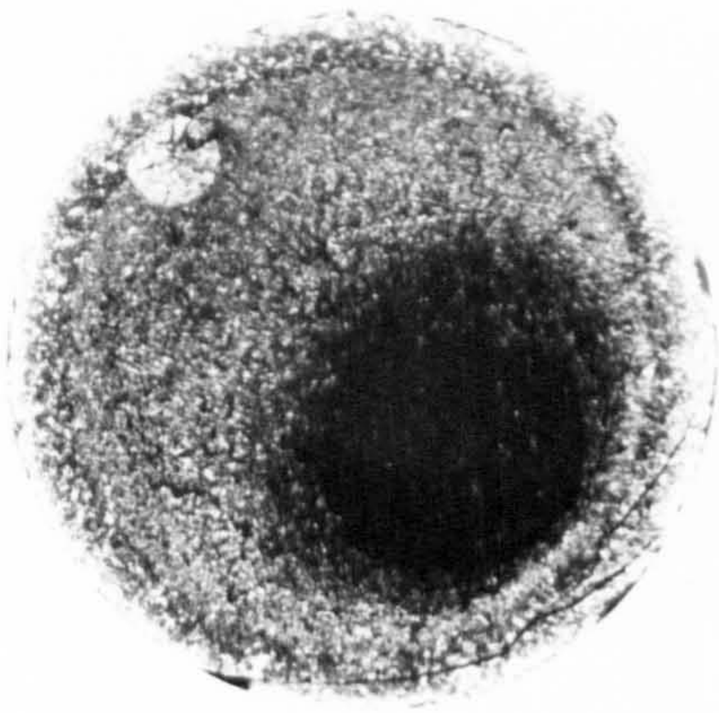

d) Nitrided
520 °C, 80% NH_3, 24h

Fig. 7.7 Optical micrographs showing characteristic fracture surfaces of the fatigue specimens

Fig. 7.8 Scanning electron micrographs of the fatigue fracture surfaces of a tempered specimen.

a - Fatigue fracture region

b - Final fracture region showing microvoids

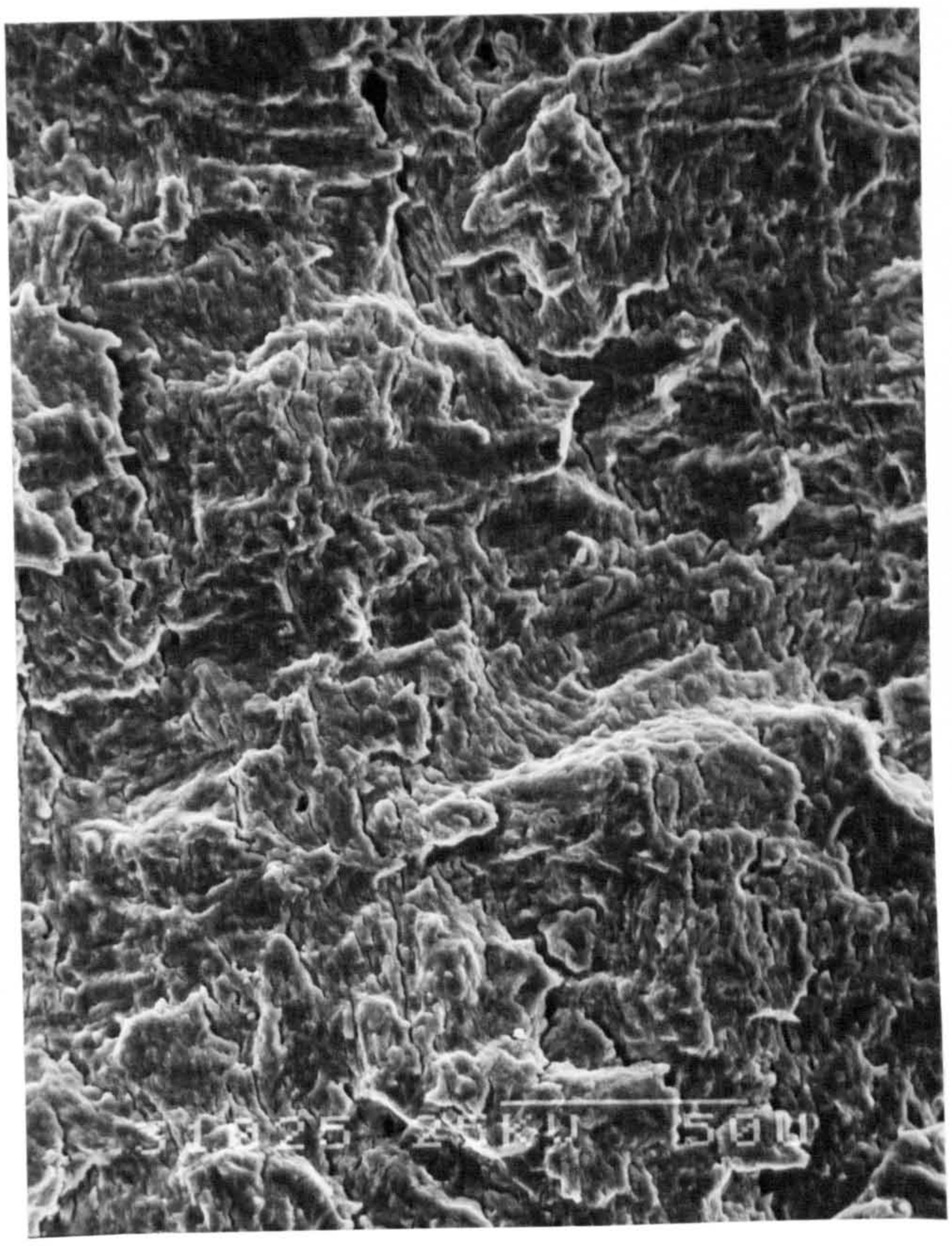

a

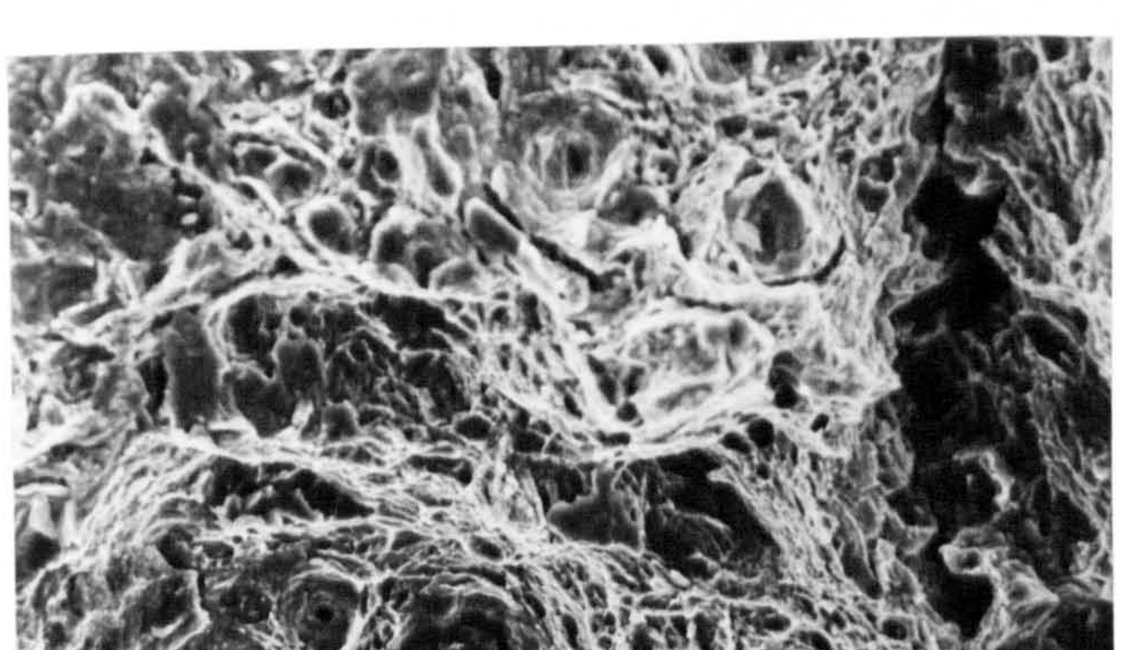

b

FIG. (7·8)

Fig. 7.9 Scanning electron micrographs of fatigue fracture of a nitrided En41A, showing transgranular tearing of the nitrided layer

a - Near the surface

b - Middle of the nitrided layer

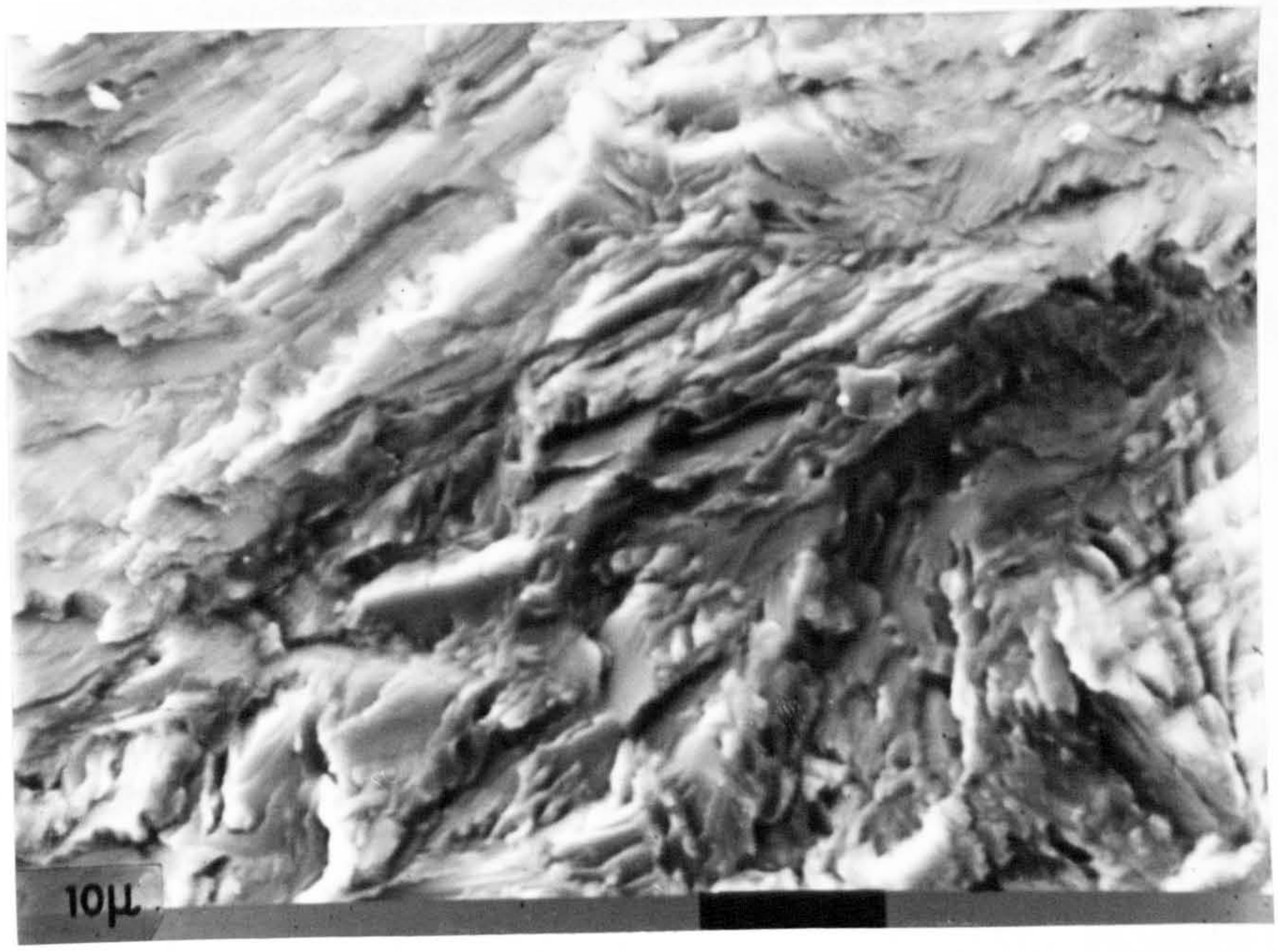

a

b

FIG. (7·9)

Fig. 7.10 Scanning electron micrograph showing the nature of the fatigue fracture of the nitrided layer up to a depth of 280 μm. Note the gradual increase in the roughness toward the core of the specimen

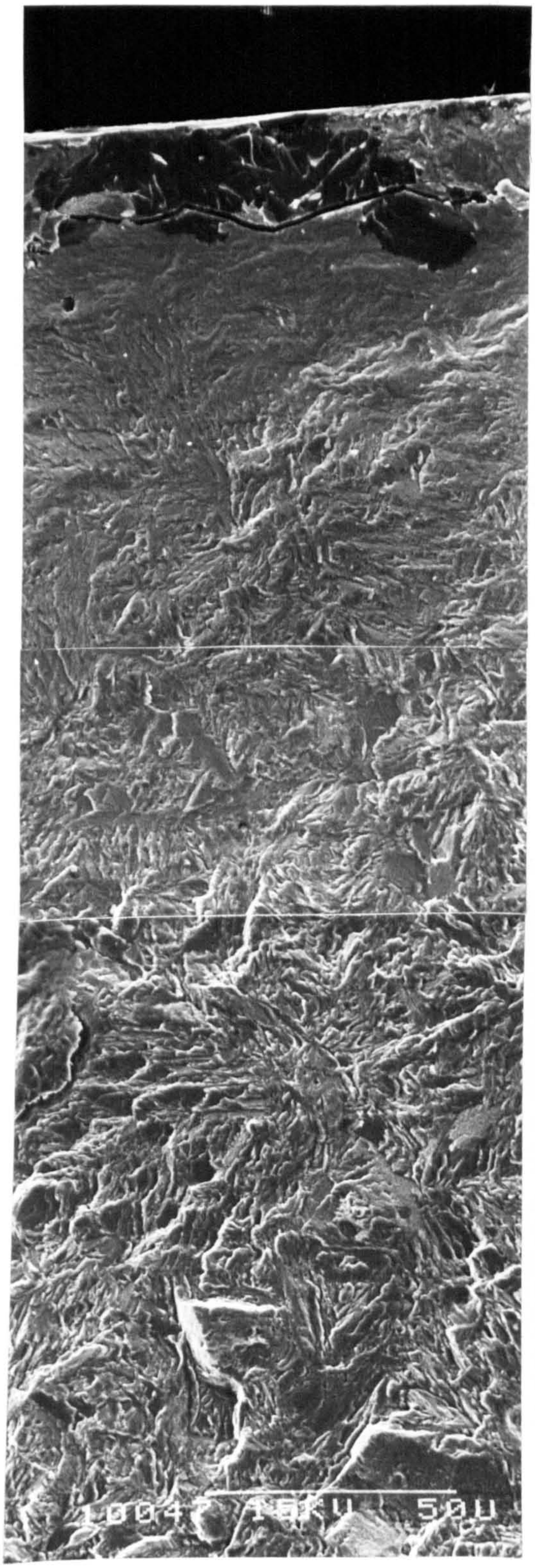

FIG (7·10)

Fig. 7.11 Scanning electron micrographs of En41A, nitrided at 520°C in 80% NH_3 for 24 h, showing the change in the fracture mode at the case/core interface. Note the intergranular facets at the interface in micrograph (b) which is a higher magnification of (a)

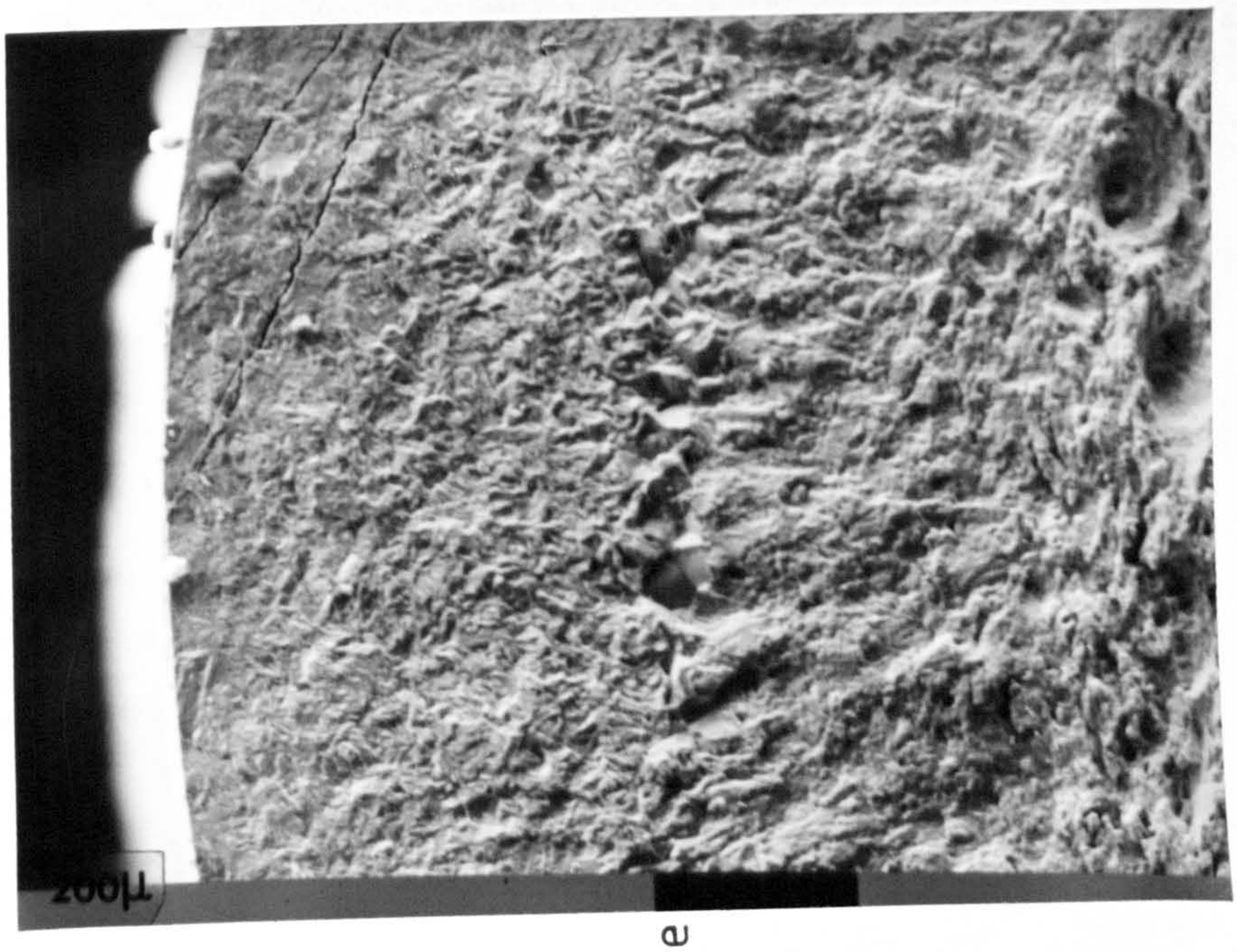

a

b

FIG. (7·11)

Fig. 7.12

a - Scanning electron micrograph of En41A, nitrided at 570°C in 10% NH_3 for 48 h, showing a combination of transgranular tearing and intergranular faceting

b - Higher magnification of (a)

c - Same as in (b) showing details of the intergranular facets

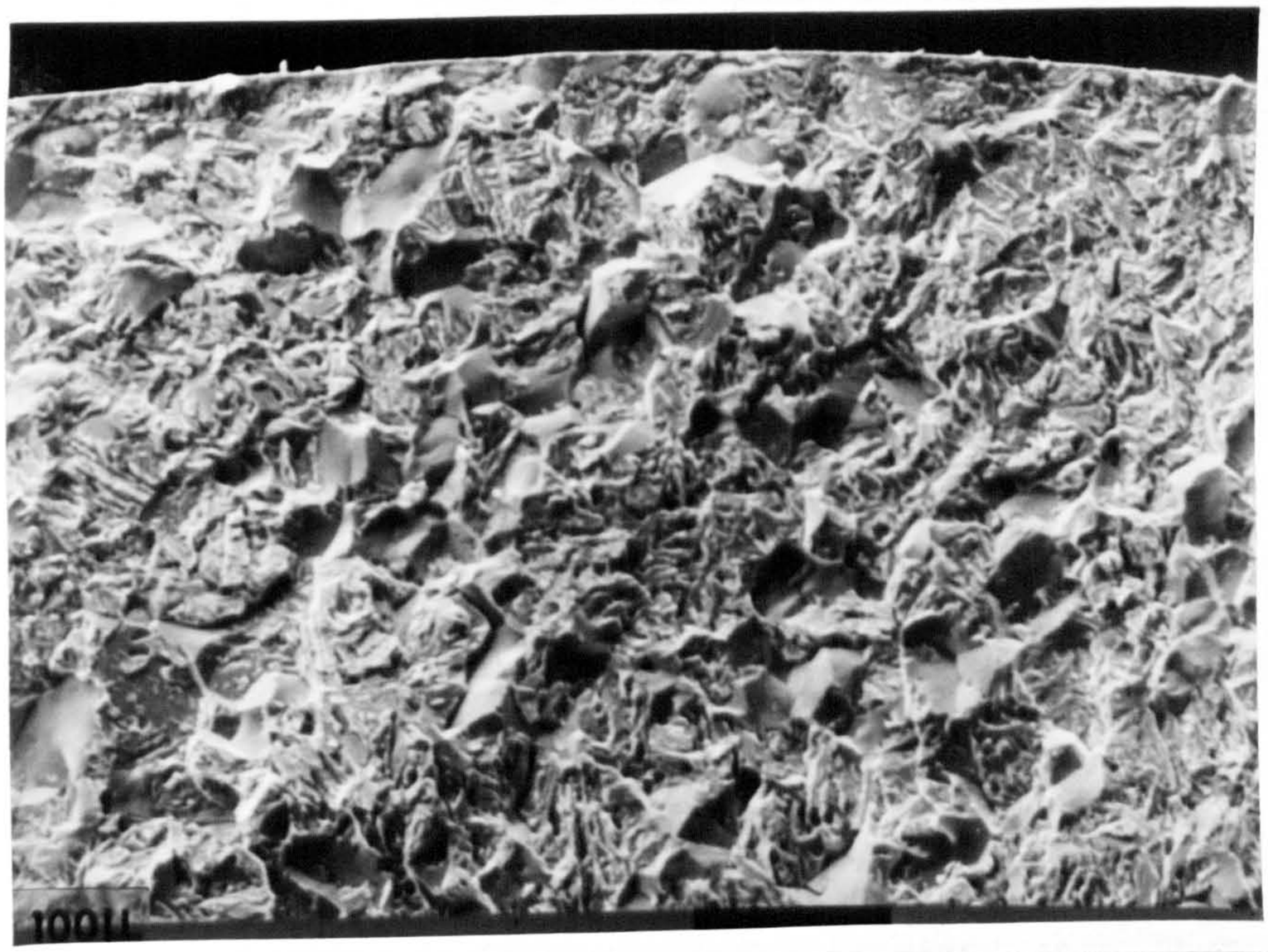

a

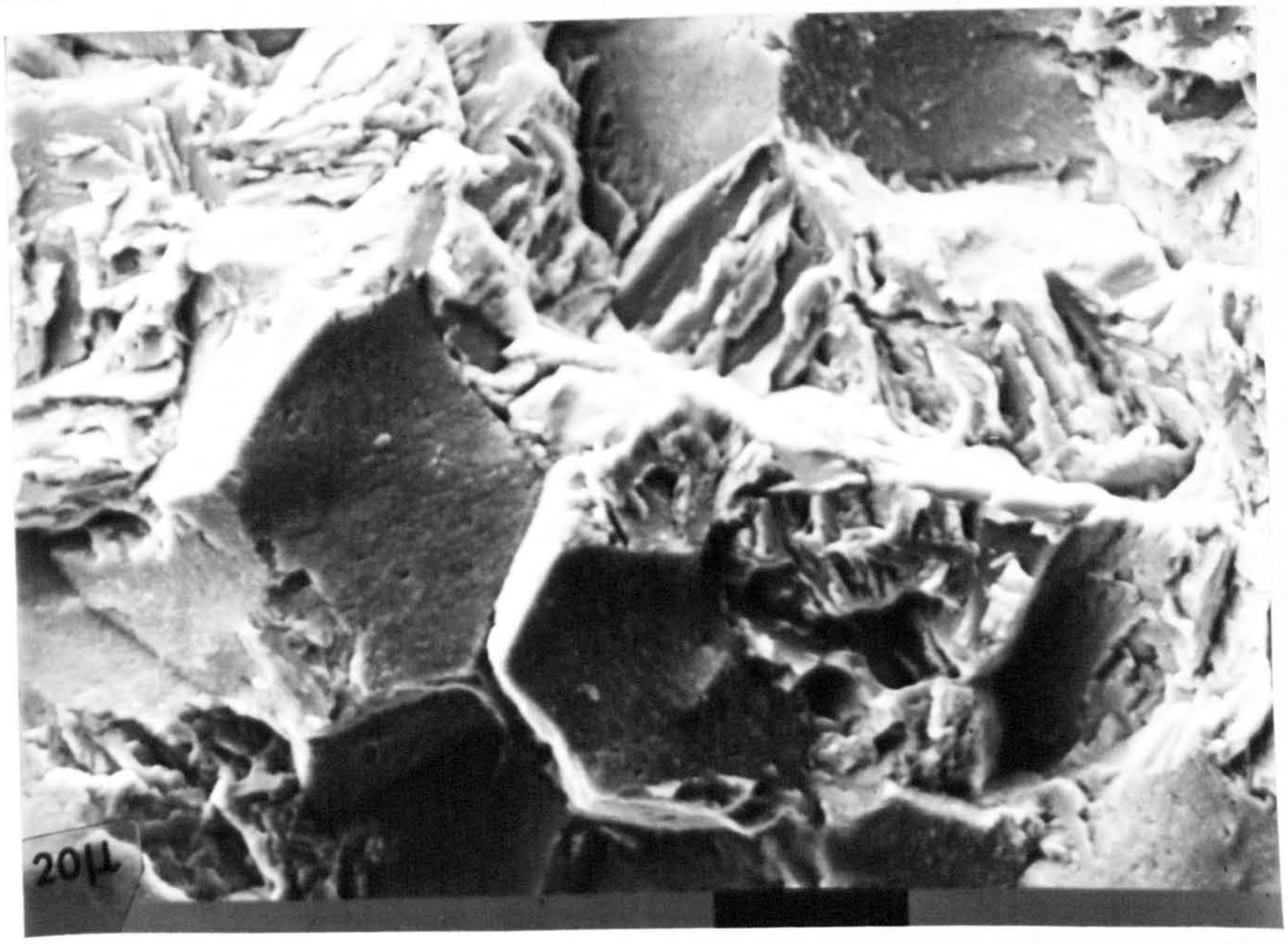

b

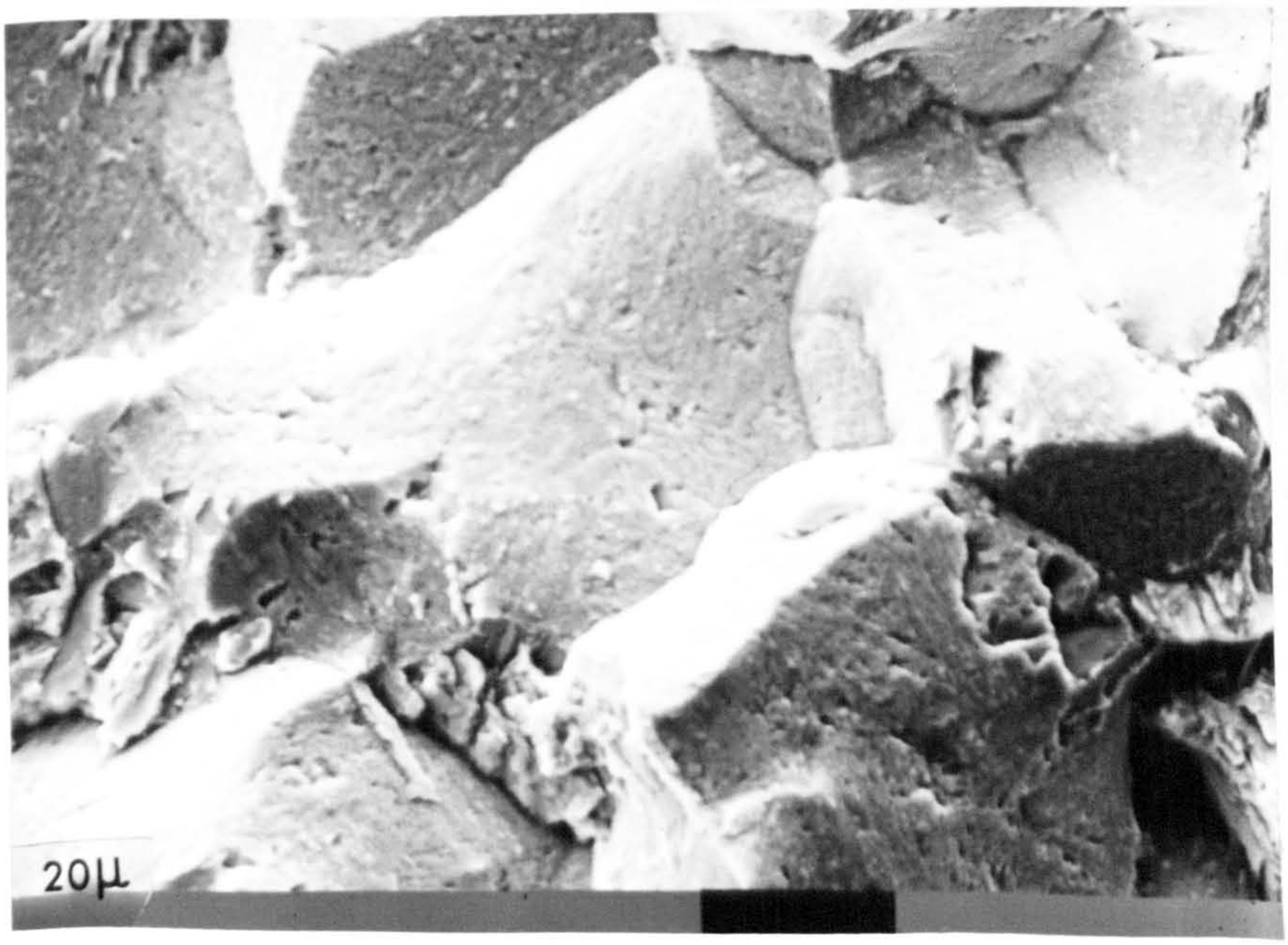

c

FIG. (7·12)

Fig. 7.13

Scanning electron micrograph showing fatigue striations. This type of fracture occurs in the annular region near to the case/core interface. Note the cracks associated with the striations

Fig. 7.14 Scanning electron micrograph showing typical fatigue fracture surface of a nitrided En41A, in which four regions are recognised;

a) transgranular fracture of the nitrided layer

b) a mixture of transgranular and inter-granular fracture mode at the interface region

c) crescent-shape annular region represent fatigue fracture of the core

d) final fracture region of the core which occurs by microvoid coalescence, is shifted to the opposite side of the s.s.c


500U

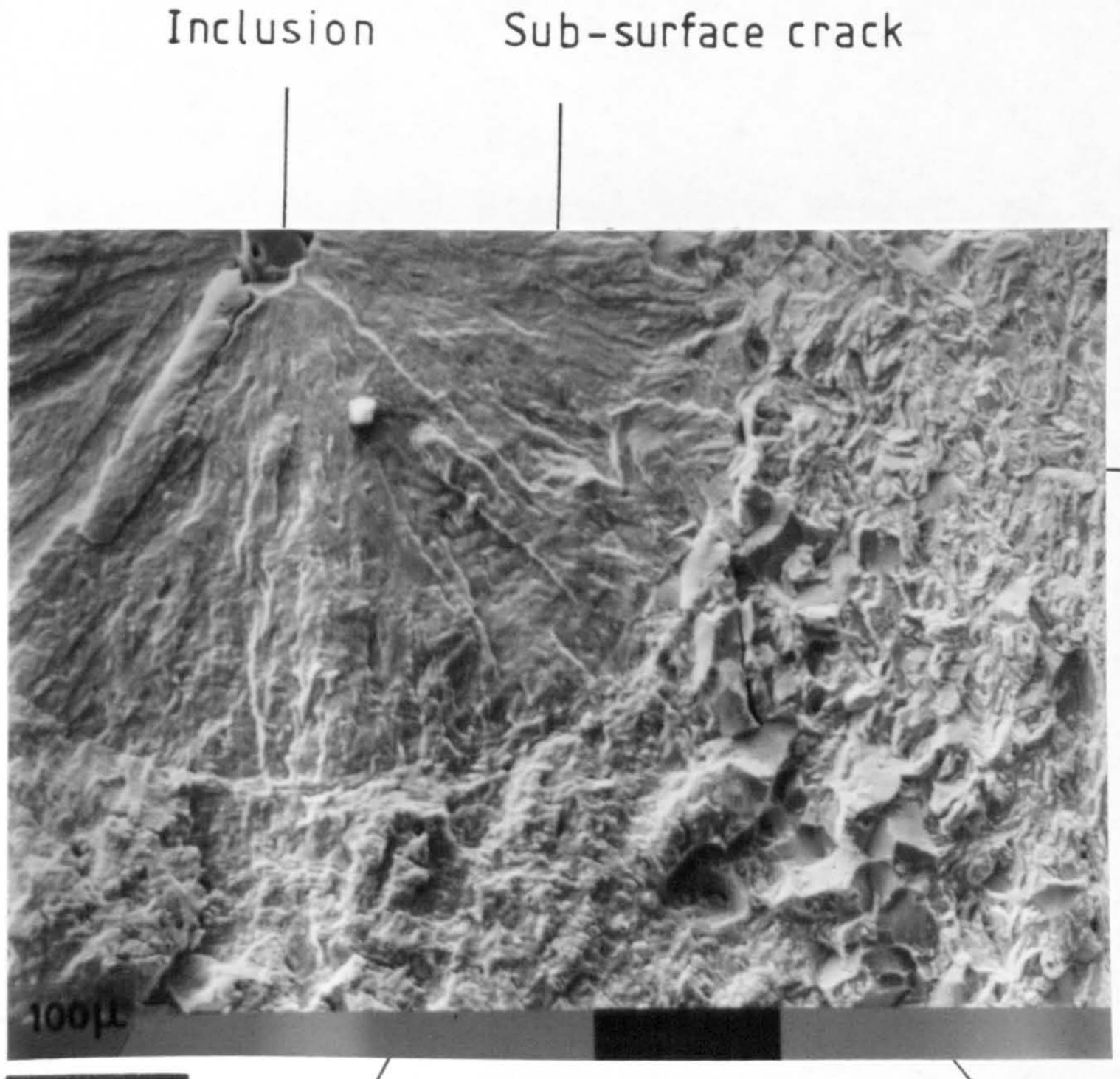

Fig. 7.15 Scanning electron micrograph showing different modes of fatigue fracture in a nitrided En41A fatigue specimen

Fig. 7.16 S-N curves for the nitrided and non nitrided specimens

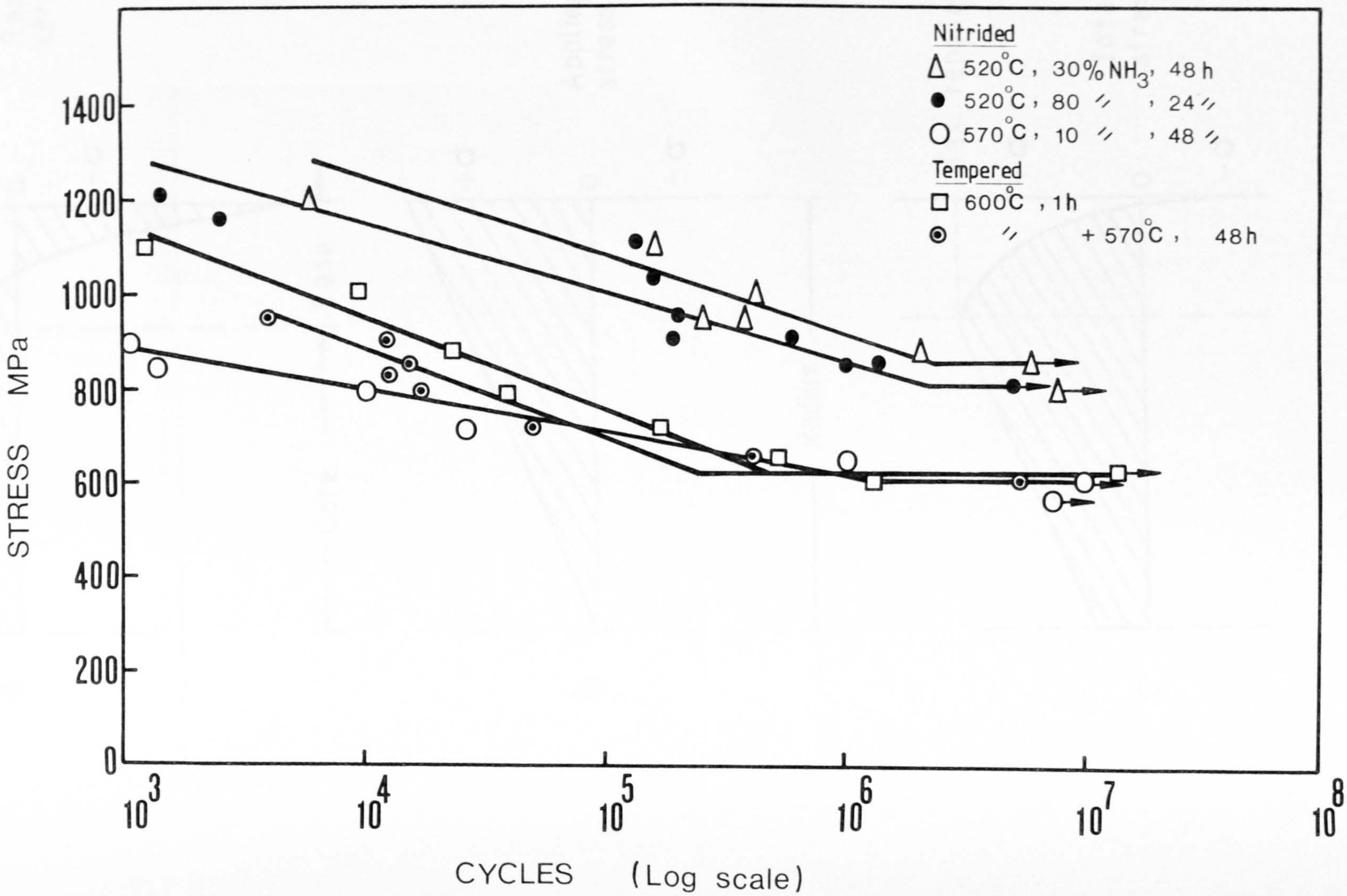

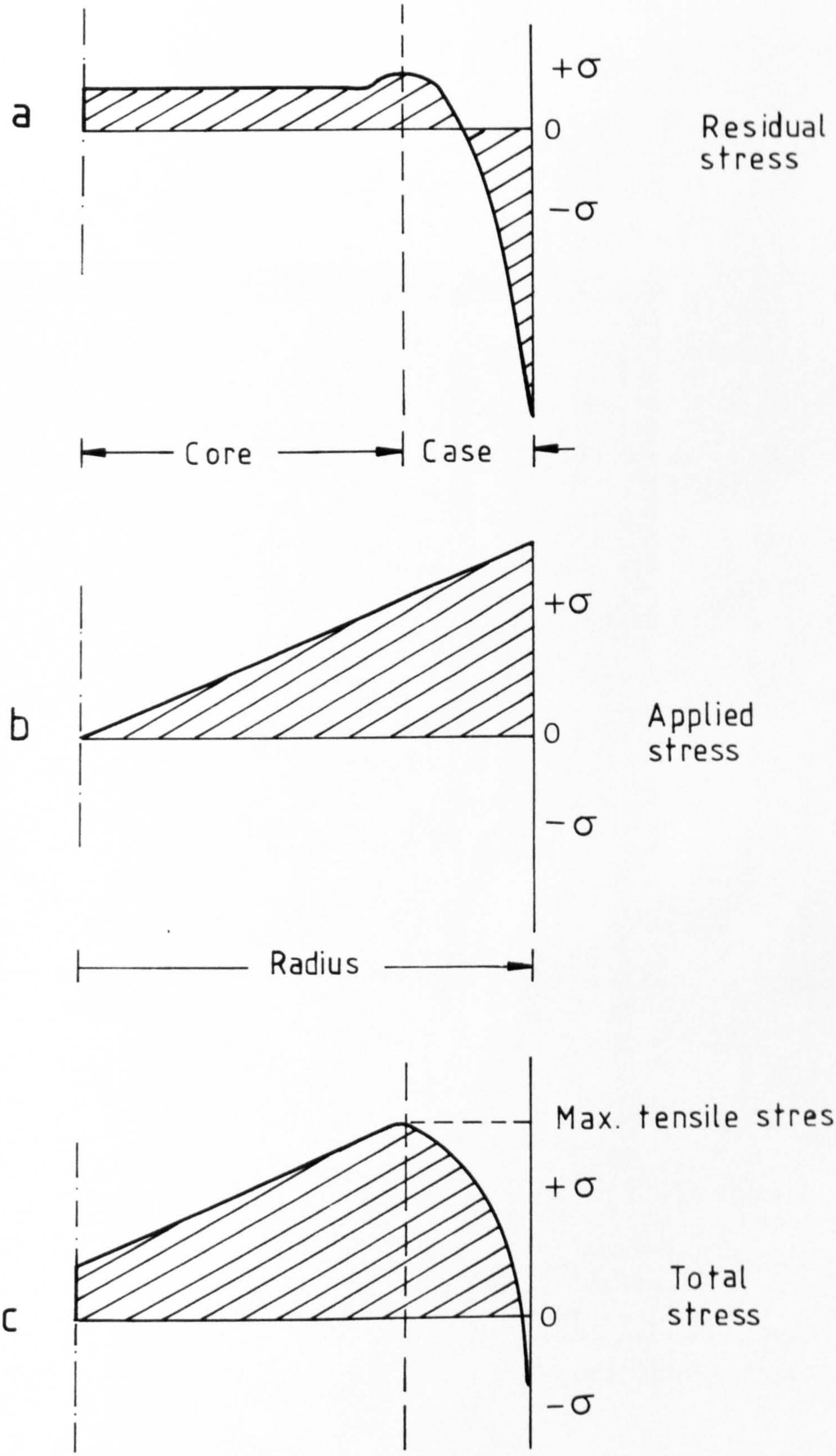

Fig. 7.17 Schematic stress distribution across the rotating bending fatigue specimens before and after applying external load

Fig. 7.18

a - Scanning electron micrograph showing a sub-surface crack initiated by an intermetalic inclusion. $r_1 < r_2$ due to the fact that crack propagation is slower in the nitrided layer than in the core, which is attributed to the high residual compressive stresses in the nitrided layer

b - Schematic drawing showing how a sub-surface crack could help to initiate a crack at the surface due to the high stress concentration in the region between the surface and the s.s.c edge.

REGION OF HIGH STRESS
CONCENTRATION

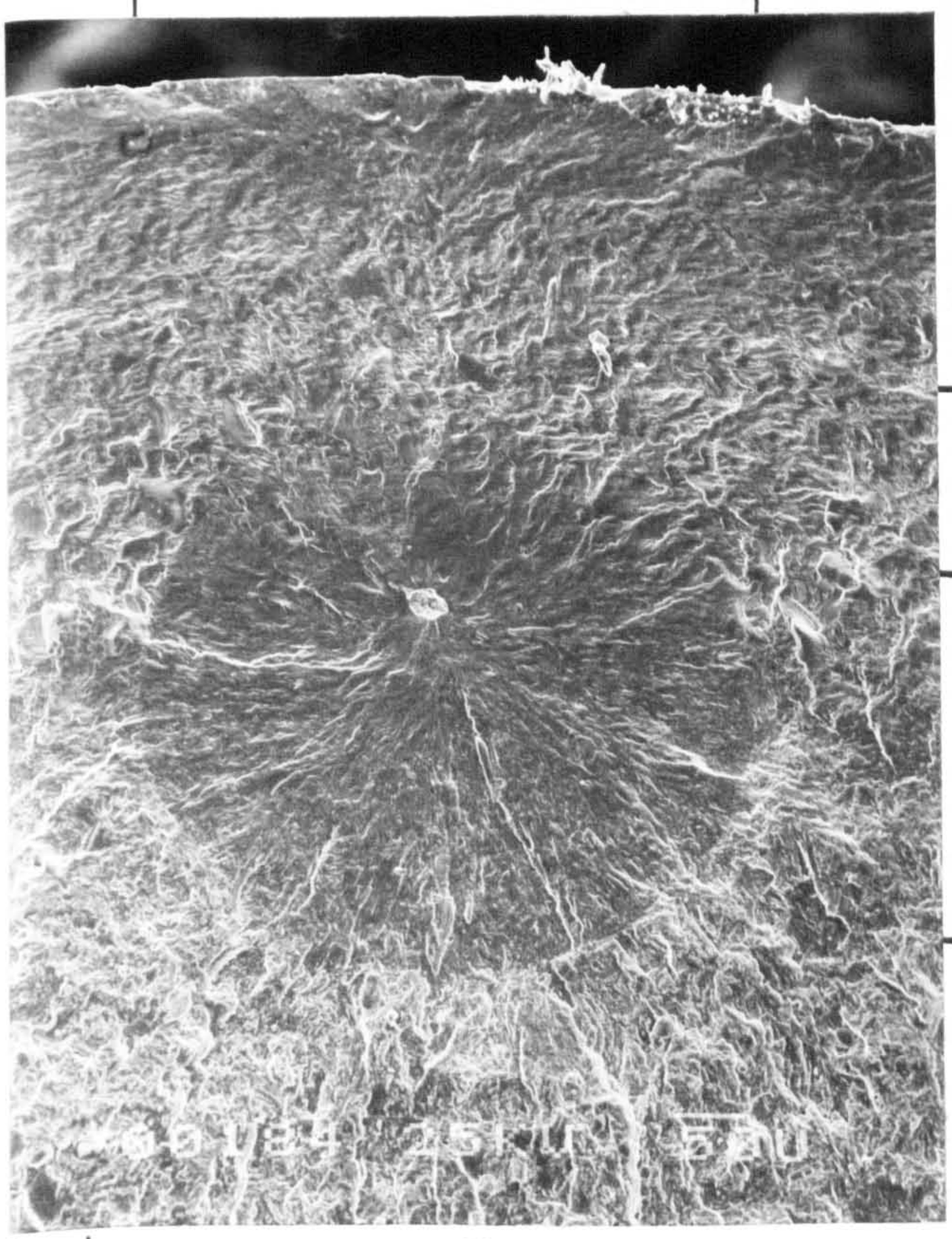

50µm

a

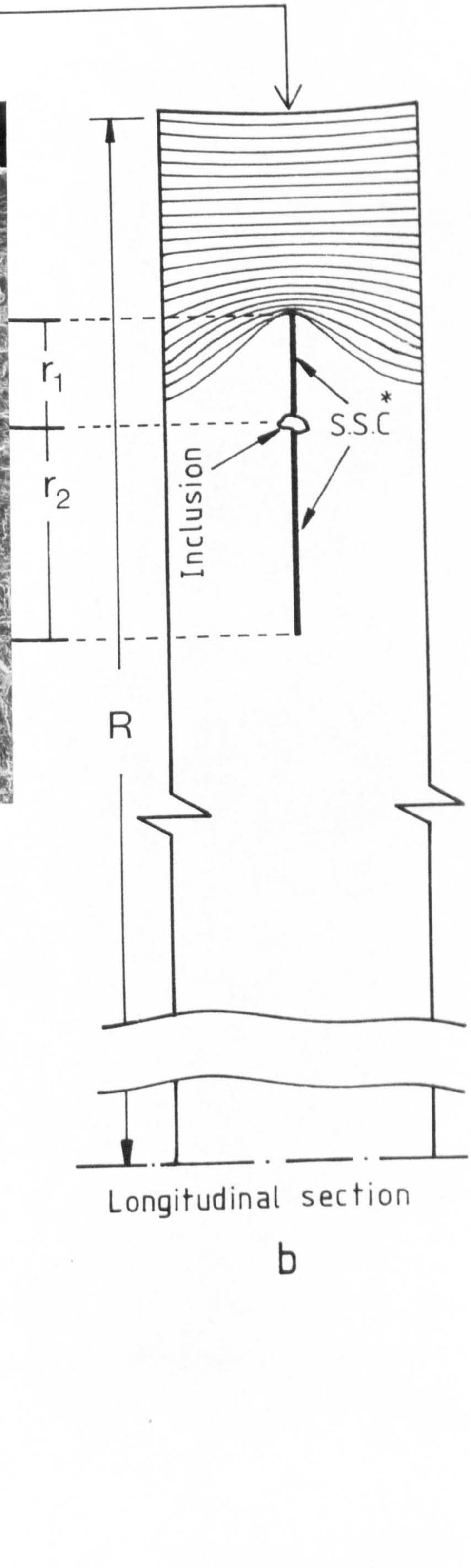

Longitudinal section

b

Fig.(7.18)

* Sub surface crack

CHAPTER 8

CONCLUSIONS

1. For aluminium containing steels, tempering at 600^{o}C for 1h produces a structure which is significantly recovered and more or less recrystallized, depending on the type of steel. The degree of recrystallization is greater with lower alloy contents.

The hardness of tempered steel depends to a large extent on the size and distribution of the carbides, which is largely influenced by the presence of alloying elements.

2. In nitrided aluminium containing steels with or without chromium, different nitrides can form. These are f.c.c. CrN, hexagonal AlN and cubic AlN. In En41B, f.c.c. CrN forms under all nitriding conditions, whereas hexagonal AlN was only detected at 570^{o}C. Cubic AlN cannot be detected because its d-spacings are similar to those of f.c.c. CrN. In chromium-free steels, hexagonal and cubic AlN forms readily at 500^{o} and 570^{o}C if nitriding is carried out in a high NH_3 content i.e. 80%.

3. In the nitrided steels that contain aluminium and silicon, the hexagonal AlN is rich in silicon

4. Cubic AlN transforms to hexagonal AlN if the nitrided specimen is annealed at 700^{o}C.

5. The f.c.c. CrN forms as a fine plates on {001} ferrite planes, whereas hexagonal AlN form randomly on dislocations with no relationship with the matrix, which explain:

the reason for its not being detected in thin foils. Cubic AlN with the NaCl structure, forms as a needle-like precipitate and can be detected by various methods.

6. The formation of the carburized layer in nitrided bulk specimens depends on the internal compressive stress of the nitrided layer, and is not solely due to chemical effects. The size of the pre-existing carbides is an important factor in the formation of the carburized layer.

Nitriding in high NH_3 content so as to form white layer on the surface of the specimen, causes carbide concentration just under the white layer.

7. The thickness of the white layer decreases with a decrease in the amount of alloying elements and the hardness of the outermost region, which consists of Fe_3N, is constant in different steels and it is softer than the innermost region, which consists of Fe_4N. The penetration of the white layer occurs preferentially down the austenite grain boundaries, and around the lath boundaries close to the advancing edge of the white layer.

8. The hardening response and the hardness profiles of En41B steel are completely different to those of the chromium-free En41(-Cr) and Fe-C-Al alloys. In En41B high hardness can be achieved at 500^{o}C due to the precipitation of finely dispersed CrN particles, whereas the hardening response of the chromium free Fe-C-Al steel is poor due to the nucleation difficulty of AlN at 500^{o}C. The hardening response of the chromium free En41(-Cr) steel is better than that of Fe-C-Al. This is attributed to the presence of silicon, which helps in

overcoming the nucleation barrier of the AlN and enhances its hardening capability.

At 570°C the hardening responses of En41B and En41(-Cr) are similar especially when nitriding is carried out in a high ammonia content.

9. In each steel the hardness profile is greatly affected by the nitriding temperature, the time of nitriding and the NH_3 content of the gas mixture. However, the effect of these variables varies according to the alloying elements in each steel. In En41B, nitriding at 500°C produces high surface hardness, a steeper hardness profile and small nitrided depth, whereas at 570°C there is a lower surface hardness, a shallower hardness profile and a greater nitrided depth. In En41(-Cr) and Fe-C-Al steels, nitriding at 570°C produces higher surface hardness, a higher general hardness level and better hardening depth than at 500°C.

10. The fatigue behaviour of the nitrided En41A depends on the quality of the nitrided case in terms of hardness, depth and microstructure. Nitriding at 520°C, with and without white layer formation, improves fatigue properties due to the high residual compressive stress level of the nitrided layer. The inferior fatigue properties at 570°C are due to the low residual stress level and due to the embrittlement effect.

11. The sub-surface cracks initiated by inclusions can reduce the fatigue life of the nitrided steel. Also, they seem to help crack initiation at the surface.

REFERENCES

1. Braune, H. — Revue de Metallurgie Memoirs 1905, 2, 497.
2. Hodkinson — Quoted by Kogan, Y.D. Metallography and Heat Treatment of Metals, 1974, March 2
3. Maclet, A.W. — U.S. Patent 884, 180, 1908 and subsequent patents
4. Fry, A. — U.S. Patent 1,487,544, 1924
5. Hobrock, R. — Trans. American Society for Steel Treating, 1929, 15, 543
6. Mahoux, G. — Comptes Rendues 1930, 191, 1328
7. Cowan, R.J. — Heat-treating and forging 1930, 16, 1277
8. Berkhin, V. Lackhtin, Yu. — Novosti Tekhniki, 1936, No. 34-35
9. Krupp. Akt Ges.F. — British Patent, No. 366838, 1932
10. Fisher, M.S. Shaw, Z. — J.I.S.I.
11. Floe, C.F. — Metal Progress, 1946, 50, 1212
12. Floe, C.F. — U.S. patent 243,7249, 1948
13. Kormanitsky, RS. — Metal Progress, 1946, 50, 655
14. — Tenifer-Mitteilungen Degussa, Frankfurt am Mein.
15. Waterfell, F.D. — 'Reducing Scuffing and Wear of Ferrous Materials', Engineering, Jan. 1959
16. Bason, G.F. — 'A New Method of Case Hardening'. Trans. American Society for Steel Treating, Vol. 14, December 1928
17. Berghaus, B. — British patent 794,174

18. Jones, C.K.
Martin, S.W.
Metal Progress 1964, 85 (2), 94

19. Hombeck, F.
Edenhofer, B.
'Symposium of physical Metallurgy, Aspects of Surface Coating', I.S.I. 1973

20. Edenhofer, B.
Metal Progress, 1976, 109, 38

21. Korotchenko, V.
Bell, T.
Heat Treatment of Metals, 1978, 4, 88

22. Jones, B.
Morgan, H.E.
J.I.S.I. Carnegie Scholarship Memoirs, 1932, 21, 39

23. Fry, A.
'Nitrogen in Iron, Steel and Special Steels', Kruppsche Monatshaft, 1923, 4, 137

24. Sergeson, R.
A.S.S.T. Nitriding Symposium, 1929

25. Erler, J.
'Cr-Mo Nitriding Steels with 2.5-3.5% Cr' Climax Molybdenum Co. New York

26. Jones, B.
J.I.S.I., 1933, 22, 51

27. Jones, B.
Ibid., 1934, 23, 139

29. Lehrer, E.
Z. Electrochem. 1930, 36, 383

30. Emett, P.H.
Hendrichs, S.B.
Brunauer, S.
J. Am. Chem. Soc., 1930, 52, 1456

31. Sutton, H.
Patent Spec. No. 345659, 1933

32. Darken, L.S.
Gurry, R.W.
'Physical Chem. of Metals'. McGraw Hill 1953, 375

33. Jack, K.H.
Proc. Roy. Soc. (London), 1948, A195, 34

34. Jack, K.H.
Ibid., 1951, A208, 200

35. Jack, K.H.
Scan. J. Met. 1972, 1, 195

36. Pope, M.
Grieveson, P.
Jack, K.H.
Scan. J. Met. 1973, 2, 29

37. Moretimer, B.
Grieveson, P.
Jack, K.H.
Ibid.
1973, 2, 29

38. Bain, E.C.
A.M.S.
1939, 229

39. Podgurski, H.H.
Knechtel, H.E.
Trans. A.I.M.E.
1969, 245, 1595

40. Jack, D.H.
Jack, K.H.
Materials Science and Engineering,
1973, 11, 1

41. Wagner, C.
Z Electrochem. 1959, 63, 772

42. Jack, D.H.
Lidster, P.C.
Grieveson, P.
Jack, K.H.
'Chemical Metallurgy of Iron and Steel', I.S.I., 1973, 374

43. Hayes, P.
Grieveson, P.
Scripta Metallurgica, 1975,
9, 39

44. Lightfoot, B.J.
Jack, K.H.
Heat treatment '73, The Metal Society

45. Meijering, J.L.
'Advances in Material Research'
Wiley Interscience, Vol. 51-81,
1971

46. Lightfoot, B.J.
Ph.D. thesis
'Nitriding of some chromium irons and Steels', Leeds University, 1973

47. Winnik, S.
Ph.D. thesis, 'The effect of process variables on the nitriding behaviour of chromium steels', Leeds University, 1979

48. Mridha, S.
Ph.D. Thesis,
"Characterization of nitrided alloy Steels", Leeds University, 1980

49. Darken, L.S.
J. Am. Chem. Soc., 1945, 67, 1398

50. Schwerdtfeger, K.
Turkdogan, E.T.
Technique for Metal Research,
Interscience 1970, 4(i), 346

51. Venkataraman, G. — Practical Metallurgy, 1979, 16, 119

52. Imai, Y. Masumoto, T. — Journal of the Japan Institute of Metals, 1963, 27, 593

53. Narita, K. Miyamoto, A. Iwakiri, H. — 'The Isolation and Determination in Steel', Trans. I.S.I.J., 1976 16, 168

54. Hodgson, C.C. Waring, H.O. — J.I.S.I. 1945, 151, 55

56. Kunz, E. — Revue Met. 1963, 60, 883

57. Baker, R. Smith, P.K. — Heat Treatment '73, The metal Society, 1975, 83

58. Hollomon, J.H. et al. — Trans. A.I.M.E., 1945, 165, 223

59. Baluffi, R.W. et al. — Trans. Am. Soc. Met. 1951, 43, 497

60. Woodhead, J.H. Quarell, A.G. — J.I.S.I. 1965, 203, 605

61. Kuo, K. — Ibid. 1953, 173, 346

62. Philips, V.A. Seybolt, A.V. — Transactions of the Metallurgy Society of A.I.M.E., 1968, 242, 2415

63. Hanai, S. Takemoto, N. Mizuyama, Y. — Transactions I.S.I.J., 1971, 11, 24

64. Takagi, S. — Kessho Kaiseki, 1968, 172, Asakura Shoten

65. Jack, D.H. Stony, I.M. — Scan. J. Met., 1972, 1, 217

66. Roberts, W. Grieveson, P. Jack, K.H. — J.I.S.I. 1972, 931

67. Driver, J.H. — Scan. J. Met., 1972, 1, 211

68. Jonsson, H.B.
Grieveson, P.
Jack, K.H.
Ibid,
1973, 2, 35

69. Stephenson, A.
Grieveson, P.
Jack, K.H.
Ibid,
1972, 1, 217

71. Minkevich, A.N.
Sorokin, Yu. V.
Met. Sci. Heat treatment,
1967, 309

72. Sumarokov, N.V.
Protective Coatings on Metals,
1970, 197

73. Lakhtin, Yu. M.
Lyubkin, A.A.
Met. Sci. Heat treatment,
1970, 234

74. Levy, S.A.
Libsch, J.F.
Wood, J.D.
Trans. A.I.M.E.
1969, 245, 753

75. Schwerdtfeger, K.
Grieveson, P.
Turkdogan, E.T.
Trans. A.I.M.E.
1969, 245, 2461

76. Bardgett, W.E.
Metal Treatment, 1943, 10, 87

77. Almen, J.O.
American Society for Metal
'Symposium on Surface Stressing of
Metals', 1946

78. Topper, T.H.
Wetzel, R.M.
J. Mat.
1969, 4, 200

79. Hengstenburg, O.
Mailander, R.
Zeitschrift des Vereines deutscher
ingenieure, 1930, 74, 1126

80. Mailander, R.
Tech. Mitt. Krup. 1933, 2, 53

81. Sutton, H.
Metal treatment, 1936, 2, 89

82. Sawert, W.
Z. Ver. Dtsch. Ing. 1943, 87, 609
quoted by R. Cazaud, Fatigue of
Metal, 185

83. Tauscher, H. — Neue- Hutt, 1974, 19, 228

84. Jones, B.K.; Martin, J.W. — Metal technology Jul. 1978, 217

85. Jack, D.H.; Winnik, S. — Heat Treatment '79, The Metal Society, 1979, 169

86. Forest, P.G. — Fatigue of Metal, Pergamon Press, 1962

87. H. Wiegand, — Revue de Metallurgie, 1948, 45, 105

88. Frith, P.H. — 'Int. Conf. on Fatigue' 1st Mech. Eng, 1956, 462

89. Teed, P.L. — Symposium: Fatigue and Fracture of Materials, M.I.T., J. Wiley, New York, 1950, 252

90. Wellinger, K. — Archive Eisench, 1952, 23, 203

91. Jones,P.K.; Martin, J.W. — Metal technology Nov. 1977, 519